UNIVERSITÀ DI PARMA

UNIVERSITA' DEGLI STUDI DI PARMA

Dottorato di Ricerca in Scienze del Farmaco, delle Biomolecole e dei Prodotti per la Salute

Ciclo XXXI

Synthesis of Irreversible Tyrosine Kinase Inhibitors and Ligand Traps as Diverse Approaches in the Antiproliferative Therapy

Coordinatore
Chiar.mo Prof. Marco Mor

Tutor
Chiar.ma Prof.ssa Silvia Rivara

Dottoranda
Nicole Bozza

Anni 2015/2018

Acknowledgements

I would like to express my gratefulness to my supervisor, Professor Silvia Rivara, for having spent so much time and attention revisioning my thesis and all the reports and presentations that I prepared during these years. I really appreciated the devotion she showed in making sure that everything was working the way it should have, the many advises she gave to me and the trust she demonstrated.

I am also indebted to Professor Marco Mor, who has guided me with strength, always congratulating and criticizing in a respectful and sincere way. I would like to express my thankfulness for his encouragement, trust and honesty.

I would also like to thank Professor Alessio Lodola for the enthusiasm he passed down to me and also for the interesting conversations about our work and the future perspectives.

I would like to express my deep gratitude to Dr. Riccardo Castelli, who really taught me much more than expectable about chemistry. I am deeply indebted for all the support he assured me during these four years in the lab, for all the canonical explanations and the magic tricks he shared.

Thanks also to Professor Federica Vacondio, for her patience and time, and for having never pulled back when I asked for details and explanations.

This experience would have not been the same without my labmate Giuseppe Marseglia: I really want to express him all my gratefulness for the great time we spent together in the lab, for all the scientific and non-scientific talks and also for having been a perfect partner during the summer schools we attended. I wish him all the success he deserves.

Thanks to the research fellows, postdocs and Ph.D. students that I met during these years: Dr. Daniele Pala, Dr. Mattia Anselmi, Dr. Michele Bassi, Dr. Laura Scalvini, Dr. Donatella Callegari, Francesca Ferlenghi, Martina Maccesi, Andrea Ghidini, Massimo Giori. Every one of them has taught me something and has contributed to a pleasant and stimulating working atmosphere.

Last but not least, I would like to thank Professor Karl-Heinz Altmann for kindly having hosted me in his group during my secondment. I am really grateful for everything I learnt

in ETH, for the enlightening group meetings and for the everyday life in the lab. Special thanks to my labmates, Simon Glauser and Melanie Zechner, for the wonderful working atmosphere and for the support they gave me. I would like to thank all the other members of the Altmann group for really having made the difference in making my experience so valuable.

Table of Contents

List of abbreviations

Ac	acetyl
ADP	adenosine diphosphate
ATP	adenosine triphosphate
BINOL	1,1′-bi-2-naphthol
Bu	butyl
Bz	benzoyl
calcd	calculated
Cp	cyclopentadienyl
DCM	dichloromethane
DDQ	2,3-dichloro-5,6-dicyano-1,4-benzoquinone
dec.	decomposition
DIBAL	diisobutylaluminium hydride
DIPEA	*N,N*-diisopropylethylamine
DMA	dimethylacetamide
DMAP	4-dimethylaminopyridine
DMF	*N,N*-dimethylformamide
DMP	Dess-Martin periodinane
DMSO	dimethylsulfoxide
ESF	ethenesulfonyl fluoride
ESI	electrospray ionization
Et	ethyl
HFA	hexafluoroacetone
HMDS	hexamethyldisilazane

HMPA	hexamethylphosphoramide
HPLC	high-performance liquid chromatography
HRMS	high-resolution mass spectrometry
HWE	Horner–Wadsworth–Emmons
IC_{50}	half maximal inhibitory concentration
IR	infrared radiation
LAH	lithium aluminium hydride
LC	liquid chromatography
LG	leaving group
Me	methyl
Mp	melting point
MS	mass spectrometry
MTT	3-(4,5-dimethylthiazol-2-yl)-2,5-diphenyltetrazolium bromide
NCS	*N*-chlorosuccinimide
NIS	*N*-iodosuccinimide
NMR	nuclear magnetic resonance
p	phospho-
PBS	phosphate-buffered saline
PCC	pyridinium chlorochromate
PG	protecting group
P_i	inorganic phosphate
Piv	pivaloyl
PMB	*p*-methoxybenzyl
Pr	propyl
PTSA	*p*-toluenesulfonic acid

r.t.	room temperature
R_f	retention factor
RP	reverse phase
SAR	Structure-Activity Relationship
SD	standard deviation
TBAF	tetrabutylammonium fluoride
TBDPS	*tert*-butyldiphenylsilyl
TBS	*tert*-butyldimethylsilyl
TBTU	2-(1*H*-benzotriazole-1-yl)-1,1,3,3-tetramethylaminium tetrafluoroborate
TEA	triethylamine
Tf	trifluoromethanesulfonate
TFA	trifluoroacetic acid
THF	tetrahydrofuran
TLC	thin-layer chromatography
TMS	trimethylsilyl
Ts	*p*-toluenesulfonyl
UV	ultraviolet
wt	wild type

1. Protein kinases: an overview

Protein phosphorylation is a post-translational modification involved in the regulation of many cellular activities.[1] This reaction is catalyzed by the protein kinase enzymes, which transfer the γ-phosphate group of adenosine triphosphate (ATP)[2] to the appropriate hydroxyl bearing side chain on a serine, threonine or tyrosine residue on the target protein, as depicted in Fig.1. Protein kinases in mammalians are therefore classified on the basis of their substrate preference as serine-threonine kinases, tyrosine kinases or dual-function kinases.[3,4] Histidine protein kinases, which are widely used in bacteria, plants and lower eukaryotes, are not expressed in animals.[5]

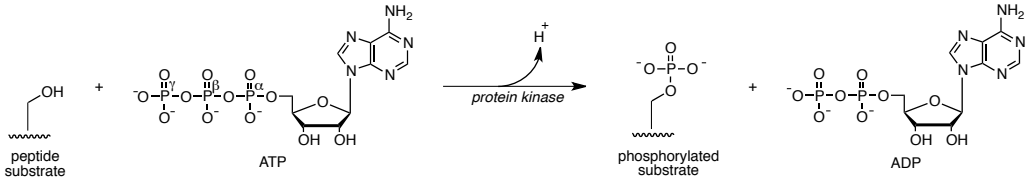

Figure 1: transfer of the γ-phosphate group of ATP catalyzed by protein kinases.

The phosphorylated proteins resulting from the kinase activity are mainly involved in a cellular downstream cascade of reactions, leading to the activation of different signaling pathways.[6] This effect derives from the capability of phosphorylated residues to act as recognition sites for other proteins involved in the signaling cascade, which are therefore recruited to eventually lead to the actual response of the cell.[7]

Phosphorylation is a reversible modification and the phosphate group can be removed by phosphatases, allowing a strict control on cell function.[8]

Protein kinases are broadly involved in the amplification and transduction of extracellular signals mediating cell growth and survival and it is now well established that deregulation of kinase activity inside the cells is one of the possible mechanisms concurring in aberrant proliferation.[9–13] Genes responsible for the transformation of

normal cells into tumor cells, also called oncogenes,[14] have been identified starting from the 1970s and some of them actually turned out to be responsible for the synthesis of protein kinases, such as the virus kinase v-SRC, the epidermal growth factor receptor (EGFR) or the fusion protein Bcr-Abl,[15] whose activity is somehow escaping the tight regulation observed in normal tissues.[16–18] Kinases thus represent an interesting target in the development of antiproliferative drugs.[10,12,19,20]

1.1. Classification of protein kinases

Protein kinases can be classified in seven different classes according to their sequence:[21] AGC, including the PKA (protein kinase A), PKG (protein kinase G) and PKC (protein kinase C) families, CAMK (calcium calmodulin-dependent kinases), CK1 (casein kinase 1), CMGC, including the CDK (cyclin-dependent kinase), MAPK (mitogen-activated protein kinase), GSK (glycogen synthase kinase) and CLK (CDC-like kinase) families, STE (homologs of yeast sterile kinases), TK (tyrosine kinases) and TKL (tyrosine kinase-like).[22] Among the 518 protein kinases encoded by the human genome, 58 proteins belonging to the tyrosine kinase class are endowed with receptor activity.[21] Among them, the Epidermal Growth Factor Receptor (EGFR)[23–26] and, more recently, the Fibroblast Growth Factor Receptor (FGFR)[27–31] have been investigated as possible targets for anticancer drugs. To date, four small-molecule inhibitors of EGFR, namely gefitinib, erlotinib, afatinib and osimertinib, are approved for the treatment of various cancer types, as well as three monoclonal antibodies, cetuximab, panitumumab and necitumumab, while no selective agent targeting the FGF/FGFR axis has been approved yet.

1.2. Structure and activity of protein kinases

Sequence similarities among protein kinases result in a conserved structure of the catalytic domain. Nevertheless, the catalytic activity of this class of proteins can be

regulated according to different mechanisms:[32] kinases can switch from an inactive state to an active one,[33] they can include a regulatory domain covalently bound to the catalytic one (e.g., Src)[34] or they can require an additional subunit to be activated (e.g., cyclin-dependent protein kinases, CDKs).[35] Receptor tyrosine kinases (e.g., EGFR) recognize their ligands through interaction with the extracellular domain and are consequently activated following a dimerization process.[36] The activity of kinases can also be regulated by post-translational modifications, such as phosphorylation by an upstream kinase or myristoylation (e.g., Abl).[37–39]

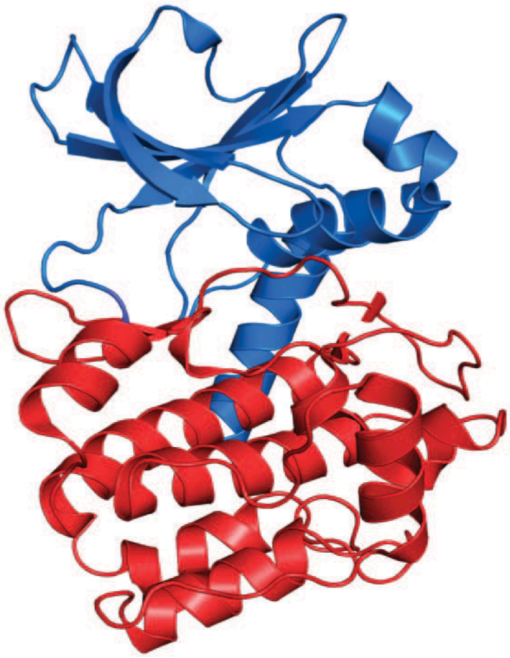

Figure 2: structure of the conserved catalytic domain of protein kinases. N-terminal lobe is shown in blue, C-terminal lobe is shown in red (picture adapted from ref.48).

The catalytic portion of kinases includes about 300 amino acid residues and 12 conserved subdomains.[40] Its tertiary structure features two distinct lobes (Fig.2), which exert different functions during regulation and catalysis.[41] The N-terminal lobe (N-lobe) of about 80 residues mainly consists of β-sheets, but also includes an α-helix (C-helix), whereas the C-terminal lobe (C-lobe) of about 200 residues is mainly α-helical, with only some short β-sheet strands. The lobes are connected by a hinge region and the ATP-binding site is located in the cleft between the two substructures.[42,43]

The catalytic domain of kinases includes some conserved structural elements, which are involved in the accommodation of the ATP molecule and in the phosphate transfer process (Fig.3). The relative spatial position of some of these substructures allows to distinguish two different conformations of the domain, which are usually described as "open" and "close" state.[42]

A peculiar, widely conserved motif embedded in the structure of the N-lobe is the "glycine-rich loop" (GxGxϕG, with ϕ usually being tyrosine or phenylalanine) or "P-loop", which is located between β1 and β2 and interacts with the γ-phosphate of ATP, positioning it for catalysis.[7] In the absence of ATP this loop exhibits high flexibility, allowing small molecule inhibitors to be accommodated into the binding cleft.[44]

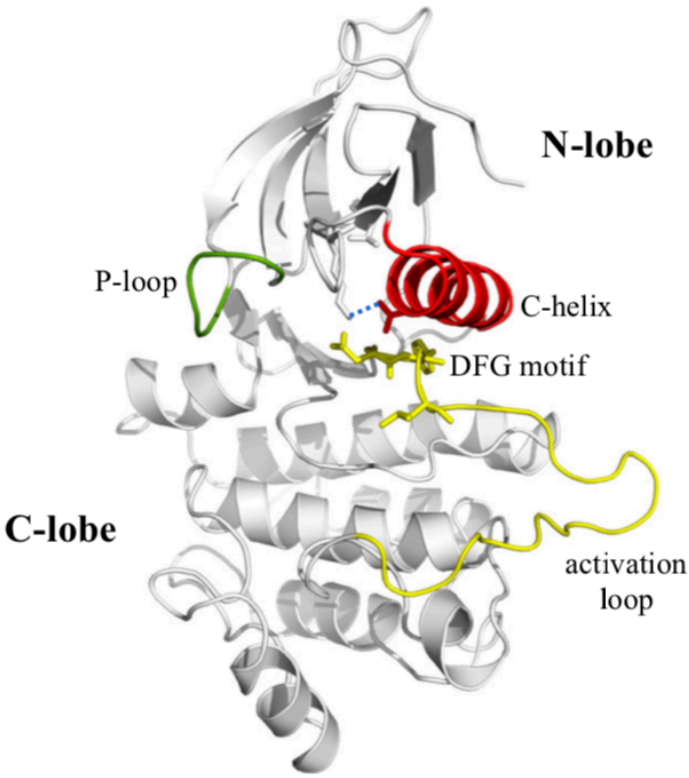

Figure 3: conserved structural elements in the catalytic domain of protein kinases. Structure of EGFR kinase domain: C-helix is colored in red, P-loop in green, activation loop in yellow. The salt-bridge between the conserved lysine and glutamate residue is highlighted as blue dotted line. Picture adapted from ref.45.

The C-helix is the only helical element included in the N-lobe and it is a dynamic structure,[7] located at the interface between the two lobes of the kinase. C-helix interfaces the N-terminal region of the "activation loop", a segment included between the DFG (aspartate-phenylalanine-glycine) and APE (alanine-proline-glutamate) motifs, the

conformation of which is crucial for the correct accommodation of the kinase substrate.[46] In many kinases, the activation loop is phosphorylated when the kinase is in the active state.[47] After activation of the kinase *via* phosphorylation on the activation loop, the position and total number of the phosphate groups are responsible for the substrate selectivity.[48]

The relative position of C-helix and the activation loop is fundamental in determining the efficiency of the catalysis. A conserved acidic residue in C-helix interacts with a lysine residue belonging to the β3-strand in the active conformation of the kinase:[33] the salt-bridge between these two residues is only maintained when the C-helix in a suitable position allowing catalysis (open state). The conserved lysine residue is buried into the interlobe cleft and interacts with the α- and β-phosphates of the ATP molecule.[44] The first three amino acid residues belonging to the activation loop represent the conserved DFG motif, which is also often used to describe the conformation of the domain and therefore its activity (the DFG "in" conformation corresponds to the open, active state of the kinase, while the DFG "out" conformer is closed and inactive).[45,49] The aspartate residue in the DFG motif contacts a magnesium ion, which is required to stabilize the triphosphate group of ATP.[50,51]

A further conserved motif in the structure of kinases is the catalytic loop HRD-motif, which is located at the N-terminus of the β7-strand. The aspartate residue serves as a weak catalytic base, required for the orientation of the substrate hydroxyl group and to trap the proton that is released during phosphorylation, while the arginine residue interacts with the phosphorylated activation loop, in order to allow its correct positioning.[52]

The active conformation of the kinase is achieved by interactions among the F-helix (C-lobe) and spatially conserved hydrophobic motifs (i.e., hydrophobic spines), as well as by correct orientation of the N-lobe.[7] The latter is only obtained when the P-loop is positioned to shield the ATP and steer the γ-phosphate for transfer and the C-helix is interacting with the activation loop in a way that allows the cleft to open and close. In some cases, C-helix can be properly positioned thanks to the interaction of a suitable peptide with two spatially conserved pockets on the surface of the kinase core. This has

been shown for instance for CDKs, which require the docking of the cyclin to one of the pockets to achieve the active conformation.[44] In other kinases, such as Fes, C-helix is oriented by the binding of a SH2 domain that also provides a priming site for docking of the substrate protein.[53] Kinases such as PKA and PKC in their active and fully phosphorylated conformation are inhibited by regulatory domains and require activation by second messengers.[54,55]

1.3. Receptor Tyrosine Kinases

1.3.1. Regulation of the activity of Receptor Tyrosine Kinases

Receptor Tyrosine Kinases (RTKs) represent a large family of membrane receptors endowed with protein kinase activity. RTKs play a crucial role in the regulation of cellular processes including proliferation, migration, metabolism, survival and differentiation.[56] The structure of these proteins includes an extracellular ligand binding domain, which is usually glycosylated, a single transmembrane domain and a cytoplasmic kinase domain. RTKs are autoinhibited by diverse mechanisms in the absence of their ligand.[36] Ligand binding induces dimerization of the receptor and phosphorylation of the cytoplasmic domain.[57,58] Different ligands can induce dimerization *via* different mechanisms: ligands can be bivalent, and in this case one molecule of ligand binds simultaneously to two receptor molecules,[59,60] or they can bind in a 1:1 ratio to the receptor on the membrane.[61]

Dimerization of the receptor causes conformational rearrangements including the rotation of the major axis of the protein and of the N- and C-lobes. The consequent movement of the activation loop enables ATP to reach its binding pocket, resulting in the phosphorylation of tyrosine residues located on the partner of dimerization.[62] The *trans*-phosphorylation of residues belonging to the activation loop is essential for the stabilization of the open conformation.

Tyrosine phosphorylation is fundamental for the recruitment and activation of intracellular signaling proteins.[56] Phosphorylated tyrosine residues are mainly located in noncatalytic regions and serve as docking sites for Src homology (SH2 or SH3) or PTB (phosphotyrosine binding) domains of different proteins. Every RTK can therefore be described as a platform for the recognition of a specific set of signaling proteins.[56]

The signaling pathways activated by RTKs autophosphorylation are well understood and mostly shared by different receptors: they include the MAPK (mitogen-activated protein kinase) pathway, which plays a crucial role in the regulation of metabolic processes, cell

proliferation, migration and differentiation,[63] as well as the PI3K-Akt,[64] the JAK/STAT and the PLC-γ pathways.[65]

The tight regulation of the cellular processes activated by RTKs requires a variety of mechanisms to terminate the signal, including, among others, inactivation of the RTK by protein tyrosine phosphatases (PTPs)[66] and receptor endocytosis.[67]

1.3.2. Targeting Receptor Tyrosine Kinases

As RTKs are deeply involved in cellular processes including proliferation and differentiation, the scientific community has spent great efforts in the development of molecules able to interfere with the aberrant activity of RTKs in tumor tissues.

To date, three approaches have been proposed to target overexpressed or mutated RTKs in neoplastic diseases (Fig.4), namely Tyrosine Kinase Inhibitors (TKIs), monoclonal antibodies (mAbs) and extracellular agents targeting the ligand (ligand-targeting mAbs[68] or peptides[69] or small molecules,[70] discussed in Chapter 3).

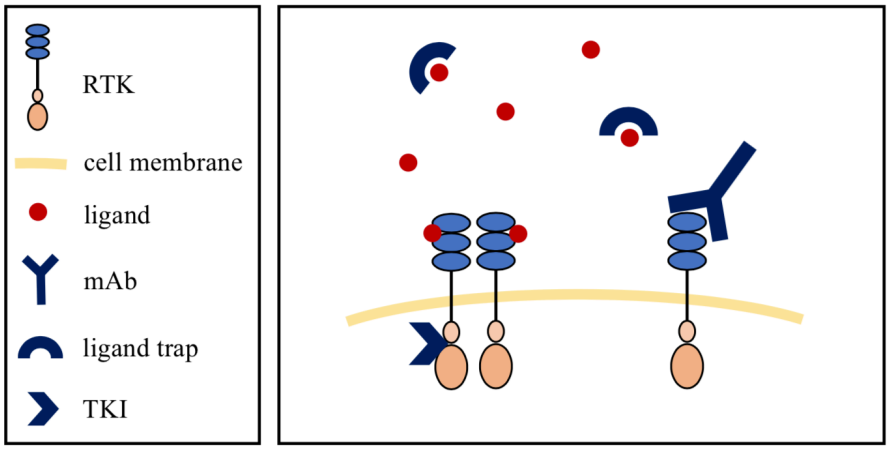

Figure 4: overview of three approaches developed to target RTKs. Monoclonal antibodies bind to the extracellular domain of the receptor, whereas ligand traps prevent ligand binding to the receptor in the extracellular environment. Tyrosine kinase inhibitors interact with the intracellular catalytic domain of RTKs.

Monoclonal antibodies bind to the extracellular domain of RTKs, thus avoiding both the binding of the natural ligand and the conformational rearrangement that is required for the receptor to activate the intracellular signaling pathways.[71] Approved mAbs available for the treatment of various cancer types are the anti-HER2 antibodies trastuzumab (Herceptin®, Genentech)[72] and pertuzumab (Perjeta®, Genentech),[73] the anti-EGFR antibodies cetuximab (Erbitux®, Imclone Systems),[74,75] panitumumab (Vectibix®, Amgen)[74,76] and necitumumab (Portrazza®, Eli Lilly),[77] and the anti-PDGFRα antibody olaratumab (Lartruvo®, Eli Lilly).[78]

Tyrosine Kinase Inhibitors are small molecules that enter the cells and inhibit the signaling cascade initiated by RTKs by binding to the catalytic domain and hampering the autophosphorylation process.[13] To date, 23 TKIs have been approved by FDA (Food&Drug Administration) for the treatment of a plethora of cancer types, ranging from leukemia to lung, liver, breast and kidney neoplasms.[79] The first strategy exploited to obtain TKIs was to develop ATP mimicking molecules. This strategy led to the development of a first generation of compounds binding to the open (active) conformation of the kinase, which are generally called type I inhibitors.[80] Type I inhibitors bind to the ATP-binding pocket and form one to three hydrogen bonds with the backbone residues of the hinge region. The type I kinase pharmacophore includes a hydrogen bond acceptor, two hydrogen bond donors and a hydrophobic portion.[81] The main drawback of type I inhibitor is that they target a conformation in which RTKs share a high degree of structural similarity. This is linked to a higher possibility to obtain non-selective compounds. Nevertheless, extensive medicinal chemistry optimization efforts have allowed the development of really potent and selective compounds, as in the case of EGFR inhibitors.[82] An example of type I inhibitor, even if targeting a non-receptor kinase, is Bcr-Abl inhibitor PD173955 (**1**), reported in Fig.5.

The inactive conformation of the kinase is targeted by type II inhibitors: these compounds bind to the ATP-binding pocket and exploit additional interaction with an allosteric pocket resulting from the displacement of the DFG residues in the DFG "out" conformation. Therefore, the type II pharmacophore includes the same structural

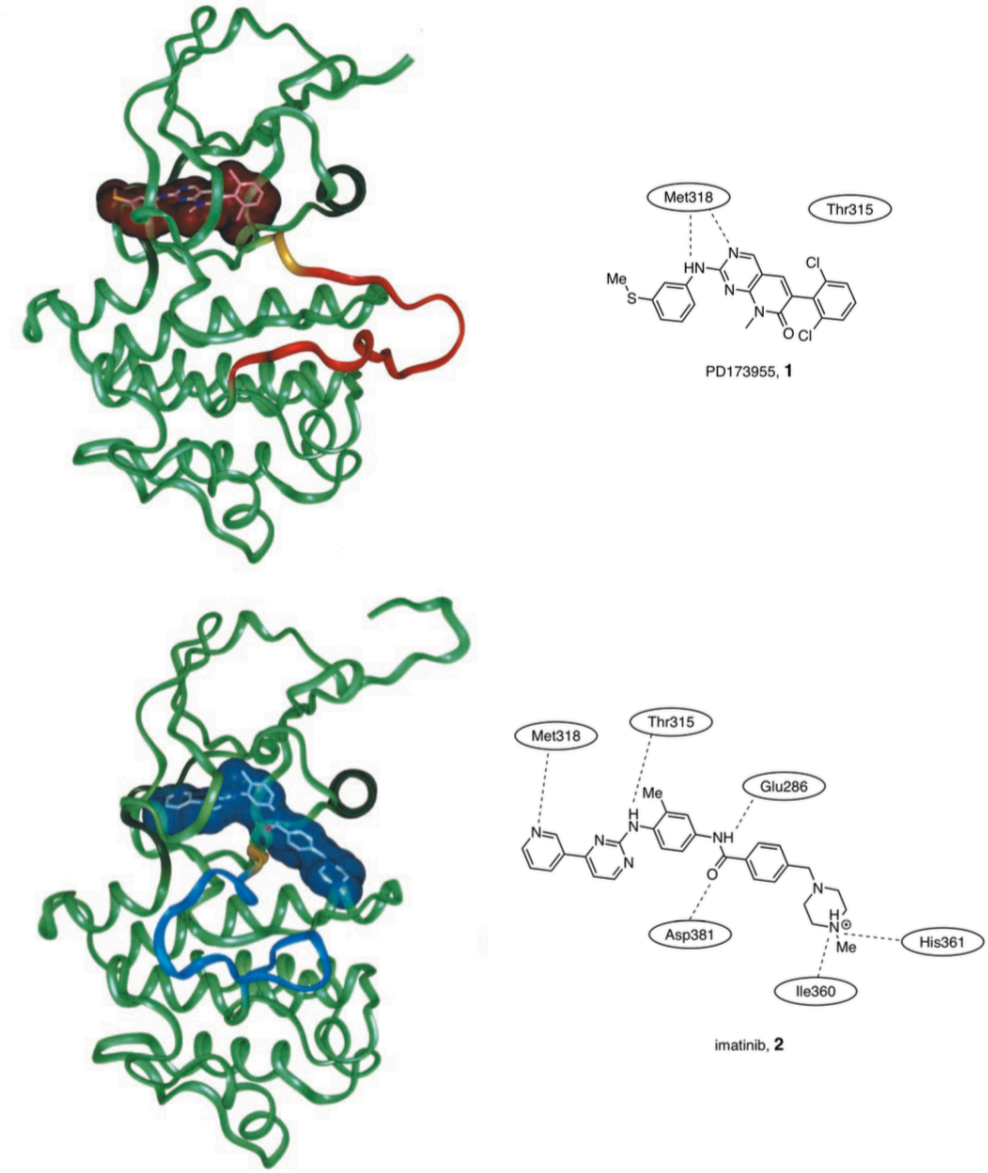

Figure 5: ribbon representation of the structure of the Abl kinase domain in complex with type I inhibitor PD173955 (**1**) and type II inhibitor imatinib (**2**). The activation loops and the van der Waals surfaces corresponding to the inhibitors are colored red for PD173955 and blue for imatinib. The structures of the inhibitors are highlighted on the right. Hydrogen bonds are indicated as dotted lines. The position of the gatekeeper residue, Thr315, is indicated. Type II inhibitor imatinib establishes additional interactions with the allosteric pocket in the inactive conformation of the kinase (picture adapted from ref.83).

elements already described for the type I pharmacophore, with the addition of a linker and a portion responsible for the interaction with the allosteric cavity. This moiety can establish hydrogen bonds with a conserved glutamate residue from the C-helix and with the aspartate residue from the DFG motif.[84] An example of a successful type II kinase inhibitor is the Bcr-Abl kinase inhibitor imatinib (**2**, Gleevec®, Novartis) (Fig.5), which is approved for the treatment of chronic myeloid leukemia.[32,85]

A promising field in the development of effective inhibitors is represented by irreversible, covalent agents, which interact with a nucleophilic residue in the ATP-binding pocket leading to the formation of a covalent bond. This class of compounds has demonstrated to be particularly useful in the treatment of acquired resistance to reversible drugs.[86–93]

2. Epidermal Growth Factor Receptor

2.1. Biology

2.1.1. The ErbB family

The Epidermal Growth Factor Receptor (EGFR) was the first receptor tyrosine kinase (RTK) to be discovered[94] and studies on this protein have led to the establishment of the general features of receptor tyrosine kinases as a class.[56] After the discovery of EGFR (also known as ErbB1 or HER1), three further members of its family have been described, namely ErbB2 (also known as HER2), ErbB3 (HER3), and ErbB4 (HER4).[95] The structure of these proteins, consistently with that of receptor tyrosine kinase family, includes an extracellular ligand binding domain, a single transmembrane domain and a cytoplasmic tail, which is endowed with catalytic activity. The absence of fundamental amino acid residues in the intracellular domain of ErbB3 renders the receptor devoid of catalytic activity.[96]

The extracellular domains of the EGFR family members are constituted of four subdomains (I to IV or L1, S1, L2, and S2), with subdomains I and III forming the ligand binding domain (Fig.6). The remaining portions of the extracellular structure are involved in receptor dimerization and interaction with other membrane proteins.[97] Intracellularly, the kinase domain includes the amino domain (also called N-lobe) and the carboxy domain (C-lobe) and all the structural features of kinases: the glycine-rich nucleotide phosphate binding loop (Gly719-Gly724 in EGFR), the DFG motif (Asp855-Gly857 in EGFR), the catalytic base (Asp837 in EGFR), the catalytic loop (Arg836-Asn842 in EGFR) and the A-loop (Asp855-Val876 in EGFR).[98]

Besides the epidermal growth factor (EGF), ErbB receptors bind to a variety of extracellular soluble ligands, including the transforming growth factor-α (TGFα), amphiregulin (AR), epiregulin (EREG), β-cellulin (BTC), and heparin-binding EGF (HB-EGF).[99]

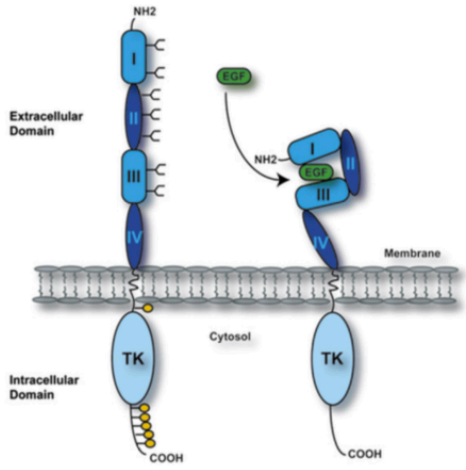

Figure 6: schematic representation of EGFR, including the extracellular domain (subdomains I, II, III and IV), the transmembrane domain and the intracellular domain (TK: Tyrosine Kinase). The ligand binding domain is formed by subdomains I and III.[100]

Ligand binding results in the formation of receptor homo- and heterodimers. The dimerization process for the ErbB receptor family has been deeply investigated. Dimerization of EGFR requires the binding of two molecules of monomeric EGF (or another ligand) to two EGFR molecules,[101] which causes a conformational change that exposes receptor-receptor interaction sites.[102–104]

While the preference of ErbB3 and ErbB4 for their ligands has been described, no natural ligand for ErbB2 has been identified. It has been proposed that ErbB2 is constitutively present in an active conformation in the absence of a ligand and that it acts as a preferred partner for heterodimerization with all members of the EGFR family.[105]

2.1.2. Activation of EGFR

Crystallographic data regarding the kinase domain of EGFR furnished a deeper insight into the activation mechanism of this receptor and highlighted its unusual behavior if compared to other RTKs.[106] The first crystallographic view of the EGFR TKD (Tyrosine

Kinase Domain) described by Stamos *et al.* confirmed that activation-loop phosphorylation is not required for it to adopt an active-like structure,[98] as already proposed by others.[107] Some years after this finding, the activation mechanism of the kinase domain was fully described by Zhang *et al.*[108] In EGFR dimer, one subunit acts as "activator", contacting the amino lobe of the other monomer, the "receiver". The interaction between the kinase domains results in the rotation of the C-helix of the "receiver", leading to its rotation from the "out" to the "in" position seen in active kinases. The disruption of key interactions resulting from this conformational change enables the activation loop to adopt the typical conformation seen in active kinases and brings the side chain of Glu762 in proximity of the side chain of Lys745, allowing the formation of a salt bridge. It has been suggested that the two monomers dissociate and reassociate rapidly enough to allow each of them to act as both "activator" and "receiver" and consequently to be trans-autophosphorylated.

2.1.3. Activation of the signaling cascades

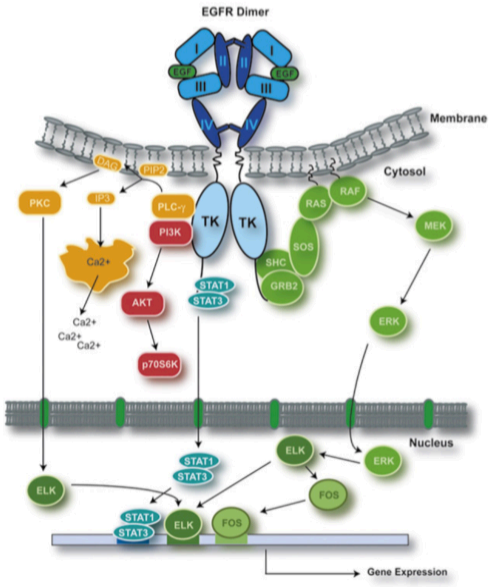

Figure 7: schematic representation of the downstream signaling pathways activated by EGFR upon dimerization.[100]

Phosphorylation of tyrosine residues leads to recruitment of proteins containing Src-homology 2 domains (SH2) such as Grb-2, SHC and PLC-γ, which in turn activate downstream signaling cascades, causing transduction of the extracellular signal to the nucleus.

The actual response is determined by the nature of the homo- or heterodimer formed by the receptors and of the specific intracellular signaling molecule recruited to the phosphorylated residues after dimerization. More precisely, different phosphorylation patterns promote the activation of different pathways through the interaction with a plethora of adaptors (for instance, pY1068 (pY: phospho-tyrosine) and pY1086 bind Grb-2 while pY992 and pY1173 interact with PLC-γ).[109] Intracellular pathways activated by ErbB receptors are the Ras-Raf-MEK-ERK1/2, STAT3 and STAT5 pathways mainly controlling proliferation and differentiation and the PI3K-Akt-mTOR cascade acting as a pro-survival and anti-apoptotic pathway (Fig.7).[53,95,110]

2.2. EGFR and cancer

2.2.1. Deregulated activity of EGFR

The tight regulation of EGFR expression and activity allows to strictly control proliferation and motility in healthy tissues. However, several diverse mechanisms can lead to aberrant activity of the system and eventually to the insurgence and progression of different cancer types, including overexpression of EGFR and/or its ligands, defective downregulation, activating mutations on the receptor.[100]

The production of EGFR ligands has been found to be increased in various neoplastic diseases.[111–114] Growth factors can act in both an autocrine or paracrine manner to activate EGFR. Moreover, it has been proposed that the co-expression of EGFR and TGF-α could serve as an independent prognostic indicator in patients affected by breast cancer.[111]

Overexpression of EGFR has been found to correlate with decreased survival in patients with head and neck, bladder, ovarian, cervical and esophageal cancer.[115] The transforming ability of EGFR overexpression is due to the tendency of the receptor to spontaneously form dimers at high concentrations, leading to constitutive activation of the intracellular signaling cascades.[116,117] EGFR overexpression can derive from EGFR gene amplification,[25] increased activity of the EGFR promoter[26,118] or deregulation at the post-translational level.[119]

Mutations of the EGFR structure can affect the extracellular domain, the intracellular portion and, in particular, the catalytic domain. Mutations in the extracellular domain of EGFR are frequently found in glioblastomas and usually result from the deletion of specific exons. For instance, the EGFRvIII mutant derives from an in-frame deletion of exons 2-7 and lacks most of the ligand-binding domain, but it is nonetheless constitutively phosphorylated and able to activate downstream effector pathways.[120,121]

The most common mutations affecting the kinase domain are small deletions in exon 19, missense mutations L858R in exon 21 and G719A/C in exon 18 and small duplications or insertions in exon 20.[122] The general result of this kind of mutations is the stabilization

of the active conformation of EGFR, which inevitably leads to a sustained stimulation of proliferation.[82,123]

2.2.2. Targeting EGFR with Tyrosine Kinase Inhibitors

Compounds targeting the EGFR kinase domain are generally classified as first, second or third generation inhibitors, according to their structure and their activity towards different EGFR mutants.

2.2.2.1. First-generation inhibitors

The first generation includes the approved drugs gefitinib (**3**) and erlotinib (**4**) (Fig.8), which are reversible inhibitors featuring a 4-anilinoquinazoline scaffold.

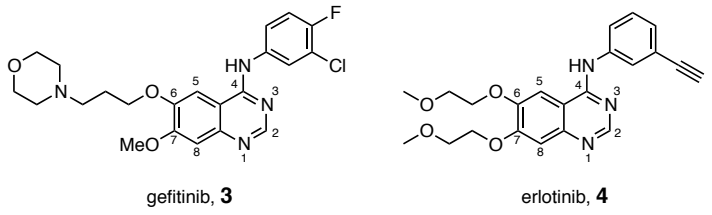

Figure 8: reversible, first-generation EGFR inhibitors.

The structure-activity relationships (SARs) for this class of compounds were established in the 1990s.[15,124,125] The publication of the crystal structure of EGFR kinase domain in complex with erlotinib allowed to better understand the interactions occurring among the inhibitor and the ATP-binding pocket residues.[98] In particular, N1 of the quinazoline ring is involved in a hydrogen bond with Met793 amide nitrogen, while N3 interacts with Thr790 side chain through a water molecule. The aniline in position 4 occupies a hydrophobic pocket in proximity of Thr790, which is not involved in the binding of ATP.[126] Finally, the groups linked to C6 and C7 on the quinazoline are projected into the solvent (Fig.9).

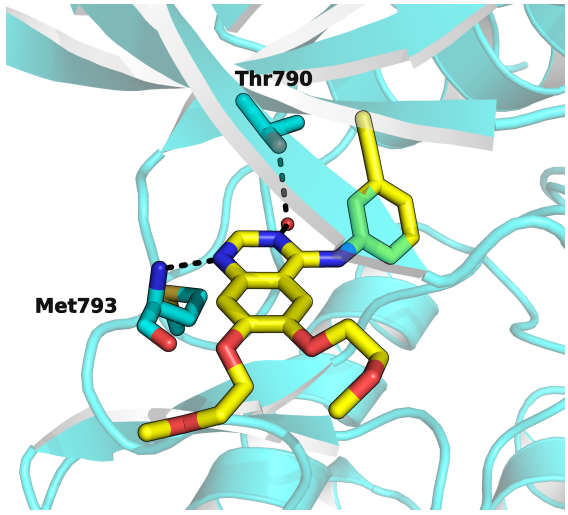

Figure 9: crystal structure of erlotinib in complex with *wt*EGFR complex (PDB ID 1M17). The EGFR kinase is shown in a ribbon representation (light blue) with the bound inhibitor in yellow. Side-chain and main-chain atoms of Thr790 and Met793 are shown. Hydrogen bonds are indicated by dashed lines. Water molecule is represented as a red dot.

Both gefitinib and erlotinib were firstly approved for the treatment of locally advanced or metastatic non-small cell lung cancer (NSCLC) in patients with tumors progressed upon previous chemotherapy treatment, but their use was later restricted to patients whose tumors present EGFR alterations, such as exon 19 deletions or exon 21 (L858R) substitution, which lead to constitutive activity of the receptor.[79]

Correlation between the presence of mutations in the kinase domain of EGFR and activity of gefitinib and erlotinib was described in 2004.[82,127,128] Notably, it was also noticed that these alterations are more frequently observed in patients affected by adenocarcinomas, in never-smokers, in women and in patients from East Asia. These mutations are located in the P-loop and in the activation loop of the kinase domain and result in a lower affinity of EGFR for ATP[129] and in an enhanced ligand-independent activation of mutated EGFR[82,130] if compared to the wild-type protein (*wt*EGFR).

Clinical efficacy of reversible inhibitors is limited by the development of acquired resistance, which is most frequently due to the "gatekeeper" mutation, T790M.[131,132] The gatekeeper residue is the first amino acid residue of the hinge region: the steric hindrance

of its side chain controls the access to a small, hydrophobic cavity, which is not occupied by ATP but accommodates the aniline ring of first-generation inhibitors.[80] Replacement of Thr790 with a methionine residue seems to be associated with the restoration of ATP affinity for its binding site:[133] given the high concentration of the nucleotide in the cell, if compared to that of the drug, the overall consequence of T790M acquisition is the loss of activity of first-generation compounds. Recent data suggest that T790M is present in about 80% of naïve NSCLC samples: mutated clones are thus selected by the therapy.[134]

2.2.2.2. Second-generation inhibitors

Second generation inhibitors were developed with the straightforward aim of circumventing acquired resistance to reversible agents.[86] These compounds feature the 4-anilinoquinazoline scaffold (the "driving portion" responsible for target affinity) equipped with an acrylamide moiety on the 6-position of the quinazoline ring: the electrophilic group, usually called "warhead", engages a hetero-Michael addition reaction with a cysteine residue (Cys797) in the binding cleft, allowing to irreversibly inhibit EGFR kinase activity.[126,135,136] Covalent inhibitors effectiveness has been demonstrated in a series of clinical trials,[137–139] resulting in FDA-approval of afatinib (Fig.10) in 2013, for the treatment of locally advanced and/or metastatic NSCLC.

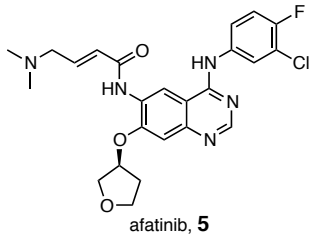

afatinib, **5**

Figure 10: irreversible, second-generation EGFR inhibitor afatinib (**5**).

Nevertheless, clinical trials on both afatinib and other acrylamide-bearing compounds highlighted the high frequency of dose-limiting toxicities, mainly diarrhea, nausea, rash

and fatigue.[140,141] These adverse effects have been related to the inhibition of *wt*EGFR (Fig.11) and are therefore due to the lack of selectivity of second-generation inhibitors towards different isoforms of the kinase.[93]

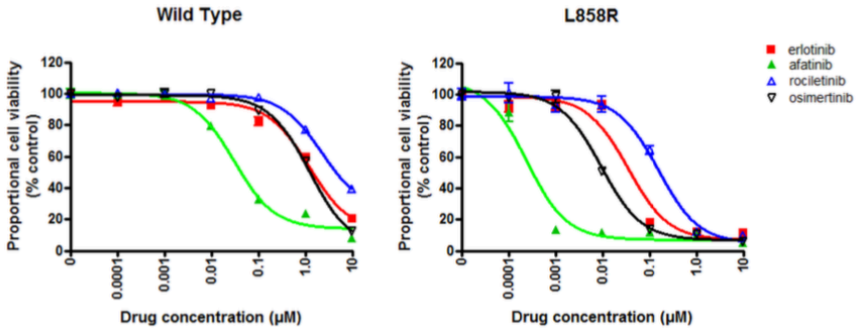

Figure 11: cell viability assays on Ba/F3 cells harboring *wt*EGFR or EGFR L858R, treated with different EGFR inhibitors (picture adapted from ref.142).

2.2.2.3. Third-generation inhibitors

Lessons learnt from these covalent inhibitors have been applied to the development of third-generation compounds: this latter class includes molecules bearing an acrylamide group, thus able to interact with Cys797 and to prolong the occupancy of the binding site, but the scaffold has been modified in order to allow selective targeting of mutated EGFR.[143]

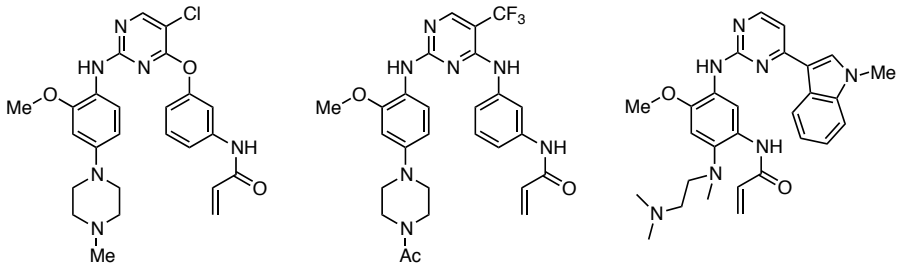

Figure 12: third-generation EGFR inhibitor WZ4002 (**6**), rociletinib (**7**) and osimertinib (**8**).

The driving portion of mutant-selective inhibitors features a 2-aminopyrimidine core (Fig.12), which is decorated with additional rings and a hydrophilic group enhancing solubility. The favored U-shaped conformation adopted by these molecules seems to be responsible for their preferential binding to EGFR T790M.[24] The crystal structure of the WZ4002/EGFR T790M complex (Fig.13) reveals the formation of a bidentate hydrogen bond between the aminopyrimidine nitrogen atoms and Met793, a residue belonging to the hinge region. Moreover, a contact has been highlighted between the chlorine atom on the pyrimidine ring of the inhibitor and the side chain of Met790, which is most likely contributing to the selectivity towards the mutated isoform of the kinase. The phenyl ring carrying the acrylamide group lies roughly orthogonal to the rest of the molecule, enabling to juxtapose the warhead with the side chain of Cys797.[143]

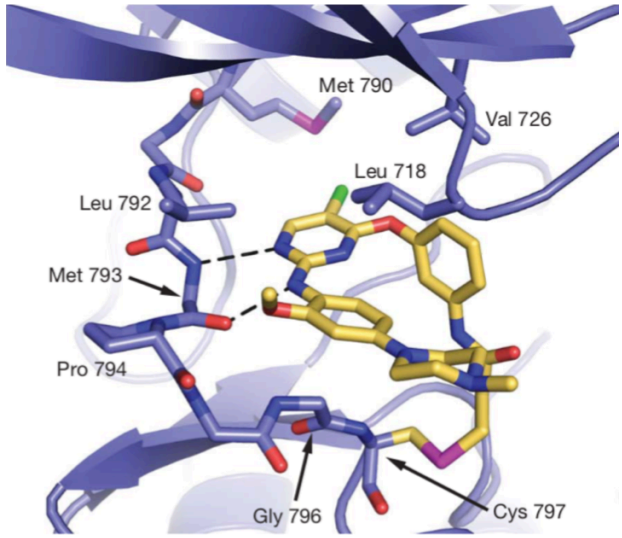

Figure 13: crystal structure of WZ4002/EGFR T790M complex as determined by Zhou *et al.*[143]

To date, only one third-generation EGFR inhibitor, namely osimertinib (**8**, Tagrisso®, AstraZeneca), has been approved for first-line treatment of patients with metastatic NSCLC harboring EGFR activating mutations.[144]

Third-generation inhibitors are actually able to prevent cell proliferation *in vitro* and to promote tumor regression *in vivo* (Fig.14), but, as for first-generation inhibitors, their

efficacy is limited by the insurgence of mutations.[90,145,146] Among them, the replacement of Lys718 with a glutamine residue results in the stabilization of a non-reactive conformation of the kinase,[147] while mutation of Cys797 to serine directly affects the capability of the residue to act as a nucleophile and therefore to engage a covalent interaction with the inhibitor (Fig.15).

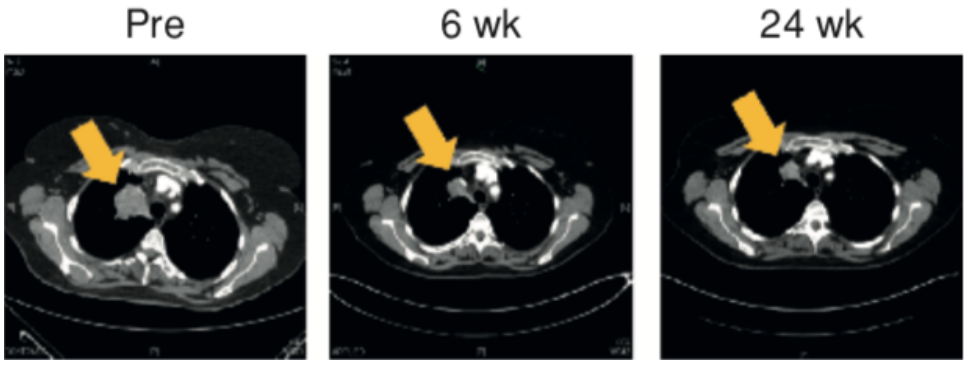

Figure 14: serial computed tomography scans of the chest from a patient highlights tumor shrinkage as a result of treatment with osimertinib (phase I AURA-trial).[148]

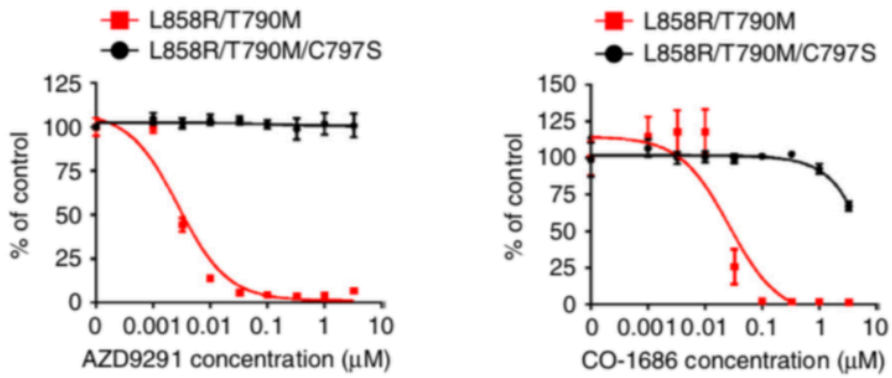

Figure 15: cell viability assay on Ba/F3 cells harboring double or triple mutated EGFR, treated with osimertinib (AZD9291) or rociletinib (CO-1686).[145]

Different strategies might be exploited to overcome acquired resistance to third-generation inhibitors: *i*) the use of drug combinations could prevent the emergence of

resistant clones,[149,150] *ii*) allosteric inhibitors could stabilize inactive conformations of the kinase,[151] *iii*) compounds bearing serine-reactive warheads could target EGFR C797S and restore the ability to covalently bind to the ATP-binding site (however, the detection of a C797G mutation[152] strongly discourages the latter hypothesis), *iv*) residues other than C797 or S797 could be targeted by covalent inhibitors bearing different warheads.

2.3. Synthesis of EGFR inhibitors: aim of the work

Two classes of EGFR tyrosine kinase inhibitors are presented in the framework of this Ph.D. thesis, which were synthesized pursuing two different aims.

2.3.1. Anilinoquinazoline-based inhibitors

The first class includes anilinoquinazoline-based inhibitors carrying non-acrylamide warheads. These compounds have been designed and synthesized to investigate the possibility to target Cys797 with selective, moderately reactive compounds, enabling long-term inhibition of EGFR. Approved covalent inhibitors of EGFR, afatinib and osimertinib, as well as other approved covalent TKIs, such as neratinib (ErbB2) and ibrutinib (BTK), include an acrylamide-based reactive portion and target a non-conserved, non-catalytic cysteine residue located in the ATP-binding site.

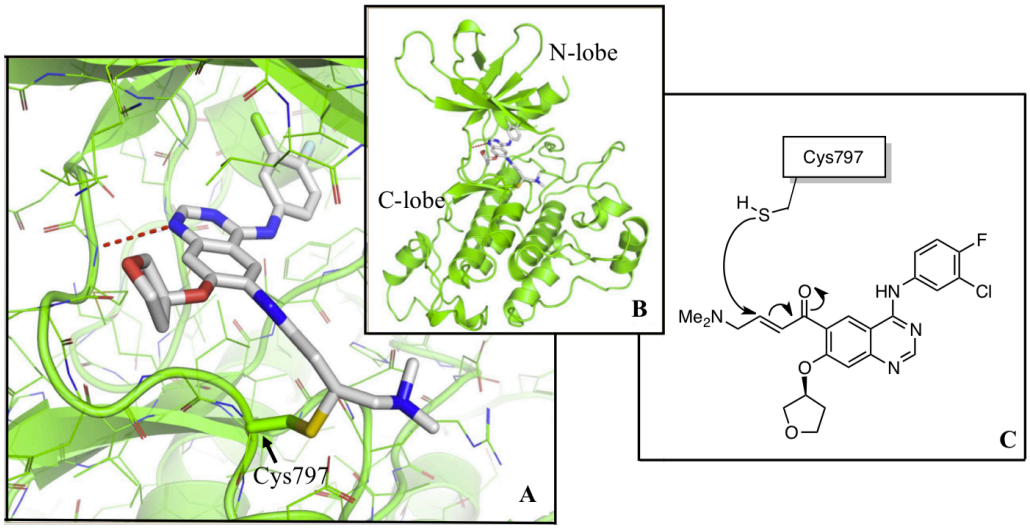

Figure 16: Covalent interaction between afatinib (**5**, Fig.10) and Cys797 in the ATP-binding site of EGFR. Panel **A**: crystal structure of *wt*EGFR in complex with afatinib, close-up of the hinge region. Panel **B**: crystal structure of *wt*EGFR in complex with afatinib, structure of the kinase domain. Panel **C**: generally accepted mechanism of the hetero-Michael addition reaction (picture adapted from ref.153)

This covalent interaction is expected to occur *via* a hetero-Michael addition of the cysteine thiol on the β-carbon of the acrylamide portion (Fig.16, panel **C**).

Despite the growing interest in the field of covalent inhibition of RTKs,[89,154–158] attempts to replace the acrylamide group are still rare in the literature, and the bulk of experimental data about new covalent compounds mainly relies on scaffold modifications.[90,159–166]

Acrylamide has proven to be a well-tolerated group in the structure of drugs, nevertheless its reactivity[167] and possible metabolic inactivation[168] suggest the usefulness of building an armory of alternative warheads to be evaluated as potential substitutes to the acrylamide function.[91]

A series of compounds bearing reactive functionalities other than acrylamide has been previously synthesized at the Department of Food and Drug of the University of Parma, where I spent my Ph.D. research period (Table 1). These agents have been tested in A431 intact cells harboring *wt*EGFR and the percentage of autophosphorylation inhibition and IC_{50} values of each molecule have been measured after 1 h of incubation and 8 h after the removal of the inhibitors from the medium.[169] In the series of 2-aryloxy-substituted acetamides, the compound bearing the 2-(pentafluorophenoxy)-acetamide warhead (**11**) resulted able to irreversibly inhibit EGFR, as suggested by the high percentage of inhibition displayed in the 8 h test (Table 1). According to Smaill *et al.*, an inhibitor can be described as "irreversible" if the target activity is inhibited by more than 80% 8 h after the removal of the inhibitor from the medium.[136] The measured effect could reasonably be ascribed to a covalent interaction of the warhead with Cys797. On the other hand, persistent inactivation of the target protein could also derive from compound accumulation inside the cell.[170] From a chemical point of view, alkylation of Cys797 can be speculated to occur *via* a substitution reaction, with the thiol acting as a nucleophile and pentafluorophenolate being released as the leaving group.

Table 1: summary of biological data obtained for 2-substituted acetamide inhibitors.

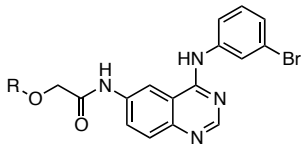

Compound	R	IC_{50} (nM)[a]		%inhibition EGFR autophosphorylation[b]	
		1 h	8 h	1 h	8 h
9		76	292	94	71
10		31	291	97	78
11	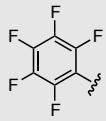	84	78	92	91

[a] Inhibition of EGFR autophosphorylation in A431 intact cells, values determined by Western blot analysis. [b] Percent inhibition of EGFR autophosphorylation determined at 1 μM concentration of the tested compounds. In both assays, values were measured immediately after 1 h of incubation and 8 h after removal of the compound from the medium. Data reported from ref.169.

Moving from the encouraging data obtained from biological assays and from the stimulating possibility of exploring a wide range of substituents to be inserted on the acetamide moiety, a series of compounds bearing a functionalized acetamide group have been synthesized (Table 2). The anilinoquinazoline scaffold was chosen as the driving portion for this class as it displays two main advantages: *i*) the affinity and selectivity of this core structure for EGFR has been largely documented in the literature,[124,125,171] allowing to only focus the analysis of biological results on the effect of the warheads, without fearing a loss of activity due to inappropriate binding to the target; *ii*) its synthesis has already been described, and minor optimization was thus required to obtain the desired precursors in gram-scale.

Table 2: summary of the structure of the synthesized compounds.

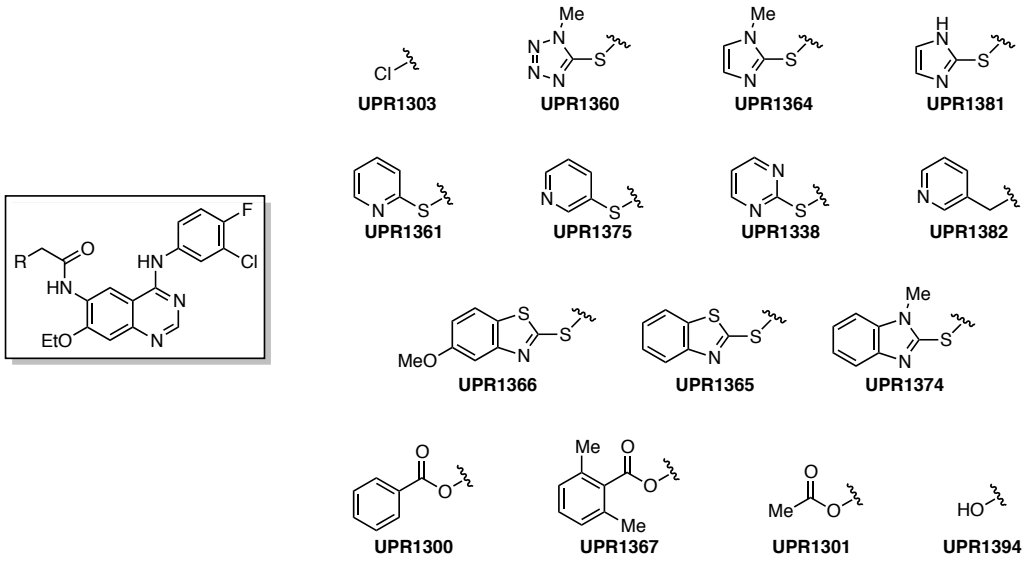

The first compound to be designed and synthesized was **UPR1303**, which carries a 2-chloroacetamide warhead: such a group has proven able to react with glutathione in solution[172], to react with cysteine residues in the binding site of kinases[173] and also to irreversibly inhibit EGFR when inserted on a 4-anilinoquinazoline scaffold similar to the one presented in this thesis.[174] The reactivity of the acetamide warhead has been consequently modulated by replacing the chlorine atom with heterocyclic thiols or carboxylate esters, in order to build a series of analogues carrying substituents with different steric and electronic features.

2.3.2. Diaminopyrimidine-based inhibitors

The second class of compounds presented in this thesis includes 2,4-diaminopyrimidine-based inhibitors of EGFR, which were designed with the aim of targeting EGFR with the C797S mutation. Replacement of the cysteine residue with a serine in the triple mutant isoform of EGFR (L858R/T790M/C797S) results in the loss of the anchor point required for covalent interaction and, consequently, in the acquisition of resistance

towards acrylamide-based inhibitor osimertinib. Development of covalent inhibitors targeting the ATP-binding site in the presence of this mutation necessarily requires the design of new warheads, in order to target Ser797 or to address other amino acid residues. Unfortunately, mutation of the residue in the 797-position from cysteine to glycine has already been detected in patients:[152] Ser797 is therefore not a reasonable target in the development of new inhibitors, as continuous selection of surviving clones in the tumor could rapidly result in the acquisition of resistance. For this reason, selection of a different residue within the ATP-binding pocket appears as the most promising approach. The strategy pursued in this work features the design and synthesis of compounds carrying a reactive portion that could lead to covalent modification of conserved Lys745. This residue has been chosen considering its essential role in the kinase catalytic activity: the formation of a salt bridge between the side chain of lysine and Glu762 is fundamental in maintaining the active conformation of the cytoplasmic domain of EGFR, and mutation of Lys745 can be therefore considered an unlikely event. On the other hand, this lysine residue is conserved across the kinome and a suitable driving portion is therefore required to confer the inhibitors a good selectivity profile.

The scaffold of the newly synthesized compounds (Fig.17) closely resembles the one of rociletinib (**7**, Fig.12), having higher affinity for T790M mutants over *wt*EGFR. It has been selected according to computational observations and synthetic reasons. Modelling studies suggest that the flexible core structure of rociletinib could be directly adapted to the development of molecules targeting a residue other than Cys797. Indeed, accessible conformations allow a favorable positioning of the reactive portion of rociletinib with respect to Lys745 (Fig.18).

This aspect is particularly favorable at the beginning of a new synthetic project, as it enables to maintain the warhead in the same position occupied in the structure of the parent compound, thus allowing the exploitation of the synthetic strategy set up for the latter. Adoption of the scaffold of osimertinib (**8**, Fig.12) has also been considered, but soon abandoned due to the necessity of heavily modifying the structure and the synthetic plan in order to target Lys745.

From a chemical point of view, the nucleus of rociletinib has been slightly modified by replacing 5-trifluoromethylpyrimidine ring with 5-chloropyrimidine, which is actually included in the structure of WZ4002 (**6**, Fig.12). Details about the rationale for this replacement are given in Paragraph 2.4.2.

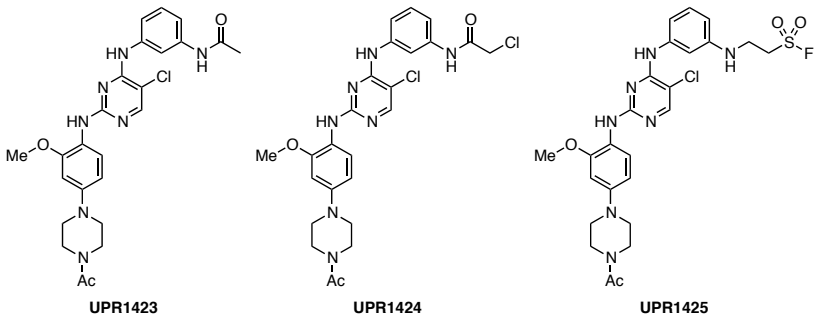

Figure 17: structure of the synthesized inhibitors.

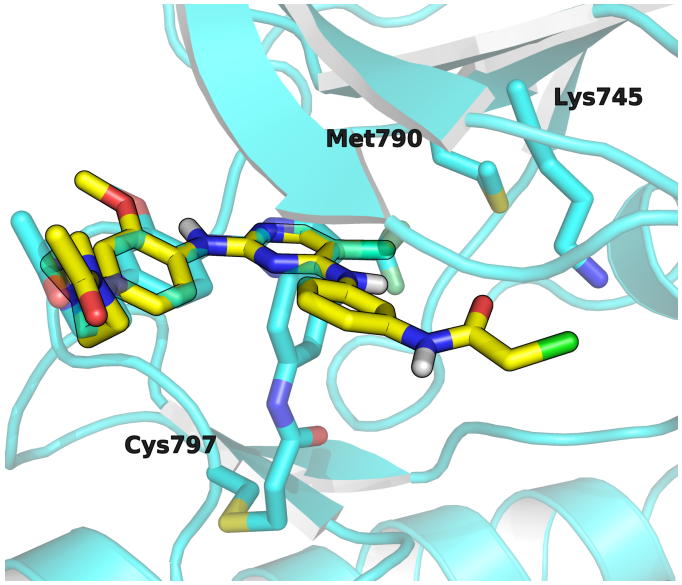

Figure 18: superimposition of crystal structure of rociletinib in complex with EGFR T790M mutant (PDB ID 5XDK) and docked pose of **UPR1424** (Fig.17). Kinase is shown in a ribbon representation (light blue). Rociletinib is colored light blue and **UPR1424** yellow. Side-chain atoms of Lys745, Met790 and Cys797 are shown.

Strongly reactive warheads have been inserted in the structure of the inhibitors: targeting Lys745 is indeed a new approach in the field of anti-EGFR TKIs and a proof of concept is required to assure that this innovative strategy can actually lead to inactivation of C797S mutant. Chloroacetamide (**UPR1424**, Fig.17) has been chosen on the basis of its high reactivity, which could actually lead to the formation of a covalent bond with the primary amine of lysine side chain. Given the flexibility of the scaffold, interaction between chloroacetamide and Ser797 cannot be excluded. The warhead of **UPR1425** (Fig.17) has been designed based on the wide use of sulfonyl fluorides (SFs) in chemical biology and molecular pharmacology, where they have been exploited to obtain probes targeting various amino acid residues, including lysine, thanks to their electrophilicity. Improved stability of SFs compared to sulfonyl chlorides renders the former an interesting functionality to be inserted in the structure of covalent inhibitors.[175] Usefulness of SFs in targeting lysine residues has been corroborated by the recent publication of the crystal structure of XO44 (**12**), a multi-kinase inhibitor with a SF warhead in complex with Src and EGFR (Fig.19).[176]

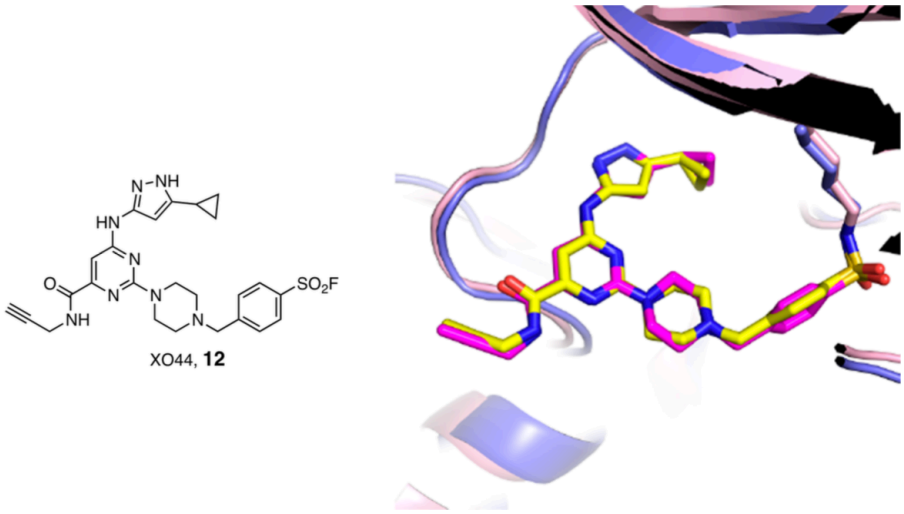

Figure 19: structure of pan-kinase inhibitor XO44 (**12**). Overlay of covalent complex of XO44 with Src (inhibitor: yellow, Lys295: blue) and EGFR (inhibitor: magenta, Lys745: pink) is reported (picture adapted from ref.176).

In both kinases, covalent interaction results from the loss of the fluorine atom from the inhibitor and modification of the conserved lysine, Lys745 in EGFR and Lys295 in Src. The flexible alkyl linker separating the sulfonyl fluoride and the aniline portion in **UPR1425** has been inserted based on modelling studies, in order to enable the warhead to reach a distance and form a suitable angle to react with the lysine side chain. A third compound has been synthesized as a negative control for biological assays: **UPR1423** (Fig.17) lacks a reactive portion and its engagement in a covalent interaction with any amino acid residue is therefore unfeasible.

2.4. Synthesis of EGFR inhibitors: chemistry

2.4.1. Anilinoquinazoline-based inhibitors

The synthesis of 4-anilinoquinazoline scaffold (Scheme 1) has been performed by adapting literature procedures.[177,178] The initial step in the synthesis featured a regioselective nitration of ethyl 4-hydroxybenzoate (**13**) in acetic acid/nitric acid mixture, affording ethyl 4-hydroxy-3-nitrobenzoate (**14**) in excellent yield. Reduction of the nitro group *via* catalytic hydrogenation and acetylation of the amino group afforded ethyl 3-acetamido-4-hydroxybenzoate (**15**). Ethyl 5-acetamido-2-amino-4-ethoxybenzoate (**18**) was then obtained through S_N reaction with ethyl bromide, regioselective nitration of compound **16** and reduction of the nitro group. Ring closure was performed by reacting compound **18** with methyl orthoformate and ammonium chloride.[179]

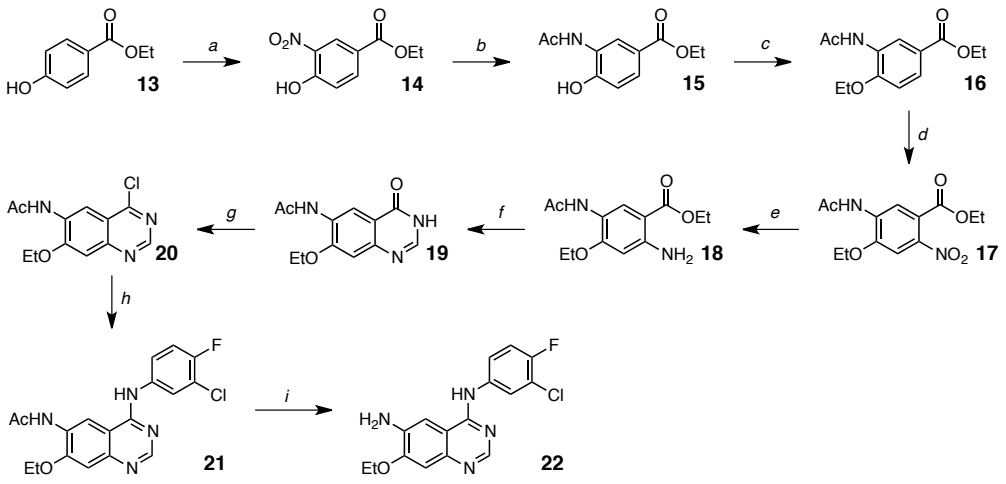

Scheme 1: synthesis of the quinazoline-based inhibitors scaffold. Reagents and conditions: *a*) AcOH, HNO_3, 40 °C, 2 h, 96% yield; *b*) $Pd(OAc)_2$, charcoal, Et_3SiH, HCOOLi, THF, r.t., 1 h; then Ac_2O, AcOH, 60 °C, 10 min, 93% yield; *c*) EtBr, K_2CO_3, DMF, 60 °C, 4 h, 92% yield; *d*) fuming HNO_3, Ac_2O, AcOH, 0 °C, 15 min, 98% yield; *e*) Fe^0, EtOH:AcOH:H_2O = 70:15:15, r.t., 15 min, 79% yield; *f*) NH_4AcO, $HC(OMe)_3$, diglyme, reflux, 90 min, 84% yield; *g*) $POCl_3$, reflux, 45 min, 86% yield; *h*) 3-chloro-4-fluoroaniline, HCl, *i*-PrOH, reflux, 45 min, 96% yield; *i*) KOH, *n*-PrOH, reflux, 2 h, 73% yield.

The obtained 6-acetamido-7-ethoxyquinazolin-4-one (**19**) was reacted with neat trichlorophosphate, leading to the 4-chloro derivative **20**. Substitution of the chlorine atom with 3-chloro-4-fluoroaniline was catalyzed by hydrochloric acid, obtaining 4-anilinoquinazoline **21**. Once the scaffold was completed, the aniline function on the 6-position (**22**) was easily restored by hydrolysis of the acetamide in basic conditions.
Synthesis of the anilino-quinazoline scaffold revealed to be easily scalable and the high purity of the intermediates allowed to use the crude product of each reaction into the following step, without further purification, with the only exception of the product of hydrolysis (**22**), which was purified by silica gel column chromatography.
Compound **22** served as starting material for the synthesis of **UPR1303**, **UPR1375** and **UPR1382**. The 2-chloroacetamide group was inserted on the 6-position of the quinazoline ring through the mixed anhydride method, which is widely used to activate carboxylic acids in acylation reactions.[180] The mixed anhydride was prepared by reacting the trialkyl ammonium salt of chloroacetic acid with pivaloyl chloride: steric hindrance in the pivalic portion of the anhydride proved to be sufficient in order to promote the sole formation of the desired amide, which could be easily purified (Scheme 2).

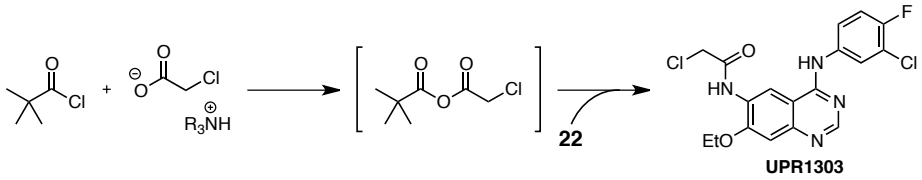

Scheme 2: synthesis of **UPR1303**. Reagents and conditions: chloroacetic acid, DIPEA, PivCl, THF, r.t., 30 min; then compound **22**, THF, r.t., 2 h, 83% yield.

UPR1375 was prepared by reacting readily available *S*-(3-pyridyl)mercaptoacetic acid[181] with aniline **22**, using TBTU (2-(1*H*-benzotriazole-1-yl)-1,1,3,3-tetramethyluronium tetrafluoroborate) as coupling agent (Scheme 3).
UPR1382 was prepared by reacting 3-pyridin-3-yl-propionyl chloride with aniline **22**. The acyl chloride resulted from treatment of 3-pyridin-3-yl-propionic acid with thionyl chloride in DCM with a catalytic amount of DMF (Scheme 3).

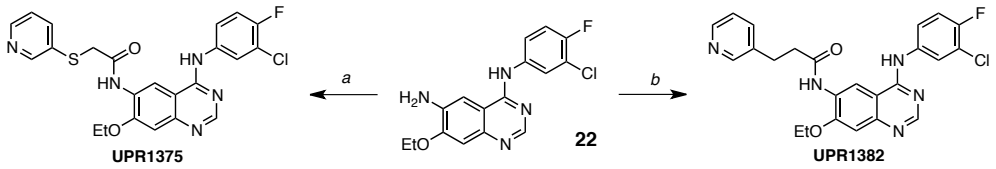

Scheme 3: synthesis of **UPR1375** and **UPR1382**. Reagents and conditions: *a*) 3-pyridylmercaptoacetic acid, TBTU, TEA, DMF, 40° C, 4 h, 25% yield; *b*) 3-pyridin-3-yl-propionic acid, $SOCl_2$, DMF (cat.), DCM, reflux 1 h; then compound **22**, pyridine, THF, r.t., 16 h, 39% yield.

All other compounds of the series, with the exception of **UPR1394**, were prepared by reacting the chloroacetamide derivative **UPR1303** with the suitable nucleophile under basic conditions (Scheme 4). Sodium hydroxide in THF or triethylamine in DMF were used according to the solubility of reactants and to the temperature required for the reaction to occur.

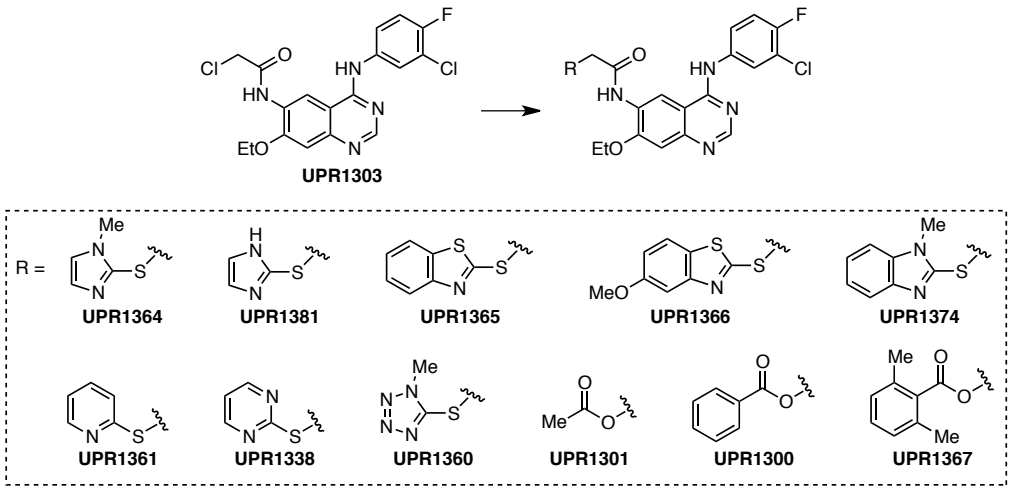

Scheme 4: synthesis of inhibitors starting from **UPR1303**. Reagents and conditions: mercaptoheterocycle or carboxylic acid, base: see Experimental Section for details (Paragraph 6.2.1), yield range: 19-89%.

The glycolic derivative **UPR1394** was easily obtained from the acetoxy precursor **UPR1301** through transesterification reaction (Scheme 5).

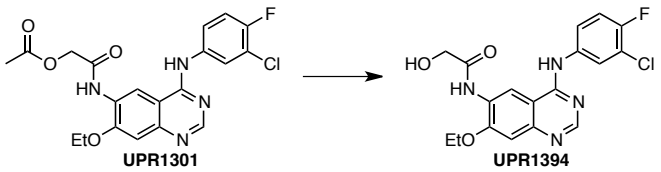

Scheme 5: synthesis of **UPR1394**. Reagents and conditions: NaOMe, THF/MeOH, r.t., 30 min, 62% yield.

2.4.2. Diaminopyrimidine-based inhibitors

As anticipated, the scaffold chosen for this series derives from the structure of rociletinib, with the sole modification of the group in position 5 on the pyrimidine ring. The synthesis of the third-generation inhibitor rociletinib has been previously reported twice in patents from two different research groups, following two different strategies.[182–185]

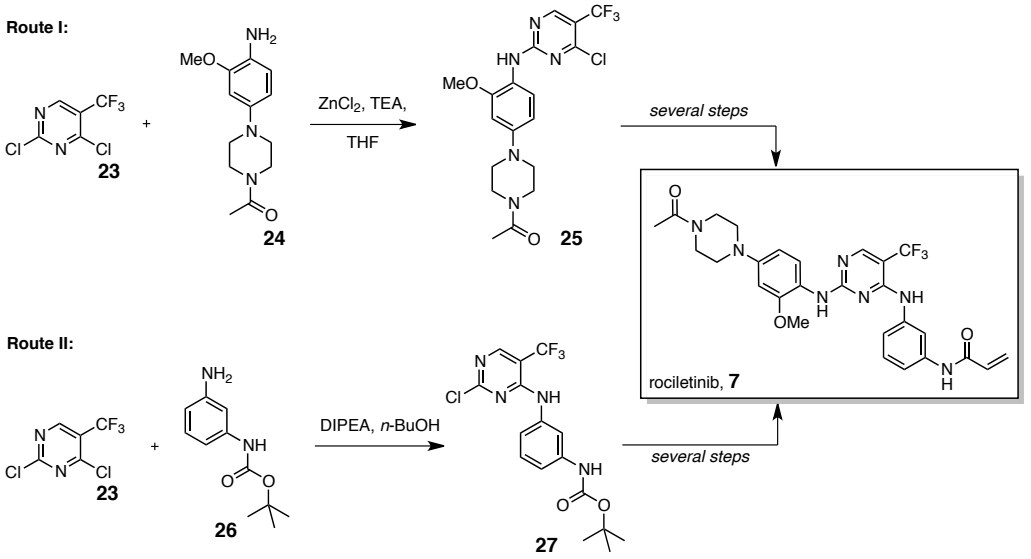

Figure 20: synthesis of rociletinib. Substitution reaction on 2,4-dichloro-5-trifluoromethylpyrimidine. Route I is reported in ref.182, route II is reported in ref.183–185.

Nonetheless, the first step in both synthetic plans was the substitution on 2,4-dichloro-5-trifluoromethylpyrimidine (**23**) (Fig.20), which is supposed to afford the 2- or 4-

substituted products (**25** or **27**, respectively) according to the reaction conditions. Authors did not comment on the formation of side products, i.e., of the undesired regioisomer.

When the conditions reported in patents were either reproduced or slightly modified, mixture of regioisomers were obtained: the compounds exhibited very similar physicochemical properties, thus hampering purification of the *major* product through standard techniques on a lab-scale.

Issues in performing this substitution reaction in a regioselective manner have already been reported in the literature: the reaction conditions usually feature the use of a base (e.g., TEA or potassium carbonate) in polar aprotic solvents (e.g., THF, acetone, diethyl ether, *tert*-butanol and mixtures thereof).[186–190] An improved regioselectivity has been reported when a stoichiometric amount of a Lewis acid (generally zinc (II) chloride) is added to the mixture,[191] favoring the 2-substituted product, which is still not obtained exclusively. This regioselectivity issue does not apply to any other 2,4-dichloropyrimidine reported in the literature. When substituent on the 5-position is fluorine, chlorine, bromine, methyl, methoxy or simply a hydrogen, the substitution only occurs at the 4-position (Fig.21).[190,191]

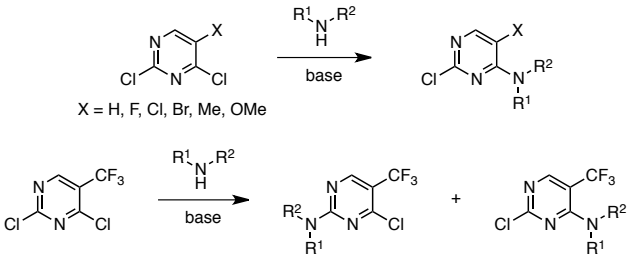

Figure 21: different behavior of 2,4-dichloro-5-trifluoromethylpyrimidine in substitution reactions if compared to 2,4-dichloropyrimidine bearing different substituents on the 5-position.

The decision to replace the 5-trifluoromethylpyrimidine core of rociletinib with the 5-chloropyrimidine one thus derived from the higher feasibility of a regioselective, reproducible procedure for the synthesis of this scaffold compared to that of rociletinib,

according to the reliable amount of data published by different research groups. Moreover, the chloropyrimidine-based nucleus is included in the structure of WZ4002 (**6**, Fig.12), which shares most of its structural features with rociletinib, suggesting that a chlorine atom in that position is tolerated in EGFR inhibitors that selectively target the T790M mutants.

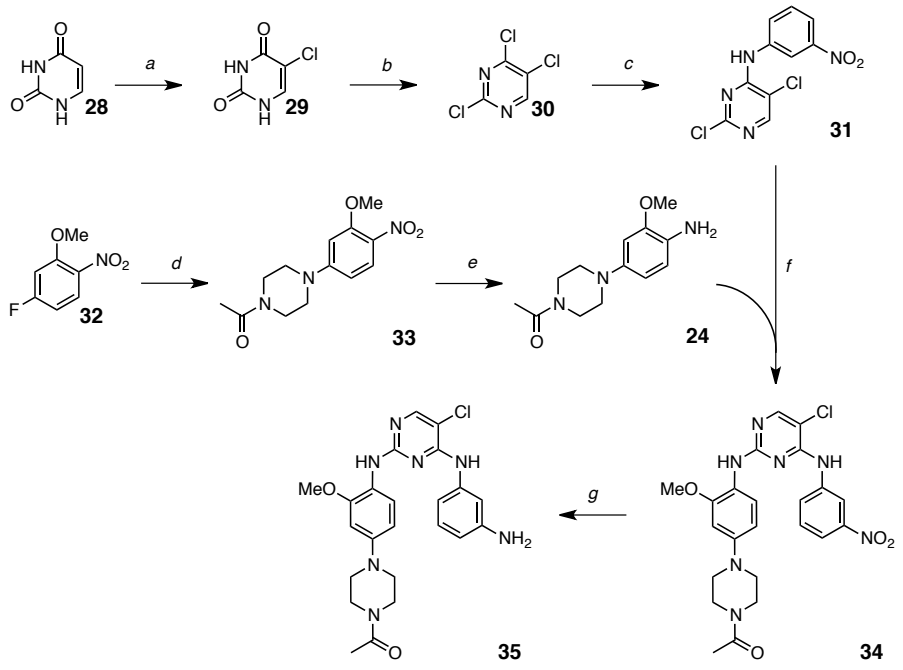

Scheme 6: synthesis of aniline **35**. Reagents and conditions: *a*) AcOH/Ac_2O, NCS, 60 °C, 5 h, 47% yield; *b*) $POCl_3$, 2,6-lutidine, 140 °C, 2 h, 64% yield; *c*) 3-nitroaniline, DIPEA, *i*-PrOH, 80 °C, 15 h, 72% yield; *d*) 1-acetylpiperazine, 40 °C, 1 h, 89% yield; *e*) Zn^0, NH_4Cl, THF/H_2O, 50 °C, 3 h, 98% yield; *f*) PTSA, *i*-PrOH, 80 °C, 15 h, 50% yield; *g*) Fe^0, HCl, EtOH, reflux, 2 h, 93% yield.

Aniline **35** is the common precursor of compounds **UPR1423**, **UPR1424** and **UPR1425**. Its synthesis was performed as reported in Scheme 6. The key intermediate 2,4,5-trichloropyrimidine (**30**) was obtained through the regioselective chlorination of position 5 of uracil (**28**), followed by exhaustive chlorination of compound **29**. The latter reaction was performed according to two different procedures: the use of $POCl_3$/2,6-lutidine[192] proved to be superior to $POCl_3/PCl_5$ in terms of reactants handling, ease of product

isolation and yield. Substitution on pyrimidine **30** only occurred at the 4-position (compound **31**): the use of DIPEA and *i*-PrOH allowed to obtain a good yield in a reproducible manner. Aniline **24** was prepared in two steps starting from 5-fluoro-2-nitroanisole **32**. The first step, i.e., the nucleophilic aromatic substitution reaction (S_N^{Ar}) on anisole employing acetylpiperazine as nucleophile, has already been reported in the literature and is usually performed using a base and a high-boiling point solvent (e.g., DIPEA in DMA at 90 °C).[193] The strategy presented in this thesis featured a convenient solvent-free procedure, affording compound **33** in excellent yield and purity and in a reproducible manner. Reduction of the nitro group of **33** to aniline proved to be quite straightforward and did not require major optimization.

In contrast, substitution reaction on chloropyrimidine **31** to afford compound **34** revealed to be quite reluctant to optimization. The best results were obtained when compounds **31** and **24** were heated at reflux in isopropanol in the presence of stoichiometric amounts of *para*-toluenesulfonic acid (PTSA). Replacement of the solvent with *n*-propanol, *n*-butanol, dioxane or dimethylsulfoxide either did not improve the yield or resulted detrimental. The yield remained unchanged when PTSA was replaced with trifluoroacetic acid (TFA), whereas the reaction did not work at all in basic conditions (use of DIPEA and cesium carbonate has been investigated). Reduction of the nitro group of compound **34** using iron under slightly acidic conditions afforded compound **35** in excellent yield and purity. This method proved superior to the use of palladium catalyst, Raney® nickel or zinc dust in terms of reaction time, yield and purity of the product, which is extremely important at this stage of the synthetic route.

Aniline **35** is finally acylated or alkylated according to different procedures. **UPR1423** was obtained through acetylation of the aniline group under standard conditions, using pyridine as a solvent and base and adding acetyl anhydride till completion of the reaction, as detected by TLC analysis. **UPR1424** was prepared following the same procedure reported above for the synthesis of **UPR1303**, which revealed to be directly applicable to the new scaffold without need of optimization (Scheme 7).

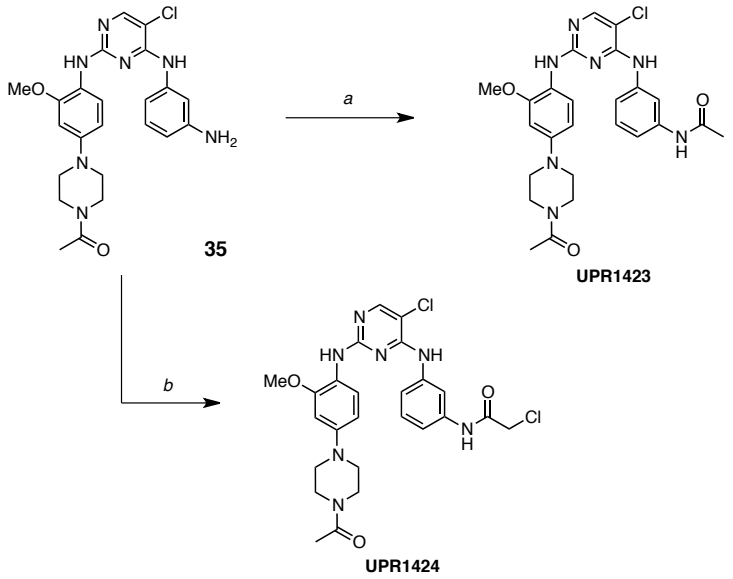

Scheme 7: synthesis of **UPR1423** and **UPR1424**. Reagents and conditions: *a*) Ac_2O, pyridine, r.t., 30 min, 82% yield; *b*) chloroacetic acid, DIPEA, PivCl, THF, r.t., 20 min; then **35**, THF, r.t., 1 h, 54% yield.

Lastly, the alkyl sulfonyl fluoride of **UPR1425** resulted from Michael addition on ethenesulfonyl fluoride (ESF) (Scheme 8). The synthetic procedure has been adapted from the one published by Krutak *et al.*[194]

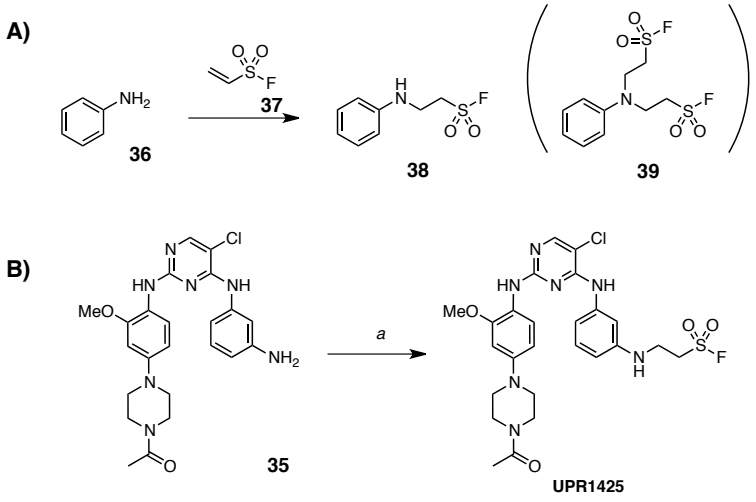

Scheme 8: A) formation of 1:1 and 1:2 adducts as reported in ref.194. **B**) synthesis of **UPR1425**. Reagents and conditions: *a*) ESF, $CHCl_3$, MeOH, r.t., 3 h, 13% yield.

Careful purification was required to separate the desired 1:1 adduct from the 1:2 adduct when the reaction was run to completion: this led to lower yields and to the loss of starting material. Pure product was easily obtained when the reaction was quenched as soon as TLC analysis detected a 40-50% conversion: at that point, the 1:2 adduct was still not formed and **UPR1425** could be effortlessly purified and the starting aniline **35** was recovered completely.

2.5. Synthesis of EGFR inhibitors: biological data

2.5.1. Anilinoquinazoline-based inhibitors

Anilinoquinazoline-based inhibitors of EGFR were tested for their reactivity towards thiol nucleophiles and for their ability to inhibit cell proliferation and EGFR autophosphorylation.

2.5.1.1. Reactivity with cysteine in solution

Reactivity towards thiols was investigated incubating the compounds with a large molar excess of cysteine (1:100) at pH 10 at 37 °C. The reaction was monitored by LC-MS.[195] Results for this assay are reported in Table 3. Acrylamide **40** was also included in the assay as a benchmark[177] and displayed a half-time ($t_{1/2}$) of 15 min, confirming the high reactivity of the typical covalent inhibitor warhead. Analogously to acrylamide, chloroacetamide **UPR1303** reacted with cysteine following pseudo first-order kinetics, with a half-time of nearly 60 min. Both compounds resulted stable in the same experimental conditions when cysteine was not added to the medium, suggesting that consumption of the starting compounds did not derive from chemical degradation.

All the other compounds presented in Table 3 displayed a reduced reactivity towards cysteine and some of them did not react at all (**UPR1375**, **UPR1382**, **UPR1394**). A qualitative ranking of reactivity was built by comparing the area of the peak of the cysteine-conjugate obtained for each compound, which was measured by LC-MS after 24 h of reaction time. The area of the adduct between **UPR1303** and cysteine was set at the reference value of 10,000 and areas for the adducts from other inhibitors were calculated referred to this value. Compounds **UPR1360**, **UPR1364**, **UPR1381**, **UPR1300** and **UPR1367** resulted to be the most reactive of the series, but their reactivity was nonetheless 600- to 2000-fold lower than the one of **UPR1303**. Compounds **UPR1382** and **UPR1394**, lacking a reactive portion able to undergo a nucleophilic

substitution, did not react with cysteine. No adduct could be detected for **UPR1375**, where the sulfur atom is not in the 2-position of a nitrogen-containing heterocycle.

Table 3: reactivity with cysteine in solution and EGFR autophosphorylation inhibition for quinazoline-based EGFR inhibitors.

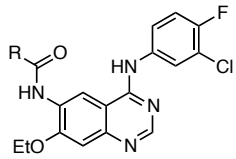

Compound	R	Reactivity Assay		EGFR autophosphorylation inhibition[c]		
		$t_{1/2}$[a] (min)	Peak Area[b]	IC_{50} (nM)[d]	% inhibition (1 μM)[e] 1 h	8 h
3	-	N.T.[f]	N.T.[f]	60 ± 25	96 ± 4.0	46 ± 5.0
40		15 ± 3.0	-	15 ± 6.4	96 ± 4.0	99 ± 1.0
UPR1303		60 ± 25	10000	7.0 ± 5.7	100 ± 0.5	81 ± 2.9
UPR1360	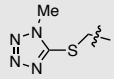	>1440	6.5	5.0 ± 1.5	100 ± 6.4	75 ± 4.1
UPR1364	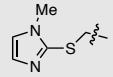	>1440	4.5	11 ± 5.0	97 ± 2.5	95 ± 4.8
UPR1381	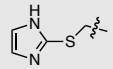	>1440	15	27 ± 3.5	99 ± 0.10	90 ± 4.6
UPR1361	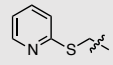	>1440	0.51	70 ± 21	73 ± 4.3	71 ± 8.1
UPR1375	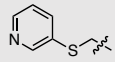	>1440	N.D.[g]	0.60 ± 0.14	96 ± 4.0	89 ± 4.6
UPR1338	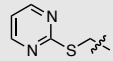	>1440	0.66	27 ± 18	99 ± 1.0	88 ± 16
UPR1382	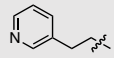	>1440	N.D.[g]	14 ± 1.4	99 ± 0.50	60 ± 2.1
UPR1374	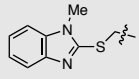	>1440	0.38	12 ± 0.71	100 ± 1.0	100 ± 1.0
UPR1365	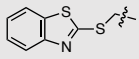	>1440	0.39	83 ± 28	88 ± 0.90	75 ± 0.50

UPR1366	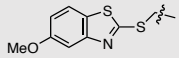	>1440	1.4	197 ± 18.4	63 ± 0.10	93 ± 0.50
UPR1301	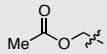	1440 ± 100	0.64	34 ± 11	97 ± 0.40	75 ± 19
UPR1300	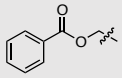	>1440	11	25 ± 12	88 ± 3.1	89 ± 5.7
UPR1367	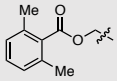	>1440	5	44 ± 0.71	97 ± 1.9	97 ± 2.6
UPR1394		>1440	N.D.[g]	27 ± 11	90 ± 3.6	77 ± 11

[a] $t_{1/2}$ measured at pH 10 and 37 °C by LC-MS. [b] Area of Cys-adduct formed by compound **UPR1303** after 24 h of incubation was set at the value of 10,000 and all the Cys-conjugate areas for other compounds were referred to this value. [c] Inhibition of EGFR autophosphorylation in A549 cells measured by Western blot analysis. [d] IC_{50} values determined after 1 h of treatment with EGFR inhibitors. [e] Percentage of inhibition at 1 μM concentration was measured after 1 h of treatment and 8 h after removal of the compound from the medium. [f] Not tested. [g] Not detected.

2.5.1.2. Inhibition of EGFR autophosphorylation

The ability of the newly synthesized compounds to inhibit EGFR autophosphorylation was tested in A549 lung cancer cells, harboring *wt*EGFR. The potency of the compounds was evaluated calculating IC_{50} values, which resulted in the nanomolar range for all the compounds (Table 3). These data suggest that the structural modifications introduced by the warheads on the 4-anilinoquinazoline nucleus did not reduce the affinity of the parent structure.

The capability of the compounds to maintain long-term inhibition of the target was evaluated measuring the percentage of inhibition obtained for each compound at 1 μM concentration both 1 h after the addition and 8 h after removal of the compound from the extra-cellular medium (1 h of incubation). Most of the compounds inhibited EGFR by more than 80% 8 h after washing: this value allowed to characterize them as "irreversible inhibitors" according to a generally accepted definition,[136] while the percentage of inhibition measured for the reversible inhibitor gefitinib was around 50%. Compounds **UPR1360**, **UPR1361**, **UPR1365** and **UPR1301** failed to reach the 80% threshold, but

were still able to guarantee a good level of inhibition. The persistency of the effect of **UPR1382** and **UPR1394**, lacking a reactive portion, could be ascribed to accumulation of the inhibitors within the cells, as already reported for reversible inhibitors.[170]

2.5.1.3. Intracellular dosage of selected compounds

Table 4: intracellular concentration of selected EGFR inhibitors in A549 cells.

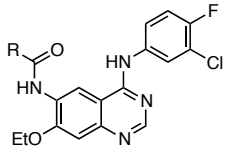

Compound	R	Intracellular concentration[a] (μM)		Ratio 1 h/8 h
		1 h	8 h	
3	-	271 ± 34	2.4 ± 0.2	112
41	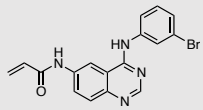	< 0.05[b]	< 0.05[b]	-
UPR1303		115 ± 10	0.80 ± 0.10	144
UPR1360	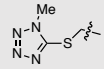	181 ± 2	5.6 ± 0.1	32
UPR1364	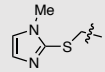	179 ± 6	10.2 ± 2.1	18
UPR1381	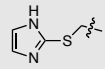	118 ± 10	0.53 ± 0.10	222
UPR1301	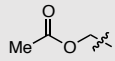	5.8 ± 0.6	<0.05	-
UPR1394		132 ± 10[c]	1.1 ± 0.1[c]	120[c]

[a] Intracellular concentration of compounds was determined after 1 h of incubation (1 μM) and 8 h after washing (1 h of incubation, 1 μM). Reported μM concentrations were calculated as ratio between compound content in each sample (pmol/mg of protein) and average cell volume (4 μL/mg of protein). Cell volume was calculated according to Kletzien *et al*.[196] [b] Data from Vacondio *et al*.[170] [c] Generated in A549 cell from the hydrolysis of compound **UPR1301**.

Intracellular dosages of selected compounds were performed in order to verify whether accumulation could effectively account, at least partially, for the persistent inhibitory effect (Table 4).

Compounds **UPR1303**, **UPR1360**, **UPR1381**, **UPR1364** and **UPR1301** were selected for this evaluation given their diverse reactivity in the presence of cysteine (Table 3): **UPR1303** was the most reactive compound, **UPR1301** was only weakly reactive, while **UPR1360**, **UPR1381** and **UPR1364** displayed a moderate reactivity. Intracellular concentrations of the compounds were measured by LC-MS after 1 h of incubation at 1 μM concentration and 8 h after removal of the compound from the extracellular medium. Reversible inhibitor gefitinib and highly reactive acrylamide-based inhibitor PD168393 (**41**)[136] were also tested in the same experimental conditions. Low concentration of PD168393 and **UPR1301** after 1 h of incubation could be ascribed to high reactivity and to hydrolytic instability, respectively. Remarkably, for **UPR1303** and **UPR1381** a significant drop in intracellular concentration was detected 8 h after compound washing. For these compounds, decrease in the intracellular concentration did not affect the capability to inhibit EGFR autophosphorylation (Table 3). These data suggest that both compounds could be covalent inhibitors of the target.

2.5.1.4. Time-resolved fluorescence resonance energy transfer

Further support to the hypothesis of covalent interaction derived from a time-resolved fluorescence resonance energy transfer (TR-FRET) assay. The assay required the use of recombinant GST-EGFR (a conjugate between recombinant EGFR L858R/T790M and glutathione S-transferase), which was incubated with an Eu-labeled anti-GST antibody and a fluorescent tracer, in the absence or in the presence of different concentrations of EGFR inhibitors. Binding of the tracer and anti-GST antibody to EGFR results in the formation of a ternary complex and in the emission of a FRET signal (665 nm), while displacement of the tracer by an EGFR inhibitor results in a loss of FRET signal.

Reduction of the obtained signal in the presence of increasing concentrations of the inhibitors is used to calculate IC_{50} values for the tested compounds. The IC_{50} values can

be determined without pre-incubation of the inhibitor with the target, or after pre-incubation: in this case, the calculated value is supposed to be independent from the incubation time when a reversible inhibitor is tested, while it should decrease after pre-incubation when covalent inhibitors are tested.[197] Variations of the IC_{50} value for covalent inhibitors is dependent on the rate of the covalent reaction. When gefitinib, **UPR1303** and **UPR1381** were tested in this assay, the IC_{50} value for gefitinib did not change after pre-incubation, as expected for reversible inhibitors (Fig.22, panel **A**). On the contrary, IC_{50} values for both **UPR1303** and **UPR1381** decreased with pre-incubation (Fig.22, panel **B** and **C**), suggesting that a covalent interaction between the compounds and the target actually occurred.

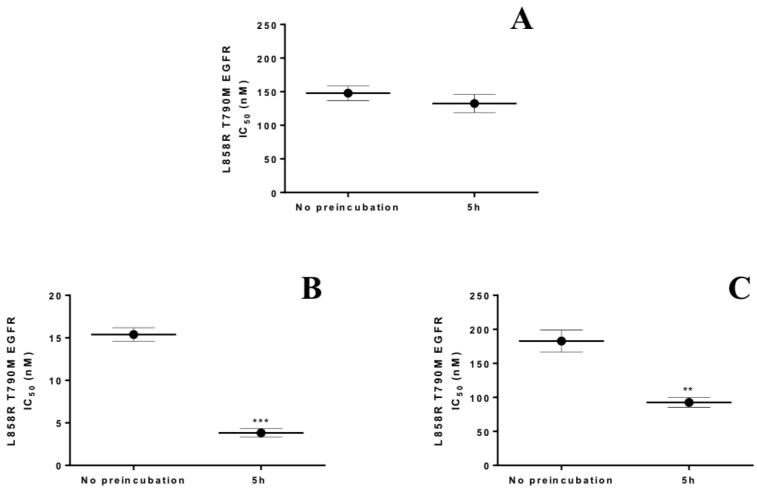

Figure 22: IC_{50} values measured by TR-FRET assay for gefitinib (panel **A**), **UPR1303** (panel **B**), and **UPR1381** (panel **C**), without and with pre-incubation. Values are reported as mean ± standard error of the mean (n = 5). Statistical significance was set at P<0.05. **: P<0.01; ***: P<0.001.

2.5.1.5. Activity on H1975 gefitinib-resistant cells

Finally, EGFR inhibitors were tested for their ability to interfere with cell proliferation and EGFR autophosphorylation in H1975 cell line, harboring EGFR L858R/T790M

double mutant and resistant to first-generation inhibitors (Table 5). Among the newly synthesized compounds, **UPR1303** and **UPR1381** were the most potent inhibitors of cell proliferation, with **UPR1303** resulting more potent than acrylamide **40**, which was included as a benchmark. Moreover, both **UPR1303** and **UPR1381** were endowed with inhibitory activity in the EGFR autophosphorylation assay, and were the most potent of the series at the lowest concentration tested (0.1 μM).

Table 5: inhibition of cell proliferation and EGFR autophosphorylation in H1975 cells.

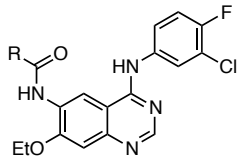

Compound	R	Proliferation inhibition[a] IC_{50} (μM)	Autophosphorylation[b] % inhibition	
			0.1 μM	1 μM
3	-	9.1 ± 1.1	8.0 ± 4.9	18 ± 4.2
40		0.70 ± 0.14	93 ± 0.70	95 ± 0.10
UPR1303		0.06 ± 0.01	100 ± 0.9	100 ± 0.10
UPR1360	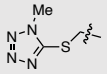	2.1 ± 0.78	16 ± 8.5	96 ± 5.7
UPR1364	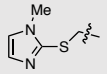	6.9 ± 0.64	45 ± 14	67 ± 8.5
UPR1381	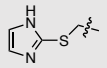	1.4 ± 0.10	80 ± 7.0	100 ± 0.71
UPR1361	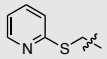	3.7 ± 0.28	1.5 ± 2.1	42 ± 7.0
UPR1375	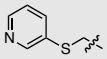	3.0 ± 0.42	29 ± 10	92 ± 9.9
UPR1338	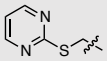	3.6 ± 1.8	40 ± 12	87 ± 9.8

UPR1374	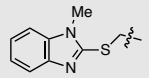	9.1 ± 1.0	6.0 ± 4.2	70 ± 6.8
UPR1365	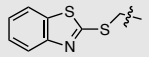	9.8 ± 0.14	29 ± 11	24 ± 7.7
UPR1366	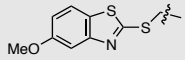	3.2 ± 0.71	30 ± 13	92 ± 0.90
UPR1301	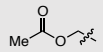	3.4 ± 0.57	27 ± 8.5	68 ± 13
UPR1300	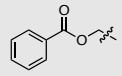	8.3 ± 1.8	0.5 ± 0.7	43 ± 4.4
UPR1367	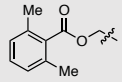	6.1 ± 1.4	20 ± 3.9	16 ± 8.0
UPR1394		>10	0.0 ± 0.1	0.0 ± 0.1

[a] Concentration able to inhibit 50% of cell proliferation as determined by the MTT assay, after 72 h of incubation with compounds (dose ranging from 0.1 to 10 μM). Osimertinib displays an IC_{50} of 0.10 ± 0.1 μM in these assay conditions. [b] Inhibition of EGFR autophosphorylation in H1975 cells was evaluated by Western blot analysis.

3. Fibroblast Growth Factors and their Receptors

3.1. Biology

3.1.1. Fibroblast Growth Factors

Fibroblast Growth Factors (FGFs) represent a family of structurally related peptides. Most FGFs share an internal core region, including 28 highly conserved residues and 6 identical amino acid residues (Fig.23).[198]

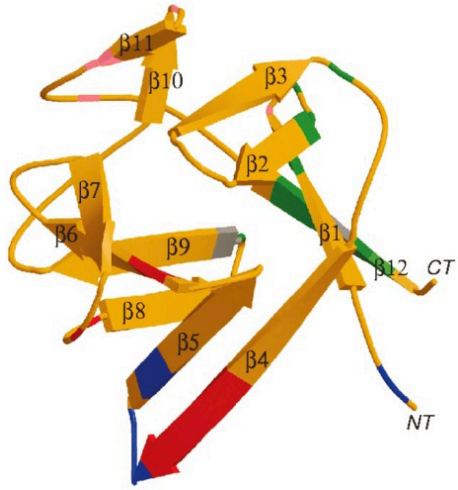

Figure 23: Three-dimensional structure of FGF2. The heparin-binding region is shown in pink, whereas regions contacting FGFR are shown in green, blue and red.[198]

The FGF family includes 22 members, which are classified in seven subfamilies according to the conserved chromosomal location of the encoding genes.[199] FGFs are also classified as canonical, intracellular and hormone-like FGFs: canonical - or paracrine - FGFs (subfamilies FGF1/2/5, FGF3/4/6, FGF7/10/22, FGF8/17/18 and

FGF9/16/20) act as local paracrine signaling molecules and bind to FGFRs to stimulate cell differentiation, proliferation and migration,[200] intracellular - or intracrine - FGFs (subfamily FGF11/12/13/14) act as autocrine, receptor-independent factors and regulate the function of voltage gated sodium channels,[201] while hormone-like - or endocrine - FGFs (subfamily FGF19/21/23) act as endocrine factors.[202] FGFs generally share a strong affinity for the glycosaminoglycan chains of proteoglycans that are expressed on the cell surface: heparan sulfate proteoglycans (HSPGs) are a family of highly glycosylated proteins expressed on the cell membrane or secreted in the extracellular matrix, which are fundamental in protecting FGFs from proteolytic degradation and in reducing FGF diffusion through the membranes, forming a sort of "reservoir" of the growth factor in the proximity of its receptor.[203] Endocrine FGFs only have a reduced affinity for HSPGs, which facilitates their diffusion in the systemic circulation. Their interaction with FGFRs is allowed by the cofactors α-Klotho and β-Klotho.[30] Hormone-like FGFs are involved in biliary acid metabolism, in the regulation of phosphate blood levels and in the metabolism of vitamin D.[204]

3.1.2. Fibroblast Growth Factor Receptors

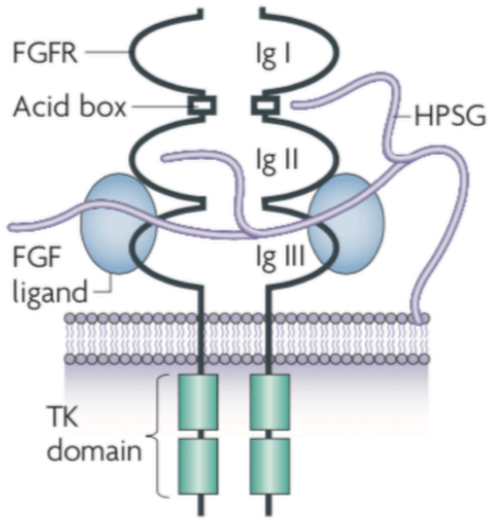

Figure 24: schematic representation of FGFR dimer in complex with FGF ligands and HSPGs.[205]

Fibroblast Growth Factor Receptors (FGFRs) are a family of Receptor Tyrosine Kinases (RTKs) and share most of the structural and functional features typical of this class. The receptors are encoded by four genes (*FGFR1-4*) and their structure includes an extracellular domain, a single transmembrane domain and a cytoplasmic domain, which is endowed with catalytic activity.[205]

The extracellular region is constituted by three immunoglobulin-like domains (IgI-IgIII). A stretch of eight acidic residues between IgI and IgII represents a conserved structural feature in the FGFR family and is usually called "acidic box" (Fig.24).[29] The amino-terminal portion of the receptor, including IgI and the acidic box, is involved in the receptor autoinhibitory mechanisms.[206] The ligand binding site is formed by structures of both IgII and IgIII. Two different isoforms of the IgIII domain have been identified in FGFR1-3 (IgIIIb and IgIIIc), which are generated by alternative splicing of exon 8 and 9. The distribution of the two isoform is tissue-specific, with IgIIIb being expressed on epithelial cells and IgIIIc on mesenchymal ones.[203] FGFR4 is only present in a single isoform, showing a ligand selectivity similar to that of FGFR2-IIIc and FGFR3-IIIc.[207]

A fifth FGF-receptor has been described: FGFR-Like1 is a protein lacking the catalytic intracellular domain, which is replaced by a histidine-rich tail. Its physiological role is still unclear, but it seems that it could act as a negative regulator inhibiting proliferation and promoting differentiation.[208]

3.1.3. Activation of the signaling cascades

Trans-phosphorylation of the intracellular domain resulting from the formation of the dimerization complex FGF/FGFR/HSPG[61] leads to the activation of different intracellular signaling cascades: the key adaptor protein FRS2 (FGFR substrate 2) can be recruited, resulting in the activation of the MAPK and PI3K-Akt pathways, while recruitment of PLC-γ and activation of PKC causes the release of calcium ions from the endoplasmic reticulum, the activation of transcription factors and the synthesis of proteins involved in the cellular motility processes.[205,209] Moreover, further signaling proteins can be engaged depending on the cellular context, such as p38, STAT or RSK2.[210] Different mechanisms leading to signal attenuation and negative feedback

control have been described, including the induction of MAPK phosphatases (MAPK3), Sprouty (SPRY) proteins and SEF family members.[211] Activated FGFRs are finally internalized and degraded or recycled on the cell membrane.[209]

3.1.4. Physiological role of FGFs and FGFRs

The FGF/FGFR axis plays a pivotal role in a variety of physiological processes: in the embryonic and fetal development it is involved in the mesenchymal-epithelial communication required for morphogenesis and tissue differentiation,[203] while in adulthood it regulates tissue homeostasis and is involved in wound healing, tissue repair, cholesterol metabolism[212] and serum phosphate regulation.[213,214] FGFs are involved in the acquisition of a "pro-angiogenic phenotype" in endothelial cells: angiogenesis is the process that allows the formation of new blood vessels from pre-existing ones and it plays a pivotal role in both physiological and pathological conditions.[215]

3.2. FGF/FGFR and cancer

3.2.1. Deregulated activity of the FGF/FGFR system

A deregulated activation of the FGF/FGFR axis has been associated with different cancer types, as well as with various other diseases, including hereditary pathologies such as craniosynostosis and dwarfism syndromes.[216]

Overexpression of the FGF receptors resulting from gene amplification has been detected in lobular breast carcinomas[217] and in triple negative breast cancers,[218] as well as in squamous cell lung cancers,[219,220] oral squamous cell carcinomas (OSCCs),[221] esophageal carcinomas,[222] and gastric cancers.[223] Intragenic FGFR translocations usually result in the fusion of the receptor kinase moiety with a transcription factor domain: the resulting fusion protein is constitutively dimerized and therefore activated.[69] Fusion protein FGFR3-TACC3 (transforming acidic coiled-coil containing protein 3) was the first gene fusion product to be characterized: it displays oncogenic activity in astrocyte cultures[224,225], but it has also been detected in human cancers, such as bladder cancer, triple negative breast cancer and head and neck cancer.[226–228] Activating mutations affecting every FGF receptor protein have been detected: they most frequently affect the extracellular and transmembrane domains of the receptors, while mutations in the kinase sequence are rarer.[27,69] Activation of the signaling pathway can also be due to the overexpression of the FGFs: for instance, high levels of serum FGF2 have been associated with poor prognosis in small cell lung cancer (SCLC) patients.[229] The increased expression of paracrine FGFs, such as FGF1, 2, 4, 5, 8 and 18, has been associated with the promotion of angiogenesis via FGFR1 and FGFR2, which are the most abundant FGF receptors expressed on the endothelium.[230] Alterations in the production of various angiogenesis inducers, such as VEGFs (Vascular Endothelial Growth Factors), angiopoietins, TGFs, PDGFs (Platelet Derived Growth Factors), interleukins, chemokines and FGFs, promote a dysregulated endothelial cell proliferation that enables tumor vascularization.[215,230] FGFs are directly involved in the stimulation of endothelial cell proliferation, but they also synergize with VEGFs and

PDGFs in promoting neoangiogenesis.[29] Experimental evidence on *in vitro* and *in vivo* models suggests that aberrant activity of FGF/FGFR axis may be involved in mechanisms of resistance to therapies targeting the VEGF/VEGFR pathway.[231–233]

3.2.2. Targeting the FGF/FGFR system

3.2.2.1. Tyrosine Kinase Inhibitors

Although different approaches have been investigated in order to target the FGF/FGFR axis, no selective agent blocking this signaling pathway has been approved for disease therapy yet. The kinase activity of the receptors can be abolished by the use of tyrosine kinase inhibitors: in this field, both selective and non-selective TKIs have been developed.

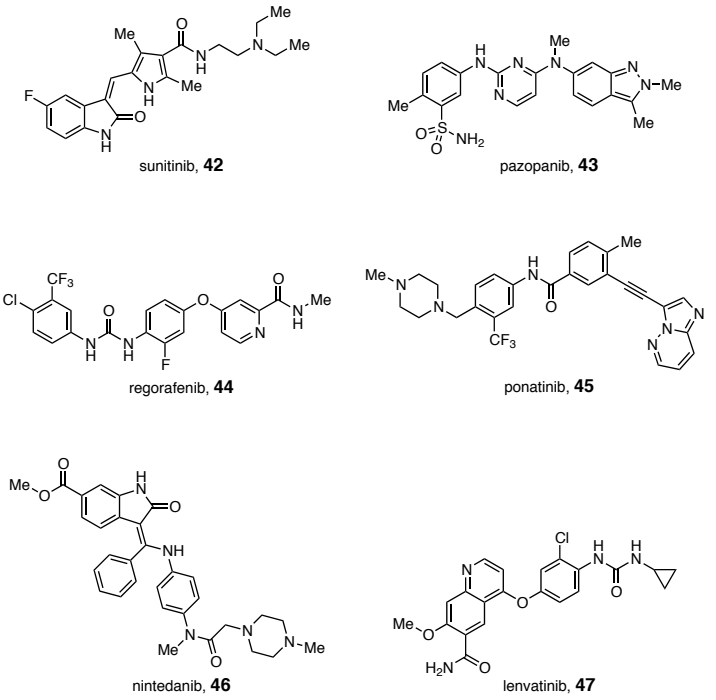

Figure 25: FDA-approved, multi-target TKIs.

As a matter of fact, a wide range of multi-kinase inhibitors targeting FGFR and other RTKs, such as VEGFR, PDGFR, c-KIT, RET and Bcr-Abl, have been described in the literature, including FDA-approved drugs sunitinib (**42**, Sutent®, Pfizer), pazopanib (**43**, Votrient®, GlaxoSmithKline), regorafenib (**44**, Stivarga®, Bayer), ponatinib (**45**, Iclusig®, Ariad Pharmaceuticals), nintedanib (**46**, Ofev®, Boehringer Ingelheim) and lenvatinib (**47**, Lenvima®, Eisai).[31,234]

Selective FGFR inhibitors include both reversible ATP-competitive and irreversible compounds. PD173074 (**48**, Fig.26) is a pyridopyrimidine-based pharmacological tool that exhibits nanomolar potency and high selectivity for the FGFR family.[235] BGJ398 (**49**, Fig.26) is a pyrimidine-based pan-FGFR selective inhibitor that displays nanomolar IC_{50} values in kinase inhibition and proliferation inhibition assays.[236]

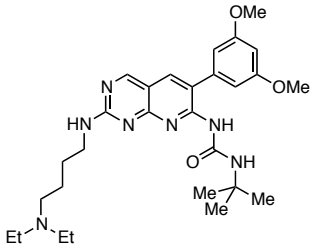

PD173074, **48**

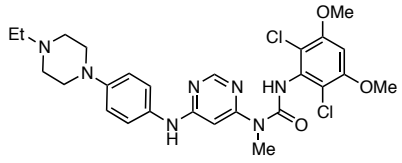

BGJ398, **49**

Figure 26: reversible, selective inhibitors of FGFR.

Irreversible FGFR-targeting TKIs share a high structural similarity with BGJ398 and PD173074 (Fig.27). FIIN-1 (**50**) features a 2-oxo-3,4-dihydropyrimido[4,5-*d*]pyrimidine core and an acrylamide moiety, which is responsible for its covalent interaction with a cysteine residue in the P-loop (Cys486 in FGFR1).[237] FIIN-1 is only a moderate inhibitor of the gatekeeper mutant V561M (FGFR1), probably because of the steric clash generated by the presence of the tetrasubstituted-aromatic ring with the methionine side chain. Optimization of the scaffold of FIIN-1 resulted in the development of covalent FGFR inhibitors FIIN-2 (**51**) and FIIN-3 (**52**).[88]

FIIN-2 features the 2-oxo-3,4-dihydropyrimido[4,5-*d*]pyrimidine core of FIIN-1, but presents some minor modification in the structure of the groups attached to this scaffold:

the chlorine atoms on the aniline ring were removed, the linear solubilizing group has been replaced with a piperazinylaniline, while the acrylamide functionality on the benzyl ring has been shifted from the *meta*- to the *para*-position.

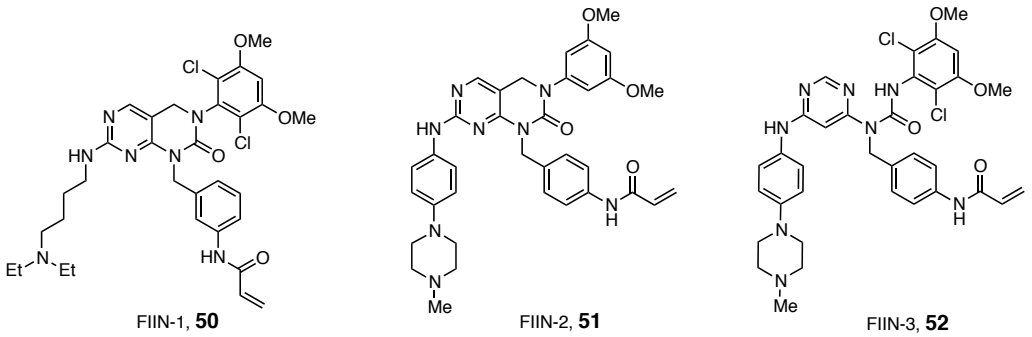

Figure 27: irreversible, selective inhibitors of FGFR.

FIIN-3 is a pyrimidine-based inhibitor bearing a urea functionality allowing the formation of an intramolecular hydrogen bond, which confers a higher degree of flexibility to the entire molecule, though maintaining a similar three-dimensional structure if compared to FIIN-2. Both FIIN-2 and FIIN-3 inhibit FGFR1 V561M in biochemical assays and they also block FGFR2 V564M gatekeeper mutant Ba/F3 cell proliferation at nanomolar concentrations.

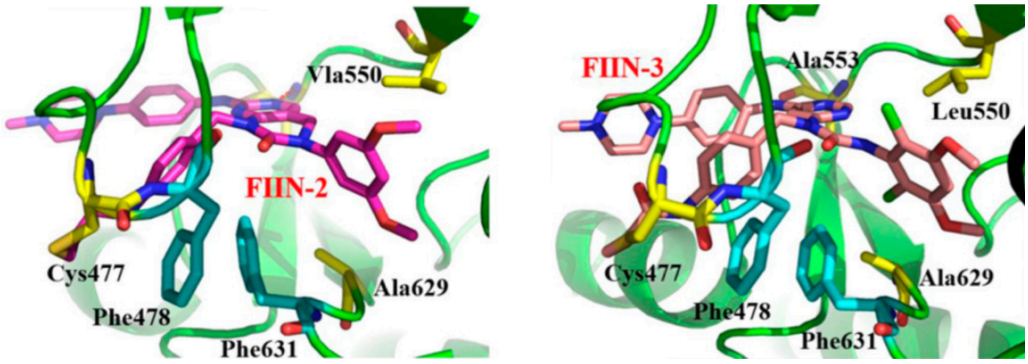

Figure 28: crystal structure of FIIN-2 and FIIN-3 covalent complex with FGFR4 (picture adapted from ref.88).

3.2.2.2. Ligand Traps

Attempts to target the FGF/FGFR axis extracellularly include the development of monoclonal antibodies, which are directed towards the extracellular portion of the receptor, and of ligand traps. The latter are molecules able to recognize and bind the growth factors and to sequester them, thus avoiding their interaction with the receptor.[69] The first example of FGF trap is the fusion protein FP-1039: its structure features the extracellular domain of FGFR1-IIIc bound to the fragment crystallizable region (Fc region) of human immunoglobulin. FP-1039 acts as a decoy receptor, able to bind paracrine and autocrine FGFs. As a result, it is endowed with antitumor and antiangiogenic activity.[238] A phase I clinical trial has highlighted the tolerability of FP-1039, which does not cause the hyperphosphatemic effects generated by the abolishment of hormonal FGF signaling derived by the use of TKIs.[239]

In 2015 the group of Professor Presta at the Department of Molecular and Translational Medicine of the University of Brescia identified the first small-molecule FGF trap able to interfere with FGF2-dependent activation of FGFR1: NSC172285 (also named NSC12 or UPR1358, **53**, Fig.29) is a steroid-based compound able to prevent the formation of HSPG/FGF2/FGFR1 complex with an $IC_{50} \sim 10\mu M$.[70]

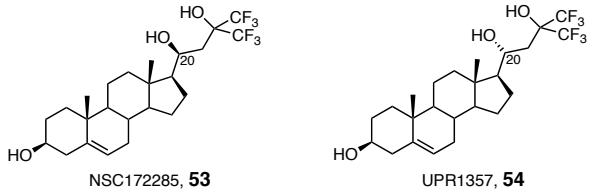

Figure 29: NSC172285, the first small-molecule FGF trap, and its C20 epimer UPR1357.

NSC12/UPR1358 was discovered through a screening of the National Cancer Institute (NCI) NCI2003 small-molecule library, but the amounts of compound available from this source were not sufficient for a complete investigation of its interesting

pharmacological properties. The collaboration between the group of Professor Presta and the group of Professor Mor at the Department of Food and Drug of the University of Parma, where I spent my Ph.D. research period, resulted in the synthesis of both NSC12/UPR1358 and its epimer at C20, namely UPR1357 (**54**, Fig.29).[240]

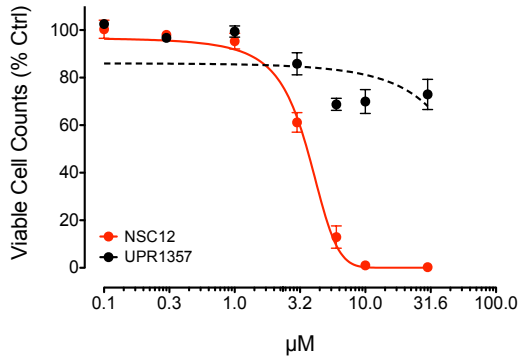

Figure 30: KMS-11 human multiple myeloma cell proliferation inhibition exerted by compounds NSC12 and UPR1357.

The latter is characterized by a lower solubility if compared to NSC12 and also by an almost complete absence of biological activity (Fig.30). As the crystal structure of NSC12 in complex with FGF2 is still not available, the difference in activity highlighted in various biological assays for the C20 epimers cannot be exclusively ascribed nor to the stereochemical configuration of the compounds nor to the scarce solubility of UPR1357.

3.3. Synthesis of FGF/FGFR targeting compounds: aim of the work

Two classes of molecules targeting the FGF/FGFR signaling system were synthesized in the framework of this Ph.D. thesis, namely Tyrosine Kinase Inhibitors (TKIs) and small-molecule FGF traps.

3.3.1. FGFR kinase inhibitors

FGFR-targeting TKIs described in this Ph.D. thesis were designed and synthesized pursuing the same goal described for anilinoquinazoline-based EGFR inhibitors, that is the achievement of long-term inhibition of the catalytic activity of FGFR replacing the acrylamide-based warhead, typical of known FGFR covalent inhibitors. A small series of inhibitors was prepared by inserting alternative reactive portions on the scaffold structure of FIIN-2, a covalent, irreversible inhibitor of FGFRs disclosed in 2014.[88]

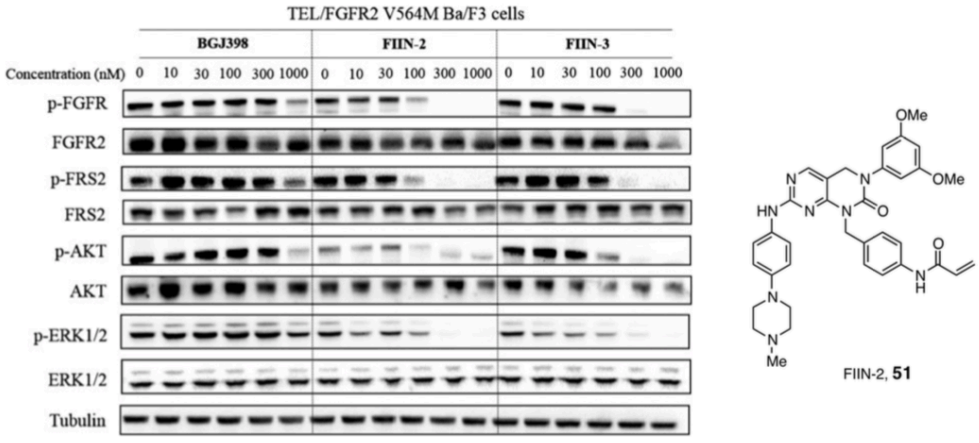

Figure 31: inhibition of FGFR-dependent signaling in Ba/F3 cells harboring FGFR2 gatekeeper mutation V564M. The effect of reversible inhibitor BGJ398 and irreversible compounds FIIN-2 (**51**) and FIIN-3 (**52**, Fig.27) was measured at different concentrations. Cells were incubated with the inhibitors for 6 h and then lysed and subjected to Western blot for the indicated proteins or phosphoproteins. Data reported from ref.88.

FIIN-2 was reported to inhibit the proliferation of cells harboring the gatekeeper mutation of FGFR1 (V561M) and FGFR2 (V564M) (Fig.31). The covalent interaction of its acrylamide portion with a cysteine residue within the ATP-binding pocket was demonstrated by the crystal structure its complex with FGFR4 (Cys477) (Fig.28).
The acrylamide portion of FIIN-2 was replaced with warheads that had also been inserted in the structure of EGFR inhibitors (Table 2).

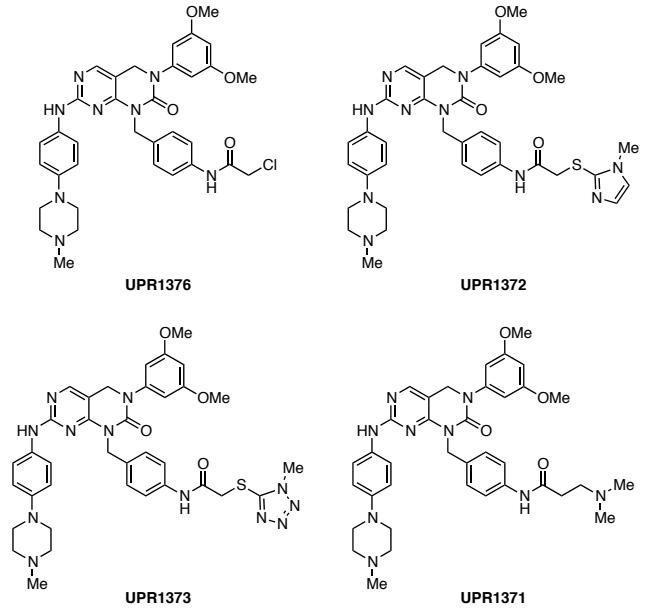

Figure 32: synthesized FIIN-2 analogues.

Besides chloroacetamide (**UPR1376**) and 2-substituted acetamides (**UPR1372** and **UPR1373**) (Fig.32), 3-aminopropanamide (**UPR1371**) was synthesized based on the promising results that such a warhead displayed in previous studies performed on cells harboring wild-type and mutated EGFR.[177,241] Anilinoquinazoline-based EGFR inhibitors bearing a Mannich base were found to be capable of maintaining long-term inhibition of EGFR autophosphorylation in A549 cells (*wt*EGFR), as well as of inhibiting proliferation of NSCLC H1975 cells (EGFR L858R/T790M), with IC_{50} values comparable to those measured for the corresponding acrylamides. When the reactivity

of 3-aminopropanamides was investigated in A549 cell lysate, formation of acrylamide and acrylamide-cysteine adduct was detected. These results suggest the possibility for compound **55**, which is non-reactive *per se,* to generate a Michael acceptor in the intracellular environment, where its inhibitory effect is actually needed (Fig.33).

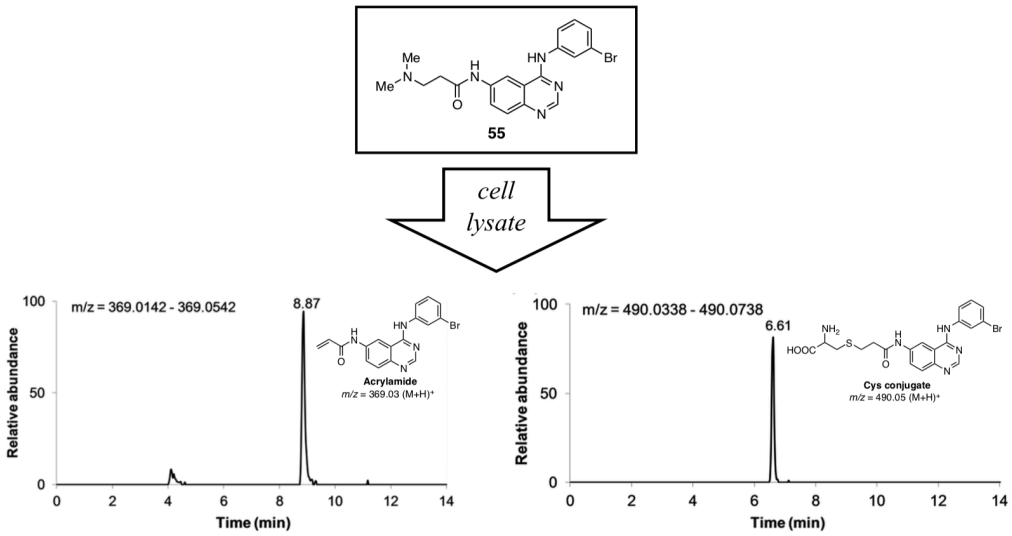

Figure 33: generation of reactive acrylamide from 3-aminopropanamide warhead. Compound **55** was incubated for 1 h in A549 cell lysate containing excess cysteine. HPLC-HRMS was then used to evaluate the formation of conjugates. Acrylamide derivative and acrylamide-cysteine adduct were detected, extracted ion chromatograms are reported. Data adapted from ref.177.

UPR1371 (Fig.32) was thus prepared with the aim of verifying whether this behavior, which is typical of a prodrug, could be replicated in different cell lines harboring a different tyrosine kinase, allowing to reduce the undesired interaction of the electrophilic warhead with nucleophiles other than the target.

3.3.2. FGF traps

The disclosure of the structure of the first small-molecule pan-FGF trap, NSC12 (also called UPR1358, Fig.29), paved the way for the investigation of this interesting class of compounds. The efficacy and tolerability of FGF traps had already been demonstrated

when peptide FP-1039 was investigated for its ability to abolish ligand-dependent activation of FGFR signaling: the soluble decoy receptor inhibits FGF2-mediated proliferation and angiogenesis in diverse tumor cell lines and exhibits antitumor activity in xenograft models.[238,239] Analogously, UPR1358 is capable of interfering with FGF2-dependent angiogenesis and tumor cell proliferation (Fig.34). Moreover, it is orally bioavailable and it produces an antitumor effect in animal models at concentrations at which no signs of toxicity are detected.[70]

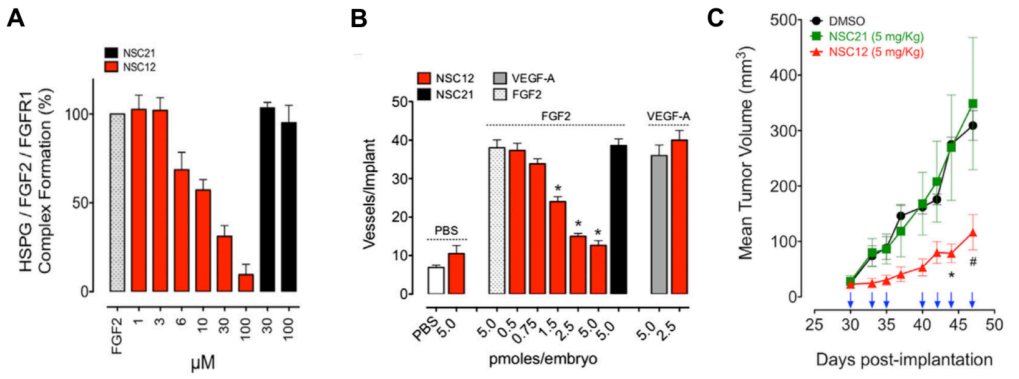

Figure 34: biological activity of NSC12. Panel **A**: inhibition of HSPG/FGF2/FGFR1 ternary complex formation by NSC12. NSC21 (methyl *N*-[6,7,8-trimethoxy-2-(methoxycarbonylamino)-4-oxo-1,3-dihydroquinazolin- 2-yl]carbamate) is used as negative control. Panel **B**: specific anti-angiogenic effect of NSC12. NSC12 impairs the angiogenic response triggered by FGF2, but has no effect on the activity of VEGF-A. Panel **C**: Growth of subcutaneous TRAMP-C2 tumor in mice treated intraperitoneally with NSC12, NSC21, or vehicle. Days of subministration are indicated with blue arrows.

As anticipated, this biological effect is not detected for UPR1357 (**54**, Fig.29), the 20*R*-epimer of NSC12/UPR1358 at 20-position, neither in *in vitro* nor in *in vivo* studies (Fig.30 and Fig.35, panel **A**). When the physicochemical properties of the epimers were investigated, a significant difference in solubility was highlighted (Fig.35, panel **B**).[240] The incapacity of UPR1357 to exert the same biological effect displayed by NSC12/UPR1358 is nevertheless observed at concentrations compatible with its

complete dissolution in the medium used in the assays, suggesting an intrinsic lower activity for the 20*R*-epimer.

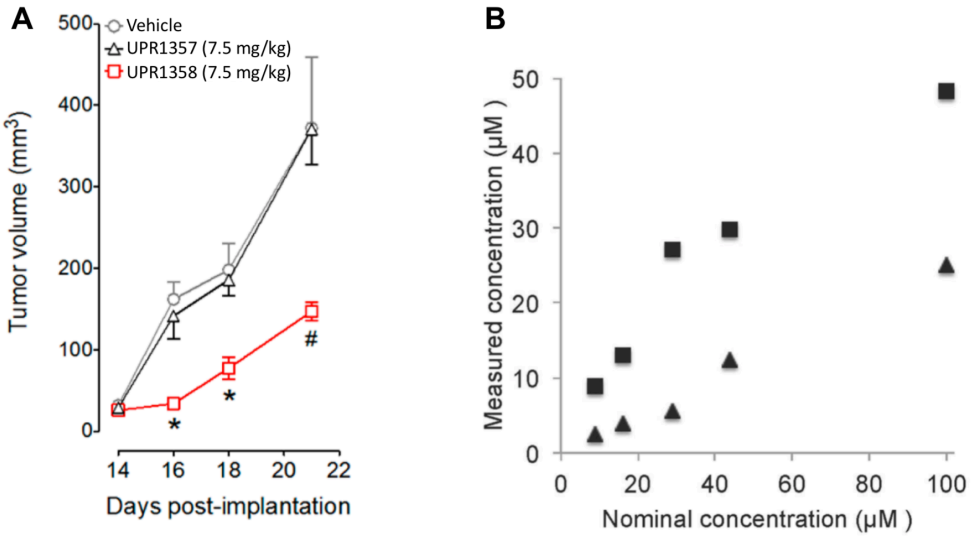

Figure 35: differences in activity and solubility between UPR1358 and UPR1357. Panel **A**: inhibition of murine Lewis lung carcinoma tumor growth exerted by oral daily administration of compounds UPR1358, UPR1357 and vehicle. Panel **B**: kinetic solubility determination for UPR1358 (squares) and UPR1357 (triangles). Solubility is determined in PBS buffer + 3% DMSO. Lower solubility of UPR1357 in the medium results in lower measured concentration at each level of nominal concentration tested in the assay. Data reported from ref.240.

To understand the role of absolute configuration at C20 and solubility in determining the different biological activity of compounds from this class of FGF traps, structure-activity relationships were investigated for a series of UPR1358 and UPR1357 analogues (Fig.36). Chemical exploration of different portion of the parent molecules was performed. The *bis*-(trifluoromethyl)propanediol side chain was modified replacing the distal portion with both a tertiary and a primary alcohol (to assess whether a change in steric hindrance and/or electronic properties was compatible with activity), with a carboxylic acid (to assess the role of an acidic group in the 22-position), with a primary amide (to verify whether replacement with a polar group was tolerated) and with a secondary alcohol linked to an aromatic group, in order to promote different spatial

conformations of the diol motif (Fig.36, Panel **I**). The relationship between the presence of a secondary alcohol in position 3 and activity was investigated by synthesizing analogues bearing various substituents on this position (Fig.36, Panel **II**) and derivatives where the alcohol group was oxidized, obtaining a ketone or an oxime (Fig.36, Panel **III**). When the 3-hydroxyl group was replaced, hydrophilic substituents were preferred to improve the solubility. Finally, the role of the double bond in the steroidal nucleus was investigated synthesizing saturated analogues of UPR1358 and UPR1357 and of their keto-derivatives (Fig.36, Panel **IV**).

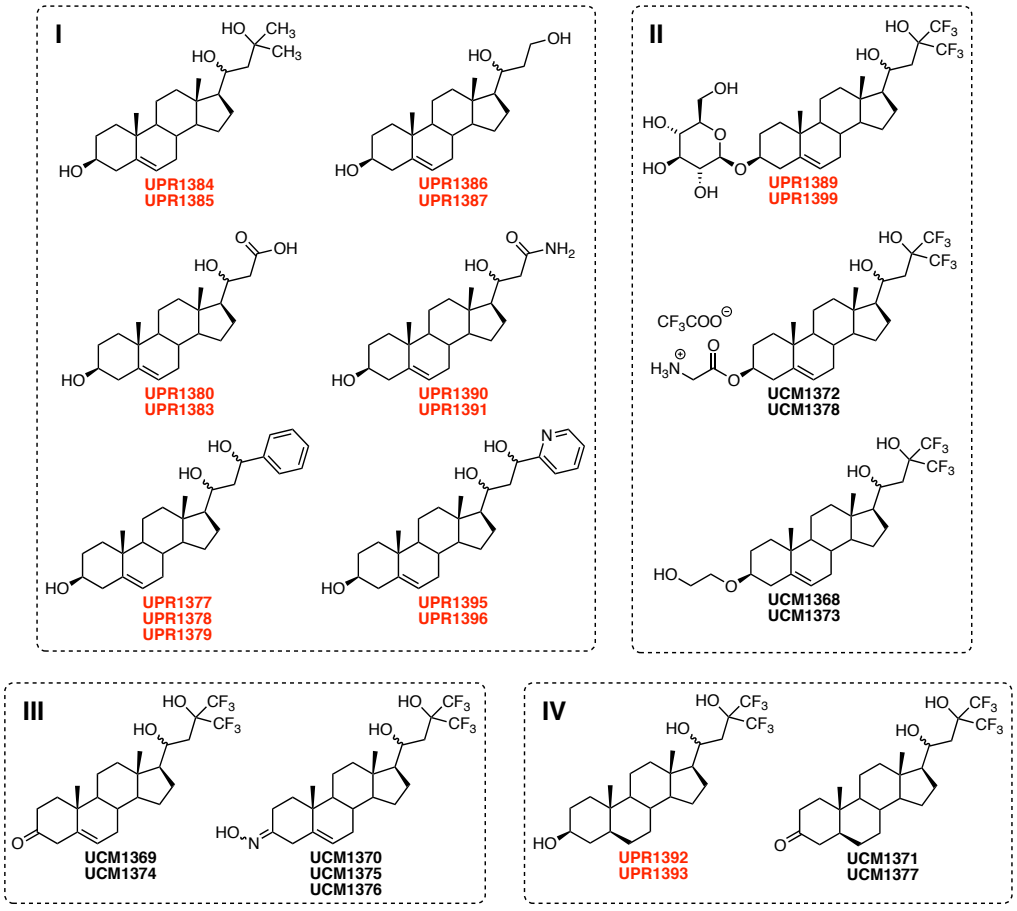

Figure 36: analogues of UPR1358 and UPR1357.

The synthesis project has been performed in the framework of a collaboration between the group of Professor Mor at the Department of Food and Drug of the University of Parma and the group of Professor Spadoni at the Department of Biomolecular Sciences of the University of Urbino. The description of the synthetic strategies reported in the following chapter is limited to the compounds that I prepared during my Ph.D. research period, reported in red in Fig.36, while discussion of the biological data is presented for the entire set of compounds.

3.4. Synthesis of FGF/FGFR targeting compounds: chemistry

3.4.1. FGFR kinase inhibitors

Synthesis of FIIN-2 scaffold was performed as previously reported by Tan *et al.*[88] with minor modifications, as depicted in Scheme 9. Compound **58** was prepared through hydroxymethylation of uracil (**28**),[242] exhaustive chlorination of 5-hydroxymethyluracil **56** and substitution of the alkyl chloride on 2,4-dichloro-5-(chloromethyl)pyrimidine (**57**) with 3,5-dimethoxyaniline in the presence of catalytic amounts of sodium iodide. The chlorine atom in position 4 of the dichloropyrimidine ring was then substituted with 4-nitrobenzylamine, obtaining compound **59**, which was subjected to a ring closure reaction with triphosgene affording intermediate **60**.

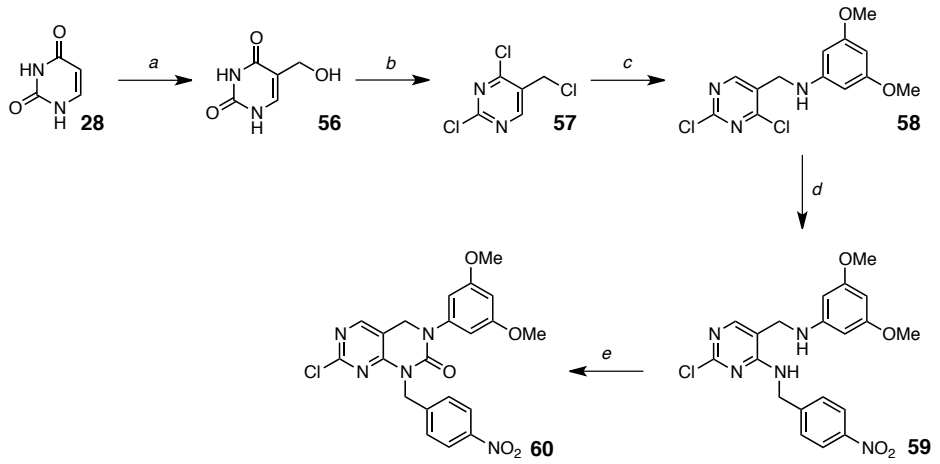

Scheme 9: synthesis of intermediate **60**. Reagents and conditions: a) paraformaldehyde, aq. KOH, 55 °C, 63 h, 81% yield; b) $POCl_3$, PCl_5, reflux, 2 h, 71% yield; c) 3,5-dimethoxyaniline, K_2CO_3, NaI (cat.), MeCN, r.t., 15 h, 34% yield; d) 4-nitrobenzylamine, DIPEA, dioxane, 60 °C, 15 h, 78% yield; e) triphosgene, TEA, THF, 70 °C, 1 h, quantitative yield.

Aniline **63** was obtained through reduction of nitro compound **62** using iron under slightly acidic conditions. Substitution of chlorine on compound **60** was performed under strongly acidic conditions and product **64** was isolated in only moderate yield.

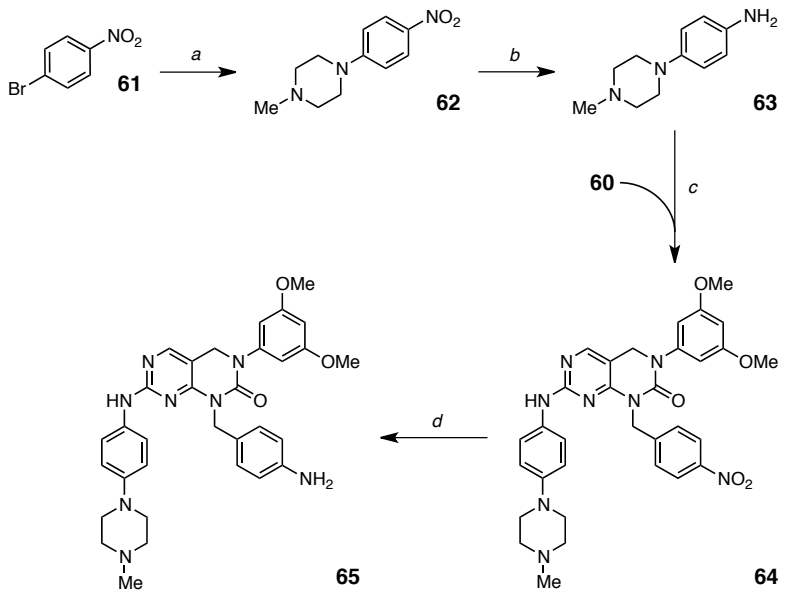

Scheme 10: synthesis of intermediate **65**. Reagents and conditions: *a*) 1-methylpiperazine, 80 °C, 6 h, 96% yield; *b*) Fe^0, NH_4Cl, EtOH, H_2O, reflux, 1 h, 95% yield; *c*) TFA, *sec*-BuOH, 100 °C, 15 h, 51% yield; *d*) Raney® nickel, MeOH/THF 1:1, 40 °C, 2 h, 71% yield.

The reaction conditions for the reduction of the nitro group to afford aniline **65** were modified from those reported in ref.88. In particular, nickel catalyst was used in the form of commercially available suspension in water (whereas the original paper described the use of a methanol suspension) and the reaction was performed under a nitrogen atmosphere, avoiding the use of gaseous hydrogen. The yield was nevertheless satisfactory and aniline **65** was isolated for characterization (analytical data are not reported in the original paper) (Scheme 10).

The reactive portion was finally inserted on aniline **65** according to procedures already described for EGFR inhibitors (Scheme 11). Chloroacetamide derivative **66** could be readily used for the synthesis of compounds **UPR1372** and **UPR1373**, but its reduced

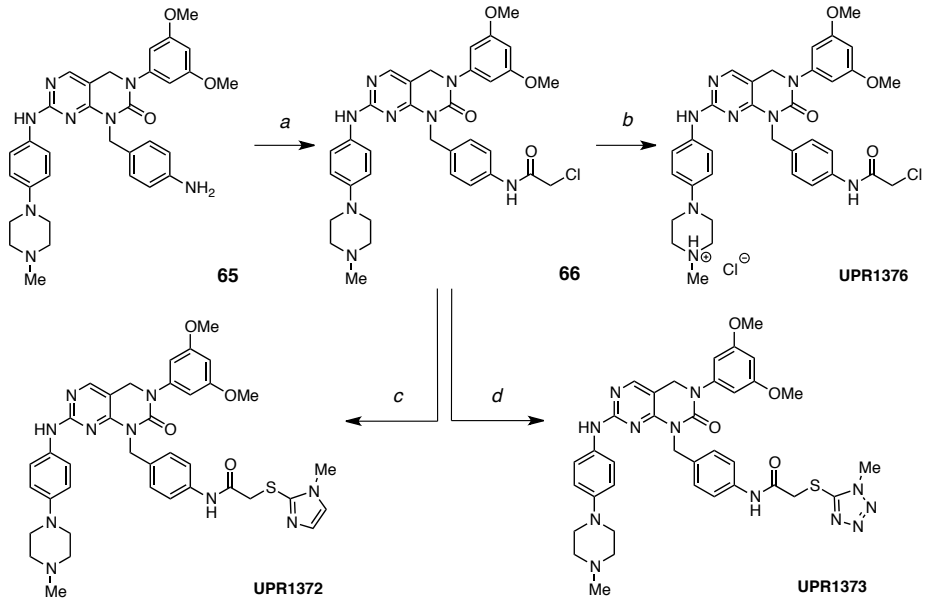

Scheme 11: synthesis of FIIN-2 analogues bearing 2-substituted acetamide warheads. Reagents and conditions: *a*) chloroacetic acid, DIPEA, PivCl, THF, 1 h, yield not calculated; *b*) TMSCl, 51% yield over two steps; *c*) 2-mercapto-1-methylimidazole, NaOH, MeCN/THF, r.t., 15 h, 78% yield; *d*) 5-mercapto-1-methyltetrazole, NaOH, MeCN/THF, r.t., 15 h, 35% yield.

stability hampered prolonged storage and also prevented definitive determination of its purity by standard analytical methods. These issues were overcome preparing hydrochloride **UPR1376**, which was tested for its biological activity.

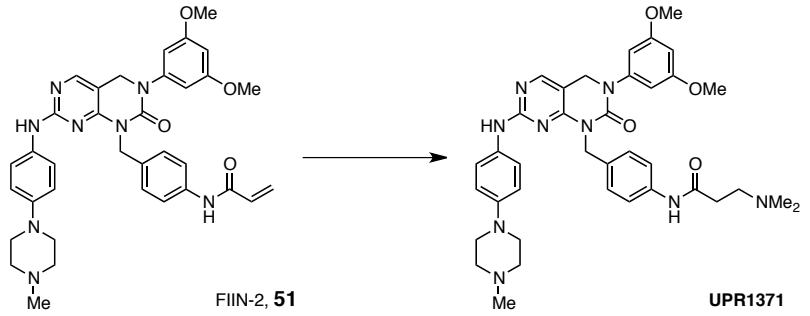

Scheme 12: synthesis of 3-aminopropanamide **UPR1371**. Reagents and conditions: Me_2NH, abs. EtOH, 70 °C, 15 min, 98% yield.

Compound **UPR1371**, bearing the 3-aminopropanamide portion, was prepared through aza-Michael addition of dimethylamine on commercially available **FIIN-2** (Scheme 12). The product was easily isolated after removal of the volatiles under reduced pressure.

3.4.2. FGF traps

Synthesis of compounds featuring modifications on the distal portion of the side chain on C17 of the steroidal nucleus was performed according to two different strategies.
Compounds carrying a primary or tertiary alcohol, a carboxylic acid and an amide were prepared starting from a common ester intermediate, which in turns was synthesized starting from an aldehyde precursor. The retrosynthetic analysis leading to this approach is depicted in Fig.37. This strategy appeared to be particularly convenient as the synthesis of the required aldehyde was already described in the literature, and conversion of the aldehyde to the suitable ester derivative allowed to prepare all the desired final products from a single precursor, instead of planning an *ad hoc* procedure for each of them.

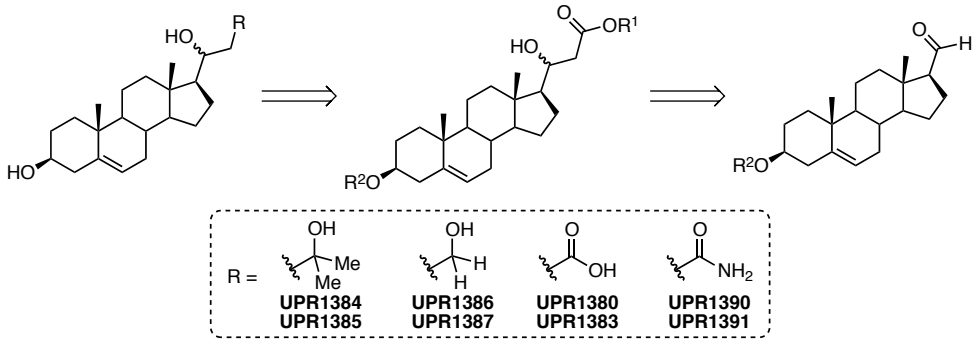

Figure 37: retrosynthetic analysis for the preparation of compounds featuring modifications on the side chain.

3β-Acetoxy-androst-5-ene-17β-carbaldehyde **70** was chosen as precursor of the required ester owing to the satisfactory amount of data about its synthesis and characterization in the literature. In particular, a convenient procedure for the synthesis of 3β-acetoxyetienic

acid **68** starting from commercially available pregnenolone acetate **67** was reported in *Organic Syntheses*.[243] Reduction of the carboxylic acid to the aldehyde group was performed in two steps. The carboxylic acid was initially transformed into the more reactive mixed anhydride, which could be easily reduced to the primary alcohol **69** using sodium borohydride in a one-pot reaction.[244] The alcohol group was then oxidized to aldehyde **70** employing pyridinium chlorochromate (PCC) (Scheme 13). The procedure was reported in the literature on the same substrate[245] and worked smoothly, allowing to obtain the target aldehyde in a suitable amount to complete the subsequent synthetic steps. For this reason, no other oxidative method was investigated.

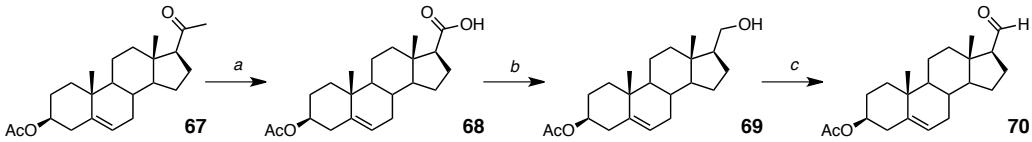

Scheme 13: synthesis of 3*β*-acetoxy-androst-5-ene-17*β*-carbaldehyde **70**. Reagents and conditions: *a*) NaOH, NaOBr, dioxane, H_2O, 0 °C, 3 h, then Ac_2O, pyridine, r.t., 18 h, 90% yield; *b*) EtOCOCl, TEA, THF, 0 °C, 90 min, then $NaBH_4$, H_2O, r.t., 15 h, 89% yield; *c*) PCC, DCM, r.t., 2 h, 56% yield.

Ester **71** was obtained through Reformatsky reaction with ethyl bromoacetate and zinc, affording a mixture of epimers that could be separated by column chromatography and employed separately in the following steps (Scheme 14).

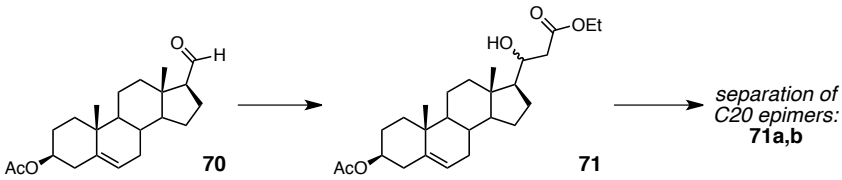

Scheme 14: synthesis of ester **71**. Reagents and conditions: ethyl bromoacetate, zinc, THF, 0 °C, 20 min, 72% yield (2:1 ratio).

The tertiary alcohol derivatives **UPR1384** and **UPR1385** were prepared by treating compound **71** with an excess of methylmagnesium bromide at reflux in toluene, which caused at the same time deprotection of the acetoxy group in position 3. The primary alcohol derivatives **UPR1386** and **UPR1387** were obtained by reducing ester **71** with sodium borohydride. The protecting group in position 3 was partially removed, and the reaction mixture was treated with excess sodium hydroxide to promote complete removal and allow isolation of the pure compounds. The carboxylic acid derivatives **UPR1380** and **UPR1383** were prepared by saponification with sodium hydroxide. The two carboxylic acids were converted to the corresponding amides **UPR1390** and **UPR1391** by condensing with ammonium chloride and TBTU (Scheme 15).

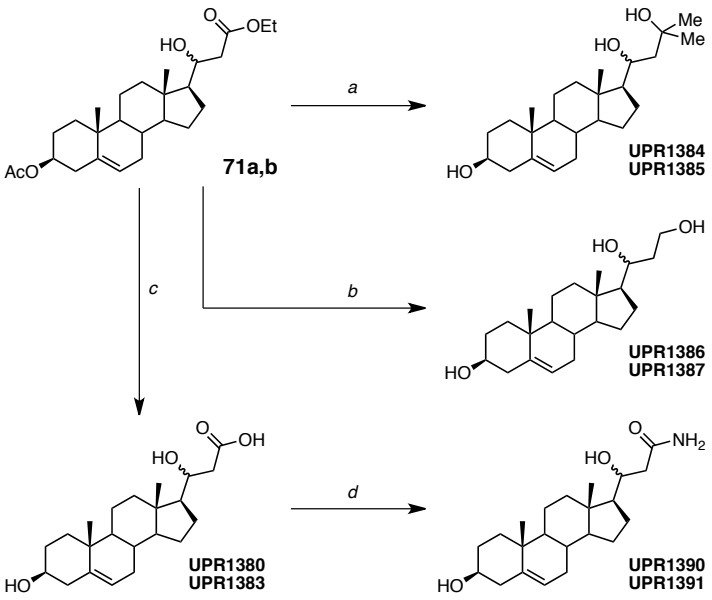

Scheme 15: Synthesis of compounds featuring modifications on the side chain starting from ester **71**. Reagents and conditions: *a*) MeMgBr, toluene, reflux, 3 h, 56-65% yield; *b*) $NaBH_4$, THF/MeOH, reflux, 1 h, 24-50% yield; *c*) NaOH, THF/H_2O, r.t., 15 h, 72-86% yield; *d*) NH_4Cl, TBTU, DIPEA, DMF, r.t., 15 h, 25% yield.

Compounds bearing a secondary alcohol and an aromatic ring were prepared through an aldol reaction between pregnenolone benzoate **72** and the suitable aldehyde, followed by

reduction of the ketone and deprotection of the hydroxyl group on position 3 (Scheme 16). While in the benzaldehyde series the two epimers at 22-position (compound **73**) could be separated by column chromatography, perfect coelution hampered the separation of the two epimers obtained for compound **75**, which were therefore reacted together in the following reduction step. Reduction of the epimers of compound **73** afforded two products in one case, and only one product in the other. Reduction of compound **75** afforded two diastereoisomers. Overall, from the sequence condensation-reduction-deprotection reactions involving benzaldehyde, three diastereoisomers were obtained (**UPR1377**, **UPR1378** and **UPR1379**), while for those bearing the pyridyl group only two were obtained (**UPR1395** and **UPR1396**).

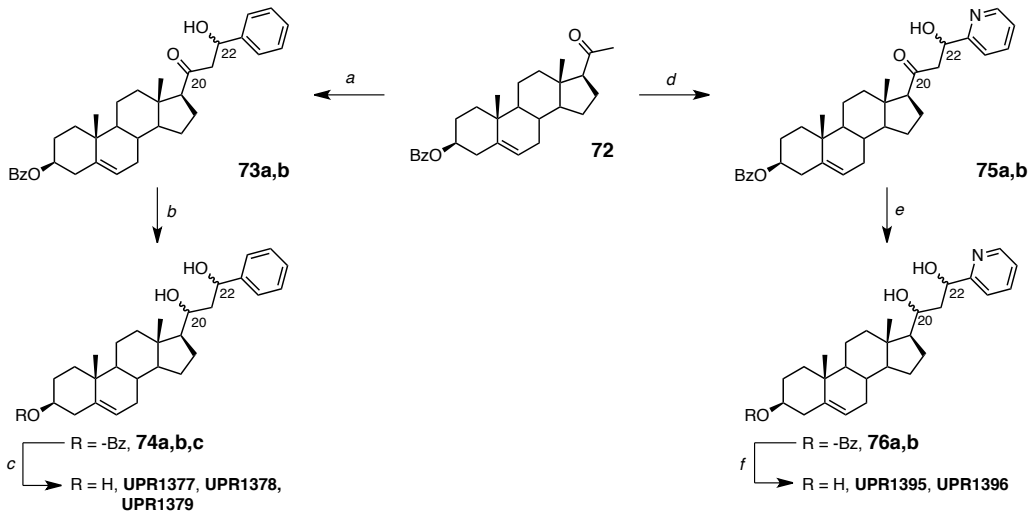

Scheme 16: synthesis of compounds bearing a secondary alcohol and an aromatic ring. Reagents and conditions: *a*) benzaldehyde, LiHMDS, THF, -78 °C, 1 h, 66% yield; *b*) $Na(OAc)_3BH$, THF, r.t., 1 h, 83% to quantitative yield; *c*) NaOH, H_2O, THF, reflux, 2 h, 68 - 88% yield; *d)* 2-pyridinecarboxaldehyde, LiHMDS, -78 °C, 1 h, 82% yield; *e*) $Na(OAc)_3BH$, THF, r.t., 1 h, 37% yield; *f*) NaOH, H_2O, THF, reflux, 2 h, 64 - 71% yield.

The glycosilated analogue of UPR1357 was obtained *via* direct glycosylation of the 3β-hydroxy group with standard imidate-coupling chemistry. Using (2,3,4,6-tetra-*O*-acetyl-α,β-D-glucopyranosyl)trichloroacetimidate, trimethylsilyl trifluoromethanesulfonate

(TMSOTf) as promoter and dichloromethane as the solvent, compound **77** could be obtained in moderate yield. Deacetylation under standard condition furnished **UPR1389** (Scheme 17).

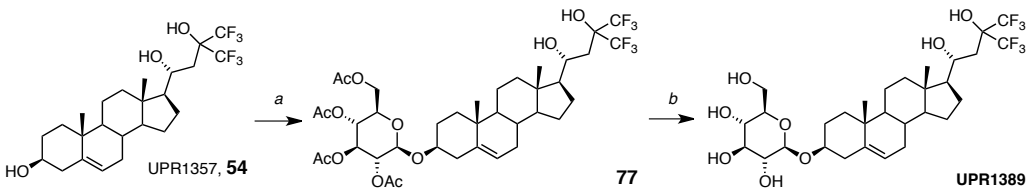

Scheme 17: synthesis of **UPR1389**. Reagents and conditions: *a*) (2,3,4,6-tetra-*O*-acetyl-*α,β*-D-glucopyranosyl)trichloroacetimidate, TMSOTf, TEA, DCM, -25°C, 15 min, 15% yield; *b*) NaOMe, MeOH, r.t., 6 h, 50% yield.

On the other hand, preparation of UPR1358 glycosylated derivative with the same protocol was hampered by a solubility issue that could not be circumvented.

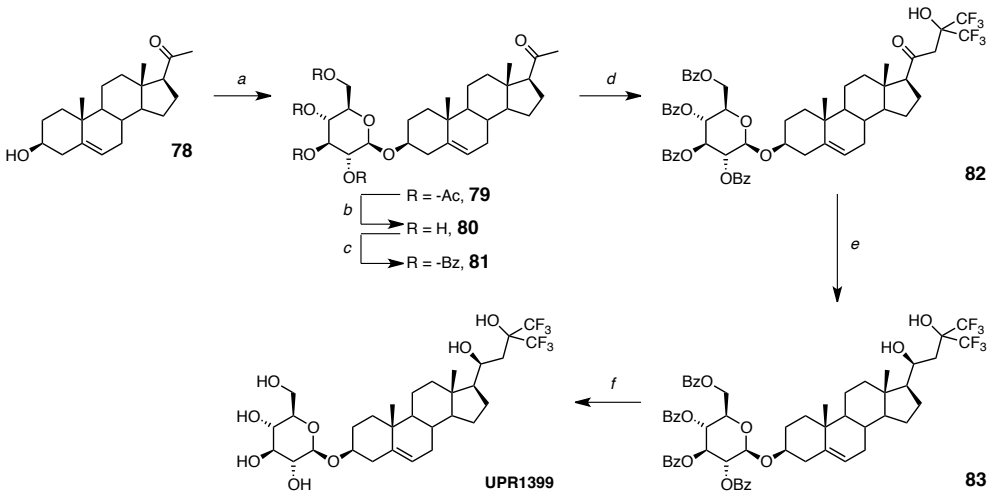

Scheme 18: synthesis of **UPR1399**. Reagents and conditions: *a*) (2,3,4,6-tetra-*O*-acetyl-*α,β*-D-glucopyranosyl)trichloroacetimidate, TMSOTf, anhydrous DCM, -25°C - 0°C, 15 min; *b*) NaOMe, THF, r.t., 1 h, 22% yield over two steps; *c)* BzCl, pyridine, r.t., 20 min, quantitative yield; *d*) LiHMDS, HFA, THF, -78°C, 1 h, 73% yield; *e*) $Na(OAc)_3BH$, THF, r.t., 1 h, 7% yield; *f*) NaOMe, THF, r.t., 2 h, 62% yield.

Owing to the lower solubility of NSC12/UPR1358 in those solvents compatible with the glycosylation reaction, the sugar moiety had to be inserted at an earlier stage during the synthesis of **UPR1399** (Scheme 18). Glycosylation of pregnenolone **78** was therefore performed. After minor protecting group manipulation, compound **82** was obtained through aldol reaction with hexafluoroacetone in the same conditions employed for the synthesis of UPR1357 and UPR1358.[240] Reduction of hydroxy-ketone **82** with sodium triacetoxyborohydride furnished two diastereoisomers, which were separated by column chromatography. The less abundant isomer (**83**) afforded **UPR1399** after deprotection. Finally, saturated analogues of UPR1358 and UPR1357, namely **UPR1392** and **UPR1393**, were prepared according to the procedure employed for the synthesis of their unsaturated parent compounds,[240] starting from commercially available 5α-pregnanolone acetate **84** (Scheme 19).

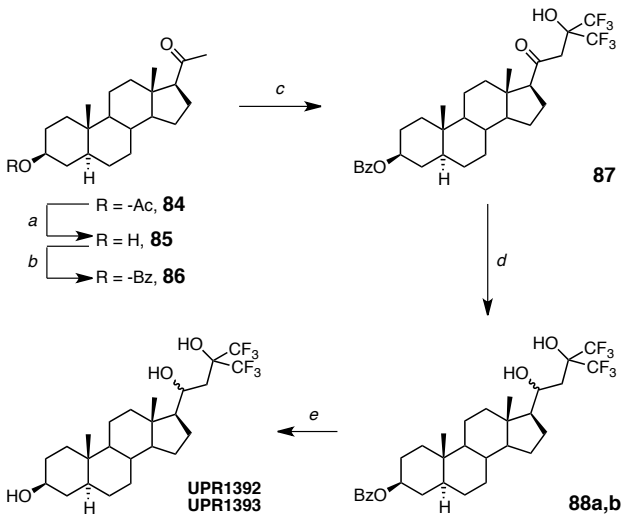

Scheme 19: synthesis of **UPR1392** and **UPR1393**. Reagents and conditions: *a*) Na^0, MeOH, THF, r.t., 2 h, quantitative yield; *b*) BzCl, pyridine, r.t., 2 h, 82% yield; *c*) LiHMDS, hexafluoroacetone, THF, -78 °C, 1 h, 85% yield; *d*) $Na(OAc)_3BH$, THF, r.t., 2 h, 48% yield for **88a** and 12% yield for **88b**; *e*) Na^0, MeOH, THF, r.t., 15 h, 75% yield for **UPR1392**, quantitative yield for **UPR1393**.

The acetyl protecting group was removed and replaced with benzoyl (compound **86**), which is non-enolizable and therefore tolerated in the following aldol reaction conditions

with hexafluoroacetone. Reduction of hydroxyketone **87** with sodium triacetoxyborohydride afforded two diastereoisomers that could be easily separated (compound **88**). Deprotection through transesterification with sodium methoxide furnished **UPR1392** and **UPR1393**.

In order to infer the absolute configuration at C20 for compounds deriving from ester **71**, ^{1}H-NMR spectra of the couples of epimers were compared to ^{1}H-NMR spectra of NSC12/UPR1358 and UPR1357 analogues prepared at the Department of Biomolecular Sciences of the University of Urbino. The strategy pursued for the synthesis of these derivatives featured late-stage modifications on the parent compounds, UPR1358 and UPR1357, the stereochemical configuration of which had already been assessed in a previous work.[240] In the UCM-series (Fig.36) the absolute configuration is therefore known for each compound. A small but appreciable difference was noticed in chemical shift of H18 methyl group based on the absolute configuration at C20, with 20*R*-derivatives displaying a higher chemical shift for the methyl signal than the 20*S*-compounds.

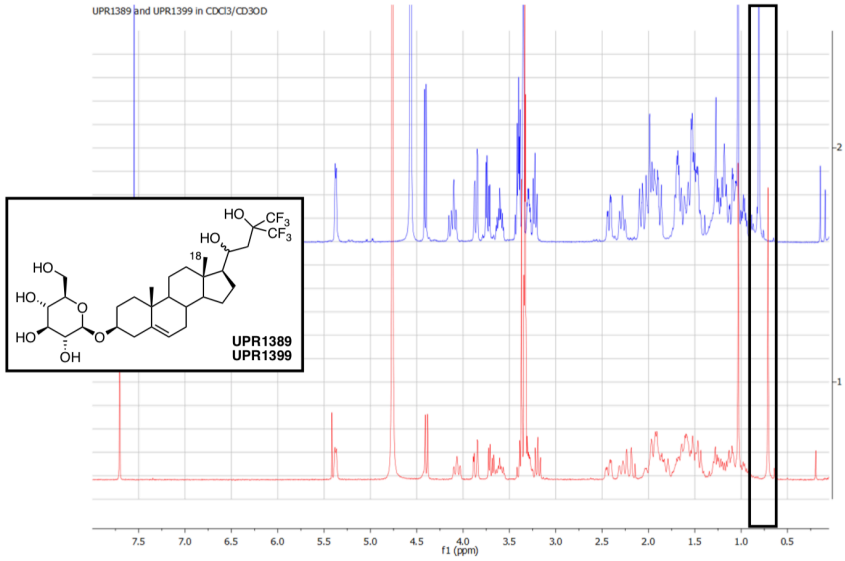

Figure 38: stacked ^{1}H-NMR spectra of **UPR1389** (blue) and **UPR1399** (red) in $CDCl_3/CD_3OD$. A higher chemical shift value for H18 in **UPR1389** spectrum is observed (0.80 ppm *vs.* 0.71 ppm).

This trend was observed also in glycosylated analogues **UPR1389** and **UPR1399**, the stereochemistry of which was known due to the preparation of **UPR1389** from UPR1357 (Fig.38). The same observation was also possible in the case of **UPR1392** and **UPR1393** (Fig.41). Moreover, **UPR1392** and **UPR1393** could also be directly prepared through catalytic hydrogenation on NSC12 and UPR1357 (reaction performed at the University of Urbino for the synthesis of 3-oxo-derivatives **UCM1371** and **UCM1377**), and their configuration was confirmed to be 20*R* for **UPR1393** and 20*S* for **UPR1392**.

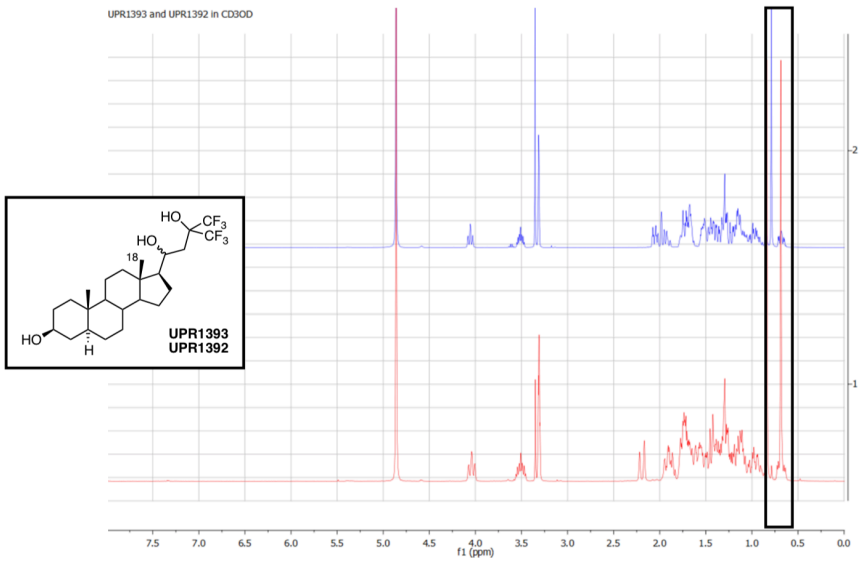

Figure 41: stacked ^{1}H-NMR spectra of **UPR1393** (blue) and **UPR1392** (red) in CD_3OD. A higher chemical shift value for H18 in **UPR1393** spectrum is observed (0.80 ppm *vs.* 0.65 ppm).

Comparison of the chemical shift of H18 methyl group of the two epimers of ester **71**, as well as of the chemical shift of the same group for all the compounds derived from that ester, allowed to infer the configuration of C20 as follows: **UPR1384**, **UPR1386**, **UPR1380** and **UPR1390**, deriving from the *major* product of the Reformatsky reaction, were assigned the 20*R*-configuration, whereas **UPR1385**, **UPR1387**, **UPR1383** and **UPR1391**, deriving from the *minor* product of the Reformatsky reaction, were assigned the 20*S*-configuration (Fig.39 and Fig.40).

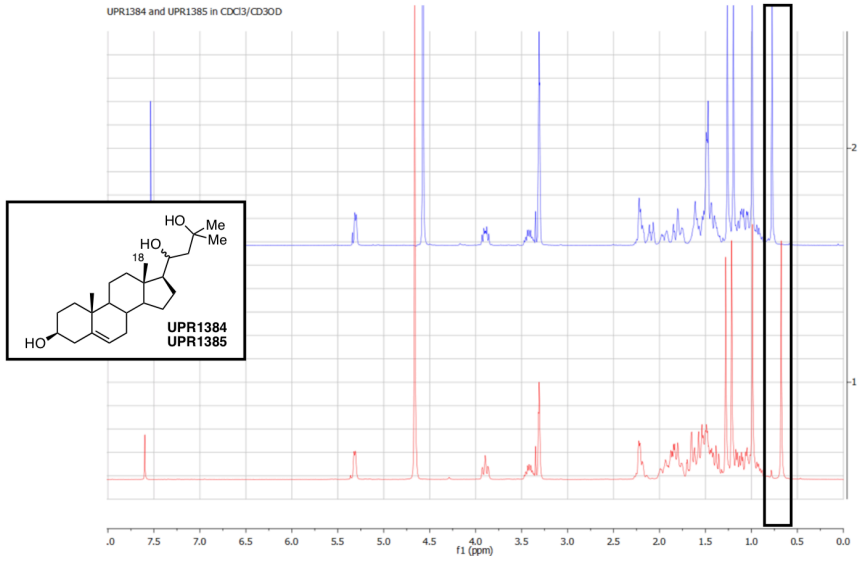

Figure 39: stacked ^{1}H-NMR spectra of **UPR1384** (blue) and **UPR1385** (red) in $CDCl_3/CD_3OD$ mixture. A higher chemical shift value for H18 in **UPR1384** spectrum is observed (0.78 ppm *vs.* 0.68 ppm).

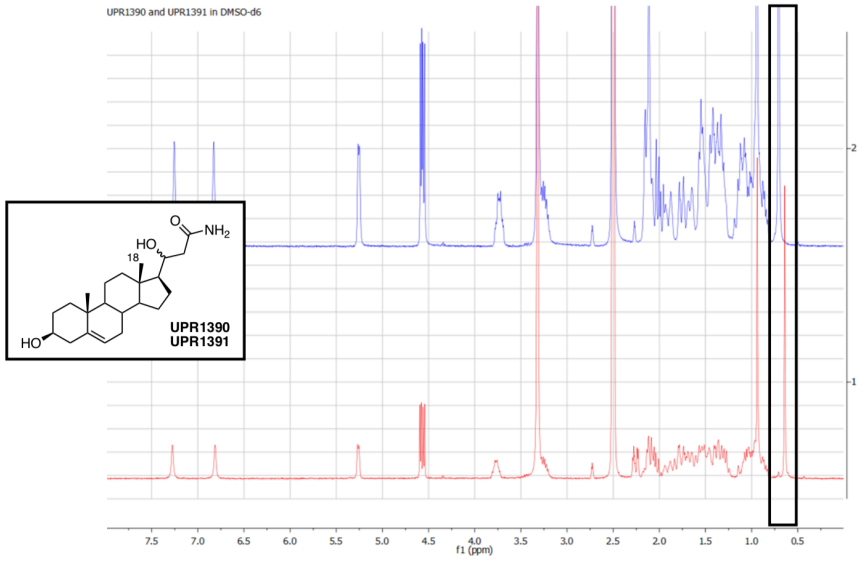

Figure 40: stacked ^{1}H-NMR spectra of **UPR1390** (blue) and **UPR1391** (red) in DMSO-*d6*. A higher chemical shift value for H18 in **UPR1390** spectrum is observed (0.71 ppm *vs.* 0.64 ppm).

In the case of derivatives bearing an aromatic or heteroaromatic ring (**UPR1377**, **UPR1378**, **UPR1379**, **UPR1395** and **UPR1396**), compounds could not be clustered according to the position of H18 methyl group peak. This is probably due to the presence of a second chiral center on C22 (Scheme 16), which leads to the possibility for these products to explore alternative conformations of the propanediol side chain. It was therefore to exclude that chemical shift of H18 could still be dependent on the sole configuration of C20.

3.5. Synthesis of FGF/FGFR targeting compounds: biological data

3.5.1. FGFR kinase inhibitors

3.5.1.1. Inhibition of *wt*FGFR autophosphorylation

FGFR inhibitors were tested for their ability to inhibit FGFR autophosphorylation in LENTI-4 cells, a cell model overexpressing FGFR1. Cells were incubated for 1 h in the presence of 1 μM concentration of the compounds and the inhibitory effect was measured immediately after and 8 h after removal of the compounds from the extracellular medium. All the compounds reduced FGF2-induced phosphorylation of FGFR1 after 1 h of treatment.

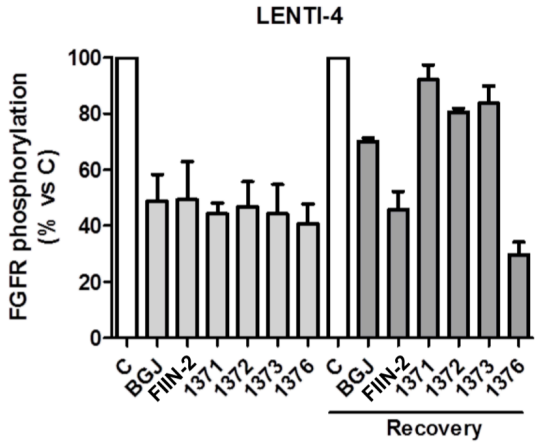

Figure 42: inhibitory effect on FGFR1 autophosphorylation in LENTI-4 cells. LENTI-4 cells were incubated with 1 μM BGJ398, FIIN-2 or the newly synthesized FGFR inhibitors for 1 h. After incubation and stimulation with FGF2 for 15 min, cells were lysed and residual autophosphorylation percentage (here reported *vs*. control) was measured by Western blot (left columns). Alternatively, cells were extensively washed with PBS after incubation and then stimulated with FGF2 for 15 min after 8 h of incubation in fresh drug-free medium ("recovery" columns). The data are means ± SD of three independent experiments.

At this time point, efficacy of the inhibitors is comparable to that of reversible FGFR inhibitor BGJ398 (**49**, Fig.26) and irreversible reference inhibitor FIIN-2 (**51**, Fig.27). After washing, autophosphorylation was recovered almost completely in the case of **UPR1371**, **UPR1372** and **UPR1373**, while **UPR1376** revealed to be more effective than FIIN-2 in maintaining the inhibition of FGFR1 autophosphorylation (Fig.42).
The antiproliferative activity of the newly synthesized compounds was also evaluated in H1581 cell line, harboring focal amplification of FGFR1. All the compounds inhibited cell proliferation with IC_{50} values in the nanomolar range (Table 6).

Table 6: inhibition of H1581 cell proliferation exerted by FGFR inhibitors.

Compound	IC_{50} (nM)[a]
BGJ398	2 ± 0.5
FIIN-2	0.15 ± 0.05
UPR1371	54.9 ± 9.2
UPR1372	5.4 ± 0.7
UPR1373	4.4 ± 1.1
UPR1376	0.8 ± 0.3

[a] H1581 cells were incubated with increasing concentrations of the FGFR inhibitors (0.001 nM - 10 μM) for 72 h. Data were obtained by MTT assay. The IC_{50} values are means ± SD of three independent experiments.

3.5.1.2. Inhibition of BGJ-resistant clone proliferation

Inhibitors were tested in two BGJ398-resistant cell lines. Resistant clones were generated treating H1581 cells with increasing doses of BGJ398 and the molecular mechanism underlying acquired resistance is not known. **UPR1376** showed a strong antiproliferative activity in H1581R1 and H1581R2 resistant clones, while reference compound FIIN-2 and the other derivatives were devoid of significant antiproliferative activity (Figure 43, panel **A**). Compound **UPR1376** inhibited cell proliferation of H1581R1 and H1581R2 resistant clones with IC_{50} values of 254 and 359 nM, respectively (Figure 43, panel **B**).

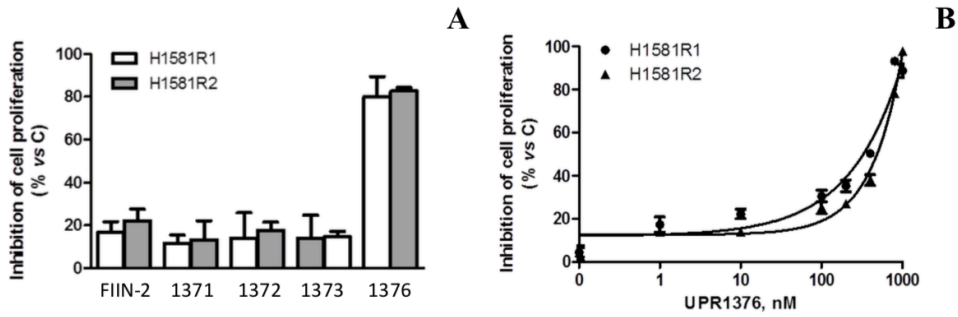

Figure 43: inhibition of cell proliferation on resistant clones. Panel **A**: H1581R1 and H1581R2 cells were incubated with 1 μM concentration of the tested compounds for 72 h. Data were obtained by MTT assay and are expressed as percent inhibition of cell proliferation *vs.* control. Panel **B**: H1581R1 and H1581R2 cells were incubated with increasing concentrations of **UPR1376** (1 - 1000 nM) for 72 h. Data were obtained by MTT assay and are expressed as percent inhibition of cell proliferation *vs.* control.

3.5.2. FGF traps

Compounds synthesized at the Department of Food and Drug of the University of Parma and at the Department of Biomolecular Sciences of the University of Urbino were tested for their ability to inhibit cell proliferation and FGFR3 phosphorylation in KMS-11 human multiple myeloma cells (data reported in Table 7). This information allows to verify whether the effect on cell growth could actually be ascribed to the inactivation of FGF/FGFR system. Analysis of IC_{50} values on KMS-11 cell proliferation revealed that replacement of the *bis*-(trifluoromethyl)propanediol side chain on C17 of the steroidal nucleus provided a reduction of compound potency (Structure A). Although stereochemical configuration was not assigned for this set of compounds, derivatives prepared from ester **71** could be clustered into two groups sharing the same configuration at C20 (see paragraph 3.4.2). Compounds **UPR1384**, **UPR1386**, **UPR1380** and **UPR1390** were indeed prepared from one single isomer, while the other isomer was used for the preparation of compounds **UPR1385**, **UPR1387**, **UPR1383** and **UPR1391**. Comparison of the biological results within the couples of isomers did not allow to state a clear dependence of the activity on the stereochemical configuration: for instance, in the tertiary alcohol couple, **UPR1384** resulted more active than **UPR1385**, while in the

Table 7: KMS-11 cell proliferation and FGFR3 phosphorylation inhibition.

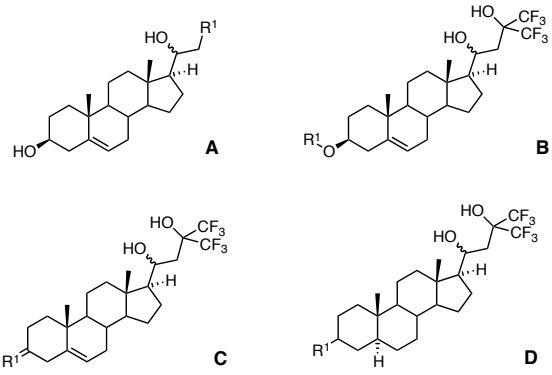

Compound	Structure	-R^1	configuration position 20[a]	IC_{50} proliferation[b] µM	pFGFR3[c] %inhibition
UPR1358 (NSC12)	A		*S*	3.4	74.2
UPR1357	A		*R*	N.A.[d]	N.A.[d]
UPR1385	A			26.6	inactive
UPR1384	A			12.2	13.9
UPR1387	A			13.3	inactive
UPR1386	A			22.8	48.6
UPR1383	A			26	65.5
UPR1380	A			inactive	34.2
UPR1391	A			inactive	16
UPR1390	A			inactive	inactive
UPR1377	A			5.5	40.3
UPR1378	A			inactive	20.3
UPR1379	A			inactive	54.8

UPR1395	A	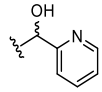		7	51.2
UPR1396	A			9.4	53.1
UPR1399	B	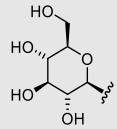	*S*	4	100
UPR1389	B		*R*	4.3	inactive
UCM1368	B		*S*	3.3	57.1
UCM1373	B		*R*	7.7	85.2
UCM1372	B	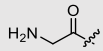	*S*	5.6	87.9
UCM1378	B		*R*	2.3	99.7
UCM1369	C		*S*	3.4	85.2
UCM1374	C		*R*	N.A.[d]	N.A.[d]
UCM1370	C		*S*	7.2	41.5
UCM1375	C		*R*	5.3	35
UCM1376	C		*R*	6.2	67.4
UPR1392	D		*S*	2.9	63.3
UPR1393	D		*R*	4.2	inactive
UCM1371	D		*S*	7.0	75.9
UCM1377	D		*R*	2.4	97.6

[a] Stereochemical configuration is reported only when assigned. For inferred configuration see paragraph 3.4.2. [b] KMS-11 human multiple myeloma cells were incubated with increasing concentrations of NSC12 derivatives for 48 h and viable cells were quantified by flow cytometry (propidium iodide staining).[c] KMS-11 human multiple myeloma cells were incubated with 6 μM concentration of the compounds for 6 h and data were collected by Western blotting after lysis. [d] N.A.: not available.

carboxylic acid couple, **UPR1380**, sharing the same configuration at C20 as **UPR1384**, was completely devoid of activity. The corresponding epimers, tertiary alcohol **UPR1385** and carboxylic acid **UPR1383**, showed the same inhibitory potency. When the *bis*-(trifluoromethyl)propanediol portion was maintained, compounds generally retained a good inhibitory activity on KMS-11 proliferation and some of them were more potent than the parent compound NSC12/UPR1358. For instance, compound **UPR1399** displayed an IC_{50} value in the proliferation assay comparable to that of NSC12 and was able to completely inhibit FGFR3 phosphorylation at the fixed concentration of 6 μM. Surprisingly, **UPR1399** epimer, **UPR1389**, displayed an IC_{50} value on cell proliferation comparable to that of NSC12, but was completely devoid of any inhibitory effect on FGFR3 phosphorylation: these data suggest that this compound could interfere with signaling pathways other than FGF/FGFR or that its effect could derive from a different mechanism. Compound **UCM1378** resulted more potent than NSC12 in both assays: interestingly, this compound had inverted C20 configuration if compared to NSC12, suggesting a limited influence of stereochemistry at C20 on inhibitory activity. **UCM1378** epimer, **UCM1372**, is among the most potent compounds as well. In the series of compounds featuring structures C and D, **UCM1369** and **UCM1377** resulted the most potent in both assays. As already observed for **UPR1399** and **UCM1378**, these compounds differed for their stereochemical configuration at C20. Analogously to **UPR1389**, compound **UPR1393** exerted a good activity in the proliferation inhibition assay, although being completely devoid of any inhibitory effect on FGFR3 phosphorylation.

4. Synthesis of zampanolide analogue NB-24

4.1. Microtubules as a target in cancer therapy

Cytoskeleton is a network of filamentous polymers and regulatory proteins involved in the maintenance of cell shape and internal organization and in fundamental processes such as division and movement.[246] Eukaryotic cells include three classes of filaments, which differ from one another for their size and composition, namely microtubules (MTs), the largest filaments, actin filaments, which are the thinnest ones, and intermediate filaments. Different polymers display diverse degrees of mechanical stiffness and rely on different assembly dynamics. Microtubules are the stiffest polymers in the cytoskeleton. They are composed of tubulin heterodimers (α and β subunits) and their polymerization occurs by a nucleation-elongation mechanism during which tubulin dimers add to the microtubule ends in a reversible and non-covalent manner (Fig.44).

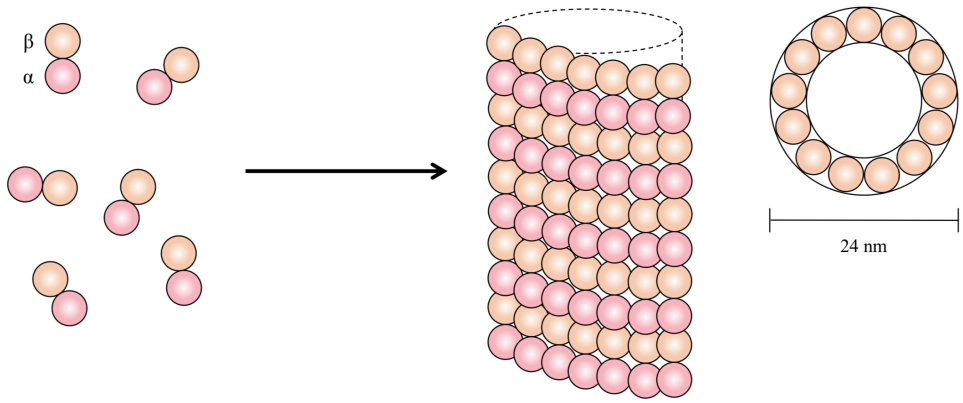

Figure 44: the assembly of tubulin heterodimers through different polymerization dynamics results in the formation of microtubules formed by 13 protofilaments, with an external diameter of 24 nm.[247]

During mitosis, MTs rearrange in a typical structure, called mitotic spindle, that allows segregation of chromosomes, preparing for cell division. The fundamental role of microtubules in mitosis renders these polymers an interesting target in the treatment of cancer and many agents affecting MTs structure and dynamics are successfully used in therapy.[247,248]

Various substances have been found to be able to bind to soluble tubulin and/or to tubulin in the MTs. Different compounds can exert different effects on MT polymerization dynamics and microtubule-targeted antimitotic agents are generally described as microtubule-destabilizing or microtubule-stabilizing agents. The former group includes compounds that inhibit MT polymerization, such as Vinca alkaloids, while the latter is composed by agents that stimulate polymerization, such as taxanes. Concentrations required for compounds from both classes to be able to modify microtubule mass are nevertheless not compatible with a therapeutic regimen. MT-targeting agents suppress microtubule dynamics at much lower concentrations and this effect results in the kinetic stabilization of microtubule, which is the most important feature responsible for their activity, leading to cell cycle arrest and apoptosis.[249,250] Microtubule Stabilizing Agents (MSAs), with the exception of laulimalide and peloruside A, all bind to the taxane binding site on β-tubulin, which is located on the inner surface of microtubules.[247]

Overexpression of membrane ATP-dependent drug efflux pumps is a well-described mechanism leading to resistance towards MT-targeting agents and many other drugs. It has been proposed that the use of covalent agents could circumvent resistance, as a drug that is covalently bound to its target cannot be pumped out of the cell by efflux pumps.[158,251]

4.2. Zampanolide: a covalent microtubule stabilizing agent

Zampanolide (**89**, Fig.45) is a natural compound that was firstly isolated in 1996 from the marine sponge *Fasciospongia rimosa*.[252] Its structure features a highly unsaturated, 20-membered macrolide ring and a rather unusual *N*-acyl hemiaminal side chain. When biological activity of zampanolide was investigated, the compound turned out to be an effective inhibitor of cancer cell proliferation, with *in vitro* IC_{50} values ranging between 1 and 5 ng/ml for different cell lines, including A549 (human lung carcinoma), P338 (leukemia), HT29 (human colon cancer) and MEL28 (human melanoma) cells.[252]

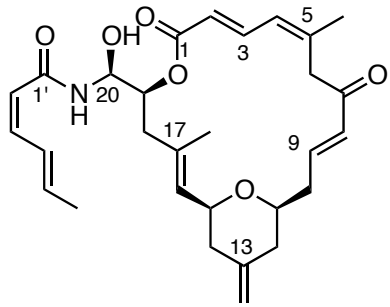

Figure 45: natural product zampanolide (**89**).

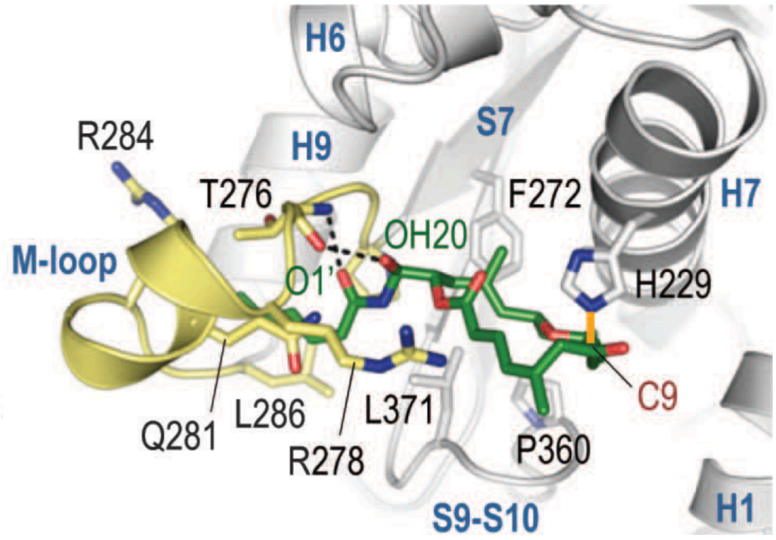

Figure 46: crystal structure of the complex between zampanolide (**89**, green sticks) and β-tubulin (gray cartoon). Interacting residues are shown in stick representation. Hydrogen bonds are indicated as black dashed lines. The covalent bond between C9 of zampanolide and His229 is shown as an orange line.[253]

The effect of zampanolide is associated with its interaction with components of the microtubule cytoskeleton. Zampanolide is actually an efficient promotor of tubulin assembly, resulting in cell cycle arrest in the G2/M phase.[254] The interaction of zampanolide with tubulin occurs at the taxane binding site *via* the formation of a covalent complex.[251,255] Asn228 and His229 have been identified as the amino acid residues reacting with zampanolide at C9 on the α,β-unsaturated ketone portion (Fig.46).[253]

In 2012, Altmann and coworkers reported their own total synthesis of zampanolide.[256] Their retrosynthetic approach includes an aza-aldol reaction, an intramolecular Horner-Wadsworth-Emmons (HWE) reaction and a Prins reaction as main steps required for the introduction of the side chain, for the macrolactonization and for the formation of the tetrahydropyran (THP) ring, respectively (Scheme 20).

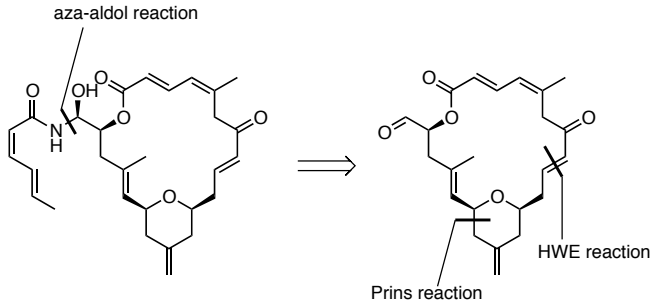

Scheme 20: retrosynthetic analysis for zampanolide, as proposed by Altmann and coworkers.

Structure-Activity Relationship (SAR) investigation for a series of zampanolide analogues revealed that only compounds carrying the same side chain and unsaturation pattern as the parent compound retained a good antitumor activity. Modifications on the tetrahydropyran ring were generally well tolerated (data not published).

4.3. Synthesis of **NB-24**

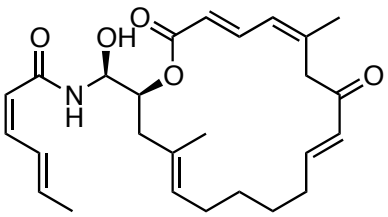

Figure 47: structure of the target compound **NB-24**.

The project presented in this Ph.D. thesis concerns the synthesis of a simplified zampanolide analogue (**NB-24**, Fig.47) featuring a methylene chain replacing the THP ring. This work has been performed during a secondment period in the group of Professor Altmann at the Department of Chemistry and Applied Biosciences at ETH Zürich.

Retrosynthetic analysis revealed that compound **NB-24** could be obtained according to the same synthetic strategy as described for the total synthesis of zampanolide, with insertion of the side chain as the last step, after HWE-based macrocyclization (Scheme 21).

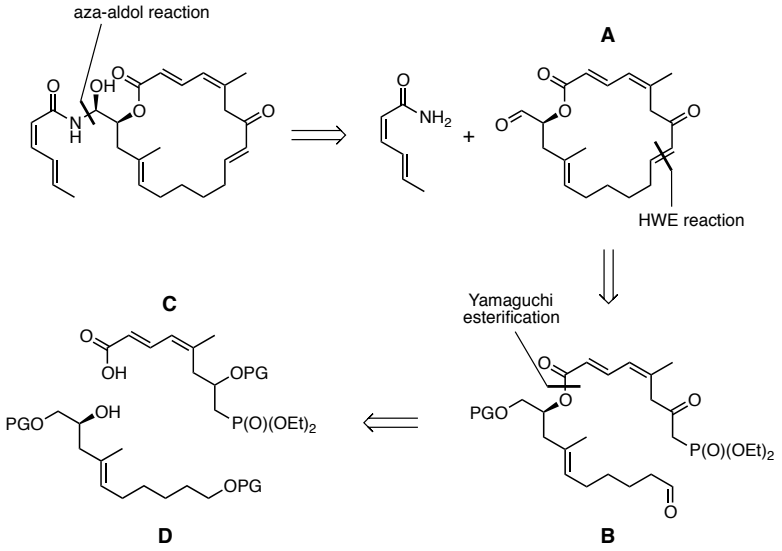

Scheme 21: retrosynthetic analysis for zampanolide analogue **NB-24** (PG: protecting group).

The synthesis of fragment **C** in the form of compound **90** (Fig.48) was already reported by Altmann and coworkers[256] and was therefore performed according to the published procedure.

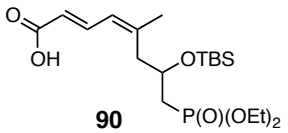

90

Figure 48: acid fragment **90**.

Retrosynthetic analysis for fragment **D** (Scheme 22) includes epoxide opening on protected (*S*)-glycidol **E** with lithiated vinyl iodide **F**. Fragment **F** was to be prepared through iodination of alkyne derivative **G**, which in turn could be prepared by a series of protection/substitution reactions from 1,5-pentanediol **I**.

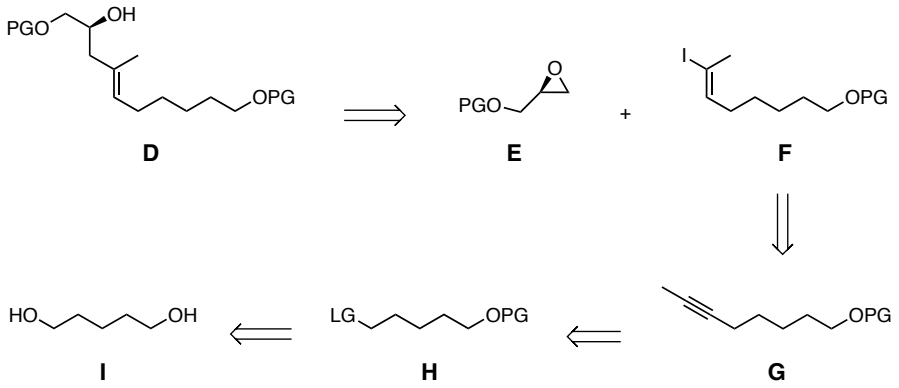

Scheme 22: retrosynthetic analysis for fragment **D** (PG: protecting group; LG: leaving group).

Synthesis of **NB-24** was performed as depicted in Scheme 23. Protection of 1,5-pentanediol (**91**) with *tert*-butyldiphenylchlorosilane (TBDPSCl) using sodium hydride as a base afforded monoprotected product **92** in good yields.[257] The second hydroxyl group was then tosylated under standard conditions to afford compound **93**. Finkelstein conditions were used for the conversion of **93** to iodide **94**, which was subsequently reacted with propyne under strongly basic conditions, yielding alkyne **95**.

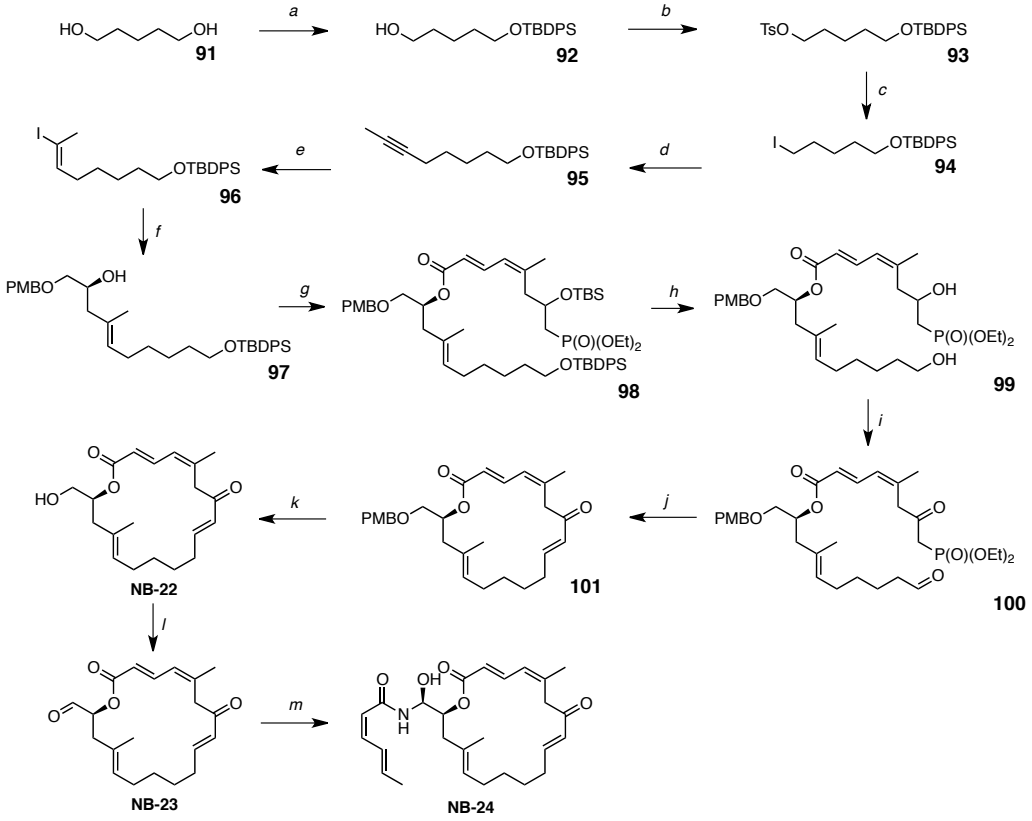

Scheme 23: synthesis of compound **NB-24**. Reagents and conditions: *a*) NaH, TBDPSCl, THF, r.t., 16 h, 64% yield; *b*) TsCl, pyridine, DCM, r.t., 16 h, 95% yield; *c*) NaI, acetone, r.t., 24 h, 98% yield; *d*) propyne, *n*-BuLi, HMPA, THF, -78 °C to r.t., 24 h, 97% yield; *e*) Cp_2ZrCl_2, DIBAL-H, THF, 65 °C, 1 h; then I_2, -78 °C, 15 min; *f*) (*S*)-2-(4-methoxy-benzyloxymethyl)-oxirane, *n*-BuLi, BF_3*OEt_2, toluene, -78 °C, 90 min, 42% yield (over two steps); *g*) compound **90**, 2,4,6-trichlorobenzoyl chloride, TEA, DMAP, toluene, r.t., 1 h, 86% yield; *h*) TBAF, THF, r.t., 4 h, 95% yield; *i*) DMP, DCM, r.t., 1 h, 49% yield; *j*) $Ba(OH)_2$, THF, H_2O, 0 °C to r.t., 1 h, 31% yield; *k*) DDQ, DCM, H_2O, r.t., 90 min, 83% yield; *l*) DMP, DCM, r.t., 90 min, 83% yield; *m*) (S)-BINOL, LAH, sorbamide, EtOH, THF, r.t., 30 min, 11% yield.

Conversion of the alkyne to vinyl iodide **96** was firstly attempted through a stannylcupration/iodination sequence.[258,259] Unfortunately, this method only allowed to obtain a 2:1 ratio of product **96** and its regioisomer **102** (Scheme 24).

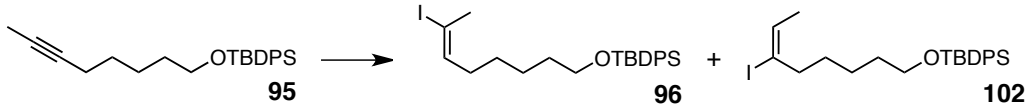

Scheme 24: synthesis of vinyl iodide **96** through stannylcupration/iodination sequence. Reagents and conditions: Bu_3SnH, *n*-BuLi, CuCN, THF, MeOH, -78 °C, then NIS, THF, -17 °C.

Conversion of **95** to **96** was then performed through a hydrozirconation/iodination sequence, which allowed to improve the yield of the desired regioisomer, although a small amount of compound **102** (about 8% as detected by ^{1}H-NMR) was still obtained. Hydrozirconation required the use of Schwartz's reagent (zirconocene hydrochloride)[260] (Fig.49), which was prepared *in situ* reacting zirconocene dichloride with DIBAL-H.[261] Alternatively, commercially available zirconocene hydrochloride could be used directly. Iodination of the alkenylzirconium intermediate with iodine yielded compound **96**.

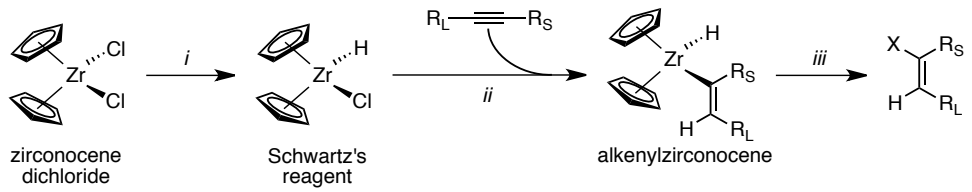

Figure 49: reaction of Schwartz's reagent with asymmetric alkynes and halogenation of the alkenylzirconocene intermediate: *i*) treatment of zirconocene dichloride with 1 eq. DIBAL-H yields the formation of zirconocene hydrochloride (Schwartz's reagent);[261] *ii*) hydrozirconation typically proceeds placing zirconium on the less-substituted carbon (R_L: large; R_S: small); *iii*) vinyl halides are obtained by electrophilic halogenation, reacting alkenylzirconocenes with iodine, bromine, iodobenzene dichloride, or *N*-halosuccinimide.[260,262]

After lithiation with either *n*-BuLi or *tert*-BuLi, vinyl iodide **96** was reacted with PMB-protected (*S*)-glycidol in toluene to afford compound **97** (Scheme 25), which was obtained in 42% yield from **95** over two steps.

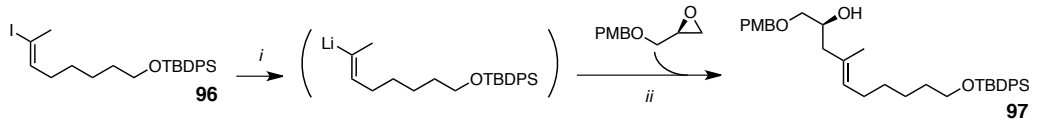

Scheme 25: synthesis of intermediate **97** starting from vinyl iodide **96**. Treatment of vinyl iodide with either *n*-BuLi or *tert*-BuLi (*i*) results in the formation of lithiated intermediate, which reacts with glycidol on the less hindered carbon, leading to epoxide opening (*ii*).

With intermediate **97** in hands, completion of the macrocyclic scaffold was performed by adapting the procedures reported for the synthesis of zampanolide. Esterification under Yamaguchi conditions allowed to obtain compound **98** in good yields. After removal of the silyl ether protecting groups with tetrabutylammonium fluoride (TBAF) (**99**) and oxidation of the hydroxyl groups with Dess-Martin periodinane (**100**), the macrolactone ring could be finally closed performing an intramolecular Horner-Wadsworth-Emmons reaction (**101**), using barium hydroxide as a base. Removal of the PMB-protecting group with 2,3-dichloro-5,6-dicyano-1,4-benzoquinone (DDQ) afforded intermediate **NB-22**, which could be oxidized to aldehyde **NB-23** employing Dess-Martin periodinane under standard conditions. Sorbamide side chain was inserted on the macrolactone scaffold through a stereoselective aza-aldol reaction, which was performed following an optimized procedure developed in the group of Professor Altmann, employing (*S*)-BINOL as a chiral bias and allowing to obtain the sole *S*-isomer of the *N*-acyl hemiaminal portion (**NB-24**), which was purified by reverse phase HPLC. Compounds **NB-22**, **NB-23** and **NB-24** will be tested for their biological activity, in particular for their antiproliferative effect on diverse cancer cell lines and their activity compared to that of zampanolide and its previously synthesized derivatives.

5. Conclusions

Demographic changes, including the growth and aging of population, and the spread of habits and conditions known as risk factors for the insurgence of neoplastic diseases, such as smoking, overweight and physical inactivity, have been associated with an increase in the occurrence of cancer in the last years.[263] According to GLOBOCAN estimates, in 2018 about 18.1 million new cancer cases have been diagnosed worldwide, and 9.6 million cancer deaths have occurred.[264] Insurgence and progression of tumors derive from the acquisition of peculiar features by cancer cells, among which a fundamental role is played by the ability to sustain chronic proliferation.

Stimuli leading to uncontrolled cell growth are largely conveyed by growth factors, which bind to their receptors on cell membranes and activate a plethora of downstream signals. Growth factors and their receptors thus represent a valuable target in the development of antiproliferative therapies, and many agents interfering with these signaling pathways have been already approved for clinical application in recent years. Epidermal Growth Factor Receptor (EGFR) and Fibroblast Growth Factor Receptor (FGFR) are two validated targets for the treatment of various cancer types. Among the diverse approaches developed so far to interfere with their aberrant activity, covalent inhibitors of their kinase domain have gained growing interest due to the possibility of circumventing acquired resistance and to maintain long-term inhibition of the catalytic activity. A typical structural feature of covalent, irreversible inhibitors is the presence of an acrylamide portion as the reactive warhead, which is responsible for the interaction with a cysteine residue within the binding site of receptor tyrosine kinases. Replacing the acrylamide with other functional groups could allow to modulate the reactivity of the covalent inhibitors, thus reducing potential

interaction with off-targets and occurrence of side effects. As a matter of fact, agents carrying substituted acetamides have already proven able to exert a prolonged inhibitory effect on EGFR autophosphorylation.[169] In this Ph.D. thesis, two classes of functionalized acetamides are presented as inhibitors of EGFR and FGFR, respectively.

In the first case, a series of quinazoline-based inhibitors with various warheads less reactive than acrylamide was synthesized adapting literature procedures and the compounds thus obtained were tested for their ability to inhibit EGFR autophosphorylation and cell proliferation on different cell lines. Compounds **UPR1303** (chloroacetamide) and **UPR1381** (*S*-imidazol-2-yl-thioacetamide) resulted the most promising agents in this series: they were able to inhibit EGFR autophosphorylation in A549 cells, harboring *wt*EGFR, and to interfere with gefitinib-resistant H1975 cell (harboring L858R activating mutation and T790M gatekeeper mutation) proliferation with a potency comparable (**UPR1381**) or superior (**UPR1303**) to that of reference acrylamide inhibitor. Quantitation of the intracellular concentration of these compounds 8 h after washing from the cell growth medium and time-dependency of IC_{50} values suggest that the long-term inhibition exerted by **UPR1303** and **UPR1381** could derive from a covalent interaction with their target. Interestingly, while chloroacetamide has already been reported to be able to covalently modify proteins, the warhead of **UPR1381** is not included in the structure of any other kinase inhibitor reported in the literature. Despite the negligible reactivity of **UPR1381** in a purely chemical environment, its prolonged effect in cell-based assays suggests that modulation of the warhead reactivity can actually allow to obtain effective, irreversible inhibitors, for which a better safety profile can be expected.

As far as FGFR inhibitors are concerned, a series of analogues of acrylamide-based inhibitor FIIN-2 was prepared according to procedures reported for the synthesis of the parent compound. Chloroacetamide **UPR1376** revealed to be a

promising inhibitor of FGFR autophosphorylation in LENTI-4 cells and inhibited the proliferation of BGJ-resistant clones, which were not affected by FIIN-2. In this case, other 2-substituted acetamides did not exert long-term inhibition of receptor phosphorylation as observed in the class of EGFR inhibitors, but the good results obtained for **UPR1376** suggest that exploration of different substituents on the acetamide portion could actually allow to achieve prolonged inhibition of the target.

A further class of kinase inhibitors is presented, which was designed to inhibit EGFR T790M/C797S mutant: the replacement of the cysteine residue with serine is reported to cause resistance to third-generation inhibitors and forces the search for new chemotypes interacting with different amino acid residues, e.g., the conserved Lys745 residue. Biological data for the synthesized compounds **UPR1423**, **UPR1424** and **UPR1425** are still not available. However, the synthetic strategies employed for their preparation proved to be easily scalable and the optimized reaction conditions devised in the framework of this Ph.D. research period could be readily adapted to the synthesis of new inhibitors, based on the activity data obtained for the compounds presented herein.

Moreover, another approach has been followed in order to target FGF/FGFR-dependent proliferation, that is, the synthesis of a series of FGF traps: these compounds are not intended to directly bind and inhibit the kinase portion, but to interact with FGFs in the extracellular environment and to avoid the formation of FGF/FGFR/HSPG signaling complexes. Based on the promising biological activity of NSC12, a series of analogues featuring modifications on the C17 side chain or on position 3 of the steroid scaffold were synthesized. Biological data obtained for these compounds allowed to assess the fundamental role played by the 1,1-*bis*-trifluoromethyl-1,3-propanediol group in determining the inhibitory activity of these products. Moreover, a reduced impact of the stereochemical

configuration at C20 on the biological activity was highlighted, compared to the previously available information coming from a limited set of data.

Despite the burgeoning interest in the field of kinase inhibitors, cancer therapy has been relying on many different targets in the last decades. Among them, a pivotal role is played by microtubules, the dynamic properties of which are modified by many successful drugs, such as Vinca alkaloids and taxanes. In this Ph.D. thesis, the synthesis of a simplified analogue of microtubule stabilizing agent zampanolide is presented. The obtained compound, **NB-24**, features a methylene linker replacing the tetrahydropyran ring included in the structure of the parent compound. This work integrates into a wider SAR investigation project and biological data obtained for **NB-24** and its precursors will furnish a deeper knowledge on the role of different substructures in determining the potency of zampanolide and its analogues.

6. Experimental Section

6.1. General procedures

Reagents were obtained from commercial suppliers and used without further purification. Solvents were purified and stored according to standard procedures. Anhydrous reactions were conducted under a positive pressure of dry N_2 or Ar, and using standard syringe/septa techniques. Reactions were monitored by TLC, on Kieselgel 60 F 254 (DC-Alufolien, Merck). Final compounds and intermediates were purified by flash chromatography (SiO_2 60, 40−63 μm). Melting points were determined with a Gallenkamp melting point apparatus and are uncorrected. NMR spectra were recorded on a Bruker 300 MHz Avance, Bruker 400 MHz Avance or Bruker 500 MHz Avance spectrometer; chemical shifts (δ scale) are reported in parts per million relative to the central peak of the solvent. ^{1}H NMR spectra are reported in the following order: multiplicity, approximate coupling constant (*J* value) in hertz, and number of protons; signals are characterized as s (singlet), d (doublet), dd (doublet of doublets), t (triplet), dt (doublet of triplets), q (quartet), m (multiplet), and br s (broad signal). All ^{13}C NMR spectra were measured with complete proton decoupling. Mass spectra of final compounds were recorded using a Thermo Scientific LTQ Orbitrap XL. Mass spectra for compounds prepared at ETH-Zürich (**92 - NB-24**) were recorded by the ETH Zurich MS service on a Bruker Daltonics maxis (UHR-TOF). Infrared spectra (IR) were recorded on a Jasco FT/IR-6200 instrument as thin film. Resonance frequencies are given as wavenumbers in cm^{-1}. Optical rotation analysis was performed using a PerkinElmer 341 polarimeter, the concentration *c* of analytes being reported as mg/mL. Optical rotations for compounds **97** – **NB-24** were measured on a Jasco P-1020 polarimeter, concentrations are reported as g/100 mL. All tested compounds (herein reported with UPR-code) were > 95% pure by HPLC/UV or HPLC/MS analysis.

6.2.1. Anilinoquinazoline-based inhibitors

Ethyl 4-hydroxy-3-nitrobenzoate (14). Concentrated nitric acid (3 ml, 71.90 mmol) is added to a solution of 4-hydroxybenzoate (**13**, 7.58 g, 45.61 mmol) in acetic acid (85 ml). The solution is stirred at 40 °C for 2 h and then cooled back to room temperature and poured into a water/ice mixture. The precipitate is recovered by suction filtration and dissolved in AcOEt. The obtained solution is washed with brine and dried over Na_2SO_4 and the solvent is removed under reduced pressure, affording the title compound (9.20 g, 96%) in the form of yellow crystals. Analytical data are in accordance with those reported in the literature.[265]

Ethyl 3-acetamido-4-hydroxybenzoate (15). To a solution of ethyl 4-hydroxy-3-nitrobenzoate (**14**, 6.84 g, 32.39 mmol) in THF (50 ml) are added $Pd(OAc)_2$ (219.1 mg, 0.98 mmol), activated charcoal (2.20 g), Et_3SiH (360 µl, 2.26 mmol) and HCOOLi (12.46 g, 178.13 mmol). The mixture is stirred at room temperature for 1 h, then it is cautiously filtered with suction and solvents are removed by the filtrate by rotary evaporation. Acetic acid (50 ml) is added to the residue and the mixture is warmed to 60 °C. Acetic anhydride (4.6 ml, 48.75 mmol) is consequently added. The suspension is slowly allowed to cool to room temperature and then poured into an ice/water mixture. Filtration of the precipitate affords the title compound (6.71 g, 93%) as a white solid. Analytical data are in accordance with those reported in the literature.[266]

Ethyl 3-acetamido-4-ethoxybenzoate (16). A suspension of ethyl 3-acetamido-4-hydroxybenzoate (**15**, 6.71 g, 30.07 mmol), K_2CO_3 (6.70 g, 48.48 mmol) and ethylbromide (2.8 ml, 37.51 mmol) in DMF (30 ml) is stirred at 60 °C for 4 h. The mixture is then allowed to cool to room temperature and poured into an ice/water mixture. The precipitate is recovered by suction filtration and dried to afford the title compound (6.92 g, 92%) as a white solid. Mp: 99-100 °C. ^{1}H NMR (300 MHz, $CDCl_3$)

δ 8.98 (d, *J* = 1.4 Hz, 1H), 7.78 (dd, *J* = 8.6, 2.0 Hz, 1H), 7.71 (bs, 1H), 6.88 (d, *J* = 8.6 Hz, 1H), 4.35 (q, *J* = 7.1 Hz, 2H), 4.17 (q, *J* = 7.0 Hz, 2H), 2.22 (s, 3H), 1.49 (t, *J* = 7.0 Hz, 3H), 1.38 (t, *J* = 7.1 Hz, 3H).

Ethyl 5-acetamido-4-ethoxy-2-nitrobenzoate (17). A mixture of acetic acid (42 ml, 734.39 mmol), fuming nitric acid (5.4 ml, 129.67 mmol) and acetic anhydride (5.4 ml, 57.23 mmol) is cautiously added to solid ethyl 3-acetamido-4-ethoxybenzoate (**16**, 6.92 g, 27.55 mmol), maintaining the suspension at 0 °C. The solution is slowly warmed to room temperature and stirred for 15 min. AcOEt (200 ml) is then added to dilute the solution and the mixture is washed with water and brine. The organic layer is dried over Na_2SO_4 and solvents are removed under reduced pressure. Trituration of the residue with diethyl ether affords, after drying, the title compound (8.06 g, 98%) as a white solid. Mp: 117-119 °C. ^{1}H NMR (400 MHz, $CDCl_3$) δ 8.73 (s, 1H), 7.94 (s, 1H), 7.44 (s, 1H), 4.37 (q, *J* = 7.2 Hz, 2H), 4.22 (q, *J* = 6.9 Hz, 2H), 2.26 (s, 3H), 1.53 (t, *J* = 6.9 Hz, 3H), 1.36 (t, *J* = 7.0 Hz, 3H).

Ethyl 5-acetamido-2-amino-4-ethoxybenzoate (18). Ethyl 5-acetamido-4-ethoxy-2-nitrobenzoate (**17**, 8.04 g, 27.13 mmol) is dissolved in a mixture of EtOH:AcOH:H_2O = 70:15:15 (100 ml) and iron powder (15.3 g, 273.95 mmol) is added. After stirring at room temperature for 15 min, the mixture is diluted with AcOEt (200 ml) and filtered. The filtrate is washed with water and brine, the organic layer is dried over Na_2SO_4 solvents are removed under reduced pressure, affording the title compound (5.74 g, 79%) as a yellow, crystalline solid. Mp: 122-124 °C. ^{1}H NMR (400 MHz, DMSO-d_6) δ 8.77 (s, 1H), 7.97 (s, 1H), 6.60 (s, 2H), 6.34 (s, 1H), 4.20 (q, *J* = 7.1 Hz, 2H), 4.01 (q, *J* = 7.0 Hz, 2H), 1.99 (s, 3H), 1.35 (t, *J* = 6.9 Hz, 3H), 1.27 (t, *J* = 7.1 Hz, 3H).

6-Acetamido-7-ethoxyquinazolin-4-one (19). A solution of ethyl 5-acetamido-2-amino-4-ethoxybenzoate (**18**, 5.74 g, 21.56 mmol), ammonium acetate (6.66 g, 86.37 mmol) and methyl orthoformate (9.4 ml, 85.92 mmol) in diglyme (100 ml) is stirred at reflux for 90 min. The mixture is then allowed to cool to room temperature and the solid

residue is recovered by suction filtration and dried to afford the title compound (4.47 g, 84%) as a white solid. Mp: 310 °C (dec.). ^{1}H NMR (300 MHz, DMSO-d_6) δ 11.92 (bs, 1H), 9.19 (s, 1H), 8.74 (s, 1H), 7.99 (s, 1H), 7.16 (s, 1H), 4.26 (q, J = 6.9 Hz, 2H), 2.16 (s, 3H), 1.44 (t, J = 6.9 Hz, 3H).

6-Acetamido-4-chloro-7-ethoxyquinazoline (20). A suspension of 6-acetamido-7-ethoxyquinazolin-4-one (**19**, 4.47 g, 18.08 mmol) in neat $POCl_3$ (16.8 ml, 179.71 mmol) is stirred at reflux 45 min. After cooling to room temperature and removing the volatile material under reduced pressure, DCM is added to the residue. The mixture is cooled to 0 °C and a saturated aqueous solution of $NaHCO_3$ is slowly added to a final pH=8. The phases are separated and the organic layer is washed with water and brine, dried over Na_2SO_4 and concentrated under reduced pressure, affording the title compound (4.14 g, 86%) as a white solid. Mp: 178-180 °C. ^{1}H NMR (300 MHz, $CDCl_3$) δ 9.24 (s, 1H), 8.88 (s, 1H), 8.07 (s, 1H), 7.33 (s, 1H), 4.34 (q, J = 6.6 Hz, 2H), 2.32 (s, 3H), 1.60 (t, J = 6.6 Hz, 3H).

6-Acetamido-4-(3-chloro-4-fluoroaniline)-7-ethoxyquinazoline (21). 6-acetamido-4-chloro-7-ethoxyquinazoline (**20**, 4.14 g, 15.58 mmol) is suspended in 2-propanol (50 ml). 3-chloro-4-fluoroaniline (2.69 g, 18.48 mmol) and HCl 1M (780 µl, 0.78 mmol) are added and the mixture is stirred at reflux for 45 min. The mixture is allowed to cool to room temperature. The precipitate is recovered by suction filtration and dried to afford the title compound (5.63 g, 96%) as a yellow solid. Mp: 249-250 °C. ^{1}H NMR (300 MHz, CD_3OD) δ 9.06 (s, 1H), 8.72 (s, 1H), 7.91 (dd, J = 6.6, 2.6 Hz, 1H), 7.64 (m, 1H), 7.35 (t, J = 8.9 Hz, 1H), 7.27 (s, 1H), 4.40 (q, J = 7.0 Hz, 2H), 2.31 (s, 3H), 1.59 (t, J = 7.0 Hz, 3H).

6-Amino-4-(3-chloro-4-fluoroaniline)-7-ethoxyquinazoline (22). A solution of KOH (1.61 g, 28.62 mmol) in water (3 ml) is added to a suspension of 6-acetamido-4-(3-chloro-4-fluoroaniline)-7-ethoxyquinazoline (**21**, 995 mg, 2.65 mmol) in 1-propanol (100 ml). After stirring the mixture at reflux for 2 h and allowing it to cool back to room

temperature, acetic acid is added until neutralization. The solvents are removed under reduced pressure and the residue is purified by silica gel column chromatography (AcOEt/hexane 4:1) to afford the title compound (647 mg, 73%) as a pale yellow solid. Mp: 208-209 °C. ^{1}H NMR (300 MHz, DMSO-d_6) δ 9.39 (s, 1H), 8.36 (s, 1H), 8.19 (dd, J = 6.9, 2.5 Hz, 1H), 7.80 (m, 1H), 7.39 (t, J = 9.0 Hz, 1H), 7.38 (s, 1H), 7.07 (s, 1H), 5.35 (s, 2H), 4.22 (q, J = 6.9 Hz, 2H), 1.44 (t, J = 6.9 Hz, 3H).

2-Chloro-*N*-(4-((3-chloro-4-fluorophenyl)amino)-7-ethoxyquinazolin-6-yl)acetamide (UPR1303). To a solution of chloroacetic acid (355 mg, 3.76 mmol) in anhydrous THF (5 ml) are added DIPEA (650 µl, 3.73 mmol) and pivaloyl chloride (460 µl, 3.73 mmol). After stirring at room temperature for 30 min, a solution of 6-amino-4-(3-chloro-4-fluoroaniline)-7-ethoxyquinazoline (**22**, 227 mg, 0.68 mmol) in anhydrous THF (3 ml) is added and the suspension is stirred for 2 h before being diluted with water. The mixture is extracted with AcOEt and the organic layer is washed with water and brine, dried over Na_2SO_4 and concentrated under reduced pressure. Purification of the solid residue by silica gel column chromatography (AcOEt/hexane 4:1) affords the title compound (231 mg, 83%) as a white solid. Mp: 278 °C (dec.). ^{1}H NMR (300 MHz, DMSO-d_6) δ 9.86 (s, 1H), 9.74 (s, 1H), 8.87 (d, J = 3.9 Hz, 1H), 8.53 (s, 1H), 8.10 (dd, J = 6.8, 2.6 Hz, 1H), 7.78 (ddd, J = 9.0, 4.3, 2.6 Hz, 1H), 7.42 (t, J = 9.1 Hz, 1H), 7.29 (s, 1H), 4.49 (d, J = 1.5 Hz, 2H), 4.30 (q, J = 6.9 Hz, 2H), 1.45 (t, J = 7.0 Hz, 3H). ^{13}C NMR (75 MHz, DMSO-d_6) δ 165.04, 156.89, 154.84, 154.28, 154.03, 151.63, 149.11, 136.73, 126.59, 123.75, 122.61 (d, J = 6.8 Hz), 118.80, 116.43 (d, J = 21.5 Hz), 115.57, 108.73, 107.37, 64.64, 43.33, 14.24. HRMS (ESI): m/z: calcd for $C_{18}H_{15}Cl_2FN_4O_2$ [$(M+H)^+$]: 409.06289; found: 409.06291.

***N*-(4-((3-Chloro-4-fluorophenyl)amino)-7-ethoxyquinazolin-6-yl)-2-(pyridin-3-ylthio)acetamide (UPR1375).** A solution of 3-pyridylmercaptoacetic acid[181] (142 mg, 0.84 mmol) and triethylamine (0.12 ml, 0.58 mmol) in DMF (6 ml) is cooled to 0 °C and TBTU (275 mg, 0.85 mmol) is added. The mixture is stirred for 30 min, then added with 6-amino-4-(3-chloro-4-fluoroaniline)-7-ethoxyquinazoline (**22**, 160 mg, 0.48

mmol) and warmed to 40 °C. After stirring for 4 h, the solution is allowed to cool to room temperature and diluted AcOEt. The organic layer is washed with water and brine, dried over Na_2SO_4 and concentrated under reduced pressure. Purification of the solid residue by silica gel column chromatography (AcOEt/MeOH 9:1) affords the title compound (58 mg, 25%) as a white solid. Mp: 210 °C. ^{1}H NMR (300 MHz, $CDCl_3/CD_3OD$) δ 8.81 (s, 1H), 8.65 (s, 1H), 8.49 (s, 1H),), 8.44 (s, 1H), 7.99 – 7.82 (m, 2H), 7.65 – 7.54 (m, 1H), 7.38 (dd, *J* = 8.3, 4.6 Hz, 1H), 7.24 – 7.10 (m, 2H), 4.30 (q, *J* = 6.9 Hz, 2H), 4.00 (s, 2H), 1.54 (t, *J* = 6.9 Hz, 3H). ^{13}C NMR (75 MHz, $CDCl_3/CD_3OD$) δ 167.82, 158.35, 157.14, 154.68, 153.89, 150.11, 148.72, 148.19, 138.50, 136.23, 127.66, 125.38, 123.15 (d, *J* = 6.7 Hz), 121.15 (d, *J* = 18.5 Hz), 116.90 (d, *J* = 22.2 Hz), 112.07, 109.78, 106.86, 65.79, 39.07, 14.63, 0.04. HRMS (ESI): m/z: calcd for $C_{23}H_{19}ClFN_5O_2S$ [$(M+H)^+$]: 484.10048; found: 484.10043.

***N*-(4-((3-Chloro-4-fluorophenyl)amino)-7-ethoxyquinazolin-6-yl)-3-(pyridin-3-yl)propenamide (UPR1382).** 3-pyridin-3-yl-propionic acid (338 mg, 2.24 mmol) is suspended in thionyl chloride (3.3 ml, 45.5 mmol) and DMF (9 µl, 0.12 mmol) is added. The mixture is stirred at reflux for 1 h, then allowed to cool to room temperature. After removing the volatile material by rotary evaporation, the residue is dissolved in anhydrous THF (3 ml) and added to a solution of 6-amino-4-(3-chloro-4-fluoroaniline)-7-ethoxyquinazoline (**22**, 194 mg, 0.58 mmol). Pyridine (230 µl, 2.84 mmol) is added. The mixture is stirred at room temperature for 16 h, then diluted with AcOEt, washed with water and brine. The organic layer is dried over Na_2SO_4 and concentrated under reduced pressure. Purification of the solid residue by silica gel column chromatography (DCM + 5% MeOH(NH_3)) affords the title compound (105 mg, 39%) as a white solid. Mp: 241 °C. ^{1}H NMR (300 MHz, $CDCl_3/CD_3OD$) δ 8.81 (s, 1H), 8.64 – 8.45 (m, 2H), 8.45 – 8.29 (m, 1H), 7.93 (dd, *J* = 6.6, 2.6 Hz, 1H), 7.75 (dt, *J* = 7.9, 2.0 Hz, 1H), 7.62 (ddd, *J* = 9.0, 4.2, 2.6 Hz, 1H), 7.35 (dd, *J* = 7.9, 4.9 Hz, 1H), 7.27 – 7.02 (m, 2H), 4.30 (q, *J* = 7.0 Hz, 2H), 3.14 (t, *J* = 7.4 Hz, 2H), 2.92 (t, *J* = 7.3 Hz, 2H), 1.55 (t, *J* = 6.9 Hz, 3H). ^{13}C NMR (75 MHz, $CDCl_3/CD_3OD$) δ 158.16, 156.98, 154.39, 149.50, 148.21, 147.45, 137.49, 137.24, 127.88, 125.16, 124.47, 122.87 (d, *J* = 6.8 Hz), 116.82 (d, *J* =

22.1 Hz), 112.06, 109.60, 106.56, 65.58, 38.48, 28.75, 14.51. HRMS (ESI): m/z: calcd for $C_{24}H_{21}ClFN_5O_2$ [$(M+H)^+$]: 466.14406; found: 466.14368.

***N*-(4-((3-Chloro-4-fluorophenyl)amino)-7-ethoxyquinazolin-6-yl)-2-((1-methyl-1*H*-imidazol-2-yl)thio)acetamide (UPR1364).** To a solution of 2-mercapto-1-methylimidazole (26 mg, 0.23 mmol) and sodium hydroxide (9.5 mg, 0.24 mmol) in THF (2 ml) is added 6-(chloroacetamido)-4-(3-chloro-4-fluoroaniline)-7-ethoxyquinazoline (**UPR1303**, 65 mg, 0.16 mmol). The mixture is stirred at 45 °C for 2 h, then it is allowed to cool to room temperature and diluted with AcOEt. The organic layer is washed with water, saturated aqueous $NaHCO_3$ and brine, dried over Na_2SO_4 and concentrated under reduced pressure. Purification of the solid residue by silica gel column chromatography (AcOEt) affords the title compound (24 mg, 31%) as a white solid. Mp: 215-217 °C. ^{1}H NMR (300 MHz, DMSO-d_6) δ 10.14 (s, 1H), 9.83 (s, 1H), 8.93 (s, 1H), 8.51 (s, 1H), 8.09 (dd, J = 6.9, 2.6 Hz, 1H), 7.77 (ddd, J = 9.1, 4.3, 2.6 Hz, 1H), 7.41 (t, J = 9.1 Hz, 1H), 7.33 – 7.20 (m, 2H), 7.00 (d, J = 1.3 Hz, 1H), 4.29 (q, J = 7.0 Hz, 2H), 4.06 (s, 2H), 3.60 (s, 3H), 1.42 (t, J = 7.0 Hz, 3H). ^{13}C NMR (75 MHz, DMSO-d_6) δ 167.22, 156.84, 154.76, 153.75, 153.60, 136.83, 128.39, 127.33, 123.67, 123.55, 122.55 (d, J = 6.7 Hz), 116.40 (d, J = 21.5 Hz), 113.85, 108.83, 107.18, 64.56, 37.44, 32.85, 14.22. HRMS (ESI): m/z: calcd for $C_{22}H_{20}ClFN_6O_2S$ [$(M+H)^+$]: 487.11138; found: 487.11123.

2-((1*H*-Imidazol-2-yl)thio)-*N*-(4-((3-chloro-4-fluorophenyl)amino)-7-ethoxyquinazolin-6-yl)acetamide (UPR1381). Triethylamine (320 µl, 2.30 mmol) is added to a solution of 2-mercaptoimidazole (231 mg, 2.31 mmol) and 6-(chloroacetamido)-4-(3-chloro-4-fluoroaniline)-7-ethoxyquinazoline (**UPR1303**, 94 mg, 0.23 mmol) in THF (6 ml). The mixture is stirred at 50 °C for 2 h, then it is allowed to cool to room temperature, diluted with AcOEt and washed with water, saturated aqueous $NaHCO_3$ and brine. The organic layer is dried over Na_2SO_4 and concentrated under reduced pressure. Purification of the solid residue by crystallization from EtOH/water 7:3 affords the title compound (97 mg, 89%) as a white solid. Mp: 243 °C.

^{1}H NMR (300 MHz, $CDCl_3/CD_3OD$) δ 8.75 (s, 1H), 8.38 (s, 1H), 7.83 (dd, *J* = 6.6, 2.6 Hz, 1H), 7.54 – 7.46 (m, 1H), 7.17 – 7.03 (m, 2H), 6.99 (s, 2H), 4.21 (q, *J* = 7.0 Hz, 2H), 3.89 (s, 2H), 1.44 (t, *J* = 7.0 Hz, 3H). ^{13}C NMR (75 MHz, DMSO-d_6) δ 167.50, 156.84, 154.77, 153.73, 153.56, 151.56, 148.68, 139.06, 136.89, 127.40, 123.64, 122.51 (d, *J* = 7.0 Hz), 118.78, 116.39 (d, *J* = 21.5 Hz), 113.71, 108.86, 107.13, 64.57, 36.99, 14.22. HRMS (ESI): m/z: calcd for $C_{21}H_{18}ClFN_6O_2S$ [$(M+H)^+$]: 473.09573; found: 473.09570.

2-(Benzo[*d*]thiazol-2-ylthio)-*N*-(4-((3-chloro-4-fluorophenyl)amino)-7-ethoxyquinazolin-6-yl)acetamide (UPR1365). 6-(chloroacetamido)-4-(3-chloro-4-fluoroaniline)-7-ethoxyquinazoline (**UPR1303**, 61 mg, 0.15 mmol) is added to a solution of 2-mercaptobenzothiazole (25 mg, 0.15 mmol) and sodium hydroxide (6.0 mg, 0.15 mmol) in THF (2 ml). The mixture is stirred at room temperature for 1 h, then it is diluted with AcOEt and washed with water, saturated aqueous $NaHCO_3$ and brine. The organic layer is dried over Na_2SO_4 and concentrated under reduced pressure. Purification of the solid by silica gel column chromatography (AcOEt/hexane 4:1), followed by crystallization from 1,2-dichloroethane, affords the title compound (15 mg, 19%) as white slender needles. Mp: 203-204 °C. ^{1}H NMR (300 MHz, DMSO-d_6) δ 9.86 (s, 1H), 9.82 (s, 1H), 8.89 (s, 1H), 8.50 (s, 1H), 8.07 - 8.01 (m, 2H), 7.86 (d, *J* = 8.0 Hz, 1H), 7.74 (ddd, *J* = 9.1, 4.4, 2.6 Hz, 1H), 7.48 (td, *J* = 8.2, 7.7, 1.4 Hz, 1H), 7.44 – 7.33 (m, 2H), 7.25 (s, 1H), 4.54 (s, 2H), 4.25 (q, *J* = 7.0 Hz, 2H), 1.36 (t, *J* = 6.9 Hz, 3H). ^{13}C NMR (75 MHz, DMSO-d_6) δ 166.07 (d, *J* = 7.2 Hz), 156.97, 154.94, 153.93, 152.57, 151.72, 148.92, 136.80 (d, *J* = 3.0 Hz), 134.95, 127.12, 126.60, 124.79, 123.86, 122.74 (d, *J* = 6.9 Hz), 122.02, 121.24, 118.76 (d, *J* = 18.6 Hz), 116.50 (d, *J* = 21.5 Hz), 114.70, 108.85, 107.32, 64.72, 37.34, 14.19. HRMS (ESI): m/z: calcd for $C_{25}H_{19}ClFN_5O_2S_2$ [$(M+H)^+$]: 540.07255; found: 540.07226.

***N*-(4-((3-Chloro-4-fluorophenyl)amino)-7-ethoxyquinazolin-6-yl)-2-((5-methoxybenzo[*d*]thiazol-2-yl)thio)acetamide (UPR1366).** 6-(chloroacetamido)-4-(3-chloro-4-fluoroaniline)-7-ethoxyquinazoline (**UPR1303**, 86 mg, 0.21 mmol) is added to a solution of 2-mercapto-5-methoxybenzothiazole (118.5 mg, 0.60 mmol) and sodium

hydroxide (24.7 mg, 0.62 mmol) in THF (4 ml). The mixture is stirred at room temperature for 1 h, then it is diluted with AcOEt and washed with water, saturated aqueous $NaHCO_3$ and brine. The organic layer is dried over Na_2SO_4 and concentrated under reduced pressure. Purification of the solid residue by silica gel column chromatography (AcOEt/hexane 4:1), followed by crystallization from 1,2-dichloroethane, affords the title compound (23 mg, 19%) as a white crystalline solid. Mp: 202-203 °C. ^{1}H NMR (300 MHz, DMSO-d_6) δ 9.83 (d, J = 3.2 Hz, 2H), 8.90 (s, 1H), 8.51 (s, 1H), 8.08 (dd, J = 6.9, 2.6 Hz, 1H), 7.89 (d, J = 8.8 Hz, 1H), 7.76 (ddd, J = 9.0, 4.3, 2.6 Hz, 1H), 7.49 – 7.33 (m, 2H), 7.27 (s, 1H), 7.02 (dd, J = 8.8, 2.5 Hz, 1H), 4.53 (s, 2H), 4.27 (q, J = 6.9 Hz, 2H), 3.82 (s, 3H), 1.38 (t, J = 6.9 Hz, 3H). ^{13}C NMR (75 MHz, DMSO-d_6) δ 166.95, 165.85, 158.74, 156.85, 154.80, 153.83, 151.58, 148.92, 136.77 (d, J = 3.2 Hz), 127.01, 126.42, 123.73, 122.60 (d, J = 6.8 Hz), 122.21, 118.63 (d, J = 18.3 Hz), 116.39 (d, J = 21.6 Hz), 114.66, 113.83, 108.78, 107.32, 104.59, 64.60, 55.52, 37.25, 14.13. HRMS (ESI): m/z: calcd for $C_{26}H_{21}ClFN_5O_5S_2$ [$(M+H)^+$]: 570.08311; found: 570.08297.

***N*-(4-((3-Chloro-4-fluorophenyl)amino)-7-ethoxyquinazolin-6-yl)-2-((1-methyl-1*H*-benzo[*d*]imidazol-2-yl)thio)acetamide (UPR1374).** 6-(chloroacetamido)-4-(3-chloro-4-fluoroaniline)-7-ethoxyquinazoline (**UPR1303**, 78 mg, 0.19 mmol) is added to a solution of 1-methylbenzimidazole (95 mg, 0.58 mmol) and sodium hydroxide (39 mg, 0.97 mmol) in THF (4 ml). The mixture is stirred at room temperature for 1 h, then it is diluted with AcOEt and washed with water, saturated aqueous $NaHCO_3$ and brine. The organic layer is dried over Na_2SO_4 and concentrated under reduced pressure. Purification of the solid residue by silica gel column chromatography (DCM + 1.5% MeOH(NH_3)) affords the title compound (56 mg, 54%) as a white solid. Mp: 226 °C. ^{1}H NMR (300 MHz, DMSO-d_6) δ 10.00 (s, 1H), 9.82 (s, 1H), 8.93 (s, 1H), 8.50 (s, 1H), 8.08 (dd, J = 6.9, 2.6 Hz, 1H), 7.76 (ddd, J = 9.1, 4.3, 2.6 Hz, 1H), 7.60 – 7.49 (m, 2H), 7.41 (t, J = 9.1 Hz, 1H), 7.26 – 7.17 (m, 3H), 4.46 (s, 2H), 4.22 (q, J = 7.0 Hz, 2H), 3.75 (s, 3H), 1.28 (t, J = 6.9 Hz, 3H). ^{13}C NMR (75 MHz, DMSO-d_6) δ 166.59, 156.82, 154.77, 153.78, 153.59, 151.55, 151.15, 148.74, 142.55, 136.95, 136.81, 127.15, 123.65, 122.52

(d, J = 6.8 Hz), 121.70 (d, J = 10.9 Hz), 117.49, 116.38 (d, J = 21.7 Hz), 114.25, 109.59, 108.80, 107.19, 64.52, 36.08, 30.00, 13.95. HRMS (ESI): m/z: calcd for $C_{26}H_{22}ClFN_6O_2S$ [$(M+H)^+$]: 537.12703; found: 537.12658.

***N*-(4-((3-Chloro-4-fluorophenyl)amino)-7-ethoxyquinazolin-6-yl)-2-(pyridin-2-ylthio)acetamide (UPR1361).** Sodium hydroxide (64.5 mg, 1.61 mmol) is suspended in THF (3 ml) and 2-mercaptopyridine (174 mg, 1.57 mmol) is added. To the clear solution is then added 6-(chloroacetamido)-4-(3-chloro-4-fluoroaniline)-7-ethoxyquinazoline (**UPR1303**, 61.4 mg, 0.15 mmol). After stirring the mixture at room temperature for 1 h, AcOEt and water are added, the layers are separated and the organic layer is washed with water, saturated aqueous $NaHCO_3$ and brine, dried over Na_2SO_4 and concentrated under reduced pressure. Trituration of the solid residue with AcOEt affords the title compound (44 mg, 61%) as a white powder. Mp: 225 °C (dec.). ^{1}H NMR (300 MHz, $CDCl_3$/CD_3OD) δ 8.86 (s, 1H), 8.53 (d, J = 5.3 Hz, 1H), 8.50 (s, 1H), 7.94 (dd, J = 6.7, 2.7 Hz, 1H), 7.68 – 7.59 (m, 2H), 7.37 (d, J = 8.1 Hz, 1H), 7.27 – 7.10 (m, 3H), 4.26 (q, J = 7.0 Hz, 2H), 4.11 (s, 2H), 1.38 (t, J = 7.0 Hz, 3H). ^{13}C NMR (75 MHz, DMSO-d_6) δ 167.34, 156.82 (d, J = 3.1 Hz), 154.79, 153.73, 153.29, 149.56, 148.62, 137.12, 136.82, 127.26, 123.69, 122.57 (d, J = 6.8 Hz), 121.94, 120.45, 118.65 (d, J = 18.1 Hz), 116.39 (d, J = 21.7 Hz), 113.46, 108.89, 107.18, 64.60, 34.02, 14.13. HRMS (ESI): m/z: calcd for $C_{23}H_{19}ClFN_5O_2S$ [$(M+H)^+$]: 484.10048; found: 484.10038.

***N*-(4-((3-Chloro-4-fluorophenyl)amino)-7-ethoxyquinazolin-6-yl)-2-(pyrimidin-2-ylthio)acetamide (UPR1338).** 6-(chloroacetamido)-4-(3-chloro-4-fluoroaniline)-7-ethoxyquinazoline (**UPR1303**, 57 mg, 0.14 mmol) is added to a solution of 2-mercaptopyrimidine (38 mg, 0.34 mmol) and sodium hydroxide (14.0 mg, 0.35 mmol) in THF (2 ml). The mixture is stirred at room temperature for 1 h, then diluted with ethyl acetate. The organic layer is washed with water, saturated aqueous $NaHCO_3$ and brine, dried over Na_2SO_4 and concentrated under reduced pressure. Purification of the solid residue by silica gel column chromatography (AcOEt) affords the title compound (59 mg, 88%) as a white solid. Mp: 243 °C. ^{1}H NMR (300 MHz, DMSO-d_6) δ 9.82 (s, 1H),

9.68 (s, 1H), 8.93 (s, 1H), 8.69 (d, *J* = 4.9 Hz, 2H), 8.50 (s, 1H), 8.08 (dd, *J* = 6.9, 2.6 Hz, 1H), 7.85 – 7.65 (m, 1H), 7.39 (t, *J* = 9.1 Hz, 1H), 7.29 (t, *J* = 4.9 Hz, 1H), 7.24 (s, 1H), 4.41 – 4.06 (m, 4H), 1.36 (t, *J* = 6.9 Hz, 3H). ^{13}C NMR (75 MHz, DMSO-d_6) δ 169.98, 166.78, 158.02, 156.81, 154.78, 153.45, 151.56, 148.65, 136.81, 127.19, 123.69, 122.56 (d, *J* = 6.9 Hz), 118.64 (d, *J* = 18.5 Hz), 117.74, 116.36 (d, *J* = 21.6 Hz), 113.83, 108.85, 107.17, 64.59, 35.14, 14.19. HRMS (ESI): m/z: calcd for $C_{22}H_{18}ClFN_6O_2S$ [$(M+H)^+$]: 485.09573; found: 485.09555.

***N*-(4-((3-Chloro-4-fluorophenyl)amino)-7-ethoxyquinazolin-6-yl)-2-((1-methyl-1H-tetrazol-5-yl)thio)acetamide (UPR1360).** To a solution of 5-mercapto-1-methyltetrazole (36.2 mg, 0.30 mmol) and sodium hydroxide (12 mg, 0.30 mmol) in THF (2 ml) is added 6-(chloroacetamido)-4-(3-chloro-4-fluoroaniline)-7-ethoxyquinazoline (**UPR1303**, 90 mg, 0.22 mmol). After stirring at room temperature for 1 h, the mixture is diluted with AcOEt. The organic layer is washed with water and brine, dried over Na_2SO_4 and concentrated under reduced pressure. Purification of the solid residue is purified by silica gel column chromatography (AcOEt) affords the title compound (65 mg, 61%) as a white solid. Mp: 232-234 °C. ^{1}H NMR (300 MHz, DMSO-d_6) δ 9.85 (s, 1H), 9.83 (s, 1H), 8.86 (s, 1H), 8.52 (s, 1H), 8.08 (dd, *J* = 6.9, 2.6 Hz, 1H), 7.76 (ddd, *J* = 9.0, 4.3, 2.6 Hz, 1H), 7.41 (t, *J* = 9.1 Hz, 1H), 7.27 (s, 1H), 4.47 (s, 2H), 4.30 (q, *J* = 7.0 Hz, 2H), 4.00 (s, 3H), 1.46 (t, *J* = 6.9 Hz, 3H). ^{13}C NMR (75 MHz, DMSO-d_6) δ 165.66, 156.85, 154.81, 153.98, 153.42, 151.59, 148.94, 136.76, 126.94, 123.71, 122.58 (d, *J* = 6.9 Hz), 118.65 (d, *J* = 18.4 Hz), 116.39 (d, *J* = 21.5 Hz), 114.88, 108.75, 107.27, 64.63, 37.39, 33.70, 14.20. HRMS (ESI): m/z: calcd for $C_{20}H_{18}ClFN_8O_2S$ [$(M+H)^+$]: 489.10187; found: 489.10161.

2-((4-((3-Chloro-4-fluorophenyl)amino)-7-ethoxyquinazolin-6-yl)amino)-2-oxoethyl acetate (UPR1301). A solution of 6-(chloroacetamido)-4-(3-chloro-4-fluoroaniline)-7-ethoxyquinazoline (**UPR1303**, 150 mg, 0.37 mmol) and sodium acetate (30 mg, 0.37 mmol) in DMF (4 ml) is stirred at reflux for 3 h. It is then allowed to cool to room temperature and diluted with water. The obtained precipitate is recovered by

suction filtration and dried to afford the title compound (141 mg, 89%) as a white solid. Mp: 221 °C. ^{1}H NMR (300 MHz, DMSO-d_6) δ 9.83 (s, 1H), 9.53 (s, 1H), 8.86 (s, 1H), 8.52 (s, 1H), 8.10 (dd, J = 6.9, 2.6 Hz, 1H), 7.78 (ddd, J = 9.1, 4.4, 2.7 Hz, 1H), 7.40 (t, J = 9.1 Hz, 1H), 7.26 (s, 1H), 4.81 (s, 2H), 4.28 (q, J = 6.9 Hz, 2H), 2.16 (s, 3H), 1.46 (t, J = 6.9 Hz, 3H). ^{13}C NMR (75 MHz, DMSO-d_6) δ 169.84, 165.88, 156.82, 154.79, 154.16, 153.91, 151.57, 149.03, 136.88, 126.58, 123.65, 122.51 (d, J = 6.9 Hz), 118.66 (d, J = 18.2 Hz), 116.39 (d, J = 21.5 Hz), 115.19, 108.83, 107.30, 64.60, 62.55, 20.47, 14.24. HRMS (ESI): m/z: calcd for $C_{20}H_{18}ClFN_4O_4$ [$(M+H)^+$]: 433.10734; found: 433.10699.

2-((4-((3-Chloro-4-fluorophenyl)amino)-7-ethoxyquinazolin-6-yl)amino)-2-oxoethyl benzoate (UPR1300). A solution of 6-(chloroacetamido)-4-(3-chloro-4-fluoroaniline)-7-ethoxyquinazoline (**UPR1303**, 70 mg, 0.17 mmol), benzoic acid (21 mg, 0.17 mmol) and triethylamine (24 µl, 0.17 mmol) in DMF (3 ml) is stirred at reflux for 3 h. The solution is allowed to cool to room temperature and diluted with water. The obtained precipitate is recovered by suction filtration and dried to afford the title compound (75 mg, 88%) as a white solid. Mp: 243 °C. ^{1}H NMR (300 MHz, $CDCl_3$/CD_3OD) δ 8.93 (s, 1H), 8.53 (s, 1H), 8.20 (s, 1H), 8.19 – 8.14 (m, 1H), 7.95 (dd, J = 6.7, 2.7 Hz, 1H), 7.71 (t, J = 7.5 Hz, 1H), 7.63 (ddd, J = 8.9, 4.1, 2.6 Hz, 1H), 7.56 (t, J = 7.6 Hz, 2H), 7.25 – 7.11 (m, 2H), 5.08 (s, 2H), 4.25 (q, J = 7.0 Hz, 2H), 1.38 (t, J = 6.9 Hz, 3H). ^{13}C NMR (75 MHz, $CDCl_3$/CD_3OD) δ 166.50, 165.63, 158.05, 156.90, 154.61, 153.64, 152.96, 148.48, 135.86, 134.54, 130.18, 129.15, 126.80, 125.12, 122.78 (d, J = 7.0 Hz), 121.02 (d, J = 18.4 Hz), 116.72 (d, J = 22.0 Hz), 111.04, 109.61, 106.77, 65.61, 63.73, 14.46. HRMS (ESI): m/z: calcd for $C_{25}H_{20}ClFN_4O_4$ [$(M+H)^+$]: 495.12299; found: 495.12263.

2-((4-((3-Chloro-4-fluorophenyl)amino)-7-ethoxyquinazolin-6-yl)amino)-2-oxoethyl 2,6-dimethylbenzoate (UPR1367). A solution of 6-(chloroacetamido)-4-(3-chloro-4-fluoroaniline)-7-ethoxyquinazoline (**UPR1303**, 65 mg, 0.16 mmol), 2,6-dimethoxy benzoic acid (70.5 mg, 0.47 mmol) and triethylamine (100 µl, 0.72 mmol) in

DMF (4 ml) is stirred at 100 °C for 30 min. The solution is allowed to cool to room temperature and diluted with water. The obtained precipitate is recovered by suction filtration and dried to afford the title compound (49 mg, 47%) as a white solid. Mp: 240 °C (dec.). ^{1}H NMR (300 MHz, DMSO-d_6) δ 9.85 (s, 1H), 9.67 (s, 1H), 8.86 (s, 1H), 8.53 (s, 1H), 8.09 (dd, J = 6.8, 2.6 Hz, 1H), 7.76 (ddd, J = 9.1, 4.4, 2.7 Hz, 1H), 7.42 (t, J = 9.1 Hz, 1H), 7.34 – 7.19 (m, 2H), 7.12 (d, J = 7.6 Hz, 2H), 5.09 (s, 2H), 4.29 (q, J = 7.0 Hz, 2H), 2.35 (s, 6H), 1.41 (t, J = 6.9 Hz, 3H). ^{13}C NMR (75 MHz, DMSO-d_6) δ 168.45, 165.69, 156.89, 154.83, 154.24, 153.97, 151.61, 149.11, 136.78 (d, J = 2.9 Hz), 134.82, 132.88, 129.68, 127.57, 126.57, 123.73, 122.61 (d, J = 7.0 Hz), 118.67 (d, J = 18.2 Hz), 116.43 (d, J = 21.6 Hz), 108.81, 107.39, 64.61, 63.13, 19.41, 14.16. HRMS (ESI): m/z: calcd for $C_{27}H_{24}ClFN_4O_4$ [$(M+H)^+$]: 523.15429; found: 523.15387.

***N*-(4-((3-Chloro-4-fluorophenyl)amino)-7-ethoxyquinazolin-6-yl)-2-hydroxyacetamide (UPR1394).** Sodium (3 mg, 0.13 mmol) is added to a solution of 6-(2-acetoyloxyacetamido)-4-(3-chloro-4-fluoroaniline)-7-ethoxyquinazoline (**UPR1301**, 93 mg, 0.22 mmol) in a mixture of THF (3 ml) and MeOH (30 µl, 0.8 mmol). The solution is stirred at room temperature for 30 min, quenched by addition of HCl 1M until neutralization and diluted with AcOEt. The organic layer is washed with water and brine, dried over Na_2SO_4 and concentrated under reduced pressure. Purification of the solid residue by silica gel column chromatography (AcOEt/hexane 4:1) affords the title compound (52 mg, 62%) as a white solid. Mp: 261 °C. ^{1}H NMR (300 MHz, DMSO-d_6) δ 9.87 (s, 1H), 9.48 (s, 1H), 9.08 (s, 1H), 8.52 (s, 1H), 8.08 (dd, J = 7.0, 2.6 Hz, 1H), 7.76 (ddd, J = 9.0, 4.3, 2.6 Hz, 1H), 7.42 (t, J = 9.1 Hz, 1H), 7.31 (s, 1H), 6.25 (t, J = 5.6 Hz, 1H), 4.33 (q, J = 6.9 Hz, 2H), 4.09 (d, J = 5.6 Hz, 2H), 1.46 (t, J = 6.9 Hz, 3H). ^{13}C NMR (75 MHz, DMSO-d_6) δ 170.42, 156.88, 154.78, 153.62, 152.71, 151.56, 148.48, 136.87, 126.73, 123.73, 122.62 (d, J = 6.9 Hz), 118.63 (d, J = 18.6 Hz), 116.38 (d, J = 21.5 Hz), 111.60, 109.09, 107.23, 64.77, 61.75, 14.28. HRMS (ESI): m/z: calcd for $C_{18}H_{16}ClFN_4O_3$ [$(M-H)^-$]: 389.08112; found: 389.08215.

6.2.2. Diaminopyrimidine-based inhibitors

5-Chlorouracil (29). Uracil (**28**, 5.00 g, 44.67 mmol) is suspended in acetic acid (130 ml). Acetic anhydride (1.30 ml, 13.32 mmol) and *N*-chlorosuccinimide (7.79 g, 58.31 mmol) are added and the mixture is stirred at 60 °C for 5 h. The suspension is then cooled to room temperature and the precipitate is recovered by suction filtration, affording the title compound (3.00 g, 47%) as a white solid. Analytical data are in accordance with those reported in the literature.[267]

2,4,5-Trichloropyrimidine (30). 5-chlorouracil (**29**, 500 mg, 3.40 mg), $POCl_3$ (0.63 ml, 6.78 mmol) and 2,6-lutidine (0.40 ml, 3.43 mmol) are heated at 140 °C for 2 h in a closed flask. The mixture is then cooled to 0 °C and ice flakes are cautiously added, followed by the addition of water. The mixture is extracted with AcOEt, the layers are separated and the organic phase is washed with brine and dried over Na_2SO_4. The solvent is evaporated under reduced pressure and the residue is purified in a short silica column (hexane/AcOEt 6:1) to afford the title compound (400 mg, 64%) as a pale yellow, sticky oil. ^{1}H NMR: (300 MHz, $CDCl_3$) δ 8.59 (s, 1H).

2,5-Dichloro-*N*-(3-nitrophenyl)pyrimidin-4-amine (31). Trichloropyrimidine (**30**, 2.89 g, 15.76 mmol) and 3-nitroaniline (1.45 g, 10.51 mmol) are suspended in *i*-PrOH (30 ml). DIPEA (3.7 ml, 21.24 mmol) is added and the mixture is stirred at 80 °C for 15 h. A precipitate is obtained when the mixture is allowed to cool temperature, which is recovered by suction filtration, washed with *i*-PrOH and water and dried, affording the title compound (2.17 g, 72%) as a pale yellow solid. ^{1}H NMR (400 MHz, $CDCl_3$/CD_3OD) δ 8.59 (t, J = 2.2 Hz, 1H), 8.21 (s, 1H), 8.04 (ddd, J = 8.2, 2.2, 1.0 Hz, 1H), 7.99 (ddd, J = 8.2, 2.3, 1.0 Hz, 1H), 7.55 (t, J = 8.2 Hz, 1H).

1-(4-(3-Methoxy-4-nitrophenyl)piperazin-1-yl)ethan-1-one (33). 5-fluoro-2-nitroanisole (**32**, 1.78 g, 10.38 mmol) and 1-acetylpiperazine (1.60 g, 12.47 mmol) are heated at 40 °C for 1 h in a closed vial. The residue is then taken with DCM and methanol and the solution is transferred into a flask and concentrated under reduced pressure. The

crude product is washed with water, dried and crystallized from toluene to afford the title compound (2.59 g, 89%) in the form of yellow, needle-like crystals. ^{1}H NMR (300 MHz, $CDCl_3$) δ 7.98 (d, *J* = 9.3 Hz, 1H), 6.40 (dd, *J* = 9.3, 2.6 Hz, 1H), 6.31 (d, *J* = 2.5 Hz, 1H), 3.94 (s, 3H), 3.83 – 3.73 (m, 2H), 3.66 (dd, *J* = 6.6, 4.0 Hz, 2H), 3.43 (ddd, *J* = 14.2, 6.5, 4.1 Hz, 4H), 2.14 (s, 3H).

1-(4-(4-Amino-3-methoxyphenyl)piperazin-1-yl)ethan-1-one (24). Compound **33** (1.33 g, 4.76 mmol) is dissolved in THF (10 ml). Zinc dust (1.58 g, 24.32 mmol) and a solution of ammonium chloride (270 mg, 4.93 mmol) in water (3 ml) are added. The mixture is stirred at 50 °C for 3 h and then filtered over a pad of cotton. The filtrate is concentrated under reduced pressure and dissolved again in DCM. The solution is washed with water and brine, dried over Na_2SO_4 and concentrated. The residue is crystallized from toluene to afford the title compound (1.17 g, 98%) in the form of purple crystals. ^{1}H NMR (400 MHz, $CDCl_3$) δ 6.61 (d, *J* = 8.3 Hz, 1H), 6.48 (d, *J* = 2.5 Hz, 1H), 6.37 (dd, *J* = 8.3, 2.4 Hz, 1H), 3.80 (s, 3H), 3.72 (t, *J* = 5.2 Hz, 2H), 3.59 – 3.54 (m, 2H), 2.97 (dt, *J* = 12.2, 5.1 Hz, 4H), 2.10 (s, 3H).

2-((2-Methoxy-4-(4-acetylpiperazin-1-yl)phenyl)amino)-4-(((3-nitro)phenyl)amino)-5-chloropyrimidine (34). Compound **31** (2.17 g, 7.61 mmol) and aniline **24** (1.26 g, 5.05 mmol) are suspended in *i*-PrOH (50 ml). PTSA*H_2O (1.92 mmol, 10.09 mmol) is added and the mixture is stirred at 80 °C for 15 h. The suspension is then cooled to room temperature and diluted with AcOEt. The solution is washed with HCl 0.2 M, causing repartition of the product in the aqueous layer. The layers are separated and $NaHCO_3$ is added to the aqueous solution (pH=8), leading to the precipitation of the product, which is recovered by suction filtration and washed thoroughly with a hot EtOH/H_2O 7:3 mixture. After drying in the air, the title compound (1.26 g, 50%) is obtained as a brownish solid. ^{1}H NMR (300 MHz, $CDCl_3$/CD_3OD) δ 8.54 (t, *J* = 2.2 Hz, 1H), 8.01 (s, 1H), 7.93 (dd, *J* = 7.8, 2.1 Hz, 1H), 7.87 (dt, *J* = 7.9, 1.5 Hz, 1H), 7.81 (d, *J* = 8.7 Hz, 1H), 7.47 (t, *J* = 8.2 Hz, 1H), 6.52 (d, *J* = 2.5 Hz, 1H), 6.33 (dd, *J* = 8.7, 2.5

Hz, 1H), 3.84 (s, 3H), 3.73 (t, *J* = 5.2 Hz, 2H), 3.63 (t, *J* = 5.1 Hz, 2H), 3.09 (dt, *J* = 13.9, 5.2 Hz, 4H), 2.12 (s, 3H).

2-((2-Methoxy-4-(4-acetylpiperazin-1-yl)phenyl)amino)-4-(((3-amino)phenyl)amino)-5-chloropyrimidine (35). Compound **34** (1.10 g, 2.21 mmol) is dissolved in EtOH (150 ml). Iron powder (1.24 g, 22.17 mmol) and HCl 1M (0.5 ml, 0.5 mmol) are added and the mixture is heated at reflux for 2 h. It is then cooled to room temperature and filtered on a pad of celite. The solvent is removed under reduced pressure and the residue is purified in a short silica column (AcOEt + 10% MeOH) to afford the title compound (965 mg, 93%) as a white solid. ^{1}H NMR (300 MHz, $CDCl_3/CD_3OD$) δ 8.00 (d, *J* = 8.8 Hz, 1H), 7.91 (s, 1H), 7.10 – 7.03 (m, 2H), 6.86 (ddd, *J* = 8.1, 2.1, 0.9 Hz, 1H), 6.56 (d, *J* = 2.6 Hz, 1H), 6.54 – 6.43 (m, 2H), 3.85 (s, 3H), 3.78 – 3.69 (m, 2H), 3.65 (t, *J* = 5.2 Hz, 2H), 3.10 (dt, *J* = 14.4, 5.1 Hz, 4H), 2.13 (s, 3H).

***N*-(3-((2-((4-(4-Acetylpiperazin-1-yl)-2-methoxyphenyl)amino)-5-chloropyrimidin-4-yl)amino)phenyl)acetamide (UPR1423).** Aniline **35** (49 mg, 0.11 mmol) is dissolved in pyridine (1 ml) and acetic anhydride (15 µl, 0.16 mmol) is slowly added. The mixture is stirred at room temperature for 30 min and diluted with water. The obtained precipitate is recovered by suction filtration and dried. Crystallization from water (10% MeOH added) affords the title compound (44 mg, 82%) as colorless, needle-like crystals. Mp: 168 °C. ^{1}H NMR (400 MHz, $CDCl_3/CD_3OD$) δ 7.96 (dd, *J* = 8.9, 1.3 Hz, 1H), 7.94 – 7.91 (m, 1H), 7.69 (s, 1H), 7.43 (dd, *J* = 7.6, 2.3 Hz, 1H), 7.36 – 7.30 (m, 1H), 7.27 (t, *J* = 8.0 Hz, 1H), 6.54 (d, *J* = 2.5 Hz, 1H), 6.45 – 6.31 (m, 1H), 3.85 (s, 3H), 3.73 (t, *J* = 5.2 Hz, 2H), 3.65 (t, *J* = 5.2 Hz, 2H), 3.09 (dt, *J* = 18.4, 5.3 Hz, 4H), 2.13 (s, 3H), 2.11 (d, *J* = 1.2 Hz, 3H). MS (ESI): m/z: calcd for $C_{25}H_{29}ClN_7O_3$ [$(M+H)^+$]: 510.19; found: 509.93.

***N*-(3-((2-((4-(4-Acetylpiperazin-1-yl)-2-methoxyphenyl)amino)-5-chloropyrimidin-4-yl)amino)phenyl)-2-chloroacetamide (UPR1424).** To a solution of chloroacetic acid (124 mg, 1.31 mmol) in anhydrous THF (2 ml) are added DIPEA (230 µl, 1.32 mmol)

and pivaloyl chloride (140 µl, 1.13 mmol). After stirring at room temperature for 20 min, a suspension of aniline **35** (97 mg, 0.21 mmol) in anhydrous THF (3 ml) is added and the mixture is stirred for 1 h before being diluted with water. The mixture is extracted with AcOEt and the organic layer is washed with water and brine, dried over Na_2SO_4 and concentrated under reduced pressure. Purification of the solid residue by silica gel column chromatography (DCM + 3% MeOH) and crystallization from EtOH/water 7:3 afford the title compound (61 mg, 54%) as colorless crystals. Mp: 172 °C. ^{1}H NMR (300 MHz, $CDCl_3$/CD_3OD) δ 7.94 (s, 1H), 7.94 (d, *J* = 11.8 Hz, 1H), 7.79 (t, *J* = 2.1 Hz, 1H), 7.42 (q, *J* = 2.1 Hz, 1H), 7.39 (t, *J* = 2.0 Hz, 1H), 7.32 (d, *J* = 7.9 Hz, 1H), 6.55 (d, *J* = 2.6 Hz, 1H), 6.37 (dd, *J* = 8.8, 2.5 Hz, 1H), 4.13 (s, 2H), 3.86 (s, 3H), 3.73 (t, *J* = 5.2 Hz, 2H), 3.66 (t, *J* = 5.2 Hz, 2H), 3.10 (dt, *J* = 14.1, 5.2 Hz, 4H), 2.13 (s, 3H). MS (ESI): m/z: calcd for $C_{25}H_{28}Cl_2N_7O_3$ [$(M+H)^+$]: 544.16; found: 543.86.

2-((3-((2-((4-(4-Acetylpiperazin-1-yl)-2-methoxyphenyl)amino)-5-chloropyrimidin-4-yl)amino)phenyl)amino)ethane-1-sulfonyl fluoride (UPR1425). Aniline **35** (200 mg, 0.43 mmol) is dissolved in chloroform/MeOH 1:1 (10 ml) and ESF (120 µl, 1.45 mmol) is added. The solution is stirred at room temperature for 3 h. TLC analysis reveals a conversion of about 40-50%. The mixture is diluted with AcOEt and washed with saturated aqueous $NaHCO_3$. The organic layer is consequently washed with water and brine, dried over Na_2SO_4 and concentrated under reduced pressure. Purification of the solid residue by silica gel column chromatography (toluene/EtOH 95:5) affords the title compound (33 mg, 13%) as a white solid. Mp: 89 °C. ^{1}H NMR (400 MHz, $CDCl_3$) δ 8.08 (d, *J* = 8.7 Hz, 1H), 8.05 (s, 1H), 7.23 – 7.16 (m, 2H), 7.00 (d, *J* = 2.0 Hz, 1H), 6.90 – 6.80 (m, 1H), 6.54 (d, *J* = 2.5 Hz, 1H), 6.48 (dd, *J* = 8.8, 2.6 Hz, 1H), 6.45 – 6.36 (m, 1H), 3.87 (s, 3H), 3.81 – 3.73 (m, 4H), 3.67 – 3.55 (m, 4H), 3.11 (dt, *J* = 12.5, 5.2 Hz, 4H), 2.15 (s, 3H). MS (ESI): m/z: calcd for $C_{25}H_{30}ClFN_7O_4$ [$(M+H)^+$]: 578.17; found: 577.90.

6.3. Synthesis of FGF/FGFR targeting compounds

6.3.1. FGFR kinase inhibitors

5-Hydroxymethyluracil (56). A mixture of uracil (**28**, 18.21 g, 162.46 mmol), paraformaldehyde (6 g) and potassium hydroxide (5.84 g, 104.08) in water (100 ml) is stirred for 63 h at 55 °C. The reaction mixture is then diluted with water (350 ml) and IRA-120 resin is added till pH=7. The mixture is concentrated under reduced pressure, yielding a solid residue that is crystallized from water to afford the title compound (18.70 g, 81%) as white solid. Analytical data are in accordance with those reported in the literature.[268]

2,4-Dichloro-5-(chloromethyl)pyrimidine (57). 5-hydroxymethyluracil (**56**, 2.12 g, 14.95 mmol) and PCl_5 (9.36 g, 44.94 mmol) are suspended in $POCl_3$ (2.6 ml, 27.81 mmol) and the mixture is gradually warmed to reflux. After stirring for 2 h, the suspension is cooled back to room temperature and volatiles are removed under reduced pressure. The residue is dissolved in DCM and the solution is washed with water and brine. The organic phase is dried over Na_2SO_4 and concentrated under reduced pressure, yielding the title compound (2.07 g, 71% yield) as a white solid. Analytical data are in accordance with those reported in the literature.[269]

***N*-((2,4-dichloropyrimidin-5-yl)methyl)-3,5-dimethoxyaniline (58).** 2,4-dichloro-5-(chloromethyl)pyrimidine (**57**, 2.07 g, 10.49 mmol), 3,5-dimethoxyaniline (1.60 g, 10.47 mmol), potassium carbonate (4.55 g, 32.91 mmol) and sodium iodide (82 mg, 0.55 mmol) are suspended in acetonitrile (30 ml) and the mixture is stirred at room temperature for 15 h. It is then diluted with chloroform and washed with water and brine. The organic layer is dried over Na_2SO_4 and concentrated under reduced pressure. The residue is purified by silica gel column chromatography (petroleum ether/AcOEt 2:1), affording the title compound (1.12 g, 34% yield) as a white solid. Analytical data are in accordance with those reported in the literature.[268]

2-Chloro-5-(((3,5-dimethoxyphenyl)amino)methyl)-*N*-(4-nitrobenzyl)pyrimidin-4-amine (59). *N*-((2,4-dichloropyrimidin-5-yl)methyl)-3,5-dimethoxyaniline (**58**, 856 mg, 2.72 mmol) and 4-nitrobenzylamine (896 mg, 5.88 mmol) are suspended in dioxane (10 ml). DIPEA (1.4 ml, 8.04 mmol) is added and the mixture is stirred at 60 °C for 15 h. The solvent is then evaporated under reduced pressure and the residue is purified by silica gel column chromatography (petroleum ether/AcOEt 2:1), affording the title compound (906 mg, 78% yield) as a pale yellow solid. Analytical data are in accordance with those reported in the literature.[88]

7-Chloro-3-(3,5-dimethoxyphenyl)-1-(4-nitrobenzyl)-3,4-dihydropyrimido[4,5-*d*]pyrimidin- 2(1*H*)-one (60). 2-chloro-5-(((3,5-dimethoxyphenyl)amino)methyl)-*N*-(4-nitrobenzyl)pyrimidin-4-amine (**59**, 906 mg, 2.11 mmol) is suspended in anhydrous THF (15 ml). Triphosgene (287 mg, 0.97 mmol) and triethylamine (0.88 ml, 6.31 mmol) are added and the mixture is stirred at 70 °C for 1 h. After being cooled to room temperature, the suspension is diluted with AcOEt and washed with saturated aqueous $NaHCO_3$, water and brine. The organic layer is dried over Na_2SO_4 and concentrated under reduced pressure, yielding the title compound (1.00 g, quantitative yield) as a pale yellow solid. Analytical data are in accordance with those reported in the literature.[88]

1-Methyl-4-(4-nitrophenyl)piperazine (62). 4-Nitrobromobenzene (**61**, 5.03 g, 24.90 mmol) and *N*-methylpiperazine (5.5 ml, 49.52 mmol) are stirred at 80 °C for 6 h. The mixture is then cooled to room temperature, diluted with AcOEt and washed with saturated aqueous $NaHCO_3$ and brine. The organic layer is dried over Na_2SO_4 and concentrated under reduced pressure, yielding the title compound (5.33 g, 96% yield) as a bright yellow solid. Analytical data are in accordance with those reported in the literature.[270]

4-(4-Methylpiperazin-1-yl)aniline (63). A mixture of 1-methyl-4-(4-nitrophenyl)piperazine (**62**, 5.20 g, 23.52 mmol), iron (13.14 g, 235.20 mmol) and

ammonium chloride (3.88 g, 70.56 mmol) in ethanol (230 ml) and water (5 ml) is is stirred at reflux for 1 h. After filtration on a pad of celite and removal of the solvent under reduced pressure, the residue is purified by silica gel column chromatography (DCM/methanol 9:1), affording the title compound (4.28 g, 95% yield) as a brown-purple solid. Analytical data are in accordance with those reported in the literature.[270]

3-(3,5-Dimethoxyphenyl)-7-((4-(4-methylpiperazin-1-yl)phenyl)amino)-1-(4-nitrobenzyl)- 3,4-dihydropyrimido[4,5-*d*]pyrimidin-2(1*H*)-one (64). 7-chloro-3-(3,5-dimethoxyphenyl)-1-(4-nitrobenzyl)-3,4-dihydropyrimido[4,5-*d*]pyrimidin-2(1*H*)-one (**60**, 1.04 g, 2.28 mmol) and 4-(4-methylpiperazin-1-yl)aniline (**63**, 654 mg, 3.42 mmol) are suspended in *sec*-butanol (20 ml). Trifluoroacetic acid (0.81 ml, 10.57 mmol) is added and the mixture is stirred at 100 °C for 15 h. After removal of the solvent, the residue is diluted with DCM and the solution is washed with saturated aqueous $NaHCO_3$ and brine. The organic layer is dried over Na_2SO_4 and concentrated under reduced pressure and the residue is purified by silica gel column chromatography (DCM/methanol 15:1), affording the title compound (718 mg, 51% yield) as a yellow solid. Analytical data are in accordance with those reported in the literature.[88]

1-(4-Aminobenzyl)-3-(3,5-dimethoxyphenyl)-7-((4-(4-methylpiperazin-1-yl)phenyl)amino)-3,4-dihydropyrimido[4,5-*d*]pyrimidin-2(1*H*)-one (65). 3-(3,5-dimethoxyphenyl)-7-((4-(4-methylpiperazin-1-yl)phenyl)amino)-1-(4-nitrobenzyl)-3,4-dihydropyrimido[4,5-*d*]pyrimidin-2(1*H*)-one (**64**, 129 mg, 0.21 mmol) is dissolved in a mixture of THF and methanol (1:1, 20 ml) and Raney nickel suspension in water (1 ml) is added. The suspension is stirred at 40 °C for 2 h, then it is cooled back to room temperature and cautiously filtered over mineral wool. The solvents are removed under reduced pressure and the residue is purified by silica gel column chromatography (DCM/methanol 15:1), affording the title compound (86 mg, 71% yield) as a pale yellow solid. ^{1}H NMR (300 MHz, $CDCl_3$) δ 7.90 (s, 1H), 7.43 (d, J = 9.0 Hz, 2H), 7.23 (d, J = 8.4 Hz, 2H), 6.92 (d, J = 8.9 Hz, 2H), 6.55 (d, J = 8.4 Hz, 2H), 6.47 (d, J = 2.3 Hz, 2H),

6.37 (t, *J* = 2.3 Hz, 1H), 5.18 (s, 2H), 4.58 (s, 2H), 3.77 (s, 6H), 3.19 (t, 4.9 Hz, 4H), 2.61 (t, *J* = 5.0 Hz, 4H), 2.37 (s, 3H).

2-Chloro-*N*-(4-((3-(3,5-dimethoxyphenyl)-7-((4-(4-methylpiperazin-1-yl)phenyl)amino)-2-oxo-3,4-dihydropyrimido[4,5-*d*]pyrimidin-1(2*H*)-yl)methyl)phenyl)acetamide (66). To a solution of chloroacetic acid (26.0 mg, 0.27 mmol) and DIPEA (47 µl, 0.27 mmol) in anhydrous THF (2 ml) is added pivaloyl chloride (28 µl, 0.23 mmol). The mixture is stirred at room temperature for 25 min, then a solution of compound **65** (63.0 mg, 0.11 mmol) in anhydrous THF (3 ml) is added. The resulting mixture is stirred for 30 min and diluted with DCM, washed with water and dried over Na_2SO_4. The organic layer is directly purified on a short silica column (DCM/MeOH 15:1) without being concentrated. Fractions containing the product are collected and the solution is either directly used in the synthesis of **UPR1376** or concentrated under reduced pressure at room temperature, yielding a solid residue that is used for the synthesis of **UPR1372** and **UPR1373**.

2-Chloro-*N*-(4-((3-(3,5-dimethoxyphenyl)-7-((4-(4-methylpiperazin-1-yl)phenyl)amino)-2-oxo-3,4-dihydropyrimido[4,5-*d*]pyrimidin-1(2*H*)-yl)methyl)phenyl)acetamide hydrochloride (UPR1376). To the solution of 2-chloro-*N*-(4-((3-(3,5-dimethoxyphenyl)-7-((4-(4-methylpiperazin-1-yl)phenyl)amino)-2-oxo-3,4-dihydropyrimido[4,5-*d*]pyrimidin-1(2*H*)-yl)methyl)phenyl)acetamide (**66**) obtained from purification by column chromatography is added TMSCl (17 µl, 0.13 mmol). The mixture is concentrated under reduced pressure at low temperature, affording the title compound (37 mg, 51% yield over two steps) as a bright yellow solid. Mp: 85 °C (dec.). ^{1}H NMR (400 MHz, CD_3OD) δ 7.95 (s, 1H), 7.46 (d, *J* = 8.2 Hz, 2H), 7.33 (d, *J* = 8.5 Hz, 2H), 7.28 (d, *J* = 8.2 Hz, 2H), 6.88 (d, *J* = 8.5 Hz, 2H), 6.48 (d, *J* = 1.9 Hz, 2H), 6.40 (t, *J* = 2.3 Hz, 1H), 5.21 (s, 2H), 4.69 (s, 2H), 4.10 (s, 2H), 3.77 (s, 6H), 3.21-3.15 (m, 4H), 2.77-2.70 (m, 4H), 2.43 (s, 3H).

2-Chloro-*N*-(4-((3-(3,5-dimethoxyphenyl)-7-((4-(4-methylpiperazin-1-yl)phenyl)amino)-2-oxo-3,4-dihydropyrimido[4,5-*d*]pyrimidin-1(2*H*)-yl)methyl)phenyl)acetamide (UPR1372). 2-Chloro-*N*-(4-((3-(3,5-dimethoxyphenyl)-7-((4-(4-methylpiperazin-1-yl)phenyl)amino)-2-oxo-3,4-dihydropyrimido[4,5-*d*]pyrimidin-1(2*H*)-yl)methyl)phenyl)acetamide (**66**, 21.5 mg, 0.03 mmol) is dissolved in a mixture of acetonitrile and THF (1:1, 4 ml). 2-mercapto-1-methylimidazole (7.5 mg, 0.07 mmol) and NaOH (3.0 mg, 0.07 mmol) are dissolved in THF (0.4 ml) and added to the solution of **66**. The mixture is stirred at room temperature for 15 h, then it is diluted with DCM and washed with saturated aqueous $NaHCO_3$ and brine. The organic layer is dried over Na_2SO_4 and concentrated under reduced pressure. The residue is purified by silica gel column chromatography (DCM/MeOH 15:1), to afford the title compound (19 mg, 78%) as a white solid. Mp: 112 °C. ^{1}H NMR (400 MHz, $CDCl_3$) δ 11.02 (s, 1H), 7.93 (s, 1H), 7.46 (d, J = 8.1 Hz, 2H), 7.41 – 7.30 (m, 4H), 7.07 (s, 1H), 6.97 (s, 1H), 6.91 (d, J = 2.7 Hz, 2H), 6.89 (s, 1H), 6.47 (d, J = 2.1 Hz, 2H), 6.38 (t, J = 2.2 Hz, 1H), 5.23 (s, 2H), 4.62 (s, 2H), 3.78 (d, J = 1.3 Hz, 6H), 3.75 (s, 2H), 3.57 (d, J = 1.4 Hz, 3H), 3.21 (t, J = 5.1 Hz, 4H), 2.64 (t, J = 5.2 Hz, 4H), 2.39 (d, J = 1.7 Hz, 3H).

***N*-(4-((3-(3,5-Dimethoxyphenyl)-7-((4-(4-methylpiperazin-1-yl)phenyl)amino)-2-oxo-3,4-dihydropyrimido[4,5-*d*]pyrimidin-1(2*H*)-yl)methyl)phenyl)-2-((1-methyl-1*H*-tetrazol-5-yl)thio)acetamide (UPR1373).** 2-Chloro-*N*-(4-((3-(3,5-dimethoxyphenyl)-7-((4-(4-methylpiperazin-1-yl)phenyl)amino)-2-oxo-3,4-dihydropyrimido[4,5-*d*]pyrimidin-1(2*H*)-yl)methyl)phenyl)acetamide (**66**, 35.0 mg, 0.05 mmol) is dissolved in a mixture of acetonitrile and THF (1:1, 4 ml). 5-mercapto-1-methyltetrazole (13.0 mg, 0.11 mmol) and NaOH (4.5 mg, 0.11 mmol) are dissolved in THF (0.45 ml) and added to the solution of **66**. The mixture is stirred at room temperature for 15 h, then it is diluted with DCM and washed with saturated aqueous $NaHCO_3$ and brine. The organic layer is dried over Na_2SO_4 and concentrated under reduced pressure. The residue is purified by silica gel column chromatography (DCM/MeOH 15:1), to afford the title compound (13 mg, 35%) as a white solid. Mp: 145 °C (dec.). ^{1}H NMR (400 MHz, $CDCl_3$) δ 9.33 (s, 1H), 7.94 (s, 1H), 7.41 (d, J = 8.2 Hz, 2H), 7.38 – 7.29 (m,

4H), 6.90 (d, *J* = 9.0 Hz, 2H), 6.47 (d, *J* = 2.2 Hz, 2H), 6.37 (t, *J* = 2.3 Hz, 1H), 5.21 (s, 2H), 4.76 – 4.51 (m, 2H), 4.01 (s, 2H), 3.94 (s, 3H), 3.77 (s, 6H), 3.28 – 3.11 (m, 4H), 2.64 (t, *J* = 5.0 Hz, 4H), 2.39 (s, 3H).

***N*-(4-((3-(3,5-Dimethoxyphenyl)-7-((4-(4-methylpiperazin-1-yl)phenyl)amino)-2-oxo-3,4-dihydropyrimido[4,5-*d*]pyrimidin-1(2*H*)-yl)methyl)phenyl)-3-(dimethylamino)propenamide (UPR1371).** Commercially available FIIN-2 (**51**, purchased from Selleckchem, 9.5 mg, 0.015 mmol) is suspended in absolute ethanol (2 ml) and dimethylamine (33% in absolute ethanol, 20 µl, 0.11 mmol) is added to the suspension. After gradually warming, a clear solution is obtained, which is cooled again to room temperature. The volatiles are removed under reduced pressure, yielding the title compound (10.0 mg, 98%) as a white powder. Mp: 117°C. ^{1}H NMR (400 MHz, $CDCl_3$) δ 10.80 (s, 1H), 7.93 (s, 1H), 7.50 – 7.30 (m, 6H), 7.00 (s, 1H), 6.96 – 6.82 (m, 2H), 6.47 (d, *J* = 2.2 Hz, 2H), 6.37 (t, *J* = 2.2 Hz, 1H), 5.24 (s, 2H), 4.62 (s, 2H), 3.78 (s, 7H), 3.19 (t, *J* = 5.0 Hz, 4H), 2.65 – 2.57 (m, 6H), 2.48 (dd, *J* = 6.6, 5.0 Hz, 2H), 2.36 (s, 3H), 2.34 (s, 6H).

6.3.2. FGF traps

3*β*-Acetoxyetienic acid (68). This compound is prepared according to a literature procedure.[243]

3*β*-Acetoxy-17*β*-hydroxymethylandrost-5-ene (69). Compound **68** (4.51 g, 12.50 mmol) is dissolved in anhydrous THF (60 ml) and the solution is cooled to -5 °C. Triethylamine (1.9 ml, 13.63 mmol) and ethyl chloroformate (1.45 ml, 15.22 mmol) are added and the mixture is stirred for 90 min at 0 °C. The white precipitate is filtered off and a solution of sodium borohydride (1.10 g, 29.06 mmol) in water (7 ml) is added to the filtrate, which is stirred for 15 h at room temperature. The reaction is quenched by the addition of a solution of tartaric acid (10.61 g, 70.72 mmol) in water (80 ml). The aqueous mixture is extracted with DCM, the layers are separated and the organic extracts are washed with brine, dried over Na_2SO_4 and concentrated under reduced pressure to afford the title compound (3.84 g, 89%) as a white solid. ^{1}H NMR (300 MHz, $CDCl_3$) δ 5.38 (d, *J* = 5.2 Hz, 1H), 4.71 – 4.49 (m, 1H), 3.84 – 3.65 (m, 1H), 3.55 (dd, *J* = 10.5, 7.4 Hz, 1H), 2.37 – 2.25 (m, 2H), 2.03 (s, 3H), 1.93 – 1.06 (m, 19H), 1.03 (s, 3H), 0.66 (s, 3H).

3*β*-Acetoxy-androst-5-ene-17*β*-carbaldehyde (70). A solution of compound **69** (3.84 g, 11.08 mmol) in anhydrous DCM (40 ml) is added to a suspension of PCC (3.84 g, 17.79 mmol) in the same solvent (150 ml) at room temperature. The mixture is stirred for 2 h at room temperature, then it is filtered on a pad of celite and the filtrate is washed with 0.1M HCl, saturated aqueous $NaHCO_3$ and brine, dried over Na_2SO_4 and concentrated under reduced pressure. The residue is purified by silica gel column chromatography (petroleum ether/AcOEt 9:1) to afford the title compound (2.13 g, 56%) as a white solid. Analytical data are in accordance with those reported in the literature.[245]

3β-Acetoxy-21-ethoxycarbonyl-pregn-5-en-20-ol (71a,b). Activated zinc dust (13.00 g, 198.8 mmol) is suspended in anhydrous THF (10 ml) and ethyl bromoacetate (5 ml, 45.1 mmol) is added portionwise (1 ml portion every 10 min). The mixture is allowed to

settle and the supernatant is added to a solution of 3β-acetoxy-androst-5-ene-17β-carbaldehyde (**70**, 1.63 g, 4.8 mmol) in anhydrous THF (10 ml) at 0 °C, until consumption of the starting material was detected by TLC. Water is then added and the mixture is extracted with AcOEt. The organic layer is washed with brine, dried over Na_2SO_4 and concentrated under reduced pressure. The residue is purified by silica gel column chromatography (petroleum ether/AcOEt 9:1) to afford *major* product **71a** (964 mg, 47%) and *minor* product **71b** (481 mg, 23%). **71a**: ^{1}H NMR (300 MHz, $CDCl_3$) δ 5.37 (d, *J* = 4.4 Hz, 1H), 4.77 – 4.48 (m, 1H), 4.17 (q, *J* = 7.1 Hz, 2H), 3.94 (ddd, *J* = 10.3, 9.1, 2.7 Hz, 1H), 2.51 (dd, *J* = 16.4, 2.6 Hz, 1H), 2.36 – 2. 28 (m, 3H), 2.17 (dt, *J* = 12.6, 3.5 Hz, 1H), 2.03 (s, 3H), 1.99 – 1.77 (m, 3H), 1.74 – 1.32 (m, 9H), 1.27 (t, *J* = 7.1 Hz, 3H), 1.21 – 0.91 (m, 8H), 0.79 (s, 3H). **71b**: ^{1}H NMR (300 MHz, $CDCl_3$) δ 5.37 (d, *J* = 4.7 Hz, 1H), 4.65 – 4.54 (m, 1H), 4.17 (q, *J* = 7.1 Hz, 2H), 3.95 (ddd, *J* = 9.3, 7.9, 2.9 Hz, 1H), 2.62 (dd, *J* = 16.4, 2.9 Hz, 1H), 2.46 – 2.26 (m, 3H), 2.02 (s, 3H), 1.98 – 1.76 (m, 5H), 1.76 – 1.35 (m, 8H), 1.27 (t, *J* = 7.1 Hz, 3H), 1.21 – 0.88 (m, 8H), 0.70 (s, 3H).

3*β*-Hydroxy-21-(1-hydroxy-1-methyl)ethyl-pregn-5-en-20-ol (UPR1384). To a solution of compound **71a** (47 mg, 0.1 mmol) in toluene (5 ml), MeMgBr (3.0M, 1 ml, 3.0 mmol) is added at 0 °C. Temperature is slowly raised till reflux and the mixture is stirred for 2 h. After cooling back to room temperature, diluted HCl (0.05M) is added till neutralization and the suspension is diluted with AcOEt and water. The layers are separated and the organic is washed with brine, dried over Na_2SO_4 and concentrated under reduced pressure. The residue is purified by silica gel column chromatography (DCM/MeOH 94:6) to afford the title compound (23 mg, 56%) as a white solid. Mp 231-233 °C. $[\alpha]_D^{20}$ = -43.33° (c = 0.6, $CHCl_3$/MeOH 1:1). ^{1}H NMR (300 MHz, $CDCl_3$/CD_3OD) δ 5.32 – 5.27 (m, 1H), 3.89 (dt, *J* = 9.9, 6.2 Hz, 1H), 3.49 – 3.35 (m, 1H), 2.29 – 2.15 (m, 2H), 2.14 – 2.05 (m, 1H), 2.03 – 1.70 (m, 3H), 1.70 – 1.32 (m, 14H), 1.26 (s, 3H), 1.20 (s, 3H), 1.14 – 0.87 (m, 7H), 0.78 (s, 3H). ^{13}C NMR (75 MHz, $CDCl_3$/CD_3OD) δ 141.6, 121.9, 72.7, 72.1, 71.8, 57.4, 57.0, 51.0, 47.8, 43.0, 42.4, 40.1,

37.9, 37.2, 32.5, 32.4, 31.7, 31.6, 28.1, 26.2, 25.1, 21.5, 19.7, 12.5. HRMS (ESI): m/z: calcd for $C_{24}H_{40}NaO_3$ [$(M+Na)^+$]: 399.28697; found: 399.28729.

3*β*-Hydroxy-21-(1-hydroxy-1-methyl)ethyl-pregn-5-en-20-ol (UPR1385). This compound is prepared according to the procedure described for compound **UPR1384** starting from ester **71b**. The title compound (27 mg, 65%) is obtained as a white solid. Mp 222-224 °C. $[\alpha]_D^{20}$ = -29.41° (c = 0.3, $CHCl_3$/MeOH 1:1). ^{1}H NMR (300 MHz, $CDCl_3/CD_3OD$) δ 5.32 (d, *J* = 5.1 Hz, 1H), 3.90 (ddd, *J* = 10.9, 8.5, 2.3 Hz, 1H), 3.51 – 3.37 (m, 1H), 2.30 – 2.08 (m, 2H), 2.00 – 1.74 (m, 5H), 1.70 – 0.88 (m, 24H), 0.68 (s, 3H). ^{13}C NMR (75 MHz, $CDCl_3/CD_3OD$) δ 141.5, 121.9, 72.5, 71.9, 71.7, 57.7, 57.3, 50.8, 47.6, 42.3, 42.0, 39.8, 37.8, 37.1, 32.4, 32.2, 31.7, 31.6, 27.7, 26.1, 24.5, 21.4, 19.6, 12.7. HRMS (ESI): m/z: calcd for $C_{24}H_{40}NaO_3$ [$(M+Na)^+$]: 399.28697; found: 399.28732.

3*β*-Hydroxy-21-hydroxymethyl-pregn-5-en-20-ol (UPR1386). Compound **71a** (95 mg, 0.2 mmol) is dissolved in THF (2 ml) and $NaBH_4$ (250 mg, 6.6 mmol) is added at room temperature. Dropwise addition of MeOH is continued until consumption of the starting material is detected by TLC analysis. The reaction is quenched by the addition of HCl 1M (7 ml). The mixture is stirred for 20 min, then aqueous NaOH (1M, excess) is added and the mixture is warmed to 50 °C until only one spot is detected by TLC analysis. The mixture is neutralized by addition of HCl 1M and extracted with AcOEt. The organic layer is washed with brine, dried over Na_2SO_4 and concentrated under reduced pressure. The residue is purified by silica gel column chromatography (DCM/MeOH 98:2) to afford the title compound (39 mg, 50%) as a white solid. Mp 176-179 °C. $[\alpha]_D^{20}$ = -39.29° (c = 0.6, $CHCl_3$/MeOH 1:1). ^{1}H NMR (300 MHz, $CDCl_3/CD_3OD$) δ 5.15 (d, *J* = 5.0 Hz, 1H), 3.60 – 3.47 (m, 3H), 3.33 – 3.20 (m, 1H), 2.11 – 2.01 (m, 2H), 1.96 (dt, *J* = 12.6, 3.3 Hz, 1H), 1.88 – 1.17 (m, 13H), 1.17 – 0.62 (m, 9H), 0.60 (s, 3H). ^{13}C NMR (75 MHz, $CDCl_3/CD_3OD$) δ 141.6, 122.0, 72.6, 71.9, 60.3, 57.0, 57.0, 51.0, 43.0, 42.4, 40.3, 39.2, 38.0, 37.2, 32.6, 32.5, 31.7, 26.1, 25.1, 21.6,

19.7, 12.5. HRMS (ESI): m/z: calcd for $C_{22}H_{36}NaO_3$ [$(M+Na)^+$]: 371.25567; found: 371.25595.

3*β*-Hydroxy-21-hydroxymethyl-pregn-5-en-20-ol (UPR1387). This compound is prepared according to the procedure described for compound **UPR1386** starting from ester **71b**. The title compound (21 mg, 24%) is obtained as a white solid. Mp 223-227 °C. $[\alpha]_D^{20}$ = -46.67° (c = 0.9, $CHCl_3$/MeOH 1:1). ^{1}H NMR (400 MHz, $CDCl_3/CD_3OD$) δ 5.33 (d, *J* = 5.0 Hz, 1H), 3.83 – 3.66 (m, 3H), 3.45 (dq, *J* = 10.5, 5.0 Hz, 1H), 2.29 – 2.15 (m, 2H), 2.02 – 1.77 (m, 6H), 1.68 – 1.36 (m, 9H), 1.30 – 0.89 (m, 8H), 0.69 (s, 3H). ^{13}C NMR (100 MHz, $CDCl_3/CD_3OD$) δ 141.7, 122.1, 72.3, 71.9, 60.5, 57.5, 51.1, 42.5, 42.3, 39.8, 39.6, 38.1, 37.3, 32.6, 32.4, 31.8, 26.4, 24.8, 21.5, 19.8, 12.8. HRMS (ESI): m/z: calcd for $C_{22}H_{36}NaO_3$ [$(M+Na)^+$]: 371.25567; found: 371.25556.

3*β*-Hydroxy-21-carboxy-pregn-5-en-20-ol (UPR1380). A solution of NaOH (39 mg, 1.0 mmol) in water (1 ml) is added to a solution of compound **71a** (36 mg, 0.1 mmol) in THF (2 ml). After stirring for 15 h at room temperature, the reaction is quenched by the addition of HCl 1M (1 ml). Solvents are removed under reduced pressure and the residue is purified by silica gel column chromatography (petroleum ether/AcOEt 3:2 + 0.5% AcOH) to afford the title compound (26 mg, 86%) as a white solid. Mp 225-227 °C. $[\alpha]_D^{20}$ = -22.83° (c = 0.9, $CHCl_3$/MeOH 1:1). ^{1}H NMR (400 MHz, $CDCl_3/CD_3OD$) δ 5.31 (d, *J* = 5.0 Hz, 1H), 3.93 (td, *J* = 9.7, 2.7 Hz, 1H), 3.46 – 3.38 (m, 1H), 2.46 (dd, *J* = 15.7, 2.8 Hz, 1H), 2.29 – 2.09 (m, 4H), 1.97 – 1.90 (m, 1H), 1.88 – 1.59 (m, 4H), 1.55 – 1.40 (m, 6H), 1.30 – 0.78 (m, 11H), 0.77 (s, 3H). ^{13}C NMR (75 MHz, $CDCl_3/CD_3OD$) δ 175.9, 141.8, 122.0, 72.0, 71.5, 57.1, 56.5, 51.1, 43.2, 42.5, 42.4, 40.2, 38.1, 37.3, 32.7, 32.6, 31.8, 26.1, 25.2, 21.6, 19.8, 12.5. HRMS (ESI): m/z: calcd for $C_{22}H_{33}O_4$ [$(M-H)^-$]: 361.23843; found: 361.23898.

3*β*-Hydroxy-21-carboxy-pregn-5-en-20-ol (UPR1383). This compound is prepared according to the procedure described for compound **UPR1380** starting from ester **71b**. The title compound (26 mg, 72%) is obtained as a white solid. Mp 235 °C (dec.). $[\alpha]_D^{20}$

= -54.17° (c = 0.7, $CHCl_3$/MeOH 1:1). ^{1}H NMR (300 MHz, $CDCl_3$/CD_3OD) δ 5.32 (d, *J* = 5.0 Hz, 1H), 3.91 (td, *J* = 9.1, 3.1 Hz, 1H), 3.43 (dq, *J* = 10.1, 4.7 Hz, 1H), 2.61 (dd, *J* = 15.5, 3.2 Hz, 1H), 2.36 – 2.15 (m, 3H), 2.08 – 1.72 (m, 6H), 1.72 – 1.35 (m, 9H), 1.32 – 0.79 (m, 9H), 0.71 (s, 3H). ^{13}C NMR (75 MHz, $CDCl_3$/CD_3OD) δ 175.7, 141.5, 121.9, 71.8, 70.5, 57.2, 56.6, 50.8, 42.3, 42.2, 42.0, 39.4, 37.9, 37.1, 32.4, 32.2, 31.6, 26.0, 24.6, 21.4, 19.7, 12.8. HRMS (ESI): m/z: calcd for $C_{22}H_{33}O_4$ [$(M-H)^-$]: 361.23843; found: 361.23850.

3*β*-Hydroxy-21-carbamoyl-pregn-5-en-20-ol (UPR1390). To a solution of compound **71a** (112 mg, 0.3 mmol) in THF (2 ml) is added a solution of NaOH (115 mg, 2.9 mmol) in water (2 ml). After stirring for 15 h at room temperature, HCl 1M (3 ml) is added and the mixture is extracted with AcOEt. The organic layer is washed with brine, dried over Na_2SO_4 and concentrated under reduced pressure. The residue is then dissolved in DMF (2 ml) and NH_4Cl (90 mg, 1.7 mmol), TBTU (98 mg, 0.3 mmol) and DIPEA (0.14 ml, 0.8 mmol) are added to the solution. After stirring for 15h at room temperature the suspension is concentrated under reduced pressure and the residue is purified by silica gel column chromatography (petroleum ether/AcOEt 1:1 + 3% AcOH) and crystallization (EtOH/water 7:3) to afford the title compound (30 mg, 25%) as colorless crystals. Mp 265 °C. $[\alpha]_D^{20}$ = -34.48° (c = 1.2, $CHCl_3$/MeOH 1:1). ^{1}H NMR (300 MHz, DMSO-*d*$_6$) δ 7.25 (s, 1H), 6.83 (s, 1H), 5.26 (d, *J* = 4.9 Hz, 1H), 4.57 (dd, *J* = 8.9, 5.1 Hz, 2H), 3.73 (qd, *J* = 7.3, 5.7, 2.9 Hz, 1H), 3.28 – 3.17 (m, 1H), 2.22 – 1.84 (m, 6H), 1.81 – 1.24 (m, 10H), 1.21 – 0.77 (m, 9H), 0.71 (s, 3H). ^{13}C NMR (100 MHz, DMSO-*d*$_6$) δ 174.0, 141.3, 120.4, 70.1, 70.0, 55.8, 55.8, 49.8, 42.4, 42.3, 42.0, 37.0, 36.1, 31.5, 31.4, 31.4, 25.0, 24.2, 20.5, 19.2, 11.9. HRMS (ESI): m/z: calcd for $C_{22}H_{35}NNaO_3$ [$(M+Na)^+$]: 384.25092; found: 384.25089.

3*β*-Hydroxy-21-carbamoyl-pregn-5-en-20-ol (UPR1391). This compound is prepared according to the procedure described for compound **UPR1390** starting from ester **71b**. The title compound (21 mg, 25%) is obtained as colorless crystals. Mp 280 °C. $[\alpha]_D^{20}$ = -44.44° (c = 0.9, $CHCl_3$/MeOH 1:1). ^{1}H NMR (300 MHz, DMSO-*d*$_6$) δ 7.28 (s, 1H), 6.81

(s, 1H), 5.26 (d, J = 4.9 Hz, 1H), 4.57 (dd, J = 10.7, 5.0 Hz, 2H), 3.81 - 3.73 (m, 1H), 3.31 – 3.20 (m, 1H), 2.32 – 2.21 (m, 1H), 2.21 – 1.98 (m, 3H), 1.98 – 1.19 (m, 13H), 1.19 – 0.81 (m, 8H), 0.64 (s, 3H). ^{13}C NMR (75 MHz, DMSO-d_6) δ 173.7, 141.3, 120.4, 70.0, 68.3, 56.1, 55.9, 49.8, 42.7, 42.2, 41.0, 38.2, 36.9, 36.1, 31.4, 31.1, 24.4, 23.7, 20.4, 19.2, 12.4. HRMS (ESI): m/z: calcd for $C_{22}H_{35}NNaO_3$ [$(M+Na)^+$]: 384.25092; found: 384.25082.

3*β*-Benzoyloxy-21-(hydroxybenzyl)-pregn-5-en-20-one (73a,b). A solution of pregnenolone benzoate (**72**, 368 mg, 0.87 mmol) in anhydrous THF (10 ml) is cooled to -78°C under a nitrogen atmosphere and LiHMDS (1.0 M, 1.80 ml, 1.80 mmol) is slowly added. After the addition of benzaldehyde (0.27 ml, 2.66 mmol), the mixture is allowed to warm to room temperature over 2 h. The reaction is quenched by the addition of acetic acid (0.12 ml, 2.10 mmol) and the mixture is diluted with DCM and washed with water. The organic layer is washed with brine, dried over Na_2SO_4 and concentrated under reduced pressure. The residue is purified by silica gel column chromatography (petroleum ether/AcOEt 9:1) to afford compound **73a** (187 mg, 41%) and compound **73b** (113 mg, 25%). **73a**: ^{1}H NMR (400 MHz, $CDCl_3$) δ 8.10 – 7.98 (m, 2H), 7.61 – 7.49 (m, 1H), 7.49 – 7.27 (m, 7H), 5.42 (d, J = 5.0 Hz, 1H), 5.17 (dd, J = 8.3, 3.9 Hz, 1H), 4.96 – 4.74 (m, 1H), 2.91 – 2.70 (m, 2H), 2.62 – 2.34 (m, 3H), 2.32 – 2.10 (m, 1H), 2.10 – 1.83 (m, 4H), 1.83 – 1.40 (m, 8H), 1.33 – 0.94 (m, 7H), 0.65 (s, 3H). **73b**: ^{1}H NMR (400 MHz, $CDCl_3$) δ 8.07 – 8.01 (m, 2H), 7.61 – 7.50 (m, 1H), 7.43 (t, J = 7.7 Hz, 2H), 7.40 – 7.32 (m, 4H), 7.32 – 7.27 (m, 1H), 5.42 (d, J = 5.0 Hz, 1H), 5.17 (dd, J = 7.7, 4.4 Hz, 1H), 5.04 – 4.74 (m, 1H), 2.83 – 2.76 (m, 2H), 2.59 – 2.46 (m, 3H), 2.28 – 2.14 (m, 1H), 2.09 – 1.90 (m, 4H), 1.82 – 1.37 (m, 8H), 1.33 – 1.13 (m, 4H), 1.07 (s, 3H), 0.65 (s, 3H).

3*β*-Benzoyloxy-21-(hydroxybenzyl)-pregn-5-en-20-ol (74a). To a solution of compound **73a** (176 mg, 0.33 mmol) in THF (5 ml) $Na(OAc)_3BH$ (702 mg, 3.31 mmol) is added at room temperature and the mixture is stirred for 2 h. The reaction is quenched by the addition of HCl (1M, 3.3 ml, 3.30 mmol). After stirring for 15 min, NaOH 2M is

added till neutralization, followed by DCM. The layers are separated and the aqueous phase is extracted again with DCM. The combined organic layers are washed with brine, dried over Na_2SO_4 and concentrated under reduced pressure. The residue is purified by silica gel column chromatography (petroleum ether/AcOEt 9:1) to afford the title compound (145 mg, 83%) as a single isomer. ^{1}H NMR (300 MHz, $CDCl_3$) δ 8.16 – 7.95 (m, 2H), 7.65 – 7.49 (m, 1H), 7.49 – 7.28 (m, 7H), 5.55 – 5.35 (m, 1H), 5.08 (dd, *J* = 9.1, 2.8 Hz, 1H), 4.87 (dtt, *J* = 12.0, 8.1, 4.5 Hz, 1H), 3.90 (ddd, *J* = 10.4, 8.1, 2.6 Hz, 1H), 2.47 (d, *J* = 8.0 Hz, 2H), 2.12 (dt, *J* = 12.2, 3.3 Hz, 1H), 2.05 – 1.88 (m, 4H), 1.85 – 1.43 (m, 10H), 1.38 – 1.00 (m, 10H), 0.78 (s, 3H).

3*β*-Benzoyloxy-21-(hydroxybenzyl)-pregn-5-en-20-ol (74b,c). These compounds are prepared according to the procedure described for compound **74a** starting from compound **73b**. The title compounds (**74b**: 41 mg, 60%; **74c**: 29 mg, 40%) are obtained as white solids. **74b**: ^{1}H NMR (300 MHz, $CDCl_3$/CD_3OD) δ 8.05 – 7.91 (m, 2H), 7.52 (t, *J* = 7.4 Hz, 1H), 7.46 – 7.13 (m, 7H), 5.38 (d, *J* = 4.9 Hz, 1H), 5.00 (dd, *J* = 9.0, 2.8 Hz, 1H), 4.89 – 4.66 (m, 1H), 3.74 (dt, *J* = 9.7, 5.1 Hz, 1H), 2.42 (d, *J* = 7.9 Hz, 2H), 2.07 – 0.62 (m, 23H), 0.58 (s, 3H). **74c**: ^{1}H NMR (300 MHz, $CDCl_3$) δ 8.12 – 7.99 (m, 2H), 7.64 – 7.50 (m, 1H), 7.43 (dd, *J* = 8.3, 6.8 Hz, 2H), 7.39 – 7.27 (m, 5H), 5.50 – 5.37 (m, 1H), 5.02 – 4.90 (m, 1H), 4.85 (ddd, *J* = 12.1, 8.0, 4.1 Hz, 1H), 3.92 (td, *J* = 9.3, 8.1, 4.6 Hz, 1H), 2.47 (d, *J* = 8.1 Hz, 2H), 2.01 – 0.91 (m, 25H), 0.83 (s, 3H).

3*β*-Hydroxy-21-(hydroxybenzyl)-pregn-5-en-20-ol (UPR1377). A mixture of compound **74a** (143 mg, 0.27 mmol) and NaOH (360 mg, 9.00 mmol) in THF (3 ml) and water (3 ml) is stirred for 2 h at reflux. After cooling to room temperature, the reaction is quenched by the addition of acetic acid (0.6 ml, 10.50 mmol). The mixture is diluted with AcOEt and the layers are separated. The aqueous phase is extracted with AcOEt and the combined organic layers are washed with brine, dried over Na_2SO_4 and concentrated under reduced pressure. The residue is purified by silica gel column chromatography (petroleum ether/AcOEt 65:35) to afford the title compound (101 mg, 88%) as a white solid. Mp 190 °C. $[\alpha]_D^{20}$ = -31.90° (c = 1.2, $CHCl_3$/MeOH 1:1). ^{1}H NMR

(300 MHz, CD_3OD) δ 7.39 – 7.22 (m, 4H), 7.22 – 7.13 (m, 1H), 5.30 (dd, *J* = 4.5, 2.8 Hz, 1H), 4.95 (dd, *J* = 10.1, 2.4 Hz, 1H), 3.84 (td, *J* = 9.7, 2.2 Hz, 1H), 3.53 – 3.37 (m, 1H), 2.32 – 2.05 (m, 3H), 2.05 – 1.70 (m, 4H), 1.66 – 1.39 (m, 8H), 1.31 – 0.85 (m, 10H), 0.77 (s, 3H). ^{13}C NMR (100 MHz, CD_3OD) δ 146.0, 141.5, 128.7, 127.5, 126.0, 121.9, 71.7, 71.3, 70.9, 56.8, 56.5, 50.9, 46.0 (d, *J* = 4.5 Hz), 43.0, 42.3, 40.2, 37.9, 37.1, 32.5, 32.4, 31.6, 25.9, 25.1, 21.5, 19.7, 12.5. HRMS (ESI): m/z: calcd for $C_{28}H_{40}NaO_3$ $[(M+Na)^+]$: 447.28697; found: 447.28687.

3*β*-Hydroxy-21-(hydroxybenzyl)-pregn-5-en-20-ol (UPR1379). This compound is prepared according to the procedure described for compound **UPR1377** starting from intermediate **74b**. The title compound (23 mg, 68%) is obtained as a white solid. Mp 223 °C. $[\alpha]_D^{20}$ = -50.00° (c = 0.4, $CHCl_3$/MeOH 1:1). ^1H NMR (300 MHz, $CDCl_3/CD_3OD$) δ 7.39 – 7.25 (m, 4H), 7.22 (ddd, *J* = 6.1, 5.0, 2.2 Hz, 1H), 5.30 (d, *J* = 4.7 Hz, 1H), 4.86 (dd, *J* = 8.2, 5.3 Hz, 1H), 3.65 (td, *J* = 9.6, 2.8 Hz, 1H), 3.43 (dq, *J* = 9.5, 4.5, 4.1 Hz, 1H), 2.19 (dd, *J* = 9.4, 3.7 Hz, 2H), 2.11 (dt, *J* = 12.5, 3.3 Hz, 1H), 1.98 – 1.27 (m, 12H), 1.27 – 0.81 (m, 10H), 0.72 (s, 3H). ^{13}C NMR (75 MHz, $CDCl_3/CD_3OD$) δ 145.4, 141.7, 129.0, 128.1, 126.8, 122.0, 74.8, 74.4, 72.0, 57.4, 57.1, 51.1, 45.8, 43.1, 42.5, 40.2, 38.1, 37.3, 32.6, 32.6, 31.8, 26.2, 25.2, 21.6, 19.8, 12.4. HRMS (ESI): m/z: calcd for $C_{28}H_{40}NaO_3$ $[(M+Na)^+]$: 447.28697; found: 447.28695.

3*β*-Hydroxy-21-(hydroxybenzyl)-pregn-5-en-20-ol (UPR1378). This compound is prepared according to the procedure described for compound **UPR1377** starting from intermediate **74c**. The title compound (33 mg, 78%) is obtained as a white solid. Mp 209 °C. $[\alpha]_D^{20}$ = -41.67° (c = 0.8, $CHCl_3$/MeOH 1:1). ^1H NMR (400 MHz, CD_3OD) δ 7.42 – 7.25 (m, 4H), 7.25 – 7.13 (m, 1H), 5.31 (d, *J* = 5.0 Hz, 1H), 4.98 (dd, *J* = 9.3, 2.6 Hz, 1H), 3.78 (td, *J* = 9.8, 9.3, 2.4 Hz, 1H), 3.41 (tt, *J* = 10.4, 4.8 Hz, 1H), 2.29 – 2.09 (m, 2H), 2.09 – 1.35 (m, 14H), 1.35 – 0.72 (m, 9H), 0.63 (s, 3H). ^{13}C NMR (100 MHz, DMSO-d_6) δ 147.3, 141.3, 128.0, 126.4, 125.5, 120.5, 70.0, 69.0, 68.1, 56.6, 56.2, 49.7, 47.4, 42.2, 41.1, 38.6, 36.9, 36.1, 31.4, 31.2, 25.3, 23.8, 20.4, 19.2, 12.3. HRMS (ESI): m/z: calcd for $C_{28}H_{40}NaO_3$ $[(M+Na)^+]$: 447.28697; found: 447.28760.

3*β*-Benzoyloxy-21-(hydroxy-pyridin-2-yl-methyl)-pregn-5-en-20-one (75a,b). To a solution of pregnenolone benzoate (**72**, 1.21 g, 2.89 mmol) in anhydrous THF (20 ml) LiHMDS (1.0 M, 4.40 ml, 4.40 mmol) is slowly added at -78 °C. After the addition of 2-pyridinecarboxaldehyde (1.60 ml, 16.82 mmol), the mixture is allowed to warm to -55 °C and excess saturated aqueous solution of NH_4Cl is added. The mixture is diluted with DCM and the layers are serapated. The organic layer is washed with water and brine, dried over Na_2SO_4 and concentrated under reduced pressure and the residue is purified by silica gel column chromatography (petroleum ether/AcOEt 4:1) to afford the mixture of epimers **75a** and **75b** (1.25 g, 82%) in about 1:0.8 ratio. ^{1}H NMR (300 MHz, $CDCl_3$) δ 8.53 (dd, *J* = 4.9, 1.6 Hz, 1H), 8.10 – 8.00 (m, 2H), 7.70 (tt, *J* = 7.6, 1.6 Hz, 1H), 7.59 – 7.35 (m, 4H), 7.24 – 7.10 (m, 1H), 5.41 (dd, *J* = 5.0, 1.8 Hz, 1H), 5.21 (dq, *J* = 7.8, 3.7 Hz, 1H), 5.00 – 4.69 (m, 1H), 4.22 (d, *J* = 4.8 Hz, 1H), 3.10 – 2.82 (m, 2H), 2.64 – 2.51 (m, 1H), 2.47 (d, *J* = 7.8 Hz, 2H), 2.33 – 1.95 (m, 4H), 1.91 (dt, *J* = 13.3, 3.4 Hz, 1H), 1.83 – 1.35 (m, 8H), 1.35 – 0.93 (m, 8H), 0.63-0.61 (m, 3H).

3*β*-Benzoyloxy-21-(hydroxy-pyridin-2-yl-methyl)-pregn-5-en-20-ol (76a,b). These compounds are prepared according to the procedure described for compound **74a** starting from compound **75**. The title compounds (**76a**: 165 mg, 16%; **76b***:* 217 mg, 21%) are obtained as white solids. **76a**: ^{1}H NMR (300 MHz, DMSO-d_6) δ 8.48 (d, *J* = 4.4 Hz, 1H), 7.96 (d, *J* = 7.5 Hz, 2H), 7.78 (td, *J* = 7.6, 1.8 Hz, 1H), 7.65 (t, *J* = 7.3 Hz, 1H), 7.52 (t, *J* = 7.7 Hz, 2H), 7.46 (d, *J* = 7.9 Hz, 1H), 7.24 (ddd, *J* = 7.5, 4.8, 1.2 Hz, 1H), 5.56 (d, *J* = 4.1 Hz, 1H), 5.39 (d, *J* = 4.8 Hz, 1H), 4.85 – 4.80 (m, 1H), 4.77 – 4.66 (m, 1H), 4.52 (d, *J* = 5.0 Hz, 1H), 3.54 – 3.46 (m, 1H), 2.42 (d, *J* = 7.8 Hz, 2H), 2.16 (d, *J* = 12.5 Hz, 1H), 2.03 – 1.28 (m, 12H), 1.28 – 0.78 (m, 10H), 0.67 (s, 3H). **76b**: ^{1}H NMR (300 MHz, DMSO-d_6) δ 8.46 (d, J = 4.5 Hz,1H), 8.04 – 7.88 (m, 2H), 7.76 (td, *J* = 7.7, 1.8 Hz, 1H), 7.71 – 7.60 (m, 1H), 7.60 – 7.40 (m, 3H), 7.21 (ddd, *J* = 7.5, 4.8, 1.2 Hz, 1H), 5.40 (d, *J* = 4.8 Hz, 1H), 5.24 (d, *J* = 5.3 Hz, 1H), 4.87 – 4.81 (m, 1H), 4.77 – 4.70 (m, 1H), 4.29 (d, *J* = 7.3 Hz, 1H), 3.70 (q, *J* = 8.9 Hz, 1H), 2.42 (d, *J* = 7.8 Hz, 2H), 2.20 (d, *J* = 12.6 Hz, 1H), 2.00 – 1.86 (m, 3H), 1.83 – 1.09 (m, 16H), 1.04 (s, 3H), 0.75 (s, 3H).

3*β*-Hydroxy-21-(hydroxy-pyridin-2-yl-methyl)-pregn-5-en-20-ol (UPR1395). This compound is prepared according to the procedure described for compound **UPR1377** starting from intermediate **76a**. The title compound (82 mg, 71%) is obtained as a white solid. Mp 225-226 °C. $[\alpha]_D^{20}$ = -73.33° (c = 0.9, $CHCl_3$/MeOH 1:1). ^{1}H NMR (400 MHz, CD_3OD) δ 8.47 (ddd, *J* = 4.9, 1.8, 0.9 Hz, 1H), 7.84 (td, *J* = 7.7, 1.8 Hz, 1H), 7.56 (dt, *J* = 7.9, 1.1 Hz, 1H), 7.31 (ddd, *J* = 7.6, 4.9, 1.2 Hz, 1H), 5.33 (d, *J* = 4.8 Hz, 1H), 4.95 (dd, *J* = 7.6, 6.1 Hz, 1H), 3.60 (td, *J* = 10.0, 2.0 Hz, 1H), 3.47 – 3.34 (m, 1H), 2.30 – 2.09 (m, 3H), 1.97 (ddd, *J* = 14.1, 6.1, 2.1 Hz, 2H), 1.87 (dt, *J* = 13.2, 3.5 Hz, 1H), 1.82 – 1.36 (m, 10H), 1.27 – 0.88 (m, 9H), 0.73 (s, 3H). ^{13}C NMR (100 MHz, $CDCl_3$/CD_3OD) δ 163.8, 148.3, 141.4, 138.0, 123.0, 121.7, 120.9, 74.9, 74.5, 71.6, 56.8, 56.6, 50.7, 44.2, 42.8, 42.2, 39.9, 37.7, 36.9, 32.3, 32.2, 31.5, 25.8, 24.9, 21.3, 19.6, 12.4. HRMS (ESI): m/z: calcd for $C_{27}H_{40}NO_3$ [$(M+H)^+$]: 426.30027; found: 426.30002.

3*β*-Hydroxy-21-(hydroxy-pyridin-2-yl-methyl)-pregn-5-en-20-ol (UPR1396). This compound is prepared according to the procedure described for compound **UPR1377** starting from intermediate **76b**. The title compound (41 mg, 64%) is obtained as a white solid. Mp 200-203 °C. $[\alpha]_D^{20}$ = -22.55° (c = 1.0, $CHCl_3$/MeOH 1:1). ^{1}H NMR (400 MHz, CD_3OD) δ 8.45 (ddd, *J* = 5.0, 1.8, 0.9 Hz, 1H), 7.82 (td, *J* = 7.7, 1.8 Hz, 1H), 7.56 (dt, *J* = 8.0, 1.2 Hz, 1H), 7.28 (ddd, *J* = 7.5, 4.9, 1.2 Hz, 1H), 5.34 (dd, *J* = 4.5, 2.8 Hz, 1H), 5.00 (dd, *J* = 10.0, 2.6 Hz, 1H), 3.86 (td, *J* = 10.1, 2.1 Hz, 1H), 3.50 – 3.35 (m, 1H), 2.27 – 2.15 (m, 3H), 2.01 – 1.94 (m, 1H), 1.88 (dt, *J* = 13.3, 3.5 Hz, 1H), 1.83 – 1.71 (m, 2H), 1.71 – 1.36 (m, 9H), 1.32 – 0.91 (m, 9H), 0.82 (s, 3H). ^{13}C NMR (75 MHz, $CDCl_3$/CD_3OD) δ 164.7, 148.3, 141.5, 138.1, 122.8, 121.9, 120.9, 71.7, 71.3, 71.1, 56.8, 56.8, 50.8, 45.0, 43.0, 42.3, 40.1, 37.8, 37.0, 32.4, 32.3, 31.6, 25.9, 25.0, 21.4, 19.7, 12.5. HRMS (ESI): m/z: calcd for $C_{27}H_{40}NO_3$ [$(M+H)^+$]: 426.30027; found: 426.30032.

(20*R*)-21-(*bis*(Trifluoromethyl)hydroxymethyl)-pregn-5-en-20-ol-*3β*-(2,3,4,6-tetra-*O*-acetyl)-*β*-D-glucopyranoside (77). To a solution of compound **54** (117 mg, 0.24 mmol) and 2,3,4,6-tetra-O-acetyl-D-glucopyranosyl trichloroacetimidate (180 mg, 0.36

mmol) in anhydrous DCM (20 ml), TMSOTf (0.004 ml, 0.024 mmol) is added at -25 °C. After stirring for 15 min at 0 °C, the reaction is quenched by the addition of triethylamine (0.20 ml, 1.43 mmol). The mixture is diluted with AcOEt and washed with water. The organic layer is washed with brine, dried over Na_2SO_4 and concentrated under reduced pressure. The residue is purified by silica gel column chromatography (hexane/AcOEt 3:1) to afford the title compound (30 mg, 15%) as a white solid. ^{1}H NMR (400 MHz, $CDCl_3$) δ 6.34 (s, 1H), 5.35 (dd, *J* = 4.9, 2.6 Hz, 1H), 5.20 (t, *J* = 9.5 Hz, 1H), 5.08 (t, *J* = 9.7 Hz, 1H), 4.95 (dd, *J* = 9.6, 8.0 Hz, 1H), 4.59 (d, *J* = 7.9 Hz, 1H), 4.30 – 4.17 (m, 2H), 4.11 (dd, *J* = 12.2, 2.5 Hz, 1H), 3.67 (ddd, *J* = 9.9, 4.8, 2.5 Hz, 1H), 3.48 (tt, *J* = 11.2, 4.8 Hz, 1H), 2.31 – 2.13 (m, 2H), 2.10 – 1.81 (m, 15H), 1.79 – 1.40 (m, 10H), 1.40 – 1.11 (m, 7H), 1.00 (s, 3H), 0.81 (s, 3H).

(20*R*)-21-(*bis*(Trifluoromethyl)hydroxymethyl)-pregn-5-en-20-ol-*3β*-*β*-D-glucopyranoside (UPR1389). A solution of compound **77** (30 mg, 0.04 mmol) and sodium (5 mg, 0.2 mmol) in MeOH (3 ml) is stirred for 2 h at room temperature, then HCl 1M (0.2 ml) is added and the mixture is diluted with AcOEt. The organic layer is washed with water and brine, dried over Na_2SO_4 and concentrated under reduced pressure. The residue is purified by silica gel column chromatography ($CHCl_3$/MeOH 9:1) to afford the title compound (13 mg, 50%) as a white solid. Mp 210 °C (dec.). $[\alpha]_D^{20}$ = -56.25° (c = 0.03, $CHCl_3$/MeOH 1:1). ^{1}H NMR (300 MHz, $CDCl_3$/CD_3OD) δ 5.33 (d, *J* = 5.0 Hz, 1H), 4.06 (t, *J* = 9.9 Hz, 1H), 3.81 (dd, *J* = 12.0, 3.0 Hz, 1H), 3.70 (dd, *J* = 11.9, 4.9 Hz, 1H), 3.64 – 3.48 (m, 1H), 3.48 – 3.33 (m, 2H), 3.22 (dddd, *J* = 17.0, 9.2, 4.6, 2.2 Hz, 2H), 2.45 – 2.31 (m, 1H), 2.23 (t, *J* = 12.4 Hz, 1H), 2.11 – 1.75 (m, 6H), 1.75 – 1.32 (m, 8H), 1.31 – 0.80 (m, 11H), 0.80 (s, 3H). ^{13}C NMR (100 MHz, $CDCl_3$/CD_3OD) δ 141.0, 125.7, 124.9, 122.8, 122.2, 101.7, 79.5, 77.1, 76.6, 74.1, 71.7, 70.8, 62.3, 57.2, 56.7, 50.7, 42.9, 39.7, 39.1, 37.8, 37.2, 33.8, 32.4, 32.2, 30.0, 25.8, 24.9, 21.3, 19.6, 12.3. HRMS (ESI): m/z: calcd for $C_{30}H_{44}F_6NaO_8$ [$(M+Na)^+$]: 669.28326; found: 669.28381.

3*β*-Pregnenolone-(2,3,4,6-tetra-*O*-acetyl)-*β*-D-glucopyranoside (79). To a solution of pregnenolone (**78**, 3.67 g, 11.60 mmol) and O-(2,3,4,6-tetra-O-acetyl-α,β-D-glucopyranosyl)trichloroacetimidate (3.80 g, 7.71 mmol) in anhydrous DCM (70 ml), TMSOTf (0.07 ml, 0.39 mmol) is added at -55 °C. The mixture is stirred 15 min at 0 °C and the reaction is quenched by the addition of TEA (0.2 ml, 1.43 mmol). The mixture is diluted with DCM and washed with water. The organic layer is washed with brine, dried over Na_2SO_4 and concentrated under reduced pressure. The residue is purified by silica gel column chromatography (hexane/AcOEt 85:15) to afford the title compound (2.52 g, 34%) as a white solid. ^{1}H NMR (400 MHz, $CDCl_3$) δ 5.33 (d, *J* = 5.1 Hz, 1H), 5.18 (t, *J* = 9.5 Hz, 1H), 5.05 (t, *J* = 9.7 Hz, 1H), 4.93 (dd, *J* = 9.6, 7.9 Hz, 1H), 4.57 (d, *J* = 7.9 Hz, 1H), 4.23 (dd, *J* = 12.2, 4.8 Hz, 1H), 4.09 (dd, *J* = 12.2, 2.5 Hz, 1H), 3.66 (ddd, *J* = 10.2, 4.9, 2.5 Hz, 1H), 3.47 (ddd, *J* = 11.2, 6.6, 4.5 Hz, 1H), 2.50 (t, *J* = 8.7 Hz, 1H), 2.31 – 2.11 (m, 3H), 2.10 (s, 3H), 2.05 (s, 3H), 2.02 (s, 3H), 2.00 (s, 3H), 1.98 (s, 3H), 1.90 – 1.80 (m, 3H), 1.71 – 1.34 (m, 9H), 1.28 – 0.99 (m, 4H), 0.96 (s, 3H), 0.60 (s, 3H).

3*β*-Pregnenolone-*β*-D-glucopyranoside (80). A solution of compound **79** (2.52 g, 3.90 mmol) and sodium (70.0 mg, 3.0 mmol) in methanol/THF 1:1 (80 ml) is stirred for 1 h at room temperature. After addition of HCl 1M till neutralization, the mixture is diluted with DCM and the layers are separated. The organic layer is washed with brine, dried over Na_2SO_4 and concentrated under reduced pressure. The residue is purified by silica gel column chromatography (DCM/EtOH 85:15) to afford the title compound (824 mg, 44%) as a white solid. ^{1}H NMR (400 MHz, CD_3OD) δ 5.45 – 5.29 (m, 1H), 4.38 (d, *J* = 7.8 Hz, 1H), 3.85 (dd, *J* = 11.9, 1.7 Hz, 1H), 3.63 (dddd, *J* = 22.9, 11.4, 8.7, 5.1 Hz, 2H), 3.35 (dd, *J* = 9.4, 5.5 Hz, 1H), 3.29 – 3.24 (m, 1H), 3.14 (dd, *J* = 9.1, 7.8 Hz, 1H), 2.64 (t, *J* = 8.8 Hz, 1H), 2.54 – 2.34 (m, 1H), 2.34 – 2.21 (m, 1H), 2.12 (s, 3H), 2.10 – 1.84 (m, 4H), 1.78 – 1.39 (m, 7H), 1.37 – 1.06 (m, 3H), 1.04 (d, *J* = 1.7 Hz, 3H), 0.63 (s, 3H).

3*β*-Pregnenolone-(2,3,4,6-tetra-*O*-benzoyl)-*β*-D-glucopyranoside (81). Benzoyl chloride (2.50 ml, 21.52 mmol) is added to a solution of pregnenolone 3β-D-

glucopyranoside (**80**, 824 mg, 1.72 mmol) in anhydrous pyridine (10 ml). After stirring for 1 h at room temperature, the mixture is diluted with DCM. The organic layer is washed with water and brine, dried over Na_2SO_4 and concentrated under reduced pressure. The residue is purified by silica gel column chromatography (hexane/AcOEt 85:15) to afford the title compound (1.54 g, quantitative yield) as a white solid. ^{1}H NMR (300 MHz, $CDCl_3$) δ 8.10 – 7.98 (m, 2H), 7.98 – 7.79 (m, 6H), 7.79 – 7.70 (m, 2H), 7.57 – 7.05 (m, 10H), 5.83 (t, *J* = 9.6 Hz, 1H), 5.57 (t, *J* = 9.7 Hz, 1H), 5.43 (dd, *J* = 9.7, 7.9 Hz, 1H), 5.15 (d, *J* = 4.8 Hz, 1H), 4.88 (d, *J* = 7.9 Hz, 1H), 4.54 (dd, *J* = 12.0, 3.5 Hz, 1H), 4.45 (dd, *J* = 12.1, 5.7 Hz, 1H), 4.09 (ddd, *J* = 9.7, 5.8, 3.6 Hz, 1H), 3.47 (tt, *J* = 10.5, 5.0 Hz, 1H), 2.45 (t, *J* = 8.7 Hz, 1H), 2.18 – 1.76 (m, 8H), 1.76 – 1.24 (m, 8H), 1.24 – 0.95 (m, 3H), 0.94 – 0.68 (m, 9H), 0.53 (s, 3H).

21-(*bis*(Trifluoromethyl)hydroxymethyl)-pregn-5-en-20-one-3*β*-(2,3,4,6-tetra-*O*-benzoyl)-*β*-D-glucopyranoside (82). To a solution of compound **81** (1.22 g, 1.36 mmol) in anhydrous THF (30 ml), LiHMDS (1M, 3.40 ml, 3.40 mmol) is added at -78 °C, followed by the addition of hexafluoroacetone (2 ml trihydrated hexafluoroacetone delivered according to ref.[240]). The mixture is allowed to warm to -50 °C. The reaction is quenched by the addition of HCl 1M (3.4 ml) and the mixture is diluted with AcOEt and washed with water. The organic layer is washed with brine, dried over Na_2SO_4 and concentrated under reduced pressure. The residue is purified by silica gel column chromatography (hexane/AcOEt 85:15) to afford the title compound (1.05 g, 73%) as a white solid. ^{1}H NMR (400 MHz, DMSO-d_6) δ 8.32 – 7.13 (m, 20H), 5.99 - 5.92 (m, 1H), 5.55 (t, *J* = 9.4 Hz, 1H), 5.34 – 5.26 (m, 2H), 5.19 (s, 1H), 4.59 – 4.38 (m, 3H), 3.53 – 3.46 (m, 1H), 3.08 (d, *J* = 15.5 Hz, 1H), 2.87 (d, *J* = 15.5 Hz, 1H), 2.78 (t, *J* = 8.6 Hz, 1H), 2.20 (d, *J* = 13.2 Hz, 1H), 2.10 – 1.02 (m, 17H), 0.94 – 0.77 (m, 5H), 0.54 (s, 3H).

(20*S*)-21-(*bis*(Trifluoromethyl)hydroxymethyl)-pregn-5-en-20-ol-3*β*-(2,3,4,6-tetra-*O*-benzoyl)-*β*-D-glucopyranoside (83). A mixture of compound **82** (606 mg, 0.57 mmol) and $Na(OAc)_3BH$ (1.21 g, 5.7 mmol) in anhydrous THF (10 ml) is stirred for 1 h at room temperature. After addition of an excess of a Rochelle's salt saturated solution

and 1 h stirring, the mixture is diluted with DCM and the layers are separated. The organic layer is washed with water and brine, dried over Na_2SO_4 and concentrated under reduced pressure. The residue is purified by silica gel column chromatography (hexane/AcOEt 4:1) to afford the title compound (43 mg, 7%) as a white solid. The major product of reduction (20*R*, 468 mg, 77%) was also isolated. ^{1}H NMR (400 MHz, $CDCl_3$) δ 8.08 – 7.79 (m, 7H), 7.60 – 7.14 (m, 13H), 5.89 (t, *J* = 9.6 Hz, 1H), 5.63 (t, *J* = 9.7 Hz, 1H), 5.49 (dd, *J* = 9.8, 7.9 Hz, 1H), 5.22 (d, *J* = 5.0 Hz, 1H), 4.94 (d, *J* = 7.9 Hz, 1H), 4.61 (dd, *J* = 12.0, 3.4 Hz, 1H), 4.52 (dd, *J* = 12.0, 5.9 Hz, 1H), 4.28 – 4.09 (m, 2H), 3.52 (tt, *J* = 10.3, 4.9 Hz, 1H), 2.28 – 0.78 (m, 27H), 0.68 (s, 3H).

(20*S*)-21-(*bis*(Trifluoromethyl)hydroxymethyl)-pregn-5-en-20-ol-*3β*-*β*-D-glucopyranoside (UPR1399). A solution of compound **83** (34 mg, 0.03 mmol) and sodium (1 mg, 0.04 mmol) in MeOH (3 ml) is stirred for 1 h at room temperature. The reaction is quenched by the addition of HCl 0.1M (0.4 ml). The mixture is diluted with AcOEt and washed with water. The organic layer is washed with brine, dried over Na_2SO_4 and concentrated under reduced pressure. The residue is purified by silica gel column chromatography (DCM/MeOH 95:5) to afford the title compound (12 mg, 62%) as a white solid. Mp 220 °C. $[\alpha]_D^{20}$ = -46.67° (c = 0.06, $CHCl_3$/MeOH 1:1). ^{1}H NMR (300 MHz, $CDCl_3$/CD_3OD) δ 5.39 (dd, *J* = 4.6, 2.6 Hz, 1H), 4.40 (d, *J* = 7.8 Hz, 1H), 4.07 (t, *J* = 10.0 Hz, 1H), 3.87 (dd, *J* = 11.9, 1.7 Hz, 1H), 3.75 – 3.52 (m, 2H), 3.46 – 3.21 (m, 2H), 3.16 (dd, *J* = 8.8, 7.8 Hz, 1H), 2.45 (ddd, *J* = 13.3, 4.9, 2.0 Hz, 1H), 2.38 – 2.13 (m, 2H), 2.13 – 1.38 (m, 13H), 1.38 – 0.80 (m, 8H), 0.71 (s, 3H). ^{13}C NMR (75 MHz, $CDCl_3$/CD_3OD) δ 141.4, 122.4, 102.1, 79.6, 77.6, 77.2, 74.6, 71.5, 71.2, 62.5, 58.5, 57.5, 51.0, 42.3, 40.0, 39.4, 38.1, 37.5, 34.3, 32.6, 32.4, 30.3, 26.1, 24.6, 21.6, 19.7, 12.7. HRMS (ESI): m/z: calcd for $C_{30}H_{44}F_6NaO_8$ [$(M+Na)^+$]: 669.28326; found: 669.28387.

3*β*-Hydroxy-5*α*-pregnan-20-one (85). Pregnanolone acetate (**84**, 2.03 g, 5.64 mmol) and sodium (0.10 g, 4.35 mmol) in methanol/THF (1:1, 30 ml) are stirred for 1 h at room temperature. The reaction is then quenched by the addition of HCl (1M, 4.3 ml, 4.3

mmol). After addition of AcOEt and water, the layers are separated and the organic phase is washed with water and brine, dried over Na_2SO_4 and concentrated under reduced pressure to afford the title compound (1.80 g, quantitative yield) as a white solid. Analytical data are in accordance with those reported in the literature.[271]

3*β*-Benzoyloxy-5*α*-pregnan-20-one (86). Isopregnanolone **85** (1.80 g, 5.64 mmol) is dissolved in anhydrous pyridine (5 ml) and benzoyl chloride (1.5 ml, 12.91 mmol) is slowly added to the solution. After stirring for 2 h at room temperature, the mixture is diluted with DCM and water and HCl is added dropwise to the aqueous layer till neutralization. Layers are then separated and the organic extract is washed with water and brine, dried over Na_2SO_4 and concentrated under reduced pressure. The residue is crystallized from isopropanol, affording the title product (1.96 g, 82%) as needle-like crystals. Analytical data are in accordance with those reported in the literature.[272]

3*β*-Benzoyloxy-21-(*bis*(trifluoromethyl)hydroxymethyl)-5*α*-pregnan-20-one (87). 3β-benzoyloxy-5α-pregnan-20-one (**86**, 0.82 g, 1.9 mmol) is dissolved in anhydrous THF (30 ml) and the solution is kept under a nitrogen atmosphere at -78 °C. LiHMDS (1.0M, 2.3 ml, 2.3 mmol) is added and the mixture is stirred for 75 min. In a separate two neck flask concentrated H_2SO_4 (10 ml) is warmed to 50 °C and linked through a cannula with the enolate flask. Trihydrate hexafluoroacetone (2 ml) is dropped inside the H_2SO_4 and through a positive nitrogen pressure, gaseous HFA is bubbled inside the enolate solution. The reaction mixture is then warmed to room temperature. HCl 1M is added till neutralization and the mixture is diluted with AcOEt. The organic phase is separated, washed with brine and dried over Na_2SO_4. Solvents are removed under reduced pressure and the residue is purified by silica gel column chromatography (petroleum ether/AcOEt 95:5) affording the title compound (965 mg, 85%) as a white solid. ^{1}H NMR (300 MHz, $CDCl_3$) δ 8.10 – 7.94 (m, 2H), 7.57 – 7.48 (m, 1H), 7.48 – 7.34 (m, 2H), 7.08 (s, 1H), 4.95 (tt, J = 11.3, 4.9 Hz, 1H), 2.93 (d, J = 17.3 Hz, 1H), 2.78 (d, J = 17.3 Hz, 1H), 2.59 (t, J = 8.7 Hz, 1H), 2.23 – 2.05 (m, 1H), 1.94 (tt, J = 10.9, 3.4

Hz, 2H), 1.83 – 1.04 (m, 18H), 1.04 – 0.92 (m, 1H), 0.87 (s, 3H), 0.74 (ddd, *J* = 13.8, 10.6, 3.8 Hz, 1H), 0.66 (s, 3H).

3*β*-Benzoyloxy-21-(*bis*(trifluoromethyl)hydroxymethyl)-5*α*-pregnan-20-ol (88). To a solution of compound 87 (0.96 g, 1.6 mmol) in THF (15 ml) is added sodium triacetoxyborohydride (3.39 g, 16.0 mmol). The mixture is stirred at room temperature for 2 h, then excess saturated aqueous solution of Rochelle salt is added and the mixture is stirred 15 h at room temperature. After dilution with AcOEt, the layers are separated and the organic phase is washed with brine, dried over Na_2SO_4 and concentrated under reduced pressure. The residue is purified by silica gel column chromatography (petroleum ether/AcOEt 97:3) to afford afford compounds **88a** (460 mg, 48%) and **88b** (112 mg, 12%) as white solids. **88a**: ^{1}H NMR (300 MHz, CD_3OD) δ 8.12 – 7.90 (m, 2H), 7.62 – 7.49 (m, 1H), 7.43 (t, *J* = 7.6 Hz, 2H), 4.90 (tt, *J* = 11.0, 5.0 Hz, 1H), 4.05 (t, *J* = 8.6 Hz, 1H), 2.12 – 2.02 (m, 1H), 1.98 – 1.87 (m, 2H), 1.81 (dt, *J* = 13.1, 3.6 Hz, 1H), 1.74 – 1.60 (m, 5H), 1.60 – 1.38 (m, 4H), 1.37 – 1.04 (m, 10H), 0.90 (s, 3H), 0.84 (td, *J* = 5.2, 4.8, 2.7 Hz, 1H), 0.77 (s, 3H), 0.71 (dd, *J* = 11.0, 3.9 Hz, 1H). **88b**: ^{1}H NMR (300 MHz, CD_3OD) δ 8.16 – 7.85 (m, 2H), 7.61 – 7.47 (m, 1H), 7.42 (dd, *J* = 8.3, 6.8 Hz, 2H), 5.06 – 4.79 (m, 1H), 4.04 (t, *J* = 10.0 Hz, 1H), 2.18 (dd, *J* = 15.1, 2.0 Hz, 1H), 2.00 – 0.68 (m, 27H), 0.67 (s, 3H).

(20*R*)-3*β*-Hydroxy-21-(*bis*(trifluoromethyl)hydroxymethyl)-5*α*-pregnan-20-ol (UPR1393). Compound **88a** (35 mg, 0.1 mmol) is dissolved in MeOH/THF 1:1 (2 ml) and sodium (33 mg, 1.4 mmol) is added at room temperature. The mixture is stirred for 1 h, then the reaction is quenched adding HCl 1M (1.4 ml) and the mixture is extracted with AcOEt. The organic layer is washed with brine and dried over Na_2SO_4. Solvents are removed under reduced pressure and the residue is purified by silica gel column chromatography (DCM/MeOH 98:2) to afford the title compound (29 mg, quantitative yield) as a white solid. Mp 199-202 °C. $[\alpha]_D^{20}$ = +8.33° (c = 1.0, $CHCl_3$/MeOH 1:1).^{1}H NMR (400 MHz, $CD_3OD/CDCl_3$) δ 4.15 – 4.02 (m, 1H), 3.53 (tt, *J* = 11.1, 4.7 Hz, 1H), 2.07 (dt, *J* = 12.6, 3.3 Hz, 1H), 2.05 – 1.86 (m, 2H), 1.80 -1.64 (m, 5H), 1.60 – 0.89 (m,

16H), 0.86 (s, 3H), 0.80 (s, 3H), 0.70 (ddd, *J* = 12.1, 10.3, 4.1 Hz, 1H). ^{13}C NMR (75 MHz, CD_3OD) δ 125.9, 125.2, 122.1, 121.4, 71.6, 71.1, 57.2, 56.2, 54. 7, 45.2, 43.0, 39.8, 37.9, 37.3, 35.7, 33.5, 32.4, 31.2, 28.9, 25.6, 24.6, 21.3, 12.4. ESI-MS $[M-H]^-$ calcd for $C_{24}H_{35}F_6O_3$: 485.24959. Found: 485.24973.

(20*S*)-3*β*-Hydroxy-21-(*bis*(trifluoromethyl)hydroxymethyl)-5*α*-pregnan-20-ol (UPR1392). This compound is prepared according to the procedure reported for compound **UPR1393** starting from intermediate **88b**. Compound **UPR1392** (62 mg, 75%) is obtained as a white solid. Mp 229-235 °C. $[\alpha]_D^{20}$ = +7.94° (c = 1.3, $CHCl_3/CH_3OH$ 1/1). ^{1}H NMR (300 MHz, $CD_3OD/CDCl_3$) δ 4.03 (t, J = 10.1 Hz, 1H), 3.50 (m, 1H), 2.17 (dd, J = 15.0, 2.0 Hz, 1H), 1.87 (m, 2H), 1.76 – 0.88 (m, 21H), 0.80 (s, 3H), 0.69 – 0.59 (m, 4H). ^{13}C NMR (75 MHz, CD_3OD) δ 129.8 (d, *J* = 64.9 Hz), 126.0 (d, *J* = 62.4 Hz), 122.2 (d, *J* = 60.3 Hz), 118.4 (d, *J* = 57.9 Hz), 71.5, 71.4, 58.5, 57.1, 55.0, 45.6, 42.4, 40.2, 38.3, 37.7, 36.2, 35.9, 34.1, 32.7, 31.6, 29.3, 26.1, 24.4, 21.7, 12.8, 12.6. ESI-MS $[M-H]^-$ calcd for $C_{24}H_{35}F_6O_3$: 485.24959. Found: 485.24924.

6.4. Synthesis of zampanolide analogue **NB-24**

5-*tert*-Butyldiphenylsilyloxy-1-pentanol (92). 1,5-pentanediol (**91**, 1.51 ml, 14.40 mmol) is added to a suspension of sodium hydride (576 mg of 60% suspension in mineral oil, washed free of oil, 14.40 mmol) in anhydrous THF (28.8 ml) at room temperature. A cloudy white precipitate is obtained. After stirring for 50 min, TBDPSCl (3.7 ml, 14.40 mmol) is added. The mixture is stirred for 16 h, then it is poured into ether (30 ml), washed with water (3 x 30 ml) and brine, dried over $MgSO_4$ and concentrated under reduced pressure. The residue is purified by silica gel column chromatography (hexane/AcOEt 9:1→7:3) to afford the title compound (3.178 g, 64%) as a thick, colourless oil. TLC: R_f = 0.37(hexane/AcOEt 7:3; UV, CPS, $KMnO_4$). ^{1}H NMR (400 MHz, $CDCl_3$) δ 7.69-7.66 (m, 4 H), 7.45-7.36 (m, 6 H), 3.68 (t, *J* = 6.4 Hz, 2 H), 3.62 (t, *J* = 6.5 Hz, 2 H), 1.63-1.52 (m, 4 H), 1.47-1.40 (m, 2 H), 1.06 (s, 9 H). ^{13}C NMR (100 MHz, $CDCl_3$) δ 135.7, 134.2, 129.7, 127.8, 63.9, 63.1, 32.6, 32.4, 27.0, 22.1, 19.4. IR (thin film): ῡ = 3331, 2931, 2858, 1427, 1108, 822, 740, 700, 613, 503, 488 cm^{-1}. HRMS (ESI): m/z: calcd for $C_{21}H_{30}NaO2Si$ [$(M+Na)^+$]: 365.1907; found: 365.1906.

5-((*tert*-Butyldiphenylsilyl)oxy)pentyl 4-methylbenzenesulfonate (93). Tosyl chloride (3.51 g, 18.41 mmol) is slowly added to a solution of compound **92** (5.26 g, 15.34 mmol) in DCM (30.0 ml) and pyridine (2.50 ml, 30.69 mmol). After stirring for 16 h, the mixture is washed with $NaHCO_3$ (2 x 50 ml). The organic layer is extracted with DCM (30 ml) and the combined organic layers are washed with 2M HCl (50 ml) and water, dried over $MgSO_4$ and concentrated under reduced pressure. The residue is purified by silica gel column chromatography (hexane/DCM 2:1) to afford the title compound (6.569 g, 95%) as a thick, colourless oil. TLC: R_f = 0.13 (hexane/DCM 2:1; UV, CPS, $KMnO_4$). ^{1}H NMR (400 MHz, $CDCl_3$) δ 7.79-7.77 (m, 2 H), 7.65-7.62 (m, 4 H), 7.44-7.7.35 (m, 6 H), 7.33-7.31 (m, 2 H), 4.00 (t, *J* = 6.5 Hz, 2 H), 3.60 (t, *J* = 6.2 Hz, 2 H), 2.43 (s, 3 H), 1.66-1.59 (m, 2 H), 1.53-1.46 (m, 2 H), 1.42-1.36 (m, 2 H), 1.03 (s, 9 H). ^{13}C NMR (100 MHz, $CDCl_3$) δ 144.8, 135.7, 134.1, 133.4, 129.9, 129.7, 128.0, 127.8, 70.7, 63.6, 31.9, 28.7, 27.0, 26.7, 21.9, 21.8, 19.3. IR (thin film): ῡ = 2931, 2857,

1472, 1428, 1360, 1189, 1176, 1110, 822, 741, 702, 664, 555, 504 cm^{-1}. HRMS (ESI): m/z: calcd for $C_{28}H_{36}NaO_4SSi$ [$(M+Na)^+$]: 519.1996; found: 519.1995.

***tert*-Butyl((5-iodopentyl)oxy)diphenylsilane (94).** Sodium iodide (9.91 g, 66.12 mmol) is added to a solution of compound **93** (6.57 g, 13.22 mmol) in acetone (140 ml) at room temperature and the mixture is stirred for 24 h. After dilution with water and extraction with diethyl ether (3 x 80 ml), the organic layer is washed with brine, dried over $MgSO_4$. and concentrated under reduced pressure. The title compound (5.855 g, 98%) is obtained as a pale orange oil and used without further purification. TLC: R_f= 0.72 (hexane/AcOEt 9:1; UV, CPS, $KMnO_4$). ^{1}H NMR (400 MHz, $CDCl_3$) δ 7.68-7.65 (m, 4 H), 7.45-7.36 (m, 6 H), 3.66 (t, *J* = 6.3 Hz, 2 H), 3.16 (t, *J* = 7.0 Hz, 2 H), 1.84-1.77 (m, 2 H), 1.61-1.53 (m, 2 H), 1.51-1.45 (m, 2 H), 1.05 (s, 9 H). ^{13}C NMR (100 MHz, $CDCl_3$) δ 135.7, 134.2, 129.7, 127.8, 63.7, 33.4, 31.6, 27.0, 19.4, 7.2. IR (thin film): ῡ = 3070, 2930, 2857, 1427, 1105, 822, 740, 700, 687, 624, 503, 487 cm^{-1}. HRMS (ESI): m/z: calcd for $C_{21}H_{30}IOSi$ [$(M+H)^+$]: 453.1005; found: 453.1092.

***tert*-Butyl(oct-6-yn-1-yloxy)diphenylsilane (95).** Propyne gas (5.0 g, 124.8 mmol) is delivered to a cooled flask (-78 °C) containing anhydrous THF (15 ml) through an argon overpressure. *n*-BuLi (8.0 ml, 12.8 mmol) is added dropwise, followed by stirring for 10 min. HMPA (3.55 ml, 20.39 mmol) is then added dropwise. The mixture is stirred for 30 min, then a further amount of *n*-BuLi (7.5 ml, 12.0 mmol) is added. After dropwise addition of a solution of compound **94** (4.855 g, 10.73 mmol) in anhydrous THF (30 ml), the mixture is allowed to warm to room temperature and stirred for 24 h. It is then poured on a saturated solution of NH_4Cl (500 ml) and extracted with diethyl ether (2 x 150 ml). The combined organic layers are washed with saturated aqueous NH_4Cl (150 ml), water (250 ml) and brine (250 ml), dried over $MgSO_4$ and concentrated under reduced pressure. The residue is purified by silica gel column chromatography (hexane/AcOEt 95:5) to afford the title compound (3.7886 g, 97%) as a colorless oil. TLC: R_f= 0.69 (hexane AcOEt 9:1, UV, CPS, $KMnO_4$). ^{1}H NMR (400 MHz, $CDCl_3$) δ 7.70-7.67 (m, 4 H), 7.45-7.37 (m, 6 H), 3.67 (t, *J* = 6.3 Hz, 2 H), 2.14-2.10 (m, 2 H), 1.78 (t, *J* = 2.6 Hz, 3 H),

1.59-1.56 (m, 2 H), 1.48-1.45 (m, 4 H), 1.06 (s, 9 H). ^{13}C NMR (100 MHz, $CDCl_3$) δ 135.7, 134.2, 129.6, 127.7, 79.4, 75.6, 63.9, 32.3, 28.9, 27.0, 25.2, 19.4, 18.9, 3.6. IR (thin film): ῡ = 3070, 2931, 2858, 1428, 1109, 822, 739, 701, 613, 504, 488 cm^{-1}. HRMS (ESI): m/z: calcd for $C_{24}H_{33}OSi$ [$(M+H)^+$]: 365.2295; found: 365.2291

(*E*)-*tert*-Butyl((7-iodooct-6-en-1-yl)oxy)diphenylsilane (96). DIBAL (1M in hexane, 18.85 ml, 18.85 mmol) is slowly added to a suspension of Cp_2ZrCl_2 (7.71 g, 26.37 mmol) in anhydrous THF (40 ml). After stirring for 30 min at 0 °C a solution of compound **95** (2.75 g, 7.53 mmol) in anhydrous THF (10 ml) is added and the suspension is warmed to 65 °C and stirred for 60 min in the dark. The mixture is then cooled to -78 °C and iodine (2.49 g, 9.79 mmol) in THF (10 ml) is added. Stirring is continued for 15 min, then the reaction is quenched by the addition of 1M HCl (120 ml). Diethyl ether (100 ml) is added and the mixture is stirred until two clear phases are obtained. The layers are separated and the organic phase is washed with saturated aqueous $Na_2S_2O_3$ (100 ml) and $NaHCO_3$ (100 ml), water (100 ml) and brine (75 ml), dried with $MgSO_4$ and concentrated under reduced pressure. The residue is purified by silica gel chromatography (hexane+0.5% AcOEt) to afford the title compound (2.60 g) as a yellow oil. The product contains an impurity that cannot be removed. TLC: R_f= 0.71 (hexane AcOEt 9:1, UV, CPS, $KMnO_4$). ^{1}H NMR (400 MHz, $CDCl_3$) δ 7.69-7.65 (m, 4 H), 7.45-7.36 (m, 6 H), 6.13 (tq, *J* = 7.5, 1.6 Hz, 1 H), 3.65 (t, *J* = 6.4 Hz, 2 H), 2.35 (d, *J* = 1.3 Hz, 3 H), 2.00 (q, *J* = 6.4 Hz, 2 H), 1.59-1.51 (m, 2 H), 1.38-1.32 (m, 4 H), 1.05 (s, 9 H). ^{13}C NMR (100 MHz, $CDCl_3$) δ 141.5, 135.7, 134.2, 129.7, 127.7, 93.6, 63.9, 32.5, 30.8, 28.8, 27.0, 25.4, 19.4. IR (thin film): ῡ = 3070, 2930, 2856, 1427, 1110, 822, 740, 701, 613, 504, 486 cm^{-1}. HRMS (ESI): m/z: calcd for $C_{24}H_{33}INaOSi$ [$(M+Na)^+$]: 515.1238; found: 515.1233.

(*S*,*E*)-10-((*tert*-Butyldiphenylsilyl)oxy)-1-((4-methoxybenzyl)oxy)-4-methyldec-4-en-2-ol (97). Compound **96** (2.60 g, 5.28 mmol) is azeotropically dried once with 10 mL of anhydrous toluene and dissolved in the same solvent (35 mL). The solution is cooled to –78 °C and *n*-BuLi (1.6M in hexane, 4.85 mL, 7.76 mmol) is added. After stirring for 30 min, the mixture is cooled –85 °C and a solution of (*S*)-2-(4-methoxy-

benzyloxymethyl)-oxirane (1.88 g, 9.68 mmol, azeotropically dried once with 5 mL of toluene right before use) in dry toluene (10 mL) is added. After adding BF_3•OEt_2 (1.17 mL, 9.50 mmol), the mixture is stirred for 1 h at –78 °C and it is poured into stirred saturated aqueous $NaHCO_3$ (200 mL). After adding AcOEt and allowing the mixture to reach room temperature, the layers are separated, the aqueous phase is extracted with AcOEt (3 x 50 mL) and the combined organic extracts are dried over $MgSO_4$ and concentrated under reduced pressure. The residue is purified by silica gel column chromatography (first column: toluene+4% AcOEt; second column: hexane/Et_2O 6:1) to afford the title compound (1.76 g, 42% over two steps) as a colorless oil. TLC: R_f = 0.10 (hexane Et_2O 4:1, UV, CPS, $KMnO_4$). ^{1}H NMR (400 MHz, $CDCl_3$) δ 7.68-7.66 (m, 4 H), 7.44-7.36 (m, 6 H), 7.28-7.25 (m, 2 H), 6.90-6.87 (m, 2 H), 6.13 (td, *J* = 7.1, 1.6 Hz, 1 H), 4.49 (s, 2 H), 3.93-3.90 (m, 1 H), 3.81 (s, 3 H), 3.65 (t, *J* = 6.5 Hz, 2 H), 3.46 (dd, *J* = 9.5, 3.4 Hz, 1 H), 3.34 (dd, *J* = 9.5, 7.1 Hz, 1 H), 2.15-2.13 (m, 2 H), 1.99 (q, *J* = 7.1 Hz, 2 H),1.62 (d, *J* = 1.2 Hz, 3 H), 1.60-1.53 (m, 2 H), 1.37-1.30 (m, 4 H), 1.05 (s, 9 H). ^{13}C NMR (100 MHz, $CDCl_3$) δ 159.4, 135.7, 134.3, 131.3, 130.3, 129.6, 129.5, 128.5, 127.7, 114.0, 74.0, 73.2, 68.3, 64.1, 55.4, 44.0, 32.2, 29.6, 28.1, 27.0, 25.6, 19.4, 16.3. IR (thin film): ῦ = 3457, 2930, 2857, 1513, 1427, 1248, 1106, 1038, 822, 740, 702, 613, 504, 489 cm^{-1}. HRMS (ESI): m/z: calcd for $C_{35}H_{48}NaO_4Si$ [$(M+Na)^+$]: 583.3214; found: 583.3216. $[\alpha]^{20}_D$: -2.00° (c=0.5, $CHCl_3$).

(*S*,*E*)-10-((*tert*-Butyldiphenylsilyl)oxy)-1-((4-methoxybenzyl)oxy)-4-methyldec-4-en-2-yl (2*E*,4*Z*)-7-((*tert*-butyldimethylsilyl)oxy)-8-(diethoxyphosphoryl)-5-methylocta-2,4-dienoate (98). Compound **90** (913.0 mg, 2.17 mmol) is azeotropically dried with anhydrous toluene (5 ml) and dissolved in the same solvent (10 mL). Triethylamine (0.66 mL, 4.70 mmol) is added, followed by the addition of 2,4,6-trichlorobenzoyl chloride (0.43 mL, 2.71 mmol). The mixture is stirred for 90 min at room temperature and a solution of compound **97** (1.01 g, 1.81 mmol, co-evaporated once with 5 mL of toluene) and DMAP (221.0 mg, 1.81 mmol) in toluene (10 mL; plus additional 10 mL form rinsing) is added. The mixture is stirred for 1 h at room temperature, then saturated aqueous $NaHCO_3$ (50 mL), H_2O (50 mL), and AcOEt (50

mL) are added and the phases are separated. The aqueous layer is extracted with AcOEt (3 x 30 mL) and the combined organic extracts are dried over $MgSO_4$ and concentrated under reduced pressure. The residue is purified by silica gel column chromatography (AcOEt/Hex 1:5→1:3) to afford the title compound (1.37 g, 79%) as a pale yellow, viscous oil. TLC: R_f= 0.36 (hexane AcOEt 1:1, UV, CPS, $KMnO_4$). ^{1}H NMR (400 MHz, $CDCl_3$) δ 7.69 – 7.64 (m, 4H), 7.57 (dd, *J* = 15.1, 11.6 Hz, 1H), 7.44 – 7.34 (m, 6H), 7.25 – 7.21 (m, 2H), 6.86 (dt, *J* = 8.6, 2.0 Hz, 2H), 6.06 (d, *J* = 11.3 Hz, 1H), 5.78 (d, *J* = 15.1 Hz, 1H), 5.21 (m, 1H), 5.15 (t, *J* = 7.3 Hz, 1H), 4.50 (d, *J* = 11.7 Hz, 1H), 4.42 (dd, *J* = 11.7, 3.0 Hz, 1H), 4.20 – 4.05 (m, 5H), 3.79 (s, 3H), 3.63 (t, *J* = 6.5 Hz, 2H), 3.50 (dd, *J* = 4.8, 1.5 Hz, 2H), 2.59 (t, *J* = 5.3 Hz, 1H), 2.29 (t, *J* = 6.1 Hz, 1H), 2.04 – 1.96 (m, 2H), 1.95 – 1.82 (m, 5H), 1.62 (s, 3H), 1.59 (s, 3H), 1.56-1.50 (m, 2H), 1.33 (td, *J* = 7.1, 3.5 Hz, 6H), 1.30 – 1.20 (m, 4H), 1.04 (s, 9H), 0.83 (s, 9H), 0.05 (s, 3H), -0.02 (s, 3H). ^{13}C NMR (100 MHz, $CDCl_3$) δ 167.0, 159.3, 146.1, 141.3, 135.7, 134.3, 130.7, 130.5, 129.6, 129.4, 128.5, 127.7, 126.9, 119.9, 113.9, 72.9, 71.1, 70.7, 66.8, 64.1, 61.7, 55.4, 41.8, 41.4, 35.9, 32.6, 29.5, 28.1, 27.0, 25.9, 25.7, 25.1, 19.4, 18.0, 16.6, 16.6, 16.4, -4.6, -4.6. IR (thin film): ῡ = 2930, 2857, 1714, 1514, 1251, 1147, 1110, 1049, 1028, 979, 962, 937, 824, 776, 703 cm^{-1}. $[\alpha]^{20}_D$: +2.00° (c=0.5, $CHCl_3$).

(*S*,*E*)-10-Hydroxy-1-((4-methoxybenzyl)oxy)-4-methyldec-4-en-2-yl (2*E*,4*Z*)-8-(diethoxyphosphoryl)-7-hydroxy-5-methylocta-2,4-dienoate (99). TBAF (1M, 0.28 ml, 0.28 mmol) is slowly added to a solution of compound **98** (132.7 mg, 0.14 mmol) in anhydrous THF (1.0 ml) at 0 °C. The mixture is then allowed to warm to room temperature and stirred for 4 h. After adding saturated aqueous $NaHCO_3$ (3 ml), the layers are separated and the aqueous phase is extracted with AcOEt (3 x 2 ml). The combined organic extracts are dried over $MgSO_4$ and concentrated under reduced pressure. The residue is purified by silica gel column chromatography (AcOEt) to afford the title compound (80.7 mg, 95%) as a colorless oil. TLC: R_f= 0.15 (AcOEt; UV, CPS, $KMnO_4$). ^{1}H NMR (400 MHz, $CDCl_3$) δ 7.53 (ddd, *J* = 15.1, 11.7, 8.2 Hz, 1H), 7.25 – 7.18 (m, 2H), 6.93 – 6.78 (m, 2H), 6.13 (d, *J* = 11.7 Hz, 1H), 5.82 (d, *J* = 15.0 Hz, 1H), 5.33 – 5.20 (m, 1H), 5.20 – 5.12 (m, 1H), 4.51 (d, *J* = 11.7 Hz, 1H), 4.43 (d, *J* = 11.7

Hz, 1H), 4.25 – 4.05 (m, 5H), 3.80 (s, 3H), 3.58 (td, *J* = 6.7, 1.2 Hz, 2H), 3.50 (dd, *J* = 4.9, 1.1 Hz, 2H), 2.74 – 2.52 (m, 1H), 2.50-2.38 (m, 1H), 2.26 (dd, *J* = 6.8, 3.8 Hz, 2H), 1.99 – 1.87 (m, 7H), 1.62 (d, *J* = 1.2 Hz, 3H), 1.59 – 1.45 (m, 2H), 1.33 (tt, *J* = 7.1, 1.9 Hz, 6H), 1.30 – 1.15 (m, 4H). ^{13}C NMR (100 MHz, $CDCl_3$) δ 167.1, 159.3, 145.8, 145.6, 140.5, 140.3, 130.8, 130.8, 130.4, 129.4, 128.4, 128.3, 126.8, 126.7, 120.4, 120.3, 113.9, 72.9, 71.1, 65.6, 65.3, 63.0, 62.3, 62.2, 62.1, 55.4, 41.6, 41.3, 41.1, 34.3, 32.9, 32.8, 31.1, 29.5, 29.5, 28.0, 28.0, 25.8, 25.4, 25.3, 24.9, 16.6, 16.4. IR (thin film): ῡ = 3374, 2931, 2855, 1709, 1633, 1612, 1514, 1275, 1248, 1223, 1148, 1030, 977 cm^{-1}. HRMS (ESI): m/z: calcd for $C_{32}H_{51}NaO_9P$ $[(M+Na)^+]$: 633.3163; found: 633.3156. $[\alpha]^{20}_D$: -2.00° (c=0.5, $CHCl_3$).

(*S*,3*E*,5*Z*,9*E*,15*E*)-18-(((4-Methoxybenzyl)oxy)methyl)-6,16-dimethyloxacyclooctadeca-3,5,9,15-tetraene-2,8-dione (100). DMP (1.017 g, 2.40 mmol) is added portionwise to a solution of compound **99** (601.0 mg, 0.98 mmol) in anhydrous DCM (15.0 ml). The mixture is stirred for 1 h at room temperature, then saturated aqueous $NaHCO_3$ (150 ml) and saturated aqueous $Na_2S_2O_3$ (150 ml) are added, the layers are separated and the aqueous phase is extracted with AcOEt (3 x 30 ml). The combined organic extracts are dried over $MgSO_4$ and concentrated under reduced pressure. The residue is purified on a short column (AcOEt) to afford the title compound (294 mg, 49 %) as an almost colorless oil. Due to instability issues, the product is directly used in the following step without being characterized. TLC: R_f= 0.42(AcOEt; UV, CPS, $KMnO_4$).

(*S*,3*E*,5*Z*,9*E*,15*E*)-18-(((4-Methoxybenzyl)oxy)methyl)-6,16-dimethyloxacyclooctadeca-3,5,9,15-tetraene-2,8-dione (101). $Ba(OH)_2$ (108.0 mg, 0.63 mmol) is added to a solution of compound **100** (294.0 mg, 0.48 mmol) in THF (160.0 ml) and water (4.0 ml) at 0 °C. The mixture is stirred for 30 min at 0 °C, then it is allowed to warm to room temperature and stirred for further 30 min. It is then diluted with Et_2O (30 ml), the layers are separated and the organic phase is washed with saturated aqueous $NaHCO_3$ (2 x 50 ml) and brine (50 ml), dried over $MgSO_4$ and

concentrated under reduced pressure. The residue is purified by silica gel column chromatography (hexane/AcOEt 4:1) to afford the title compound (68 mg, 31%) as a colorless oil. TLC: R_f = 0.31 (hexane/AcOEt 4:1; UV, CPS, $KMnO_4$). ^{1}H NMR (400 MHz, $CDCl_3$) δ 7.63 (dd, *J* = 15.1, 11.5 Hz, 1H), 7.27-7.25 (m, 2 H), 6.90 – 6.86 (m, 2 H), 6.83 (dt, *J* = 16.0, 7.0 Hz, 1H), 6.12 (d, *J* = 11.5 Hz, 1H), 5.99 (dt, *J* = 16.0, 1.5 Hz, 1H), 5.91 (d, *J* = 15.1 Hz, 1H), 5.39 (dt, *J* = 12.6, 5.0 Hz, 1H), 5.11 – 5.07 (m, 1H), 4.54 (d, *J* = 11.7 Hz, 1H), 4.47 (d, *J* = 11.7 Hz, 1H), 4.02 (d, *J* = 12.8 Hz, 1H), 3.81 (s, 3H), 3.55 (dd, *J* = 10.4, 5.8 Hz, 1H), 3.50 (dd, *J* = 10.4, 4.6 Hz, 1H), 2.97 (d, *J* = 12.8 Hz, 1H), 2.29 – 2.00 (m, 6H), 1.88 (d, *J* = 1.3 Hz, 3H), 1.66 (d, *J* = 1.2 Hz, 3H), 1.36 (dt, *J* = 11.4, 6.6 Hz, 2H), 1.30 – 1.18 (m, 2H). ^{13}C NMR (100 MHz, $CDCl_3$) δ 197.2, 166.7, 159.4, 149.9, 142.8, 139.9, 131.1, 130.3, 129.6, 129.5, 127.7, 125.7, 121.2, 114.0, 76.8, 73.0, 71.9, 70.1, 55.4, 45.7, 42.3, 32.7, 28.7, 28.3, 27.5, 16.4. IR (thin film): ῡ = 2929, 2858, 1714, 1668, 1634, 1513, 1280, 1250, 1149, 1035, 978 cm^{-1}. HRMS (ESI): m/z: calcd for $C_{28}H_{36}NaO_5$ [$(M+Na)^+$]: 475.2455; found: 475.2455. $[\alpha]^{20}_D$: -173.97° (c=0.5, $CHCl_3$).

(*S*,3*E*,5*Z*,9*E*,15*E*)-18-(Hydroxymethyl)-6,16-dimethyloxacyclooctadeca-3,5,9,15-tetraene-2,8-dione (NB-22). Water (1.0 mL) and DDQ (75.0 mg, 0.33 mmol) are added to a solution of compound **101** (100.0 mg, 0.22 mmol) in DCM (5 mL) at room temperature under vigorous stirring. The mixture is stirred for 90 min, then it is diluted with saturated aqueous $NaHCO_3$ (30 mL) and DCM (5 mL). The clear phases are separated and the aqueous phase is extracted with DCM (3 x 5 mL). The combined organic extracts are dried over $MgSO_4$ and concentrated under reduced pressure. The residue is purified by silica gel column chromatography (hexane/AcOEt 2:1) to afford the title compound (61 mg, 83%) as a colorless oil. TLC: R_f = 0.36 (hexane/AcOEt 1:1; UV, $KMnO_4$, CPS). ^{1}H NMR (400 MHz, $CDCl_3$) δ 7.65 (dd, *J* = 15.1, 11.6 Hz, 1H), 6.83 (dt, *J* = 16.0, 7.0 Hz, 1H), 6.13 (d, *J* = 11.6 Hz, 1H), 6.00 (dt, *J* = 16.0, 1.6 Hz, 1 H), 5.91 (d, *J* = 15.0 Hz, 1H), 5.33 – 5.26 (m, 1H), 5.10 (dd, *J* = 9.2, 5.4 Hz, 1H), 4.02 (d, *J* = 12.9 Hz, 1H), 3.76 (dd, *J* = 11.9, 3.8 Hz, 1H), 3.70 (dd, *J* = 11.8, 6.3 Hz, 1H), 2.98 (d, *J* = 12.8 Hz, 1H), 2.28 – 2.03 (m, 5H), 1.88 (d, *J* = 1.3 Hz, 3H), 1.88-1-78 (m, 1H), 1.68

(d, *J* = 1.2 Hz, 3H), 1.42 – 1.32 (m, 2H), 1.29 – 1.19 (m, 2H). ^{13}C NMR (100 MHz, $CDCl_3$) δ 197.0, 166.9, 149.8, 143.3, 140.3, 130.9, 129.6, 127.8, 125.7, 120.8, 72.4, 65.6, 45.8, 41.8, 32.6, 28.6, 28.3, 27.5, 24.5, 16.5. IR (thin film): ῡ = 3435, 2928, 2857, 1712, 1693, 1666, 1631, 1440, 1360, 1281, 1151, 979 cm^{-1}. HRMS (ESI): m/z: calcd for $C_{20}H_{29}O_4$ [$(M+H)^+$]: 333.2060; found: 333.2053. $[\alpha]^{20}_D$: -204.96° (c=0.2, $CHCl_3$).

(*S*,4*E*,10*E*,14*Z*,16*E*)-4,14-Dimethyl-12,18-dioxooxacyclooctadeca-4,10,14,16-tetraene-2-carbaldehyde (NB-23). DMP (99.0 mg, 0.23 mmol) and pyridine (0.10 ml) are added to a solution of compound **NB-22** (51.8 mg, 0.16 mmol) in DCM (2.0 mL) at room temperature. After stirring for 45 min, a further amount of DMP (100.0 mg, 0.23 mmol) is added and the mixture is stirred for 90 min. It is then diluted with saturated aqueous $NaHCO_3$ (7 mL) and saturated aqueous $Na_2S_2O_3$ (7 mL). The clear phases are separated and the aqueous phase is extracted with DCM (3 x 4 mL). The combined organic layers are dried over $MgSO_4$ and concentrated under reduced pressure. The residue is purified by silica gel column chromatography (hexane/AcOEt 2:1) to afford the title compound (28 mg, 50%) as a colorless thick oil. TLC: R_f= 0.38 (hexane/AcOEt 2:1; UV, $KMnO_4$, CPS). ^{1}H NMR (400 MHz, $CDCl_3$) δ 9.67 (s, 1H), 7.68 (dd, *J* = 15.0, 11.6 Hz, 1H), 6.82 (dt, *J* = 16.0, 6.9 Hz, 1H), 6.17 (d, *J* = 11.8 Hz, 1H), 6.02 (dt, *J* = 16.0, 1.5 Hz, 1 H), 5.97 (d, *J* = 15.0 Hz, 1 H), 5.43 (dd, *J* = 11.1, 2.6 Hz, 1H), 5.15 (t, *J* = 7.3 Hz, 1H), 3.83 (d, *J* = 13.0, 1H), 3.19 (d, *J* = 13.0 Hz, 1H), 2.59 (d, *J* = 14.1 Hz, 1H), 2.29 (dd, *J* = 14.3, 11.2 Hz, 1H), 2.28 – 2.02 (m, 4H), 1.91 (s, 3H), 1.67 (d, *J* = 1.2 Hz, 3H), 1.42-1.35 (m, 2 H), 1.28-1.20 (m, 2 H). ^{13}C NMR (100 MHz, $CDCl_3$) δ 199.3, 196.6, 166.3, 149.8, 144.1, 141.0, 129.6, 129.56, 129.0, 125.7, 119.9, 45.9, 39.8, 32.5, 28.5, 28.1, 27.1, 24.7, 16.0. IR (thin film): ῡ = 2927, 2857, 2360, 1715, 1667, 1632, 1279, 1146, 980 cm^{-1}. HRMS (ESI): m/z: calcd for $C_{20}H_{26}NaO_4$ [$(M+Na)^+$]: 353.1723; found: 353.1720. $[\alpha]^{20}_D$: -179.96° (c=0.5, $CHCl_3$).

(2*Z*,4*E*)-*N*-((*S*)-((*S*,4*E*,10*E*,14*Z*,16*E*)-4,14-Dimethyl-12,18-dioxooxacyclooctadeca-4,10,14,16-tetraen-2-yl)(hydroxy)methyl)hexa-2,4-dienamide (NB-24). Lithium aluminium hydride (11.3 mg, 0.30 mmol), (*S*)-BINOL (94.1 mg, 0.33 mmol) and

sorbamide (36.3 mg, 0.33 mmol) are dried for 15 h at high vacuum. Lithium aluminium hydride is then suspended in anhydrous THF (1.0 ml) and EtOH (0.02 ml) in THF (1.0 ml) is slowly added to the suspension, followed by (*S*)-BINOL in THF (1.0 ml) and sorbamide. 2.0 ml of the resulting clear grey solution are added to a solution of compound **NB-23** (26.8 mg, 0.08 mmol) in THF (2 ml). After stirring for 30 min, the reaction is quenched by the addition of saturated aqueous $NaHCO_3$ (5 ml). The aqueous phase is extracted with AcOEt (3 x 5 ml) and the combined organic extracts are dried on $MgSO_4$ and concentrated under reduced pressure. The residue is purified by silica gel column chromatography (hexane AcOEt 3:2 + 3% TEA) and RP-HPLC (Waters, SymmetryPrep®C18, 5µm, 19x100mm, ACN/H_2O 40:60 to 70:30, 254 nm) to afford the pure title compound (4 mg, 11%) as a white solid. TLC: R_f = 0.71 (AcOEt hexane 2.5:1, UV, $KMnO_4$). ^{1}H NMR (400 MHz, $CDCl_3$) δ 7.66 (dd, *J* = 15.1, 11.6 Hz, 1H), 7.42 (app.t., *J* = 13.3 Hz, 1H), 6.81 (dt, *J* = 16.0, 7.1 Hz, 1H), 6.45 (t, *J* = 11.3 Hz, 1H), 6.36 (d, *J* = 7.9 Hz, 1H), 6.13 (d, *J* = 11.5 Hz, 1H), 6.05 (dd, *J* = 15.0, 7.0 Hz, 1H), 5.99 (d, *J* = 15.9 Hz, 1H), 5.90 (d, *J* = 15.1 Hz, 1H), 5.48-5.41 (m, 2 H), 5.29 (ddd, *J* = 11.2, 5.7, 1.9 Hz, 1H), 5.11 (app.t., *J* = 7.2 Hz, 1H), 4.01 (d, *J* = 13.0 Hz, 1H), 3.53 (d, *J* = 3.9 Hz, 1H), 2.98 (d, *J* = 12.8 Hz, 1H), 2.44 (d, *J* = 14.1 Hz, 1H), 2.30 – 1.99 (m, 4H), 1.89 (s, 3H), 1.87 (dd, *J* = 6.8, 1.7 Hz, 3H), 1.67 (s, 3H), 1.40-1.33 (m, 2 H), 1.27-1.21 (m, 2 H). ^{13}C NMR (125 MHz, $CDCl_3$) δ 196.9, 167.4, 167.0, 149.8, 143.6, 143.3, 140.8, 139.8, 130.7, 129.5, 128.4, 127.9, 125.5, 120.3, 117.4, 75.2, 72.4, 45.6, 41.5, 32.6, 28.6, 28.2, 27.4, 24.5, 18.7, 16.5. IR (thin film): ῡ = 3338, 2928, 2952, 1697, 1661, 1634, 1604, 1521, 1508, 1273, 1208, 1155, 1134, 1046, 979 cm^{-1}. HRMS (ESI): m/z: calcd for $C_{26}H_{35}NNaO_5$ [$(M+Na)^+$]: 464.2407; found: 464.2394. $[\alpha]^{20}_D$: -299.94° (c=0.5, EtOH).

7. References

(1) Mann, M.; Jensen, O. N. Proteomic Analysis of Post-Translational Modifications. *Nat. Biotechnol.* **2003**, *21*, 255.

(2) Fisher, E.; Krebs, E. Conversion of Phophorylase b to Phosphorylase a in Muscle Extracts. *J. Biol. Chem.* **1955**, *216*, 121–132.

(3) Adams, J. A. Kinetic and Catalytic Mechanisms of Protein Kinases. *Chem. Rev.* **2001**, *101* (8), 2271–2290.

(4) Olsen, J. V.; Blagoev, B.; Gnad, F.; Macek, B.; Kumar, C.; Mortensen, P.; Mann, M. Global, In Vivo, and Site-Specific Phosphorylation Dynamics in Signaling Networks. *Cell* **2006**, *127* (3), 635–648.

(5) Wolanin, P. M.; Thomason, P. A.; Stock, J. B. Histidine Protein Kinases: Key Signal Transducers Outside the Animal Kingdom. *Genome Biol.* **2002**, *3* (10), reviews3013.1-reviews3013.8.

(6) Ardito, F.; Giuliani, M.; Perrone, D.; Troiano, G.; Lo Muzio, L. The Crucial Role of Protein Phosphorylation in Cell Signaling and Its Use as Targeted Therapy (Review). *Int. J. Mol. Med.* **2017**, 271–280.

(7) Taylor, S. S.; Kornev, A. P. Protein Kinases: Evolution of Dynamic Regulatory Proteins. *Trends Biochem. Sci.* **2011**, *36* (2), 65–77.

(8) Li, X.; Wilmanns, M.; Thornton, J.; Köhn, M. Elucidating Human Phosphatase-Substrate Networks. *Sci. Signal.* **2013**, *6* (275), 1–15.

(9) Konopka, J. B.; Watanabe, S. M.; Witte, O. N. An Alteration of the Human C-Abl Protein in K562 Leukemia Cells Unmasks Associated Tyrosine Kinase Activity. *Cell* **1984**, *37* (3), 1035–1042.

(10) Cohen, P. Protein Kinases-the Major Drug Targets of the Twenty-First Century? *Nat. Rev. Drug Discov.* **2002**, *1*, 309–315.

(11) Hanahan, D.; Weinberg, R. A. Hallmarks of Cancer: The Next Generation.

Cell **2011**, *144* (5), 646–674.

(12) Giamas, G.; Stebbing, J.; Vorgias, C. E.; Knippschild, U. Protein Kinases as Targets for Cancer Treatment. *Pharmacogenomics* **2007**, *8* (8), 1005–1016.

(13) Arora, A.; Scholar, E. M. Role of Tyrosine Kinase Inhibitors in Cancer Therapy. *J Pharmacol Exp Ther* **2005**, *315* (3), 971–979.

(14) Weinstein, I. B. Addiction to Oncogenes-the Achilles Heal of Cancer. *Science (80-.).* **2002**, *297* (5578), 63–64.

(15) Bridges, A. J. Chemical Inhibitors of Protein Kinases. *Chem. Rev.* **2001**, *101* (8), 2541–2572.

(16) Weinstein, I. B.; Joe, A. Oncogene Addiction. *Cancer Res.* **2008**, *68* (9), 3077–3080.

(17) Weinstein, I. B.; Joe, A. K. Mechanisms of Disease: Oncogene Addiction—a Rationale for Molecular Targeting in Cancer Therapy. *Nat. Clin. Pract. Oncol.* **2006**, *3*, 448–457.

(18) Weinstein, I. B.; Begemann, M.; Zhou, P.; Han, K.; Sgambato, A.; Doki, Y.; Arber, N.; Ciaparrone, M.; Yamamoto, H. Disorders in Cell Circuitry Associated with Multistage Carcinogenesis: Exploitable Targets for Cancer Prevention and Therapy. *Clin. Cancer Res.* **1997**, *3*, 2696–2702.

(19) Bhullar, K. S.; Lagarón, N. O.; McGowan, E. M.; Parmar, I.; Jha, A.; Hubbard, B. P.; Rupasinghe, H. P. V. Kinase-Targeted Cancer Therapies: Progress, Challenges and Future Directions. *Mol. Cancer* **2018**, *17*, 48.

(20) Krause, D. S.; Van Etten, R. A. Tyrosine Kinases as Targets for Cancer Therapy. *N. Engl. J. Med.* **2005**, *353* (2), 172–187.

(21) Manning, G.; Whyte, D. B.; Martinez, R.; Hunter, T.; Sudarsanam, S. The Protein Kinase Complement of the Human Genome. *Science* **2002**, *298* (5600), 1912–1934.

(22) Fedorov, O.; Sundström, M.; Marsden, B.; Knapp, S. Insights for the

Development of Specific Kinase Inhibitors by Targeted Structural Genomics. *Drug Discov. Today* **2007**, *12* (9–10), 365–372.

(23) Sharma, S. V.; Bell, D. W.; Settleman, J.; Haber, D. A. Epidermal Growth Factor Receptor Mutations in Lung Cancer. *Nat. Rev. Cancer* **2007**, *7* (3), 169–181.

(24) Song, Z.; Ge, Y.; Wang, C.; Huang, S.; Shu, X.; Liu, K.; Zhou, Y.; Ma, X. Challenges and Perspectives on the Development of Small-Molecule EGFR Inhibitors against T790M-Mediated Resistance in Non-Small-Cell Lung Cancer: Miniperspective. *J. Med. Chem.* **2016**, *59* (14), 6580–6594.

(25) Hanawa, M.; Suzuki, S.; Dobashi, Y.; Yamane, T.; Kono, K.; Enomoto, N.; Ooi, A. EGFR Protein Overexpression and Gene Amplification in Squamous Cell Carcinomas of the Esophagus. *Int. J. Cancer* **2005**, *118* (5), 1173–1180.

(26) Nomura, M.; Shigematsu, H.; Li, L.; Suzuki, M.; Takahashi, T.; Estess, P.; Siegelman, M.; Feng, Z.; Kato, H.; Marchetti, A.; Shay, J.W.; Spitz, M.R.; Wistuba, I.I.; Minna, J.D.; Gazdar, A.F. Polymorphisms, Mutations, and Amplification of the EGFR Gene in Non-Small Cell Lung Cancers. *PLOS Med.* **2007**, *4* (4), e125.

(27) Touat, M.; Ileana, E.; Postel-Vinay, S.; André, F.; Soria, J. C. Targeting FGFR Signaling in Cancer. *Clin. Cancer Res.* **2015**, *21* (12), 2684–2694.

(28) Katoh, M. FGFR Inhibitors: Effects on Cancer Cells, Tumor Microenvironment and Whole-Body Homeostasis. *Int. J. Mol. Med.* **2016**, *38* (1), 3–15.

(29) Dienstmann, R.; Rodon, J.; Prat, A.; Perez-Garcia, J.; Adamo, B.; Felip, E.; Cortes, J.; Iafrate, A. J.; Nuciforo, P.; Tabernero, J. Genomic Aberrations in the FGFR Pathway: Opportunities for Targeted Therapies in Solid Tumors. *Ann. Oncol.* **2014**, *25* (3), 552–563.

(30) Giacomini, A.; Chiodelli, P.; Matarazzo, S.; Rusnati, M.; Presta, M.;

Ronca, R. Blocking the FGF/FGFR System as a “Two-Compartment” Antiangiogenic/Antitumor Approach in Cancer Therapy. *Pharmacol. Res.* **2016**, *107*, 172–185.

(31) Porta, R.; Borea, R.; Coelho, A.; Khan, S.; Araújo, A.; Reclusa, P.; Franchina, T.; Van Der Steen, N.; Van Dam, P.; Ferri, J.; Sirera, R.; Naing, A.; Hong, D.; Rolfo, C. FGFR a Promising Druggable Target in Cancer: Molecular Biology and New Drugs. *Crit. Rev. Oncol. Hematol.* **2017**, *113*, 256–267.

(32) Johnson, L. N. Protein Kinase Inhibitors: Contributions from Structure to Clinical Compounds. *Q. Rev. Biophys.* **2009**, *42* (1), 1–40.

(33) Johnson, L. N.; Noble, M. E. M.; Owen, D. J. Active and Inactive Protein Kinases: Structural Basis for Regulation. *Cell* **1996**, *85*, 149–158.

(34) Xu, W.; Doshi, A.; Lei, M.; Eck, M. J.; Harrison, S. C. Crystal Structures of C-Src Reveal Features of Its Autoinhibitory Mechanism. *Mol. Cell* **1999**, *3* (5), 629–638.

(35) Morgan, D. O. The Dynamics of Cyclin Dependent Kinase Structure. *Curr. Opin. Cell Biol.* **1996**, *8* (6), 767–772.

(36) Lemmon, M. A.; Schlessinger, J. Cell Signaling by Receptor Tyrosine Kinases. *Cell* **2010**, *141* (7), 1117–1134.

(37) Vertommen, D.; Rider, M.; Ni, Y.; Waelkens, E.; Merlevede, W.; Vandenheede, J. R.; Van Lint, J. Regulation of Protein Kinase D by Multisite Phosphorylation. *J. Biol. Chem.* **2000**, *275* (26), 19567–19576.

(38) Chong, H.; Lee, J.; Guan, K.-L. Positive and Negative Regulation of Raf Kinase Activity and Function by Phosphorylation. *EMBO J.* **2001**, *20* (14), 3716–3727.

(39) Hantschel, O.; Nagar, B.; Guettler, S.; Kretzschmar, J.; Dorey, K.; Kuriyan, J.; Superti-Furga, G. A Myristoyl/Phosphotyrosine Switch Regulates c-Abl. *Cell* **2003**, *112* (6), 845–857.

(40) Hanks, S. K.; Hunter, T. Protein Kinases 6. The Eukaryotic Protein Kinase Superfamily: Kinase (Catalytic) Domain Structure and Classification. *FASEB J.* **1995**, *9* (8), 576–596.

(41) Hubbard, S. R.; Till, J. H. Protein Tyrosine Kinase Structure and Function. *Annu. Rev. Biochem.* **2000**, *69* (1), 373–398.

(42) Möbitz, H. The ABC of Protein Kinase Conformations. *Biochim. Biophys. Acta - Proteins Proteomics* **2015**, *1854* (10), 1555–1566.

(43) Schwartz, P. A.; Murray, B. W. Protein Kinase Biochemistry and Drug Discovery. *Bioorg. Chem.* **2011**, *39* (5–6), 192–210.

(44) Huse, M.; Kuriyan, J. The Conformational Plasticity of Protein Kinases. *Cell* **2002**, *109*, 275–282.

(45) Sutto, L.; Gervasio, F. L. Effects of Oncogenic Mutations on the Conformational Free-Energy Landscape of EGFR Kinase. *Proc. Natl. Acad. Sci. U. S. A.* **2013**, *11* (26), 10616–10621.

(46) Nolen, B.; Taylor, S.; Ghosh, G. Regulation of Protein Kinases: Controlling Activity through Activation Segment Conformation. *Mol. Cell* **2004**, *15* (5), 661–675.

(47) Adams, J. A. Activation Loop Phosphorylation and Catalysis in Protein Kinases: Is There Functional Evidence for the Autoinhibitor Model? *Biochemistry* **2003**, *42* (3), 601–607.

(48) Oliveira, P. S. L. De; Ferraz, F. A. N.; Pena, D. A.; Pramio, D. T.; Morais, F. A.; Schechtman, D. Revisiting Protein Kinase – Substrate Interactions : Toward Therapeutic Development. *Sci. Signal.* **2016**, *9* (420), 1–13.

(49) Treiber, D. K.; Shah, N. P. Ins and Outs of Kinase DFG Motifs. *Chem. Biol.* **2013**, *20* (6), 745–746.

(50) Yu, L.; Xu, L.; Xu, M.; Wan, B.; Yu, L.; Huang, Q. Role of Mg2+ Ions in Protein Kinase Phosphorylation: Insights from Molecular Dynamics Simulations of ATP-Kinase Complexes. *Mol. Simul.* **2011**, *37* (14), 1143–

1150.

(51) Summerton, J. C.; Martin, G. M.; Evanseck, J. D.; Chapman, M. S. Common Hydrogen Bond Interactions in Diverse Phosphoryl Transfer Active Sites. *PLoS One* **2014**, *9* (9), e108310.

(52) Zhang, L.; Wang, J.C.; Hou, L.; Cao, P.R.; Wu, L.; Zhang, Q.S.; Yang, H.Y.; Zang, Y.; Ding, J.P.; Li, J. Functional Role of Histidine in the Conserved His-x-Asp Motif in the Catalytic Core of Protein Kinases. *Sci. Rep.* **2015**, *5*, 10115.

(53) Yarden, Y.; Sliwkowski, M. X. Untangling the ErbB Signalling Network. *Nat. Rev. Mol. Cell Biol.* **2001**, *2* (2), 127–137.

(54) Anjum, R.; Blenis, J. The RSK Family of Kinases: Emerging Roles in Cellular Signalling. *Nat. Rev. Mol. Cell Biol.* **2008**, *9* (10), 747–758.

(55) Kannan, N.; Haste, N.; Taylor, S. S.; Neuwald, A. F. The Hallmark of AGC Kinase Functional Divergence Is Its C-Terminal Tail, a Cis-Acting Regulatory Module. *Proc. Natl. Acad. Sci. U. S. A.* **2008**, *104* (4), 1272–1277.

(56) Schlessinger, J. Cell Signaling by Receptor Tyrosine Kinases. *Cell* **2000**, *103* (2), 211–225.

(57) Schlessinger, J. Signal Transduction by Allosteric Receptor Oligomerization. *Trends Biochem. Sci.* **1988**, *13* (11), 443–447.

(58) Lemmon, M. A.; Schlessinger, J. Regulation of Signal Transduction and Signal Diversity by Receptor Oligomerization. *Trends Biochem. Sci.* **1994**, *19* (11), 459–463.

(59) Kossiakoff, A. A.; De Vos, A. M. Structural Basis for Cytokine Hormone-Receptor Recognition and Receptor Activation. *Adv. Protein Chem.* **1998**, *52*, 67–108.

(60) Jiang, G.; Hunter, T. When Dimerization Is Not Enough. *Curr Biol* **1999**, *12* (9), R568–R571.

(61) Schlessinger, J.; Plotnikov, A. N.; Ibrahimi, O. A.; Eliseenkova, A. V.; Yeh, B. K.; Yayon, A.; Linhardt, R. J.; Mohammadi, M. Crystal Structure of a Ternary FGF-FGFR-Heparin Complex Reveals a Dual Role for Heparin in FGFR Binding and Dimerization. *Mol. Cell* **2000**, *6* (3), 743–750.

(62) Ségaliny, A. I.; Tellez-Gabriel, M.; Heymann, M. F.; Heymann, D. Receptor Tyrosine Kinases: Characterisation, Mechanism of Action and Therapeutic Interests for Bone Cancers. *J. Bone Oncol.* **2015**, *4* (1), 1–12.

(63) Davis, R. J. Signal Transduction by the JNK Group Review of MAP Kinases. *Cell* **2000**, *103*, 239–252.

(64) Porta, C.; Paglino, C.; Mosca, A. Targeting PI3K/Akt/MTOR Signaling in Cancer. *Front. Oncol.* **2014**, *4*, 64.

(65) Fambrough, D.; McClure, K.; Kazlauskas, A.; Lander, E. S. Diverse Signaling Pathways Activated by Growth Factor Receptors Induce Broadly Overlapping, Rather Than Independent, Sets of Genes. *Cell* **1999**, *97* (6), 727–741.

(66) Östman, A.; Böhmer, F.-D. Regulation of Receptor Tyrosine Kinase Signaling by Protein Tyrosine Phosphatases. *Trends Cell Biol.* **2001**, *11* (6), 258–266.

(67) Goh, L.; Sorkin, a D. Endocytosis of Receptor Tyrosine Kinases. *Cold Spring Harb. Perspect. Biol.* **2013**, *5* (5), a017459–a017459.

(68) Wang, L.; Park, H.; Chhim, S.; Ding, Y.; Jiang, W.; Queen, C.; Kim, K. J. A Novel Monoclonal Antibody to Fibroblast Growth Factor 2 Effectively Inhibits Growth of Hepatocellular Carcinoma Xenografts. *Mol. Cancer Ther.* **2012**, *11* (4), 864–872.

(69) Presta, M.; Chiodelli, P.; Giacomini, A.; Rusnati, M.; Ronca, R. Fibroblast Growth Factors (FGFs) in Cancer: FGF Traps as a New Therapeutic Approach. *Pharmacol. Ther.* **2017**, *179*, 171–187.

(70) Ronca, R.; Giacomini, A.; Di Salle, E.; Coltrini, D.; Pagano, K.; Ragona, L.; Matarazzo, S.; Rezzola, S.; Maiolo, D.; Torrella, R.; et al. Long-Pentraxin 3 Derivative as a Small-Molecule FGF Trap for Cancer Therapy. *Cancer Cell* **2015**, *28* (2), 225–239.

(71) Fauvel, B.; Yasri, A. Antibodies Directed against Receptor Tyrosine Kinases: Current and Future Strategies to Fight Cancer. *MAbs* **2014**, *6* (4), 838–851.

(72) Harries, M.; Smith, I. The Development and Clinical Use of Trastuzumab (Herceptin). *Endoc. Relat. Cancer* **2002**, *9*, 75–85.

(73) Barthélémy, P.; Leblanc, J.; Goldbarg, V.; Wendling, F.; Kurtz, J.-E. Pertuzumab: Development beyond Breast Cancer. *Anticancer Res.* **2014**, *34* (4), 1483–1492.

(74) You, B.; Chen, E. X. Anti-EGFR Monoclonal Antibodies for Treatment of Colorectal Cancers: Development of Cetuximab and Panitumumab. *J. Clin. Pharmacol.* **2012**, *52* (2), 125–155.

(75) Cohen, M. H.; Chen, H.; Shord, S.; Fuchs, C.; He, K.; Zhao, H.; Sickafuse, S.; Keegan, P.; Pazdur, R. Approval Summary: Cetuximab in Combination With Cisplatin or Carboplatin and 5-Fluorouracil for the First-Line Treatment of Patients With Recurrent Locoregional or Metastatic Squamous Cell Head and Neck Cancer. *Oncologist* **2013**, *18*, 460–466.

(76) Giusti, R. M.; Shastri, K. A.; Cohen, M. H.; Keegan, P.; Pazdur, R. FDA Drug Approval Summary: Panitumumab (VectibixTM). *Oncologist* **2007**, *12* (5), 577–583.

(77) Garnock-Jones, K. P. Necitumumab: First Global Approval. *Drugs* **2016**, *76* (2), 283–289.

(78) van der Graaf, W. T. A. Olaratumab in Soft-Tissue Sarcomas. *Lancet* **2016**, *388* (10043), 442–444.

(79) https://www.accessdata.fda.gov/ visited on 6th September 2018.

(80) Zuccotto, F.; Ardini, E.; Casale, E.; Angiolini, M. Through the "Gatekeeper Door": Exploiting the Active Kinase Conformation. *J. Med. Chem.* **2010**, *53* (7), 2681–2694.

(81) Zhang, J.; Yang, P. L.; Gray, N. S. Targeting Cancer with Small Molecule Kinase Inhibitors. *Nat. Rev. Cancer* **2009**, *9* (1), 28–39.

(82) Lynch, T. J.; Bell, D. W.; Sordella, R.; Gurubhagavatula, S.; Okimoto, R. A.; Brannigan, B. W.; Harris, P. L.; Haserlat, S. M.; Supko, J. G.; Haluska, F. G.; et al. Activating Mutations in the Epidermal Growth Factor Receptor Underlying Responsiveness of Non-Small-Cell Lung Cancer to Gefitinib. *N. Engl. J. Med.* **2004**, *350*, 2129–2139.

(83) Nagar, B.; Bornmann, W. G.; Pellicena, P.; Schindler, T.; Veach, D. R.; Miller, W. T.; Clarkson, B.; Kuriyan, J. Crystal Structures of the Kinase Domain of C-Abl in Complex with the Small Molecule Inhibitors PD173955 and Imatinib (STI-571). *Cancer Res.* **2002**, *62* (15), 4236–4243.

(84) Knight, Z. A.; Shokat, K. M. Features of Selective Kinase Inhibitors. *Chem. Biol.* **2005**, *12* (6), 621–637.

(85) Schindler, T. Structural Mechanism for STI-571 Inhibition of Abelson Tyrosine Kinase. *Science* **2000**, *289* (5486), 1938–1942.

(86) Kwak, E. L.; Sordella, R.; Bell, D. W.; Godin-Heymann, N.; Okimoto, R. A.; Brannigan, B. W.; Harris, P. L.; Driscoll, D. R.; Fidias, P.; Lynch, T. J.; et al. Irreversible Inhibitors of the EGF Receptor May Circumvent Acquired Resistance to Gefitinib. *Proc. Natl. Acad. Sci. U. S. A.* **2005**, *102* (21), 7665–7670.

(87) Walter, A. O.; Sjin, R. T. T.; Haringsma, H. J.; Sun, J.; Ohashi, K.; Lee, K.; Dubrovskiy, A.; Labenski, M.; Wang, Z.; Zhu, Z.; et al. Discovery of a Mutant-Selective Covalent Inhibitor of EGFR That Overcomes T790M Mediated Resistance in NSCLC. *Cancer Discov.* **2013**, *3* (12), 1404–1415.

(88) Tan, L.; Wang, J.; Tanizaki, J.; Huang, Z.; Aref, A. R.; Rusan, M.; Zhu, S.-J.; Zhang, Y.; Ercan, D.; Liao, R. G.; et al. Development of Covalent Inhibitors That Can Overcome Resistance to First-Generation FGFR Kinase Inhibitors. *Proc. Natl. Acad. Sci. U. S. A.* **2014**, *111* (45), E4869–E4877.

(89) Zhao, Z.; Bourne, P. E. Progress with Covalent Small-Molecule Kinase Inhibitors. *Drug Discov. Today* **2018**, *23* (3), 727–735.

(90) Engel, J.; Lategahn, J.; Rauh, D. Hope and Disappointment: Covalent Inhibitors to Overcome Drug Resistance in Non-Small Cell Lung Cancer. *ACS Med. Chem. Lett.* **2016**, *7* (1), 2–5.

(91) Carmi, C.; Mor, M.; Petronini, P. G.; Alfieri, R. R. Clinical Perspectives for Irreversible Tyrosine Kinase Inhibitors in Cancer. *Biochem. Pharmacol.* **2012**, *84* (11), 1388–1399.

(92) Chong, C. R.; Jänne, P. A. The Quest to Overcome Resistance to EGFR-Targeted Therapies in Cancer. *Nat. Med.* **2013**, *19* (11), 1389–1400.

(93) Juchum, M.; Günther, M.; Laufer, S. A. Fighting Cancer Drug Resistance: Opportunities and Challenges for Mutation-Specific EGFR Inhibitors. *Drug Resist. Updat.* **2015**, *20*, 12–28.

(94) Carpenter, G.; King Jr, L.; Cohen, S. Epidermal Growth Factor Stimulates Phosphorylation in Membrane Preparations in Vitro. *Nature* **1978**, *276*, 409–410.

(95) Schlessinger, J. Ligand-Induced, Receptor-Mediated Dimerization and Activation of EGF Receptor. *Cell* **2002**, *110* (6), 669–672.

(96) Citri, A.; Skaria, K. B.; Yarden, Y. The Deaf and the Dumb: The Biology of ErbB-2 and ErbB-3. *Exp. Cell Res.* **2003**, *284*, 57–68.

(97) Lax, I.; Bellot, F.; Howk, R.; Ullrich, A.; Givol, D.; Schlessinger, J. Functional Analysis of the Ligand Binding Site of EGF-Receptor Utilizing Chimeric Chicken/Human Receptor Molecules. *EMBO J.* **1989**, *8* (2),

421–427.

(98) Stamos, J.; Sliwkowski, M. X.; Eigenbrot, C. Structure of the Epidermal Growth Factor Receptor Kinase Domain Alone and in Complex with a 4-Anilinoquinazoline Inhibitor. *J. Biol. Chem.* **2002**, *277* (48), 46265–46272.

(99) Yarden, Y. The EGFR Family and Its Ligands in Human Cancer. Signalling Mechanisms and Therapeutic Opportunities. *Eur. J. Cancer* **2001**, *37*, S3–S8.

(100) Zandi, R.; Larsen, A. B.; Andersen, P.; Stockhausen, M. T.; Poulsen, H. S. Mechanisms for Oncogenic Activation of the Epidermal Growth Factor Receptor. *Cell. Signal.* **2007**, *19* (10), 2013–2023.

(101) Lemmon, M. A.; Bu, Z.; Ladbury, J. E.; Zhou, M.; Pinchasi, D.; Lax, I.; Engelman, D. M.; Schlessinger, J. Two EGF Molecules Contribute Additively to Stabilization of the EGFR Dimer. *EMBO J.* **1997**, *16* (2), 281–294.

(102) Garrett, T. P.; McKern, N. M.; Lou, M.; Elleman, T. C.; Adams, T. E.; Lovrecz, G. O.; Zhu, H. J.; Walker, F.; Frenkel, M. J.; Hoyne, P. A.; Jorissen, R.N.; Nice, E.C.; Burgess, A.W.; Ward, C.W. Crystal Structure of a Truncated Epidermal Growth Factor Receptor Extracellular Domain Bound to Transforming Growth Factor A. *Cell* **2002**, *110*, 763–773.

(103) Ogiso, H.; Ishitani, R.; Nureki, O.; Fukai, S.; Yamanaka, M.; Kim, J. H.; Saito, K.; Sakamoto, a; Inoue, M.; Shirouzu, M.; et al. Crystal Structure of the Complex of Human Epidermal Growth Factor and Receptor Extracellular Domains. *Cell* **2002**, *110* (6), 775–787.

(104) Dawson, J. P.; Berger, M. B.; Lin, C.; Schlessinger, J.; Lemmon, M. A.; Kathryn, M.; Ferguson, K. M. Epidermal Growth Factor Receptor Dimerization and Activation Require Ligand-Induced Conformational Changes in the Dimer Interface Epidermal Growth Factor Receptor

Dimerization and Activation Require Ligand-Induced Conformational Changes in the Dimer Inter. *Mol. Cell. Biol.* **2005**, *25* (17), 7734–7742.

(105) Graus-Porta, D.; Beerli, R. R.; Daly, J. M.; Hynes, N. E. EebB-2, the Preferred Hereodimerization Partner of All ErbB Receptors, Is a Mediator of Lateral Signalling. *EMBO J.* **1997**, *16* (7), 1647–1655.

(106) Lemmon, M. A.; Schlessinger, J.; Ferguson, K. M. The EGFR Family: Not so Prototypical Receptor Tyrosine Kinases. *Cold Spring Harb. Perspect. Biol.* **2014**, *6* (4), 1–18.

(107) Burgess, A. W.; Cho, H. S.; Eigenbrot, C.; Ferguson, K. M.; Garrett, T. P. J.; Leahy, D. J.; Lemmon, M. a; Sliwkowski, M. X.; Ward, C. W.; Yokoyama, S.; et al. An Open-and-Shut Case ? Recent Insights into the Activation of EGF / ErbB Receptors CSIRO Health Science and Nutrition. *Mol. Cell* **2003**, *12*, 541–552.

(108) Zhang, X.; Gureasko, J.; Shen, K.; Cole, P. A.; Kuriyan, J. An Allosteric Mechanism for Activation of the Kinase Domain of Epidermal Growth Factor Receptor. *Cell* **2006**, *125* (6), 1137–1149.

(109) Jorissen, R. N.; Walker, F.; Pouliot, N.; Garrett, T. P. J.; Ward, C. W.; Burgess, A. W. Epidermal Growth Factor Receptor: Mechanisms of Activation and Signalling. *Exp. Cell Res.* **2003**, *284* (1), 31–53.

(110) Hynes, N. E.; Lane, H. A. ERBB Receptors and Cancer: The Complexity of Targeted Inhibitors. *Nat. Rev. Cancer* **2005**, *5* (5), 341–354.

(111) Umekita, Y.; Ohi, Y.; Sagara, Y.; Yoshida, H. Co-Expression of Epidermal Growth Factor Receptor and Transforming Growth Factor-Alpha Predicts Worse Prognosis in Breast-Cancer Patients. *Int. J. Cancer* **2000**, *89* (6), 484–487.

(112) Billings, S. D.; Southall, M. D.; Li, T.; Cook, P. W.; Baldridge, L.; Moores, W. B.; Spandau, D. F.; Foley, J. G.; Travers, J. B. Amphiregulin Overexpression Results in Rapidly Growing Keratinocytic Tumors. *Am. J.*

Pathol. **2003**, *163* (6), 2451–2458.

(113) Sunaga, N.; Kaira, K.; Imai, H.; Shimizu, K.; Nakano, T.; Shames, D. S.; Girard, L.; Soh, J.; Sato, M.; Iwasaki, Y.; et al. Oncogenic KRAS-Induced Epiregulin Overexpression Contributes to Aggressive Phenotype and Is a Promising Therapeutic Target in Non-Small-Cell Lung Cancer. *Oncogene* **2012**, *32*, 4034.

(114) Venugopal, C.; Wang, X. S.; Manoranjan, B.; McFarlane, N.; Nolte, S.; Li, M.; Murty, N.; Siu, K. W. M.; Singh, S. K. GBM Secretome Induces Transient Transformation of Human Neural Precursor Cells. *J. Neurooncol.* **2012**, *109* (3), 457–466.

(115) Nicholson, R. .; Gee, J. M. .; Harper, M. . EGFR and Cancer Prognosis. *Eur. J. Cancer* **2001**, *37*, 9–15.

(116) Pedersen, M. W.; Tkach, V.; Pedersen, N.; Berezin, V.; Poulsen, H. S. Expression of a Naturally Occurring Constitutively Active Variant of the Epidermal Growth Factor Receptor in Mouse Fibroblasts Increases Motility. *Int. J. Cancer* **2004**, *108* (5), 643–653.

(117) Pedersen, M. W.; Pedersen, N.; Damstrup, L.; Villingshøj, M.; Sønder, S. U.; Rieneck, K.; Bovin, L. F.; Spang-Thomsen, M.; Poulsen, H. S. Analysis of the Epidermal Growth Factor Receptor Specific Transcriptome: Effect of Receptor Expression Level and an Activating Mutation. *J. Cell. Biochem.* **2005**, *96* (2), 412–427.

(118) Araújo, A.; Ribeiro, R.; Azevedo, I.; Coelho, A.; Soares, M.; Sousa, B.; Pinto, D.; Lopes, C.; Medeiros, R.; Scagliotti, G. V. Genetic Polymorphisms of the Epidermal Growth Factor and Related Receptor in Non-Small Cell Lung Cancer—A Review of the Literature. *Oncol.* **2007**, *12* (2), 201–210.

(119) Lindsey, S.; Langhans, S. A. Epidermal Growth Factor Signaling in Transformed Cells. *Int. Rev. Cell Mol. Biol.* **2015**, *314*, 1–41.

(120) An, Z.; Aksoy, O.; Zheng, T.; Fan, Q.-W.; Weiss, W. A. Epidermal Growth Factor Receptor and EGFRvIII in Glioblastoma: Signaling Pathways and Targeted Therapies. *Oncogene* **2018**, 1561–1575.

(121) Nishikawa, R.; Ji, X. D.; Harmon, R. C.; Lazar, C. S.; Gill, G. N.; Cavenee, W. K.; Huang, H. J. A Mutant Epidermal Growth Factor Receptor Common in Human Glioma Confers Enhanced Tumorigenicity. *Proc. Natl. Acad. Sci. U. S. A.* **1994**, *91* (16), 7727–7731.

(122) Graham, R. P.; Treece, A. L.; Lindeman, N. I.; Vasalos, P.; Shan, M.; Jennings, L. J.; Rimm, D. L. Worldwide Frequency of Commonly Detected EGFR Mutations. *Arch. Pathol. Lab. Med.* **2018**, *142* (2), 163–167.

(123) Sordella, R.; Bell, D. W.; Haber, D. A.; Settleman, J. Gefitinib-Sensitizing EGFR Mutations in Lung Cancer Activate Anti-Apoptotic Pathways. *Science (80-.).* **2004**, *305* (5687), 1163–1167.

(124) Bridges, A. J.; Zhou, H.; Cody, D. R.; Rewcastle, G. W.; Mcmichael, A.; Showalter, H. D. H.; Fry, D. W.; Kraker, A. J.; Denny, W. A. Tyrosine Kinase Inhibitors 8. An Unusually Steep Structure-Activity Relationship for Analogues of 4-(3-Bromoanilino)-6,7-Dimethoxyquinazoline (PD 153035), a Potent Inhibitor of the Epidermal Growth Factor Receptor. *J. Med. Chem.* **1996**, *39*, 267–276.

(125) Thompson, A. M.; Bridges, A. J.; Fry, D. W.; Kraker, A. J.; Denny, W. A. Tyrosine Kinase Inhibitors. 7. 7-Amino-4-(Phenylamino)- and 7-Amino-4-[(Phenylmethyl)Amino]Pyrido[4,3d]Pyrimidines: A New Class of Inhibitors of the Tyrosine Kinase Activity of the Epidermal Growth Factor Receptor. *J. Med. Chem.* **1995**, *38* (7), 3780–3788.

(126) Denny, W. A. Irreversible Inhibitors of the ErbB Family of Protein Tyrosine Kinases. *Pharmacol. Ther.* **2002**, *93* (2–3), 253–261.

(127) Paez, J. G.; Jänne, P.; Lee, J. C.; Tracy, S.; Greulich, H.; Gabriel, S.;

Herman, P.; Kaye, F. J.; Lindeman, N.; Boggon, T. J.; et al. EGFR Mutations in Lung Cancer: Correlation with Clinical Response to Gefitinib Therapy. *Science (80-.).* **2004**, *304* (5676), 1497–1500.

(128) Pao, W.; Miller, V.; Zakowski, M.; Doherty, J.; Politi, K.; Sarkaria, I.; Singh, B.; Heelan, R.; Rusch, V.; Fulton, L.; et al. EGF Receptor Gene Mutations Are Common in Lung Cancers from "Never Smokers" and Are Associated with Sensitivity of Tumors to Gefitinib and Erlotinib. *Proc. Natl. Acad. Sci.* **2004**, *101* (36), 13306–13311.

(129) Carey, K. D.; Garton, A. J.; Romero, M. S.; Kahler, J.; Thomson, S.; Ross, S.; Park, F.; Haley, J. D.; Gibson, N.; Sliwkowski, M. X. Kinetic Analysis of Epidermal Growth Factor Receptor Somatic Mutant Proteins Shows Increased Sensitivity to the Epidermal Growth Factor Receptor Tyrosine Kinase Inhibitor, Erlotinib. *Cancer Res.* **2006**, *66* (16), 8163–8171.

(130) Yun, C. H.; Boggon, T. J.; Li, Y.; Woo, M. S.; Greulich, H.; Meyerson, M.; Eck, M. J. Structures of Lung Cancer-Derived EGFR Mutants and Inhibitor Complexes: Mechanism of Activation and Insights into Differential Inhibitor Sensitivity. *Cancer Cell* **2007**, *11* (3), 217–227.

(131) Kobayashi, S.; Boggon, T. J.; Dayaram, T.; Janne, P. J.; Kocher, O.; Meyerson, M.; Johnson, B. E.; Eck, M. J.; Tenen, D. G.; Almos, B. EGFR Mutation and Resistance of Non-Small-Cell Lung Cancer to Gefitinib. *N Engl J Med* **2005**, *352* (8), 786–792.

(132) Pao, W.; Miller, V. A.; Politi, K. A.; Riely, G. J.; Somwar, R.; Zakowski, M. F.; Kris, M. G.; Varmus, H. Acquired Resistance of Lung Adenocarcinomas to Gefitinib or Erlotinib Is Associated with a Second Mutation in the EGFR Kinase Domain. *PLoS Med.* **2005**, *2* (3), 0225–0235.

(133) Yun, C.-H.; Mengwasser, K. E.; Toms, A. V.; Woo, M. S.; Greulich, H.; Wong, K.-K.; Meyerson, M.; Eck, M. J. The T790M Mutation in EGFR

Kinase Causes Drug Resistance by Increasing the Affinity for ATP. *Proc. Natl. Acad. Sci. U. S. A.* **2008**, *105* (6), 2070–2075.

(134) Watanabe, M.; Kawaguchi, T.; Isa, S. I.; Ando, M.; Tamiya, A.; Kubo, A.; Saka, H.; Takeo, S.; Adachi, H.; Tagawa, T.; et al. Ultra-Sensitive Detection of the Pretreatment EGFR T790M Mutation in Non-Small Cell Lung Cancer Patients with an EGFR-Activating Mutation Using Droplet Digital PCR. *Clin. Cancer Res.* **2015**, *21* (15), 3552–3560.

(135) Smaill, J. B.; Rewcastle, G. W.; Loo, J. A.; Greis, K. D.; Chan, O. H.; Reyner, E. L.; Lipka, E.; Showalter, H. D. H.; Vincent, P. W.; Elliott, W. L.; et al. Tyrosine Kinase Inhibitors. 17. Irreversible Inhibitors of the Epidermal Growth Factor Receptor: 4-(Phenylamino)Quinazoline- and 4-(Phenylamino)Pyrido[3,2-d]Pyrimidine-6-Acrylamides Bearing Additional Solubilizing Functions. *J. Med. Chem.* **2000**, *43* (7), 1380–1397.

(136) Smaill, J. B.; Palmer, B. D.; Rewcastle, G. W.; Denny, W. a; Mcnamara, D. J.; Dobrusin, E. M.; Bridges, A. J.; Zhou, H.; Showalter, H. D. H.; Winters, R. T.; et al. 4- (Phenylamino) Pyrido [d] Pyrimidine Acrylamides as Irreversible Inhibitors of the ATP Binding Site of the Epidermal Growth Factor Receptor. *J. Med. Chem.* **1999**, *42* (10), 1803–1815.

(137) Miller, V. A.; Hirsh, V.; Cadranel, J.; Chen, Y.-M.; Park, K.; Kim, S.-W.; Zhou, C.; Su, W.-C.; Wang, M.; Sun, Y.; et al. Afatinib versus Placebo for Patients with Advanced, Metastatic Non-Small-Cell Lung Cancer after Failure of Erlotinib, Gefitinib, or Both, and One or Two Lines of Chemotherapy (LUX-Lung 1): A Phase 2b/3 Randomised Trial. *Lancet Oncol.* **2012**, *13* (5), 528–538.

(138) Yang, J. C.-H.; Shih, J.-Y.; Su, W.-C.; Hsia, T.-C.; Tsai, C.-M.; Ou, S.-H. I.; Yu, C.-J.; Chang, G.-C.; Ho, C.-L.; Sequist, L. V; et al. Afatinib for

Patients with Lung Adenocarcinoma and Epidermal Growth Factor Receptor Mutations (LUX-Lung 2): A Phase 2 Trial. *Lancet Oncol.* **2012**, *13* (5), 539–548.

(139) Katakami, N.; Atagi, S.; Goto, K.; Hida, T.; Horai, T.; Inoue, A.; Ichinose, Y.; Koboyashi, K.; Takeda, K.; Kiura, K.; et al. LUX-Lung 4: A Phase II Trial of Afatinib in Patients With Advanced Non–Small-Cell Lung Cancer Who Progressed During Prior Treatment With Erlotinib, Gefitinib, or Both. *J. Clin. Oncol.* **2013**, *31* (27), 3335–3341.

(140) Wong, K.-K.; Fracasso, P. M.; Bukowski, R. M.; Lynch, T. J.; Munster, P. N.; Shapiro, G. I.; Jänne, P. A.; Eder, J. P.; Naughton, M. J.; Ellis, M. J.; et al. A Phase I Study with Neratinib (HKI-272), an Irreversible Pan ErbB Receptor Tyrosine Kinase Inhibitor, in Patients with Solid Tumors. *Clin. Cancer Res.* **2009**, *15* (7), 2552 LP-2558.

(141) Yang, J. C.-H.; Schuler, M. H.; Yamamoto, N.; O'Byrne, K. J.; Hirsh, V.; Mok, T.; Geater, S. L.; Orlov, S. V; Tsai, C.-M.; Boyer, M. J.; et al. LUX-Lung 3: A Randomized, Open-Label, Phase III Study of Afatinib versus Pemetrexed and Cisplatin as First-Line Treatment for Patients with Advanced Adenocarcinoma of the Lung Harboring EGFR-Activating Mutations. *J. Clin. Oncol.* **2012**, *30* (18_suppl), LBA7500-LBA7500.

(142) Hirano, T.; Yasuda, H.; Tani, T.; Hamamoto, J.; Oashi, A.; Ishioka, K.; Arai, D.; Nukaga, S.; Miyawaki, M.; Kawada, I.; et al. In Vitro Modeling to Determine Mutation Specificity of EGFR Tyrosine Kinase Inhibitors against Clinically Relevant EGFR Mutants in Non-Small-Cell Lung Cancer. *Oncotarget* **2015**, *6* (36), 38789–38803.

(143) Zhou, W.; Ercan, D.; Chen, L.; Yun, C. H.; Li, D.; Capelletti, M.; Cortot, A. B.; Chirieac, L.; Iacob, R. E.; Padera, R.; et al. Novel Mutant-Selective EGFR Kinase Inhibitors against EGFR T790M. *Nature* **2009**, *462* (7276), 1070–1074.

(144) https://www.fda.gov/drugs/informationondrugs/approveddrugs/ visited on 7th September 2018.

(145) Thress, K. S.; Paweletz, C. P.; Felip, E.; Cho, B. C.; Stetson, D.; Dougherty, B.; Lai, Z.; Markovets, A.; Vivancos, A.; Kuang, Y.; et al. Acquired EGFR C797S Mutation Mediates Resistance to AZD9291 in Non-Small Cell Lung Cancer Harboring EGFR T790M. *Nat. Med.* **2015**, *21* (6), 560–562.

(146) Bersanelli, M.; Minari, R.; Bordi, P.; Gnetti, L.; Bozzetti, C.; Squadrilli, A.; Lagrasta, C. A. M.; Bottarelli, L.; Osipova, G.; Capelletto, E.; et al. L718Q Mutation as New Mechanism of Acquired Resistance to AZD9291 in EGFR-Mutated NSCLC. *J. Thorac. Oncol.* **2016**, *11* (10), e121–e123.

(147) Callegari, D.; Ranaghan, K. E.; Woods, C. J.; Minari, R.; Tiseo, M.; Mor, M.; Mulholland, A. J.; Lodola, A. L718Q Mutant EGFR Escapes Covalent Inhibition by Stabilizing a Non-Reactive Conformation of the Lung Cancer Drug Osimertinib. *Chem. Sci.* **2018**, *9* (10), 2740–2749.

(148) Cross, D. A. E.; Ashton, S. E.; Ghiorghiu, S.; Eberlein, C.; Nebhan, C. A.; Spitzler, P. J.; Orme, J. P.; Finlay, M. R. V.; Ward, R. A.; Mellor, M. J.; et al. AZD9291, an Irreversible EGFR TKI, Overcomes T790M-Mediated Resistance to EGFR Inhibitors in Lung Cancer. *Cancer Discov.* **2014**, *4* (9), 1046–1061.

(149) Ercan, D.; Choi, H. G.; Yun, C. H.; Capelletti, M.; Xie, T.; Eck, M. J.; Gray, N. S.; Jänne, P. A. EGFR Mutations and Resistance to Irreversible Pyrimidine-Based EGFR Inhibitors. *Clin. Cancer Res.* **2015**, *21* (17), 3913–3923.

(150) La Monica, S.; Madeddu, D.; Tiseo, M.; Vivo, V.; Galetti, M.; Cretella, D.; Bonelli, M.; Fumarola, C.; Cavazzoni, A.; Falco, A.; et al. Combination of Gefitinib and Pemetrexed Prevents the Acquisition of TKI Resistance in NSCLC Cell Lines Carrying EGFR-Activating Mutation. *J.*

Thorac. Oncol. **2016**, *11* (7), 1051–1063.

(151) Jia, Y.; Yun, C. H.; Park, E.; Ercan, D.; Manuia, M.; Juarez, J.; Xu, C.; Rhee, K.; Chen, T.; Zhang, H.; et al. Overcoming EGFR(T790M) and EGFR(C797S) Resistance with Mutant-Selective Allosteric Inhibitors. *Nature* **2016**, *534* (7605), 129–132.

(152) Lee, J.; Shim, J. H.; Park, W.-Y.; Kim, H. K.; Sun, J.-M.; Lee, S.-H.; Ahn, J. S.; Park, K.; Ahn, M.-J. Rare Mechanism of Acquired Resistance to Osimertinib in Korean Patients with EGFR-Mutated Non-Small Cell Lung Cancer . *J Korean Cancer Assoc* **2018**, *0* (0), 0.

(153) Solca, F.; Dahl, G.; Zoephel, A.; Bader, G.; Sanderson, M.; Klein, C.; Kraemer, O.; Himmelsbach, F.; Haaksma, E.; Adolf, G. R. Target Binding Properties and Cellular Activity of Afatinib (BIBW 2992), an Irreversible ErbB Family Blocker. *J. Pharmacol. Exp. Ther.* **2012**, *343* (2), 342–350.

(154) Baillie, T. A. Targeted Covalent Inhibitors for Drug Design. *Angew. Chemie - Int. Ed.* **2016**, *55* (43), 13408–13421.

(155) Lonsdale, R.; Ward, R. A. Structure-Based Design of Targeted Covalent Inhibitors. *Chem. Soc. Rev.* **2018**, *47* (11), 3816–3830.

(156) Lagoutte, R.; Patouret, R.; Winssinger, N. Covalent Inhibitors: An Opportunity for Rational Target Selectivity. *Curr. Opin. Chem. Biol.* **2017**, *39*, 54–63.

(157) Bauer, R. A. Covalent Inhibitors in Drug Discovery: From Accidental Discoveries to Avoided Liabilities and Designed Therapies. *Drug Discov. Today* **2015**, *20* (9), 1061–1073.

(158) Singh, J.; Petter, R. C.; Baillie, T. A.; Whitty, A. The Resurgence of Covalent Drugs. *Nat. Rev. Drug Discov.* **2011**, *10* (4), 307–317.

(159) Cheng, H.; Nair, S. K.; Murray, B. W.; Almaden, C.; Bailey, S.; Baxi, S.; Behenna, D.; Cho-Schultz, S.; Dalvie, D.; Dinh, D. M.; et al. Discovery of 1-{(3R,4R)-3-[({5-Chloro-2-[(1-Methyl-1H-Pyrazol-4-Yl)Amino]-7H-

Pyrrolo[2,3-d]Pyrimidin-4-Yl}oxy)Methyl]-4-Methoxypyrrolidin-1-Yl}prop-2-En-1-One (PF-06459988), a Potent, WT Sparing, Irreversible Inhibitor of T790M-Containing EGFR Mutants. *J. Med. Chem.* **2016**, *59* (5), 2005–2024.

(160) Wurz, R. P.; Pettus, L. H.; Ashton, K.; Brown, J.; Chen, J. J.; Herberich, B.; Hong, F.-T.; Hu-Harrington, E.; Nguyen, T.; St. Jean, D. J.; et al. Oxopyrido[2,3-d]Pyrimidines as Covalent L858R/T790M Mutant Selective Epidermal Growth Factor Receptor (EGFR) Inhibitors. *ACS Med. Chem. Lett.* **2015**, *6* (9), 987–992.

(161) Xie, H.; Lin, L.; Tong, L.; Jiang, Y.; Zheng, M.; Chen, Z.; Jiang, X.; Zhang, X.; Ren, X.; Qu, W.; et al. AST1306, A Novel Irreversible Inhibitor of the Epidermal Growth Factor Receptor 1 and 2, Exhibits Antitumor Activity Both In Vitro and In Vivo. *PLoS One* **2011**, *6* (7), e21487.

(162) Qiu, H.; Liu-Bujalski, L.; Caldwell, R. D.; Follis, A. V.; Gardberg, A.; Goutopoulos, A.; Grenningloh, R.; Head, J.; Johnson, T.; Jones, R.; et al. Discovery of Potent, Highly Selective Covalent Irreversible BTK Inhibitors from a Fragment Hit. *Bioorg. Med. Chem. Lett.* **2018**, *28* (17), 2939–2944.

(163) Brameld, K. A.; Owens, T. D.; Verner, E.; Venetsanakos, E.; Bradshaw, J. M.; Phan, V. T.; Tam, D.; Leung, K.; Shu, J.; Lastant, J.; et al. Discovery of the Irreversible Covalent FGFR Inhibitor 8-(3-(4-Acryloylpiperazin-1-Yl)Propyl)-6-(2,6-Dichloro-3,5-Dimethoxyphenyl)-2-(Methylamino)Pyrido[2,3-d]Pyrimidin-7(8H)-One (PRN1371) for the Treatment of Solid Tumors. *J. Med. Chem.* **2017**, *60* (15), 6516–6527.

(164) Wu, H.; Wang, W.; Liu, F.; Weisberg, E. L.; Tian, B.; Chen, Y.; Li, B.; Wang, A.; Wang, B.; Zhao, Z.; et al. Discovery of a Potent, Covalent BTK Inhibitor for B-Cell Lymphoma. *ACS Chem. Biol.* **2014**, *9* (5), 1086–1091.

(165) Günther, M.; Lategahn, J.; Juchum, M.; Döring, E.; Keul, M.; Engel, J.;

Tumbrink, H. L.; Rauh, D.; Laufer, S. Trisubstituted Pyridinylimidazoles as Potent Inhibitors of the Clinically Resistant L858R/T790M/C797S EGFR Mutant: Targeting of Both Hydrophobic Regions and the Phosphate Binding Site. *J. Med. Chem.* **2017**, *60* (13), 5613–5637.

(166) Song, Z.; Huang, S.; Yu, H.; Jiang, Y.; Wang, C.; Meng, Q.; Shu, X.; Sun, H.; Liu, K.; Li, Y.; et al. Synthesis and Biological Evaluation of Morpholine-Substituted Diphenylpyrimidine Derivatives (Mor-DPPYs) as Potent EGFR T790M Inhibitors with Improved Activity toward the Gefitinib-Resistant Non-Small Cell Lung Cancers (NSCLC). *Eur. J. Med. Chem.* **2017**, *133*, 329–339.

(167) Lanning, B. R.; Whitby, L. R.; Dix, M. M.; Douhan, J.; Gilbert, A. M.; Hett, E. C.; Johnson, T. O.; Joslyn, C.; Kath, J. C.; Niessen, S.; et al. A Road Map to Evaluate the Proteome-Wide Selectivity of Covalent Kinase Inhibitors. *Nat. Chem. Biol.* **2014**, *10* (9), 760–767.

(168) Dickinson, P. A.; Cantarini, M. V.; Collier, J.; Frewer, P.; Martin, S.; Pickup, K.; Ballard, P. Metabolic Disposition of Osimertinib in Rats, Dogs, and Humans: Insights into a Drug Designed to Bind Covalently to a Cysteine Residue of Epidermal Growth Factor Receptor. *Drug Metab. Dispos.* **2016**, *44* (8), 1201–1212.

(169) Carmi, C.; Cavazzoni, A.; Vezzosi, S.; Bordi, F.; Vacondio, F.; Silva, C.; Rivara, S.; Lodola, A.; Alfieri, R. R.; Monica, S. La; et al. Novel Irreversible Epidermal Growth Factor Receptor Inhibitors by Chemical Modulation of the Cysteine-Trap Portion. *J. Med. Chem.* **2010**, *53* (5), 2038–2050.

(170) Vacondio, F.; Carmi, C.; Galvani, E.; Bassi, M.; Silva, C.; Lodola, A.; Rivara, S.; Cavazzoni, A.; Alfieri, R. R.; Petronini, P. G.; et al. Long-Lasting Inhibition of EGFR Autophosphorylation in A549 Tumor Cells by Intracellular Accumulation of Non-Covalent Inhibitors. *Bioorganic Med.*

Chem. Lett. **2013**, *23* (19), 5290–5294.

(171) Thompson, A. M.; Murray, D. K.; Elliott, W. L.; Fry, D. W.; Nelson, J. A.; Showalter, H. D.; Roberts, B. J.; Vincent, P. W.; Denny, W. A. Tyrosine Kinase Inhibitors. 13. Structure-Activity Relationships for Soluble 7-Substituted 4-[(3-Bromophenyl)Amino]Pyrido[4,3-d]Pyrimidines Designed as Inhibitors of the Tyrosine Kinase Activity of the Epidermal Growth Factor Receptor. *J. Med. Chem.* **1997**, *40* (24), 3915–3925.

(172) Flanagan, M. E.; Abramite, J. A.; Anderson, D. P.; Aulabaugh, A.; Dahal, U. P.; Gilbert, A. M.; Li, C.; Montgomery, J.; Oppenheimer, S. R.; Ryder, T.; et al. Chemical and Computational Methods for the Characterization of Covalent Reactive Groups for the Prospective Design of Irreversible Inhibitors. *J. Med. Chem.* **2014**, *57* (23), 10072–10079.

(173) Kung, A.; Chen, Y. C.; Schimpl, M.; Ni, F.; Zhu, J.; Turner, M.; Molina, H.; Overman, R.; Zhang, C. Development of Specific, Irreversible Inhibitors for a Receptor Tyrosine Kinase EphB3. *J. Am. Chem. Soc.* **2016**, *138* (33), 10554–10560.

(174) Mishani, E.; Abourbeh, G.; Jacobson, O.; Dissoki, S.; Ben Daniel, R.; Rozen, Y.; Shaul, M.; Levitzki, A. High-Affinity Epidermal Growth Factor Receptor (EGFR) Irreversible Inhibitors with Diminished Chemical Reactivities as Positron Emission Tomography (PET)-Imaging Agent Candidates of EGFR Overexpressing Tumors. *J. Med. Chem.* **2005**, *48* (16), 5337–5348.

(175) Narayanan, A.; Jones, L. H. Sulfonyl Fluorides as Privileged Warheads in Chemical Biology. *Chem. Sci.* **2015**, *6* (5), 2650–2659.

(176) Zhao, Q.; Ouyang, X.; Wan, X.; Gajiwala, K. S.; Kath, J. C.; Jones, L. H.; Burlingame, A. L.; Taunton, J. Broad-Spectrum Kinase Profiling in Live Cells with Lysine-Targeted Sulfonyl Fluoride Probes. *J. Am. Chem. Soc.*

2017, *139* (2), 680–685.

(177) Carmi, C.; Galvani, E.; Vacondio, F.; Rivara, S.; Lodola, A.; Russo, S.; Aiello, S.; Bordi, F.; Costantino, G.; Cavazzoni, A.; et al. Irreversible Inhibition of Epidermal Growth Factor Receptor Activity by 3-Aminopropanamides. *J. Med. Chem.* **2012**, *55*, 2251–2264.

(178) Mao, Y.; Liu, Z.; Yang, X.; Xia, X.; Zhang, R.; Li, J.; Jiang, X.; Xie, K.; Zheng, J.; Zhang, H.; et al. A New and Improved Process for N - (4-Chloro-3-Cyano-7- Ethoxyquinolin-6-Yl)Acetamide. *Org. Process Res. Dev.* **2012**, *16*, 1970–1973.

(179) EP1477481 (A1) — 2004-11-17, 2004.

(180) Montalbetti, C. A. G. N.; Falque, V. Amide Bond Formation and Peptide Coupling. *Tetrahedron* **2005**, *61* (46), 10827–10852.

(181) Tschitschibabin, A. E.; Woroshtzow, N. N. Über Einige Derivate Des a,b-Pyridin-Thioindoxyls. *Chem. Ber.* **1933**, *66*, 364–372.

(182) CN105461640, 2016, A.

(183) WO2013/138495, 2013, A1.

(184) WO2013/138502, 2013, A1.

(185) WO2014/182593, 2014, A1.

(186) JP2015/218155, 2015, A.

(187) JP2015/218132, 2015, A.

(188) US2007/32514, 2007, A1.

(189) Yang, E. H.; Yun, J. I.; Latif, M.; Lee, H. J.; Yun, C. S.; Lee, K.; Park, C. H.; Cho, S. Y.; Jung, H. J.; Kim, P.; et al. New Pyrimidine Derivatives Possessing ALK Inhibitory Activities. *Bull. Korean Chem. Soc.* **2013**, *34* (10), 3129–3132.

(190) Walker, D. P.; Christopher Bi, F.; Kalgutkar, A. S.; Bauman, J. N.; Zhao, S. X.; Soglia, J. R.; Aspnes, G. E.; Kung, D. W.; Klug-McLeod, J.; Zawistoski, M. P.; et al. Trifluoromethylpyrimidine-Based Inhibitors of

Proline-Rich Tyrosine Kinase 2 (PYK2): Structure-Activity Relationships and Strategies for the Elimination of Reactive Metabolite Formation. *Bioorganic Med. Chem. Lett.* **2008**, *18* (23), 6071–6077.

(191) Richter, D. T.; Kath, J. C.; Luzzio, M. J.; Keene, N.; Berliner, M. A.; Wessel, M. D. Selective Addition of Amines to 5-Trifluoromethyl-2,4-Dichloropyrimidine Induced by Lewis Acids. *Tetrahedron Lett.* **2013**, *54* (35), 4610–4612.

(192) Wang, H.; Wen, K.; Wang, L.; Xiang, Y.; Xu, X.; Shen, Y.; Sun, Z. Large-Scale Solvent-Free Chlorination of Hydroxy-Pyrimidines,-Pyridines,-Pyrazines and-Amides Using Equimolar POCl3. *Molecules* **2012**, *17* (4), 4533–4544.

(193) Ward, R. A.; Anderton, M.; Ashton, S.; Bethel, P.; Box, M.; Butterworth, S.; Colclough, N.; Chorley, C. G.; Chuaqui, C.; Cross, D.; et al. Structure and Reactivity Based Development of Covalent Inhibitors of the Activating and Gatekeeper Mutant Forms of the Epidermal Growth Factor Receptor (EGFR). *J. Med. Chem.* **2013**, *56* (17), 7025–7048.

(194) Krutak, J. J.; Burpitt, R. D.; Moore, W. H.; Hyatt, J. A. Chemistry of Ethenesulfonyl Fluoride. Fluorosulfonylethylation of Organic Compounds. *J. Org. Chem.* **1979**, *44* (22), 3847–3858.

(195) Berteotti, A.; Vacondio, F.; Lodola, A.; Bassi, M.; Silva, C.; Mor, M.; Cavalli, A. Predicting the Reactivity of Nitrile-Carrying Compounds with Cysteine: A Combined Computational and Experimental Study. *ACS Med. Chem. Lett.* **2014**, *5* (5), 501–505.

(196) Kletzien, R. F.; Pariza, M. W.; Becker, J. E.; Potter, V. R. A Method Using 3-O-Methyl-D-Glucose and Phloretin for the Determination of Intracellular Water Space of Cells in Monolayer Culture. *Anal. Biochem.* **1975**, *68* (2), 537–544.

(197) Barf, T.; Kaptein, A. Irreversible Protein Kinase Inhibitors: Balancing the

Benefits and Risks. *J. Med. Chem.* **2012**, *55* (14), 6243–6262.

(198) Ornitz, D. M.; Itoh, N. Fibroblast Growth Factors. *Genome Biol.* **2001**, *2* (reviews), 1–12.

(199) Itoh, N.; Ornitz, D. M. Fibroblast Growth Factors: From Molecular Evolution to Roles in Development, Metabolism and Disease. *J. Biochem.* **2011**, *149* (2), 121–130.

(200) Beenken, A.; Mohammadi, M. The FGF Family: Biology, Pathophysiology and Therapy. *Nat. Rev. Drug Discov.* **2009**, *8* (3), 235–253.

(201) Goldfarb, M.; Schoorlemmer, J.; Williams, A.; Diwakar, S.; Wang, Q.; Huang, X.; Giza, J.; Tchetchik, D.; Kelley, K.; Vega, A.; et al. Fibroblast Growth Factor Homologous Factors Control Neuronal Excitability through Modulation of Voltage-Gated Sodium Channels. *Neuron* **2007**, *55* (3), 449–463.

(202) Kharitonenkov, A. FGFs and Metabolism. *Curr. Opin. Pharmacol.* **2009**, *9* (6), 805–810.

(203) Mohammadi, M.; Olsen, S. K.; Ibrahimi, O. A. Structural Basis for Fibroblast Growth Factor Receptor Activation. *Cytokine Growth Factor Rev.* **2005**, *16*, 107–137.

(204) Itoh, N.; Ohta, H.; Konishi, M. Endocrine FGFs: Evolution, Physiology, Pathophysiology, and Pharmacotherapy. *Front. Endocrinol. (Lausanne).* **2015**, *6*, 154.

(205) Turner, N.; Grose, R. Fibroblast Growth Factor Signalling: From Development to Cancer. *Nat. Rev. Cancer* **2010**, *10* (2), 116–129.

(206) Olsen, S. K.; Ibrahimi, O. A.; Raucci, A.; Zhang, F.; Eliseenkova, A. V; Yayon, A.; Basilico, C.; Linhardt, R. J.; Schlessinger, J.; Mohammadi, M. Insights into the Molecular Basis for Fibroblast Growth Factor Receptor Autoinhibition and Ligand-Binding Promiscuity. *Proc. Natl. Acad. Sci. U.*

S. A. **2004**, *101* (4), 935–940.

(207) Itoh, N.; Ornitz, D. M. Evolution of the Fgf and Fgfr Gene Families. *Trends Genet.* **2004**, *20* (11), 563–569.

(208) Trueb, B.; Zhuang, L.; Taeschler, S.; Wiedemann, M. Characterization of FGFRL1, a Novel Fibroblast Growth Factor (FGF) Receptor Preferentially Expressed in Skeletal Tissues. *J. Biol. Chem.* **2003**, *278* (36), 33857–33865.

(209) Wesche, J.; Haglund, K.; Haugsten, E. M. Fibroblast Growth Factors and Their Receptors in Cancer. *Biochem. J.* **2011**, *437* (2), 199–213.

(210) Desai, A.; Adjei, A. A. FGFR Signaling as a Target for Lung Cancer Therapy. *J. Thorac. Oncol.* **2016**, *11* (1), 9–20.

(211) Brooks, A. N.; Kilgour, E.; Smith, P. D. Molecular Pathways: Fibroblast Growth Factor Signaling: A New Therapeutic Opportunity in Cancer. *Clin. Cancer Res.* **2012**, *18* (7), 1855–1862.

(212) Yu, C.; Wang, F.; Kan, M.; Jin, C.; Jones, R. B.; Weinstein, M.; Deng, C. X.; McKeehan, W. L. Elevated Cholesterol Metabolism and Bile Acid Synthesis in Mice Lacking Membrane Tyrosine Kinase Receptor FGFR4. *J. Biol. Chem.* **2000**, *275* (20), 15482–15489.

(213) Shimada, T.; Kakitani, M.; Yamazaki, Y.; Hasegawa, H.; Takeuchi, Y.; Fujita, T.; Fukumoto, S.; Tomizuka, K.; Yamashita, T. Targeted Ablation of Fgf23 Demonstrates an Essential Physiological Role of FGF23 in Phosphate and Vitamin D Metabolism. *J. Clin. Invest.* **2004**, *113* (4), 561–568.

(214) Shimada, T.; Hasegawa, H.; Yamazaki, Y.; Muto, T.; Hino, R.; Takeuchi, Y.; Fujita, T.; Nakahara, K.; Fukumoto, S.; Yamashita, T. FGF-23 Is a Potent Regulator of Vitamin D Metabolism and Phosphate Homeostasis. *J. Bone Miner. Res.* **2004**, *19* (3), 429–435.

(215) Carmeliet, P.; Jain, R. K. Angiogenesis in Cancer and Other Diseases.

Nature **2000**, *407*, 249–257.

(216) Helsten, T.; Schwaederle, M.; Kurzrock, R. Fibroblast Growth Factor Receptor Signaling in Hereditary and Neoplastic Disease: Biologic and Clinical Implications. *Cancer Metastasis Rev.* **2015**, *34*, 479–496.

(217) Reis-Filho, J. S.; Simpson, P. T.; Turner, N. C.; Lambros, M. B.; Jones, C.; Mackay, A.; Grigoriadis, A.; Sarrio, D.; Savage, K.; Dexter, T.; et al. FGFR1 Emerges as a Potential Therapeutic Target for Lobular Breast Carcinomas. *Clin. Cancer Res.* **2006**, *12* (22), 6652–6662.

(218) Turner, N.; Lambros, M. B.; Horlings, H. M.; Pearson, A.; Sharpe, R.; Natrajan, R.; Geyer, F. C.; Van Kouwenhove, M.; Kreike, B.; MacKay, A.; et al. Integrative Molecular Profiling of Triple Negative Breast Cancers Identifies Amplicon Drivers and Potential Therapeutic Targets. *Oncogene* **2010**, *29* (14), 2013–2023.

(219) Heist, R. S.; Mino-Kenudson, M.; Sequist, L. V.; Tammireddy, S.; Morrissey, L.; Christiani, D. C.; Engelman, J. A.; Iafrate, A. J. FGFR1 Amplification in Squamous Cell Carcinoma of the Lung. *J. Thorac. Oncol.* **2012**, *7* (12), 1775–1780.

(220) Hammerman, P. S.; Lawrence, M. S.; Voet, D.; Jing, R.; Cibulskis, K.; Sivachenko, A.; Stojanov, P.; McKenna, A.; Lander, E. S.; Gabriel, S.; et al. Comprehensive Genomic Characterization of Squamous Cell Lung Cancers. *Nature* **2012**, *489* (7417), 519–525.

(221) Freier, K.; Schwaenen, C.; Sticht, C.; Flechtenmacher, C.; Mühling, J.; Hofele, C.; Radlwimmer, B.; Lichter, P.; Joos, S. Recurrent FGFR1 Amplification and High FGFR1 Protein Expression in Oral Squamous Cell Carcinoma (OSCC). *Oral Oncol.* **2007**, *43* (1), 60–66.

(222) Von Loga, K.; Kohlhaussen, J.; Burkhardt, L.; Simon, R.; Steurer, S.; Burdak-Rothkamm, S.; Jacobsen, F.; Sauter, G.; Krech, T. FGFR1 Amplification Is Often Homogeneous and Strongly Linked to the

Squamous Cell Carcinoma Subtype in Esophageal Carcinoma. *PLoS One* **2015**, *10* (11), e0141867.

(223) Matsumoto, K.; Arao, T.; Hamaguchi, T.; Shimada, Y.; Kato, K.; Oda, I.; Taniguchi, H.; Koizumi, F.; Yanagihara, K.; Sasaki, H.; et al. FGFR2 Gene Amplification and Clinicopathological Features in Gastric Cancer. *Br. J. Cancer* **2012**, *106* (4), 727–732.

(224) Singh, D.; Chan, J. M.; Zoppoli, P.; Niola, F.; Sullivan, R.; Castano, A.; Liu, E. M.; Reichel, J.; Porrati, P.; Pellegatta, S.; et al. Transforming Fusions of FGFR and TACC Genes in Human Glioblastoma. *Science (80-.).* **2012**, *337* (6099), 1231–1235.

(225) Parker, B. C.; Annala, M. J.; Cogdell, D. E.; Granberg, K. J.; Sun, Y.; Ji, P.; Li, X.; Gumin, J.; Zheng, H.; Hu, L.; et al. The Tumorigenic FGFR3-TACC3 Gene Fusion Escapes MiR-99a Regulation in Glioblastoma. *J. Clin. Invest.* **2013**, *123* (2), 855–865.

(226) Williams, S. V.; Hurst, C. D.; Knowles, M. A. Oncogenic FGFR3 Gene Fusions in Bladder Cancer. *Hum. Mol. Genet.* **2013**, *22* (4), 795–803.

(227) Shaver, T. M.; Lehmann, B. D.; Beeler, J. S.; Li, C.-I.; Li, Z.; Jin, H.; Stricker, T. P.; Shyr, Y.; Pietenpol, J. A. Diverse, Biologically Relevant, and Targetable Gene Rearrangements in Triple-Negative Breast Cancer and Other Malignancies. *Cancer Res.* **2016**, *76* (16), 4850 LP-4860.

(228) Daly, C.; Castanaro, C.; Zhang, W.; Zhang, Q.; Wei, Y.; Ni, M.; Young, T. M.; Zhang, L.; Burova, E.; Thurston, G. FGFR3-TACC3 Fusion Proteins Act as Naturally Occurring Drivers of Tumor Resistance by Functionally Substituting for EGFR/ERK Signaling. *Oncogene* **2016**, *36*, 471.

(229) Ruotsalainen, T.; Joensuu, H.; Mattson, K. High Pretreatment Serum Concentration of Basic Fibroblast Growth Factor Is a Predictor of Poor Prognosis in Small Cell Lung Cancer 1. *Cancer Epidemiol. Biomarkers*

Prev. **2002**, *11*, 1492–1495.

(230) Presta, M.; Dell'Era, P.; Mitola, S.; Moroni, E.; Ronca, R.; Rusnati, M. Fibroblast Growth Factor/Fibroblast Growth Factor Receptor System in Angiogenesis. *Cytokine Growth Factor Rev.* **2005**, *16*, 159–178.

(231) Lieu, C.; Heymach, J.; Overman, M.; Tran, H.; Kopetz, S. Beyond VEGF: Inhibition of the Fibroblast Growth Factor Pathway and Antiangiogenesis. *Clin. Cancer Res.* **2011**, *17* (19), 6130–6139.

(232) Bello, E.; Colella, G.; Scarlato, V.; Oliva, P.; Berndt, A.; Valbusa, G.; Serra, S. C.; D'Incalci, M.; Cavalletti, E.; Giavazzi, R.; et al. E-3810 Is a Potent Dual Inhibitor of VEGFR and FGFR That Exerts Antitumor Activity in Multiple Preclinical Models. *Cancer Res.* **2011**, *71* (4), 1396 LP-1405.

(233) Allen, E.; Walters, I. B.; Hanahan, D. Brivanib, a Dual FGF/VEGF Inhibitor, Is Active Both 1(St) and 2(Nd) Line against Mouse Pancreatic Neuroendocrine Tumors (PNET) Developing Adaptive/Evasive Resistance to VEGF Inhibition. *Clin. Cancer Res.* **2011**, *17* (16), 5299–5310.

(234) Chae, Y. K.; Ranganath, K.; Hammerman, P. S.; Vaklavas, C.; Mohindra, N.; Kalyan, A.; Matsangou, M.; Costa, R.; Carneiro, B.; Villaflor, V. M.; et al. Inhibition of the Fibroblast Growth Factor Receptor (FGFR) Pathway: The Current Landscape and Barriers to Clinical Application. *Oncotarget* **2017**, *8* (9), 16052–16074.

(235) Mohammadi, M.; Froum, S.; Hamby, J. M.; Schroeder, M. C.; Panek, R. L.; Lu, G. H.; Eliseenkova, A. V.; Green, D.; Schlessinger, J.; Hubbard, S. R. Crystal Structure of an Angiogenesis Inhibitor Bound to the FGF Receptor Tyrosine Kinase Domain. *EMBO J.* **1998**, *17* (20), 5896–5904.

(236) Guagnano, V.; Furet, P.; Spanka, C.; Bordas, V.; Le Douget, M.; Stamm, C.; Brueggen, J.; Jensen, M. R.; Schnell, C.; Schmid, H.; et al. Discovery

of 3-(2,6-Dichloro-3,5-Dimethoxy-Phenyl)-1-{6-[4-(4-Ethyl-Piperazin-1-Yl)-Phenylamino]-Pyrimidin-4-Yl}-1-Methyl-Urea (NVP-BGJ398), A Potent and Selective Inhibitor of the Fibroblast Growth Factor Receptor Family of Receptor Tyrosine Kinase. *J. Med. Chem.* **2011**, *54* (20), 7066–7083.

(237) Zhou, W.; Hur, W.; McDermott, U.; Dutt, A.; Xian, W.; Ficarro, S. B.; Zhang, J.; Sharma, S. V.; Brugge, J.; Meyerson, M.; et al. A Structure-Guided Approach to Creating Covalent FGFR Inhibitors. *Chem. Biol.* **2010**, *17* (3), 285–295.

(238) Harding, T. C.; Long, L.; Palencia, S.; Zhang, H.; Sadra, A.; Hestir, K.; Patil, N.; Levin, A.; Hsu, A. W.; Charych, D.; et al. Blockade of Nonhormonal Fibroblast Growth Factors by FP-1039 Inhibits Growth of Multiple Types of Cancer. *Sci. Transl. Med.* **2013**, *5* (178), 178ra39-178ra39.

(239) Tolcher, A. W.; Papadopoulos, K. P.; Patnaik, A.; Wilson, K.; Thayer, S.; Zanghi, J.; Gemo, A. T.; Kavanaugh, W. M.; Keer, H. N.; LoRusso, P. M. A Phase I, First in Human Study of FP-1039 (GSK3052230), a Novel FGF Ligand Trap, in Patients with Advanced Solid Tumors. *Ann. Oncol.* **2016**, *27* (3), 526–532.

(240) Castelli, R.; Giacomini, A.; Anselmi, M.; Bozza, N.; Vacondio, F.; Rivara, S.; Matarazzo, S.; Presta, M.; Mor, M.; Ronca, R. Synthesis, Structural Elucidation, and Biological Evaluation of NSC12, an Orally Available Fibroblast Growth Factor (FGF) Ligand Trap for the Treatment of FGF-Dependent Lung Tumors. *J. Med. Chem.* **2016**, *59* (10), 4651–4663.

(241) Galvani, E.; Giovannetti, E.; Saccani, F.; Cavazzoni, A.; Leon, L. G.; Dekker, H.; Alfieri, R.; Carmi, C.; Mor, M.; Ardizzoni, A.; et al. Molecular Mechanisms Underlying the Antitumor Activity of 3-Aminopropanamide Irreversible Inhibitors of the Epidermal Growth Factor Receptor in Non–

Small Cell Lung Cancer. *Neoplasia* **2013**, *15* (1), 61-IN18.

(242) Chu, C. K. Acyclopyrimidine C-nucleosides. Synthesis of Acyclopseudoisocytidine and Its Derivatives. *J. Heterocycl. Chem.* **1984**, *21* (1), 9–11.

(243) 3β-Acetoxyetienic Acid. *Org. Synth.* **1962**, *42*, 4.

(244) Ishizumi, K.; Koga, K.; Yamada, S. Chemistry of Sodium Borohydride and Diborane. IV. Reduction of Carboxylic Acids to Alcohols with Sodium Borohydride through Mixed Carbonic-Carboxylic Acid Anhydrides. *Chem. Pharm. Bull. (Tokyo).* **1968**, *16* (3), 492–497.

(245) Drašar, P.; Pouzar, V.; Černý, I.; Havel, M. Alternative Syntheses of Steroidal Maleimides. *Collect. Czechoslov. Chem. Commun.* **1983**, *48*, 1224–1232.

(246) Fletcher, D. A.; Mullins, R. D. Cell Mechanics and the Cytoskeleton. *Nature* **2010**, *463* (7280), 485–492.

(247) Jordan, M. A.; Wilson, L. Microtubules as a Target for Anticancer Drugs. *Nat. Rev. Cancer* **2004**, *4* (4), 253–265.

(248) Rusan, N. M.; Fagerstrom, C. J.; Yvon, A. M.; Wadsworth, P. Cell Cycle-Dependent Changes in Microtubule Dynamics in Living Cells Expressing Green Fluorescent Protein-Alpha Tubulin. *Mol. Biol. Cell* **2001**, *12* (4), 971–980.

(249) Kelling, J.; Sullivan, K.; Wilson, L.; Jordan, M. A. Suppression of Centromere Dynamics by Taxol in Living Osteosarcoma Cells. *Cancer Res.* **2003**, *63* (11), 2794–2801.

(250) Okouneva, T.; Hill, B. T.; Wilson, L.; Jordan, M. A. The Effects of Vinflunine, Vinorelbine, and Vinblastine on Centromere Dynamics. *Mol. Cancer Ther.* **2003**, *2*, 427–436.

(251) Field, J. J.; Calvo, E.; Northcote, P. T.; Miller, J. H.; Altmann, K. H.; Díaz, J. F. Methods for Studying Microtubule Binding Site Interactions.

Zampanolide as a Covalent Binding Agent. *Methods Cell Biol.* **2013**, *115*, 303–325.

(252) Tanaka, J.; Higa, T. Zampanolide, a New Cytotoxic Macrolide from a Marine Sponge. *Tetrahedron Lett.* **1996**, *37* (31), 5535–5538.

(253) Prota, A. E.; Bargsten, K.; Zurwerra, D.; Field, J. J.; Díaz, J. F.; Altmann, K.-H.; Steinmetz, M. O. Molecular Mechanism of Action of Microtubule-Stabilizing Anticancer Agents. *Science (80-.).* **2013**, *339*, 587–590.

(254) Field, J. J.; Singh, A. J.; Kanakkanthara, A.; Halafihi, T.; Northcote, P. T.; Miller, J. H. Microtubule-Stabilizing Activity of Zampanolide, a Potent Macrolide Isolated from the Tongan Marine Sponge Cacospongia Mycofijiensis. *J. Med. Chem.* **2009**, *52* (22), 7328–7332.

(255) Field, J. J.; Pera, B.; Calvo, E.; Canales, A.; Zurwerra, D.; Trigili, C.; Rodríguez-Salarichs, J.; Matesanz, R.; Kanakkanthara, A.; Wakefield, S. J.; et al. Zampanolide, a Potent New Microtubule-Stabilizing Agent, Covalently Reacts with the Taxane Luminal Site in Tubulin α,β-Heterodimers and Microtubules. *Chem. Biol.* **2012**, *19* (6), 686–698.

(256) Zurwerra, D.; Glaus, F.; Betschart, L.; Schuster, J.; Gertsch, J.; Ganci, W.; Altmann, K. H. Total Synthesis of (-)-Zampanolide and Structure-Activity Relationship Studies on (-)-Dactylolide Derivatives. *Chem. - A Eur. J.* **2012**, *18* (52), 16868–16883.

(257) McDougal, P. G.; Rico, J. G.; Oh, Y. I.; Condon, B. D. A Convenient Procedure for the Monosilylation of Symmetric 1,n-Diols. *J. Org. Chem.* **1986**, *51* (17), 3388–3390.

(258) Betzer, J.-F.; Delaloge, F.; Muller, B.; Pancrazi, A.; Prunet, J. Radical Hydrostannylation, Pd(0)-Catalyzed Hydrostannylation, Stannylcupration of Propargyl Alcohols and Enynols: Regio- and Stereoselectivities. *J. Org. Chem.* **1997**, *62* (22), 7768–7780.

(259) Betzer, J.-F.; Ardisson, J.; Lallemand, J.-Y.; Pancrazi, A. An Efficient

Method in Stannylcupration of a Methyl Substituted Enyne or Alkyne by Kinetic Control Using Methanol. *Tetrahedron Lett.* **1997**, *38* (13), 2279–2282.

(260) Hart, D. W.; Schwartz, J. Hydrozirconation. Organic Synthesis via Organozirconium Intermediates. Synthesis and Rearrangement of Alkylzirconium(IV) Complexes and Their Reaction with Electrophiles. *J. Am. Chem. Soc.* **1974**, *96* (26), 8115–8116.

(261) Huang, Z.; Negishi, E. A Convenient and Genuine Equivalent to HZrCp2Cl Generated in Situ from ZrCp2Cl2−DIBAL-H. *Org. Lett.* **2006**, *8* (17), 3675–3678.

(262) Wipf, P.; H, T.; Nian, Z. Kinetic vs. Thermodynamic Control in Hydrozirconation Reactions. *Pure and Applied Chemistry*. 1998, p 1077.

(263) Torre, L. A.; Bray, F.; Siegel, R. L.; Ferlay, J.; Lortet-tieulent, J.; Jemal, A. Global Cancer Statistics, 2012. *CA a cancer J. Clin.* **2015**, *65* (2), 87–108.

(264) https://gco.iarc.fr/today/data/factsheets/cancers/39-All-cancers-fact-sheet.pdf visited on 17th October 2018.

(265) Ortiz, A.; Shanahan, C. S.; Sisk, D. T.; Perera, S. C.; Rao, P.; McGrath, D. V. Improved Iterative Synthesis of Linearly Disassembling Dendrons. *J. Org. Chem.* **2010**, *75* (18), 6154–6162.

(266) Wang, X.; Gensch, T.; Lerchen, A.; Daniliuc, C. G.; Glorius, F. Cp*Rh(III)/Bicyclic Olefin Cocatalyzed C–H Bond Amidation by Intramolecular Amide Transfer. *J. Am. Chem. Soc.* **2017**, *139* (18), 6506–6512.

(267) Asakura, J.; Robins, M. J. Cerium(IV)-Mediated Halogenation at C-5 of Uracil Derivatives. *J. Org. Chem.* **1990**, *55* (16), 4928–4933.

(268) WO2014/144737, 2014, A1.

(269) Coterón, J. M.; Catterick, D.; Castro, J.; Chaparro, M. J.; Díaz, B.;

Fernández, E.; Ferrer, S.; Gamo, F. J.; Gordo, M.; Gut, J.; et al. Falcipain Inhibitors: Optimization Studies of the 2-Pyrimidinecarbonitrile Lead Series. *J. Med. Chem.* **2010**, *53* (16), 6129–6152.

(270) Yang, J.; Wang, L.-J.; Liu, J.-J.; Zhong, L.; Zheng, R.-L.; Xu, Y.; Ji, P.; Zhang, C.-H.; Wang, W.-J.; Lin, X.-D.; et al. Structural Optimization and Structure–Activity Relationships of N2-(4-(4-Methylpiperazin-1-Yl)Phenyl)-N8-Phenyl-9H-Purine-2,8-Diamine Derivatives, a New Class of Reversible Kinase Inhibitors Targeting Both EGFR-Activating and Resistance Mutations. *J. Med. Chem.* **2012**, *55* (23), 10685–10699.

(271) Shibuya, H.; Murakami, N.; Shimada, F.; Yoshikawa, M.; Kitagwa, I. Oxygen-Functionalization of C13-Angular Methyl Group in Pregnane Steroid by Means of Intramolecular Carbonyl-Mediated Anodic Oxidation. *Chem. Pharm. Bull. (Tokyo)*. **1992**, *40* (5), 1143–1147.

(272) Barton, D. H. R.; Cox, J. D. 158. The Application of the Method of Molecular Rotation Differences to Steroids. Part IV. Optical Anomalies. *J. Chem. Soc.* **1948**, 783–793.